



Validation and robust optimization of deep drawing process by simulation in the presence of uncertainty

von Dim Nguyen

► To cite this version:

von Dim Nguyen. Validation and robust optimization of deep drawing process by simulation in the presence of uncertainty. Materials and structures in mechanics [physics.class-ph]. Université de Technologie de Troyes, 2015. English. NNT : 2015TROY0006 . tel-03358892

HAL Id: tel-03358892

<https://theses.hal.science/tel-03358892>

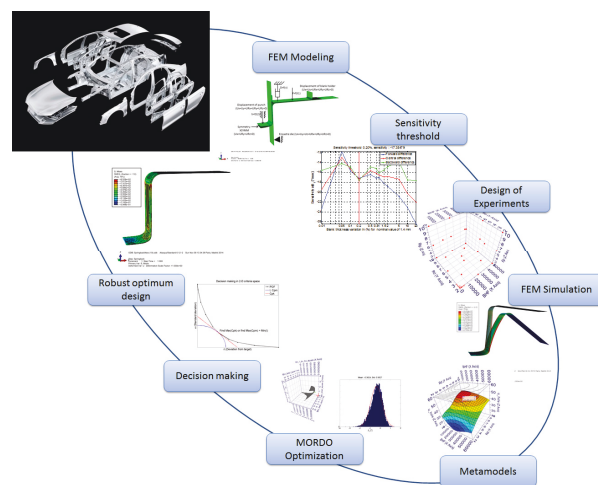
Submitted on 29 Sep 2021

HAL is a multi-disciplinary open access archive for the deposit and dissemination of scientific research documents, whether they are published or not. The documents may come from teaching and research institutions in France or abroad, or from public or private research centers.

L'archive ouverte pluridisciplinaire **HAL**, est destinée au dépôt et à la diffusion de documents scientifiques de niveau recherche, publiés ou non, émanant des établissements d'enseignement et de recherche français ou étrangers, des laboratoires publics ou privés.

Von Dim NGUYEN

Validation and Robust Optimization of Deep Drawing Process by Simulation in the Presence of Uncertainty



Spécialité :
Systèmes Mécaniques et Matériaux

THESE

pour l'obtention du grade de

**DOCTEUR de l'UNIVERSITE
DE TECHNOLOGIE DE TROYES
Spécialité : SYSTEMES MECANQUES ET MATERIAUX**

présentée et soutenue par

Von Dim NGUYEN

le 26 février 2015

**Validation and Robust Optimization of Deep Drawing Process by
Simulation in the Presence of Uncertainty**

JURY

M. S. CHATTI	DOCTOR INGENIEUR - HDR	Président
M. P.-A. ADRAGNA	MAITRE DE CONFERENCES	Directeur de thèse
M. P. BREITKOPF	INGENIEUR DE RECHERCHE CNRS - HDR	Rapporteur
M. J.-Y. DANTAN	PROFESSEUR DES UNIVERSITES	Examineur
M. P. LAFON	PROFESSEUR DES UNIVERSITES	Directeur de thèse
M. S. SAMPER	PROFESSEUR DES UNIVERSITES	Rapporteur

Personnalité invitée

M. F. CHOQUART	DOCTEUR INGENIEUR
----------------	-------------------

Acknowledgments

First and foremost, I would like to express my most sincere gratitude to my supervisors, Pr. Pascal LAFON and Associate Pr. Pierre-Antoine ADRAGNA for their excellent support and guidance during my research work at LASMIS laboratory. Thanks to their priceless advice in scientific research, I have overcome many difficult problems of my thesis.

I would like to acknowledge Pr. Serge SAMPER and Dr. Piotr BREITKOPF who have accepted to read and examine my dissertation. Thank you for your brilliant comments and suggestions. I would also like to thank the members of the jury, Pr. Jean-Yves DANTAN, Dr. Sami CHATTI, and Dr. François CHOQUART for having accepted to be part of the jury and for their remarks and interesting questions in my PhD defense.

I acknowledge my colleagues in the LASMIS lab, particularly Laurent DANIEL for his installation of software and calculation server which helped run computer experiments. I also thank Carl LABERGÈRE for our discussion on FEM simulation.

Thank you all Vietnamese students in Troyes for our good time after scientific works, exchanges of knowledge, skills during my study which helped enrich the experience.

Last but not least, I would like to thank my family and my best friends for their support and encouragement during the time far away from home. I must acknowledge my dear parents, Tien Truc and Mai Thu, without whose love and encouragement, I would not have finished this thesis.

Abstract

The ultimate objective of this thesis is to evaluate the possibility to validate and optimize a manufacturing process using numerical simulation and taking into account the irreducible uncertainties in the process, materials and geometry of manufactured product. Taking into account the uncertainties requires quantifying the effects of variations of model parameters on the outputs, by propagating these variations via computer simulation to assess their effects on the outputs. In this work, we have proposed a procedure to determine the sensitivity threshold of the numerical model to build numerical Design of Experiments consistent with this threshold. We have also shown that, given the uncertainties in the materials and the geometry of the product, it is possible to optimize certain process parameters to control the effects of uncertainties on the dimensional and morphological variations of the product. For this, we have proposed an optimization procedure based on NSGA-II algorithm and a meta-modeling of the process. The application for deep drawing of a U-shaped sheet metal part, springback included, shows that it is a robust design problem for which we get all the compromise between the deviation from the mean and standard deviation of a "performance" depending on the process correctly chosen. Finally, the analysis of these results allows us to quantify the relationship between the notion of robustness of an optimized solution of the process and criteria for measuring the quality of the product.

Keywords: uncertainty, sheet-metal forming, robust design, numerical simulation, sensitivity threshold, uncertainty propagation, robust design optimization, multiple criteria decision making.

Dedicated to my dear parents, Tien-Truc and Mai-Thu, with love and respect.

"The apple never falls far from the tree."

Proverb

List of Tables

2.1	Uniaxial tension test data [75].	16
2.2	Modes of deformation of sheet metal forming	19
2.3	Commonly used metamodeling techniques [200].	28
2.4	Beam bending data	36
2.5	Material constant for yield function Hill 48 [75].	38
2.6	A comparison of springback results obtained by using three different versions of Abaqus.	41
2.7	Input data for comparison with experimental results of Numisheet 2011.	43
2.8	Numerical and experimental comparison of Numisheet 2011.	43
2.9	Nominal values of input parameters for sensitivity threshold analysis	43
2.10	Output parameters	43
2.11	Synthesis of sensitivity threshold of FE numerical beam bending model in 1D with different element sizes	52
2.12	Synthesis of the seven input parameters' minimum sensitivity threshold	57
2.13	Sensitivity of springback responses with respect to the input parameters	57
2.14	Input data for DOE strategy	63
2.15	Input data for DOE strategy	64
2.16	Comparison of accuracy between radial functions of RBF	67
2.17	Comparison of accuracy of metamodels	71
3.1	Methodologies for uncertainty propagation	78
3.2	Relations between probability distributions and orthogonal polynomials	82
3.3	Relationship between C_{pk} and process yield and process fallout	92
3.4	Probabilistic modeling and representation of uncertainties in the in- put parameters	98
3.5	The two first statistical moments of β_1 , β_2 and ρ	98
3.6	Comparison of accuracy of metamodels for U_T	108
4.1	Synthesis of classification of robust design	116
4.2	The interval bounds of input variables	142
4.3	Parameters of NSGA-II	142
4.4	The best compromise solution obtained by the WSM.	145
4.5	The best compromise solution obtained by the WSM for springback parameters β_1 , β_2 , ρ	147
4.6	Analysis results of the effects of aleatory uncertainties in uncontrol- lable parameters on the output parameters of β_1 , β_2 , ρ	149
4.7	Parameters of NSGA-II	151
4.8	Probabilistic modeling and representation of uncertainties in the pa- rameters for the case of hole displacement U_T	151

4.9	Probabilistic modeling and representation of uncertainties in the parameters for the case of three output variables of β_1, β_1, ρ	153
4.10	Relationship between the values of C_{pk} and the IT and design ID	156
4.11	The best solution when $C_{pk}^i = 0.33$	157
4.12	The best solution when $C_{pk} = 0.67, C_{pk} = 1.00$ and $C_{pk} = 1.33$	157
4.13	The best solution when $C_{pk} = 1.67$ and $C_{pk} = 2.00$	157
4.14	Relationship between the values of C_{pm} and the IT and design ID	158
4.15	The best solution found by using the C_{pm} index	159
4.16	Comparison of the IT values between using C_{pk} and C_{pm}	159
4.17	The best compromise solution found by finding maximum value of MC_{pk} of three springback parameters $\beta_1, \beta_2, 1/\rho$	163
4.18	The best compromise solution found by finding maximum value of MC_{pk} of three springback parameters $\beta_1, \beta_2, 1/\rho$	163
4.19	The best compromise solution found by finding maximum value of MC_{pm} of three springback parameters $\beta_1, \beta_2, 1/\rho$	165
4.20	Synthesis of the best solutions based on the capability indices	165
5.1	Synthèse du seuil de sensibilité minimale des sept paramètres d'entrée	189
5.2	La sensibilité de réponse du retour élastique par rapport aux paramètres d'entrée	190
5.3	Les données d'entrée pour la stratégie DOE	194
5.4	Comparaison de la précision de métamodèles	195
5.5	Modélisation probabiliste : représentation des incertitudes dans les paramètres d'entrée	198
5.6	Les deux premiers moments statistiques de β_1, β_2 and ρ	199
5.7	Comparaison de la précision des méta-modèles pour U_T	203
5.8	Modélisation probabiliste et la représentation des incertitudes dans les paramètres pour le cas de déplacement de trou U_T	206
5.9	Modélisation probabiliste et la représentation des incertitudes dans les paramètres pour le cas de déplacement de trou U_T	207
5.10	Modélisation probabiliste et représentation des incertitudes sur les paramètres dans le cas des 3 sorties β_1, β_1 et ρ	209
5.11	Synthèse des meilleures solutions sur la base des indices de capacité	212
5.12	La meilleure solution de compromis trouvé en trouvant valeur maximale de MC_{pk} de trois paramètres retour élastique $\beta_1, \beta_2, 1/\rho$	213
5.13	La meilleure solution lors de $C_{pk} = 0.67, C_{pk} = 1.00$ and $C_{pk} = 1.33$	213
5.14	La meilleure solution de compromis trouvé en trouvant valeur maximale de MC_{pm} de trois paramètres retour élastique $\beta_1, \beta_2, 1/\rho$	214
5.15	La meilleure solution trouvée par l'aide de l'indice de C_{pm}	214
A.1	The input parameters for indentifying sensitivity threshold	222
A.2	Synthesis of punch radius sensitivity threshold	223
A.3	Synthesis of die radius sensitivity threshold	224
A.4	Synthesis of blank holder force sensitivity threshold	225

A.5	Synthesis of friction coefficient sensitivity threshold	226
A.6	Synthesis of blank thickness sensitivity threshold	227
A.7	Synthesis of UTS sensitivity threshold	228
A.8	Synthesis of yield strength sensitivity threshold	229
A.9	Available radial functions	233

List of Figures

1.1	Metal sheet components in Body-In-White of a car	4
1.2	The life-cycle of a product [6]	6
1.3	Design process [162],[188], [55].	6
1.4	Ishikawa diagram for sheet metal forming simulation process [204]	7
1.5	Uncertainty sources in a sheet metal forming process [154].	8
2.1	U-bending process [1].	13
2.2	Typical part formed in stamping [83].	13
2.3	Typical example of deep drawing [95].	14
2.4	Engineering stress-strain curve of DP780 steel [75].	15
2.5	True stress-strain curve of DP780 steel.	16
2.6	A general plane stress sheet process.	17
2.7	An element of a sheet showing: (a) the undeformed state with circle and square grids marked on it; (b) the deformed state with the grid circles deformed to ellipses of major diameter d_1 and minor diameter d_2 and (c) the tractions, T , or forces transmitted per unit width [83].	18
2.8	Strain distributions of different modes [83].	18
2.9	Law of Hollomon.	20
2.10	Comparison of experimental data with material laws.	21
2.11	Design and manufacturing process of stamping tools in automobile industry at present [128].	22
2.12	Design and manufacturing process of stamping tools in automobile industry in the future [128].	23
2.13	Metamodeling and its role in support of engineering design optimization [232].	26
2.14	Principle of metamodeling [103].	27
2.15	Basic three-factor designs. (a) 2^3 full factorial; (b) 2^{3-1} fractional factorial; (c) composite design [200].	29
2.16	(a) "Classical" Design and (b) "Space filling" Design [17].	30
2.17	A typical FEM simulation-based uncertainty propagation approach.	35
2.18	Cantilever beam problem.	36
2.19	Comparison of deflection calculated by analytic formula and FE numerical analysis in 1D with different element sizes enlarged.	37
2.20	A schematic view of tools and dimensions for the open-channel.	37
2.21	A schematic view of springback profile and parameters proposed by Numisheet 2011.	38
2.22	A schematic modeling of draw bending process.	39
2.23	Sensitivity threshold analysis of FEM numerical simulation in sheet metal draw bending.	41
2.24	Representation of Swift's law with different values of R_e and R_m	42

2.25	Evolution of blank thickness with respect to the wall opening angle β_1 .	44
2.26	Evolution of blank thickness with respect to the flange angle β_2 .	45
2.27	Evolution of blank thickness with respect to the side wall curl ρ .	45
2.28	Different geometric interpretations of the first-order finite difference approximation related to forward, backward and central difference approximation.	47
2.29	Sensitivity of $f(x)$ at $x = 1.5$ using the finite difference approximations.	48
2.30	Comparison of ε relative error in the first derivative computed using FDM with respect to analytical derivative.	49
2.31	Sensitivity threshold of FE numerical beam bending model in 1D with element size of 0.2.	50
2.32	Relative error in the estimates using FDM with respect to theoretical result.	51
2.33	Proposed methodology for identifying sensitivity threshold of FE numerical simulation.	53
2.34	The minimum sensitivity threshold of FE numerical sheet metal draw bending regarding β_1 when having the blank thickness variations from 20% to 0.01%.	54
2.35	The minimum sensitivity threshold of FE numerical sheet metal draw bending regarding β_2 when having the blank thickness variations from 20% to 0.01%.	55
2.36	The minimum sensitivity threshold of FE numerical sheet metal draw bending regarding ρ when having the blank thickness variations from 20% to 0.01%.	55
2.37	Sensitivity analysis result of the input variables contributing to β_1 at their nominal value	58
2.38	Sensitivity analysis result of the input variables contributing to β_2 at their nominal value	59
2.39	Sensitivity analysis result of the input variables contributing to ρ at their nominal value	59
2.40	Flowchart of metamodeling process	61
2.41	Workflow of metamodeling for sheet metal forming process	62
2.42	Graphical representation of the FFD of the factors.	65
2.43	Metamodels of β_1 , β_2 and ρ in function of F_{BHF} , R_d built by RSM.	67
2.44	Metamodels of β_1 , β_2 , ρ in function of F_{BHF} , R_d built by Kriging.	68
2.45	Metamodels of β_1 , β_2 , ρ in function of F_{BHF} , R_d built by Radial Basis Functions.	69
2.46	Metamodels of β_1 , β_2 , ρ in function of F_{BHF} , R_d built by Neural Networks.	70
3.1	Uncertainty types [74]	74
3.2	Methodologies for uncertainty propagation and distribution propagation [37]	76
3.3	Uncertainty analysis using surrogate models.	80

3.4	Monter Carlo Sampling generation based on Gaussian distribution. . .	84
3.5	Latin Hypercube Sampling generation based on Uniform distribution. . .	85
3.6	A schematic view of springback profile and parameters.	86
3.7	Springback map and its section [132].	87
3.8	Shapes of the modes of stamped part [112].	87
3.9	Approach of geometric deviation determination based on the sheet metal part's node coordinates.	88
3.10	Procedure of the principal component analysis.	89
3.11	Graphical illustration of process capability.	90
3.12	Normal distribution with a mean shift causes an increase in rejects. .	91
3.13	Taxonomy of uncertainty in sheet metal forming process design based on FEM numerical simulation.	94
3.14	P-Diagram.	94
3.15	An proposed approach for uncertainty propagation.	96
3.16	Probability density function and cumulative distribution function for a normal distribution	97
3.17	Illustration of proposed approach for distribution propagation. . . .	99
3.18	The probability density of β_1 , β_2 and ρ	100
3.19	Geometric tolerances of the sheet metal part.	101
3.20	Probability density of geometric tolerances of $T1$, $T2$, $T3$	102
3.21	Probability density of geometric tolerances of $T4$ and $T5$	103
3.22	Probability density of geometric tolerances of $T1$, $T2$, $T3$	104
3.23	Probability density of geometric tolerances of $T4$ and $T5$	105
3.24	Components assembled in the system [72].	106
3.25	Cross-sections in the assembly system [72].	106
3.26	The variability of hole position before and after springback.	107
3.27	Metamodel of U_T with respect to F_{BHF} and R_d	109
3.28	The probability density of hole displacemnt U_T	109
4.1	The quality loss function and performance target for three manu- factured products whose performance varies through different ranges and whose values of mean performance may or may not coincide with the desired performance [4]	115
4.2	Different types of performance variations [246].	115
4.3	A P -diagram showing information input and response in a product or process model [4].	116
4.4	Taguchi robust design matrix [248].	117
4.5	Two steps of Taguchi method [166].	119
4.6	A comparison of two types of robust design [30].	121
4.7	Type III Robust design [33].	122
4.8	Type IV Robust design [33].	123
4.9	Limit state function in reliability analysis. The region where $g(X) <$ 0 is the failure domain whereas the region where $g(X) > 0$ is the safe domain [99].	124

4.10	Reliability-based design [249].	124
4.11	FORM reliability analysis method.	126
4.12	(a) Deterministic constrained optimisation; (b) Robustness and reliability of a deterministic constrained optimum where noise is present [15].	128
4.13	Robust and reliability based optimization[15].	130
4.14	The principle of robust design optimization [15], [236].	131
4.15	Generic Pareto front.Full blue points indicate members of the pareto set. Point (a) is the optimum for objective function for a given value of (red points). Point (b) minimizes for another value of (compared to green points). For a member of the Pareto set, say (c), any attempt to improve a goal involves worsening the other, point (d) for comparison. Empty blue points are other possible solutions that are worse than those in the Pareto set [175].	136
4.16	Trade-off of two-objective minimization problem, which is represented by non-dominated solutions [186].	137
4.17	NSGA-II flowchart.	139
4.18	A deterministic process design optimization strategy	141
4.19	1000 random designs for R_d , R_p and F_{BHF}	143
4.20	Design of experiments based on a random sequence for the design variables.	143
4.21	The POF obtained by NSGA-II.	144
4.22	Numerical illustration of the optimal design solution obtained when optimizing the springback parameters β_1, β_2, ρ by NSGA-II.	146
4.23	Results of uncertainty analysis of β_1 , β_2 and ρ	148
4.24	Robust design strategy applied for sheet metal forming process design.150	
4.25	Pareto optimal front obtained from MORDO of hole displacement of U_T	152
4.26	Pareto multiple-objective criteria decision making based on capability indices in 2-D space.	155
4.27	Graphical representation of different values of the C_{pk} with respect to the POF	156
4.28	Graphical representation of the C_{pm} of 1.33 with respect to the POF .158	
4.29	The principle of the proposed approach in decision-making support in higher dimensions	161
4.30	The best compromise solution found by finding maximum value of MC_{pk} with $IT = 8$	162
5.1	Des composantes de "caisse en blanc" d'une voiture.	175
5.2	Le cycle de vie d'un produit [6]	177
5.3	Le processus de conception [162],[188], [55].	178
5.4	Diagramme d'Ishikawa pour simuler le procédé d'emboutissage [204] .178	
5.5	Sources d'incertitude dans un procédé de formage de tôle en acier [154].179	

5.6	Comparaison de flèche calculée analytiquement (5.1) et l'analyse numérique EF en 1D avec différentes tailles d'élément.	182
5.7	évolution d'épaisseur de la tôle par rapport à l'angle β_1	183
5.8	évolution d'épaisseur de la tôle par rapport à l'angle β_2	184
5.9	évolution d'épaisseur de la tôle par rapport à le rayon ρ	184
5.10	Méthodologie proposée pour identifier seuil de sensibilité de la simulation numérique EF.	186
5.11	Le seuil de sensibilité minimale de la simulation numérique EF du processus de pliage de la tôle par rapport à β_1 pour des variations d'épaisseur de 20% à 0,01%.	187
5.12	Le seuil de sensibilité minimale de la simulation numérique EF du processus de pliage de la tôle par rapport à β_1 pour des variations d'épaisseur de 20% à 0,01%.	188
5.13	Le seuil de sensibilité minimale de la simulation numérique EF du processus de pliage de la tôle par rapport à ρ pour des variations d'épaisseur de 20% à 0,01%.	188
5.14	L'analyse de sensibilité des variables d'entrée contribuant à la réponse du retour élastique de β_1 à leur valeur nominale	191
5.15	L'analyse de sensibilité des variables d'entrée contribuant à la réponse du retour élastique de β_2 à leur valeur nominale	191
5.16	L'analyse de sensibilité des variables d'entrée contribuant à la réponse du retour élastique de ρ à leur valeur nominale	192
5.17	Organigramme du processus de métamodélisation	193
5.18	Taxonomie des incertitudes dans la conception d'un procédé d'emboutissage de tôle basée sur la simulation numérique MEF.	197
5.19	P-diagramme	198
5.20	Démarche proposée pour la propagation de l'incertitude.	199
5.21	Les points d'échantillonnage générés par LHS pour les paramètres d'entrée	200
5.22	La densité de probabilité de β_1 , β_2 and ρ	201
5.23	La variabilité de la position du trou avant et après le retour élastique.	202
5.24	Méta-modèle de U_T par rapport à F_{BHF} et R_d	203
5.25	La densité de probabilité du déplacement de trou U_T	204
5.26	A multi-objective design strategy using robust design optimization	207
5.27	Front optimal de Pareto obtenu de MORDO de déplacement de trou de U_T	208
5.28	La prise de décision dans l'espace des critères 2-D basée sur des indices de capacité	210
A.8	Typical neuron and architecture. (a) Single unit per caption; (b) feedforward two-layer architecture [200].	234

Contents

I	English version	1
1	Introduction	3
1.1	Background and motivation	3
1.2	Problem definition and Objective of thesis	5
1.2.1	Research scope and purpose of thesis	5
1.2.2	Problem statement	5
1.2.3	Objective of thesis	9
1.3	Dissertation outline	9
2	Numerical approaches and qualification of FEM model	11
2.1	Introduction to sheet metal forming processes	12
2.1.1	Die-bending process	12
2.1.2	Deep drawing process	13
2.2	Determination of sheet material properties	14
2.2.1	Uniaxial tension test	15
2.2.2	The true stress-strain curve	15
2.3	Deformation of sheet in plane stress	17
2.3.1	Strain diagram	17
2.3.2	Effective stress-strain laws	19
2.4	State-of-the-art of FEM simulation in sheet metal forming	20
2.4.1	Role of finite element simulation applied in automotive industry	20
2.4.2	Literature review on FEM simulation of sheet metal forming process for springback prediction	22
2.5	State-of-the-art of metamodeling techniques for computer based en- gineering design	25
2.5.1	Role of metamodeling in support of engineering design	25
2.5.2	Metamodeling process	26
2.5.3	Literature review of metamodeling techniques	27
2.6	Identification of sensitivity threshold of a FEM numerical model	33
2.6.1	Problem statement	33
2.6.2	Sensitivity in FEM analysis: illustrating sensitivity threshold	34
2.6.3	Elaboration of numerical model of sheet metal draw bending	36
2.7	Finite Difference Method (FDM)-based sensitivity threshold identifi- cation of FEM numerical simulation	46
2.7.1	Sensitivity analysis method	46
2.7.2	Illustration of analytic function	48
2.7.3	Illustration of FE numerical beam bending model in 1D	50
2.7.4	Proposed methodology for identifying sensitivity threshold of FE numerical simulation	52

2.8	Example of application	54
2.8.1	Identification of minimum sensitivity threshold	54
2.8.2	Sensitivity analysis of sheet metal draw bending	56
2.9	Building surrogate-models for computer experiments	60
2.9.1	Proposed strategy	60
2.9.2	Metamodeling for sheet metal forming process	62
2.10	Summary of the chapter	71
3	Uncertainty and geometric dispersion	73
3.1	State-of-the-art	73
3.1.1	Uncertainty definition, categorization and propagation	73
3.1.2	Uncertainty modeling, representation and propagation	77
3.1.3	Sampling techniques	84
3.1.4	Determination of sheet metal part variations	86
3.1.5	Quality evaluation of sheet metal part with multiple characteristics	90
3.2	Uncertainty propagation in sheet metal forming process design	93
3.2.1	Uncertainty classification	93
3.2.2	Strategy for uncertainty propagation	95
3.2.3	Analysis of the effects of uncertainties on the product performance	98
3.3	Summary of the chapter	110
4	Optimization under uncertainty of sheet metal forming	113
4.1	State-of-the-art	113
4.1.1	Robust design and Reliability-based design	113
4.1.2	Optimization under uncertainty	127
4.1.3	Multi-objective optimization and Pareto optimality	134
4.1.4	Algorithms for multi-objective optimization	137
4.2	Multi-objective optimization strategy under uncertainty for sheet metal forming process	140
4.2.1	Deterministic process design optimization	141
4.2.2	Uncertainty analysis	147
4.2.3	Multi-objective robust design optimization (MORDO)	149
4.2.4	Pareto multiple objective criteria decision-making support based on capability indices	153
4.2.5	Synthesis of results	164
4.3	Summary of the chapter	166
5	Conclusions and perspectives	167
5.1	Conclusions	167
5.2	Perspectives	168

II	Summary in French	171
A	Appendix	219
A.1	Equations for calculating the springback paramters	219
A.2	Numerical analysis procedures	220
A.2.1	Dynamic explicit procedure	220
A.2.2	Static implicit procedure	221
A.3	Input data for sensitivity threshold identification	222
A.4	Results of sensitivity threshold identification	223
A.4.1	Punch radius	223
A.4.2	Die radius	224
A.4.3	Blank holder force	225
A.4.4	Friction coefficient	226
A.4.5	Blank thickness	227
A.4.6	Ultimate tensile strength	228
A.4.7	Yield strength	229
A.5	Metamodeling techniques	229
A.5.1	Response Surface Methodology	229
A.5.2	Kriging	230
A.5.3	Radial Basis Functions	231
A.5.4	Neural Networks	233
	Nomenclature	235
	Bibliography	237
B	Publications	259

Part I

English version

Introduction

Contents

1.1 Background and motivation	3
1.2 Problem definition and Objective of thesis	5
1.2.1 Research scope and purpose of thesis	5
1.2.2 Problem statement	5
1.2.3 Objective of thesis	9
1.3 Dissertation outline	9

1.1 Background and motivation

In a context where it is necessary to respond industrial challenges towards shorter lead times, lower cost and better customer satisfaction. Concurrent Engineering (CE) was born as a solution to these issues. The solution of the CE is carried out in a manner that the different tasks in the product and production development process are integrated and performed at the same time rather than in sequence. Due to the tasks being implemented in parallel, by integrating product and process design, this makes decrease the development lead time and enhance the quality [201]. In order to improve further the CE, tools and methods of design of product, process and manufacturing systems based on computer simulation need to be more developed [201].

In the other side, sheet metal stamping is a productive process which is mainly used in mass production, particularly to produce the components for "body in white" in the automotive industry as illustrated in Figure 1.1. More specifically, there are around 100 to 150 stamped metal panels on vehicles produced nowadays such as automobiles, light trucks, and minivans [126]. Due to ever increasing competition, the cost reduction and productivity improvement are demands at which the automotive manufacturers aim. However, the sheet metal stamping design process is very expensive and time-consuming because of the costly trial-and-error procedures. Indeed, an automotive plant needs to produce about 40-50 critical panels per a car model that require 150-200 stamping dies [86]. Hence, it is very necessary to shorten the process design time and eliminate costly physical trials which add to the manufacturing cost. As a solution for this issue, CAD software and FEM-based numerical simulation tools have been widely used to design and support in the design and

product development process. A designer can use sheet metal stamping simulation to assess the possibility of successfully manufacturing a sheet metal stamping part without the expense of making a physical tool. Nevertheless, it still has the discrepancy between results from computer simulation and physical experiment. The discrepancy can be provoked by either approximations and errors in FEM models, or variations of the input variables [88].

On the other hand, searching a manufacturing process design producing the parts of which specifications are as close as possible to the nominal values, meanwhile reducing variations of the part performance caused by uncertainties of input variables. Unfortunately, the automobile manufacturers often cope with several defects on the stamped parts in which shape defect due to springback, thinning, wrinkling and tearing are conspicuous defects in the sheet metal stamping process.

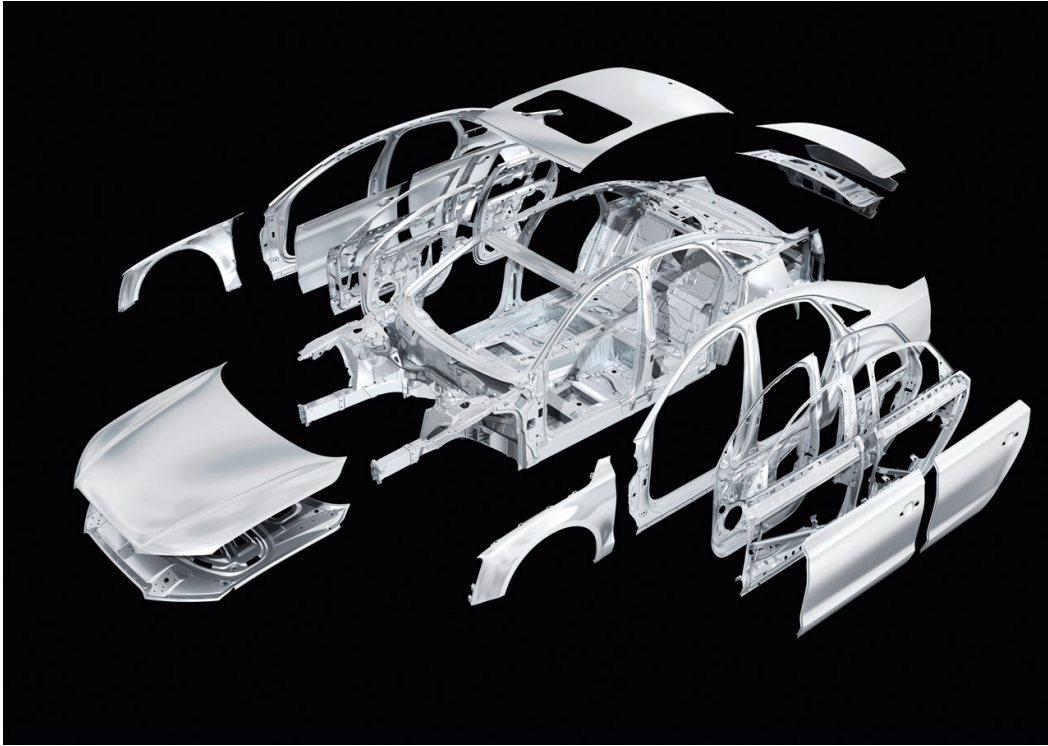


Figure 1.1: Metal sheet components in Body-In-White of a car

The variations in material properties, blank thickness, lubrication, tooling dimensions and process parameters can be causes of those variations in performance of the output. As a consequence, it leads to amplified variations and problems in the downstream assembly process, and in turn, results in quality issues. The sources of the inherent variations stems from the part-to-part, batch-to-batch, and within batch variation during production process [126]. Thus, taking irreducible inherent variability into account and optimization of the process design are major issues should be tackled to obtain a robust process design in the sheet metal stamping

process design.

In the context of Concurrent Engineering and Robust Design, this thesis is motivated by a demand to elaborate a strategy in which engineering activities in the product and production development process are integrated and carried out simultaneously, more particularly searching a robust process design insensitive to variations is included. Moreover, this research challenge is one of the problems which is posed by French research group of Design for Producing Robust Product from the French Association of Mechanical Engineering (AFM) as follows:

" How to manage the uncertainties in the early product life cycle, in particular at the production level?"

1.2 Problem definition and Objective of thesis

1.2.1 Research scope and purpose of thesis

In order to capture research scope of the thesis, the product life-cycle is used as the reference. Altung [6] indicated that the life-cycle of a product goes through six phases including:

- Need recognition
- Design/development
- Production
- Distribution
- Usage
- Disposal/recycling

These phases of the life-cycle of a product is illustrated in Figure 1.2. The framework of this research work in relation to this representation of a product life-cycle will touch the early three phases comprising the need recognition, the product design/development and the product production.

In particular, this thesis addresses the design process in which a part of the embodiment design and detailed design phase are focused on as shaded in Figure 1.3. More specifically, robust design for a sheet metal forming process is taken into account in detail.

The purpose of the thesis is to propose a methodology to manage uncertainties in the sheet metal forming process based on FEM numerical simulation, served for Research & Development (R & D) stage.

1.2.2 Problem statement

Using high performance FEM-based numerical simulation solutions to design sheet metal parts and to support in the product development process is more and more

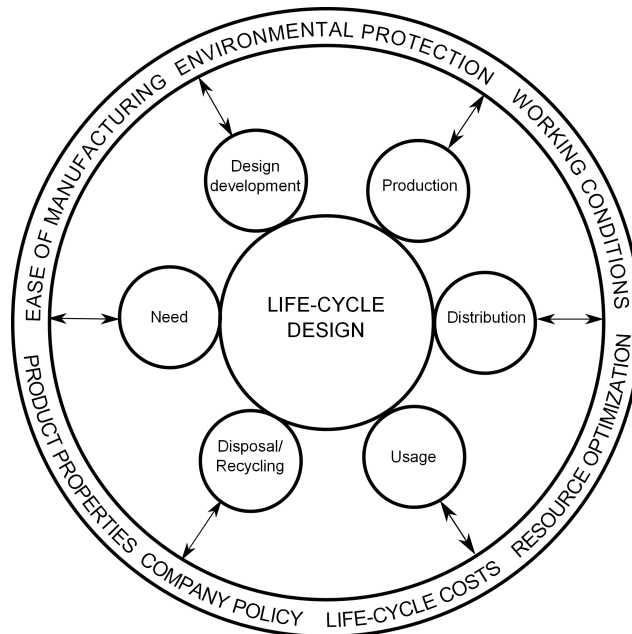


Figure 1.2: The life-cycle of a product [6]

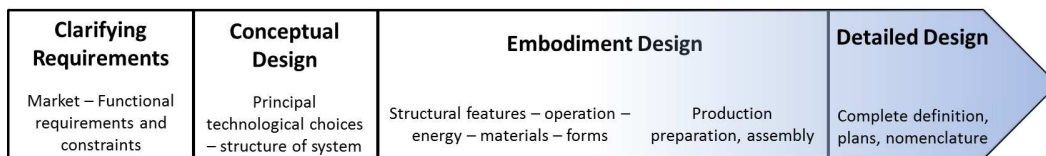


Figure 1.3: Design process [162],[188], [55].

common in the automotive industry. The progress on numerical simulation tools can increase the level of predictability and precision, but these numerical tools remain dependent on many factors including primary causes such as software factors, numeric factors, process parameters, material and workpiece as listed in Figure 1.4 [204]. Moreover, FEM-based numerical models are deterministic - rerunning the

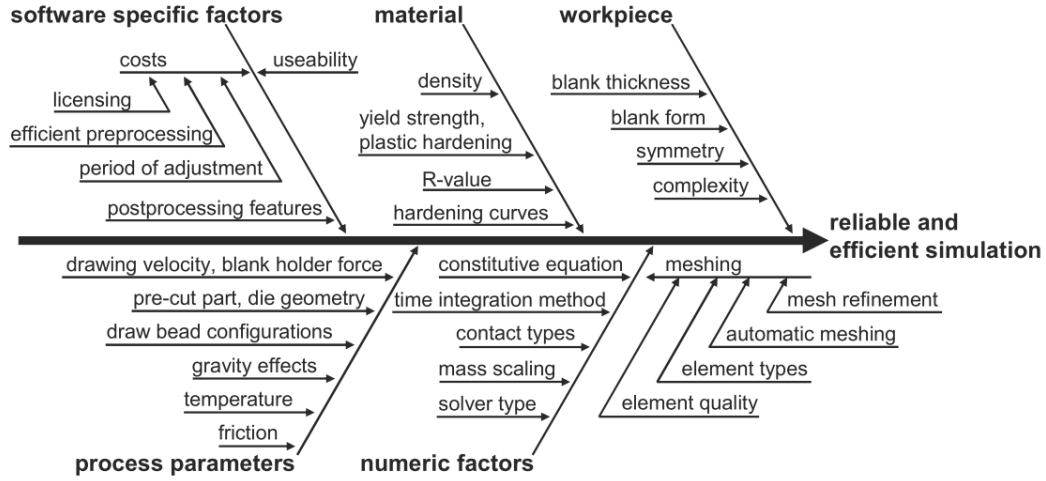


Figure 1.4: Ishikawa diagram for sheet metal forming simulation process [204]

code with the same inputs gives identical observations. It is this lack of random error that makes computer experiments different from physical experiments [183].

While uncertainty is inevitable in any manufacturing process, at any stages of product development, and throughout a product life-cycle. Uncertainties can lead to variations in performance of the outputs. Uncertainties emanate from various sources such as manufacturing imprecision, variations in material properties, variations in geometric dimensions of workpiece, and variations in process parameters. Uncertainty sources in a sheet metal forming process is synthesized in Figure 1.5 [154]. The sources of these inherent variations stem from the part-to-part, batch-to-batch, and within batch variation during production process [126]. In particular, the variability in material properties differs from coil-to-coil, laboratory-to-laboratory and test-to-test. It is indicated that the scatter laboratory-to-laboratory is approximately equal to test-to-test scatter at one laboratory. Coil-to-coil variations are typically greater than the observed test-to-test scatter, particularly in the transverse direction[98]. As a consequence, it leads to amplified variations and problems in the downstream assembly process, and in turn, results in quality issues. Therefore, in order to improve the quality, uncertainty quantification in the design process is required to take into account. Computer experiments based on FEM numerical simulations are the most common approach to study problems in uncertainty quantification [183]. However, these computer experiments consider FEM-based numerical tools as a black-box, thus it is impossible to modify inside to improve their precision. In addition, since FEM-based numerical software has finite precision (due to the errors introduced the

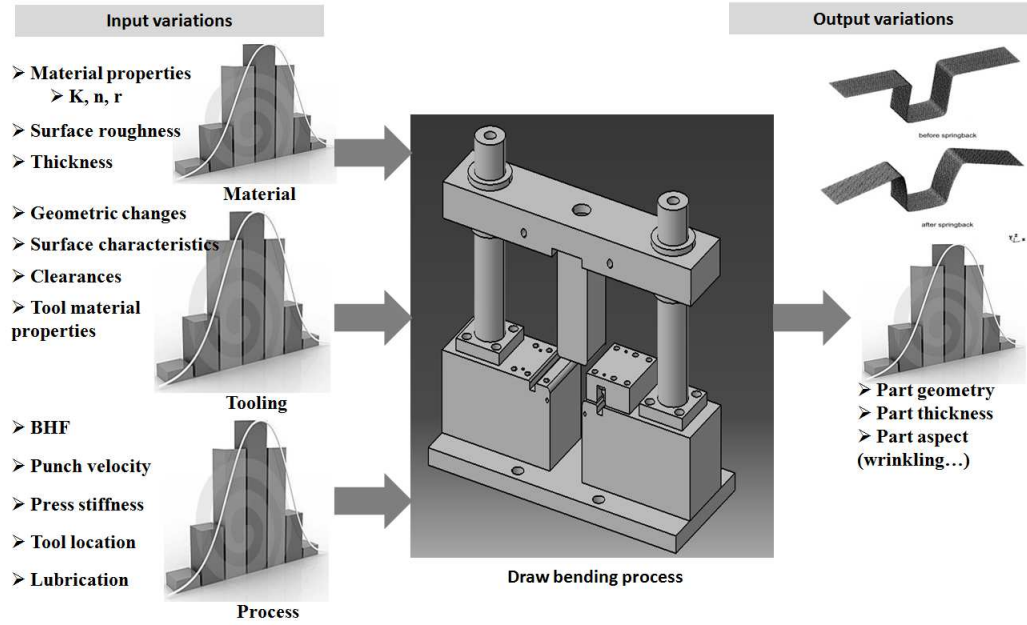


Figure 1.5: Uncertainty sources in a sheet metal forming process [154].

numerical solution methods used such as discretization error, approximation error, convergence problems, modeling error, etc), its sensitivity threshold to input parameters' variation intervals is necessary to study. This contributes to enhancing the confidence of the results in uncertainty propagation.

In the detailed design phase, to ensure the desired behaviour and functional requirements of a part in spite of uncertainties, the part features are assigned a tolerance zone within which the value of feature. Therefore, tolerance design is a key element in industry for improving product quality and decreasing the manufacturing cost. Since the sheet metal part's performance variation induced by uncertainties of the inputs is quite large due to springback, geometric tolerance analysis for the sheet metal part is a problem to consider.

Due to variations being unavoidable in manufacturing process, minimizing the variations of the performance under uncertainty are required from automotive industry. In order to solve this problem, Robust Design proposed by Taguchi (also known as Taguchi method) [208], [211] was given. Nevertheless, the Taguchi method has several drawbacks. Since Taguchi generates experimental designs based on orthogonal arrays, the optimum designs can be only obtained at these sampling points, while the points between them are not evaluated. Another drawback of the Taguchi method is the impossibility of taking into account interaction effects between design variables [221]. In addition to the shortcomings of the Taguchi method, the variance in response is caused solely by uncertainties in noise factors. Hence, it is essential to build a multi-objective optimization strategy based on Robust Design Optimization (RDO) to the performance variations under uncertainties in both design variables and noise factors.

For multi-objective optimization problem, the Pareto optimal front (POF) represents optimum solutions in the objective space. A designer selects the ultimate solution among the Pareto set on the basis of additional requirements, which may be subjective.

1.2.3 Objective of thesis

The general goal of this thesis is to respond the question: "How to manage the uncertainties in the early product life-cycle, in particular at the production level?" for a sheet metal forming process using FEM-based numerical simulations.

The specific objectives are carried out in this thesis as follows:

- Identify the credibility of a FEM-based numerical simulation of a sheet metal forming process.
- Analyze the effect of uncertainties in the input parameters on part performance via FEM simulation and metamodels
- Optimize the process in the presence of uncertainties and identify the best optimal design configurations based on process capability indices.

1.3 Dissertation outline

The dissertation is organized into 5 chapters as follows:

- **Chapter 1:** This chapter introduces the background and motivation in product development in industry. The problem statements as well as objectives of the thesis are presented.
- **Chapter 2:** One of the focuses of the thesis, this chapter reviews numerical approaches including FEM-based numerical simulations for sheet metal forming process and metamodeling techniques. *Particularly, an approach identifying sensitivity threshold of the FEM-based numerical models is proposed.* An application of U-shaped part draw bending process is taken into account. A strategy for building metamodels is suggested.
- **Chapter 3:** The literature review on uncertainty, sampling techniques, and process capability indices are employed. Geometric tolerance analysis and determination of sheet metal part's performance variations are presented. *Analysis of the effects of uncertainties on the part performance are carried out.*
- **Chapter 4:** A strategy for multi-objective robust design optimization of the sheet metal forming process is built based on metamodels and multi-objective algorithms. *An approach is proposed to address the best optimal design configuration based on the capability indices applied for Robust Design.*

- **Chapter 5:** Key conclusions and perspectives are given in this chapter.

Numerical approaches and qualification of FEM model

Contents

2.1	Introduction to sheet metal forming processes	12
2.1.1	Die-bending process	12
2.1.2	Deep drawing process	13
2.2	Determination of sheet material properties	14
2.2.1	Uniaxial tension test	15
2.2.2	The true stress-strain curve	15
2.3	Deformation of sheet in plane stress	17
2.3.1	Strain diagram	17
2.3.2	Effective stress-strain laws	19
2.4	State-of-the-art of FEM simulation in sheet metal forming	20
2.4.1	Role of finite element simulation applied in automotive industry	20
2.4.2	Literature review on FEM simulation of sheet metal forming process for springback prediction	22
2.5	State-of-the-art of metamodeling techniques for computer based engineering design	25
2.5.1	Role of metamodeling in support of engineering design	25
2.5.2	Metamodeling process	26
2.5.3	Literature review of metamodeling techniques	27
2.6	Identification of sensitivity threshold of a FEM numerical model	33
2.6.1	Problem statement	33
2.6.2	Sensitivity in FEM analysis: illustrating sensitivity threshold	34
2.6.3	Elaboration of numerical model of sheet metal draw bending	36
2.7	Finite Difference Method (FDM)-based sensitivity threshold identification of FEM numerical simulation	46
2.7.1	Sensitivity analysis method	46
2.7.2	Illustration of analytic function	48
2.7.3	Illustration of FE numerical beam bending model in 1D	50
2.7.4	Proposed methodology for identifying sensitivity threshold of FE numerical simulation	52
2.8	Example of application	54

2.8.1	Identification of minimum sensitivity threshold	54
2.8.2	Sensitivity analysis of sheet metal draw bending	56
2.9	Building surrogate-models for computer experiments	60
2.9.1	Proposed strategy	60
2.9.2	Metamodeling for sheet metal forming process	62
2.10	Summary of the chapter	71

The main objective of this chapter is to qualify the level of predictability of a FEM-based numerical simulation of a sheet metal forming process.

2.1 Introduction to sheet metal forming processes

Sheet metal forming processes are those in which force is applied to a piece of sheet metal to modify its geometry rather than remove any material. The applied force stresses the metal beyond its yield strength, causing the material to plastically deform, but not to fail. By doing so, the sheet can be bent or stretched into a variety of complex shapes. Sheet metal forming processes are mainly used in mass production for producing automobiles, domestic appliances, building products, aircraft, food and drink cans. Sheet-metal parts have the advantage that the material has a high elastic modulus and high yield strength so that the parts produced can be stiff and have a good strength-to-weight ratio [83]. There is a large number of techniques to make sheet metal parts in which the most common sheet metal forming techniques including deep drawing process is interested in this research work.

2.1.1 Die-bending process

Bending is the simplest metal forming process in which a force is applied to a piece of sheet metal, causing it to bend at an angle and form the desired shape. Plastic deformation occurs only in the bend region and the material away from the bend is not deformed. If the material lacks ductility, cracking may appear on the outside bend surface, but the greatest difficulty is usually to obtain an accurate and repeatable bend angle. Elastic springback is appreciable [83].

U-bending sometimes called deep drawing process (the depth larger than the width) requires a blank, blank holder, die, and punch as shown Figure 2.1. To form U-part, the blank is clamped by the blank holder over the die which has a cavity where the punch moves downward into the blank. As the punch is pushed into the sheet, tensile forces are generated at the centre. These are the forces that cause the deformation and the contact stress between the punch and the sheet is very much lower than the yield stress of the sheet. The tensile forces are resisted by the material at the flange of the blank and compressive stresses will develop in this region. As a result, the U-bent part is generated after removing the tools. Ideally, the bent part meets desired functional and technical requirements. However, geometrical defect of the bent part due to springback is an inherent problem in the bending

process. Reducing and compensating the springback occurred are still challenges to the industry.

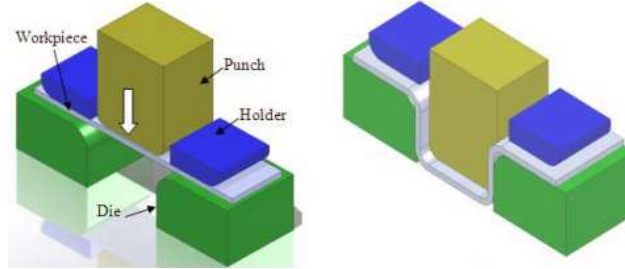


Figure 2.1: U-bending process [1].

2.1.2 Deep drawing process

Deep drawing process is a process in which thin walled metal parts are also shaped by punches and dies. The punch pushes downward on the sheet metal, forcing it into a die cavity in the shape of the desired part. In stamping, most of the final part is formed by stretching over the punch although some material around the sides may have been drawn inwards from the flange. As there is a limit to the stretching that is possible before tearing, stamped parts are typically shallow. This process is widely used to form auto-body panels and a variety of appliance parts. A typical part formed in stamping is shown in Figure 2.2.

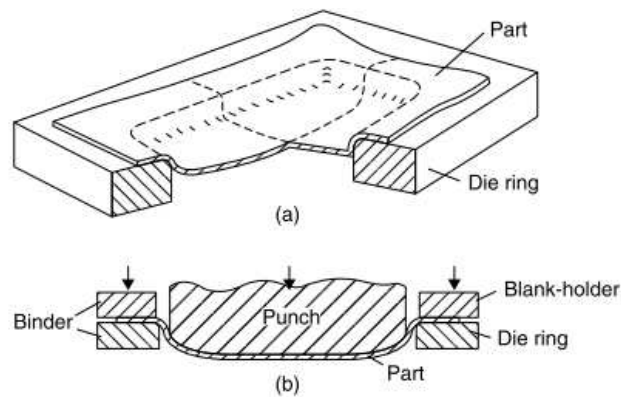


Figure 2.2: Typical part formed in stamping [83].

To form deeper parts, much more material must be drawn inwards to form the sides and such a process is termed deep drawing. Deep drawn parts are characterized by a depth equal to more than half of the diameter of the part. Typical example of deep drawing is presented in Figure 2.3.

The deep drawing process requires a blank, blank holder, punch, and die. The blank is a piece of sheet metal, typically a disc or rectangle, which is pre-cut from stock material and will be formed into the part. The blank is clamped down by

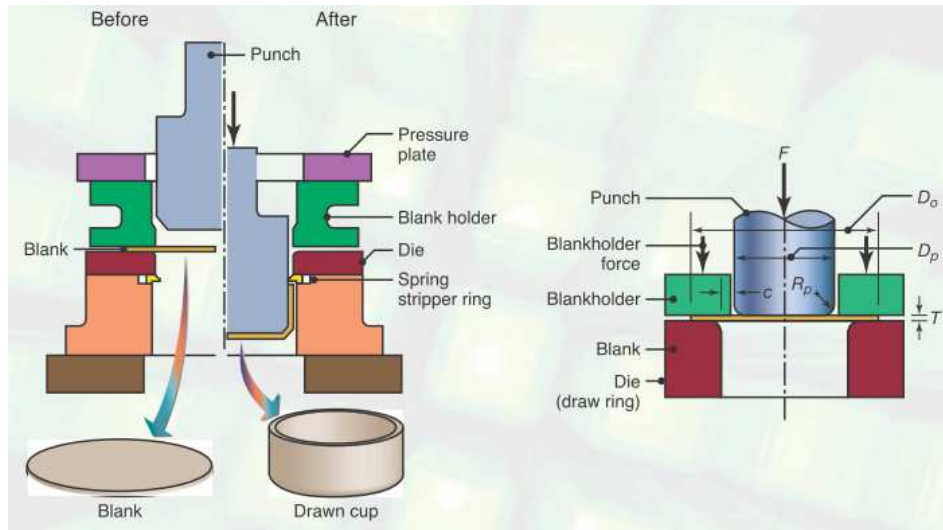


Figure 2.3: Typical example of deep drawing [95].

the blank holder over the die, which has a cavity in the external shape of the part. A tool called a punch moves downward into the blank and draws, or stretches, the material into the die cavity. The movement of the punch is usually hydraulically powered to apply enough force to the blank. Both the die and punch experience wear from the forces applied to the sheet metal and are therefore made from tool steel or carbon steel. The process of drawing the part sometimes occurs in a series of operations, called draw reductions. In each step, a punch forces the part into a different die, stretching the part to a greater depth each time. After a part is completely drawn, the punch and blank holder can be raised and the part removed from the die. The portion of the sheet metal that was clamped under the blank holder may form a flange around the part that can be trimmed off.

2.2 Determination of sheet material properties

In sheet metal forming, there are two regimes of interest consisting of elastic and plastic deformation. Forming a sheet to some shape obviously involves permanent plastic flow and the strains in the sheet could be quite large. While elastic strain has an important effect to give rise to springback when the sheet metal part is released from the tools.

Moreover, advanced high strength Dual Phase (DP) steels are ever increasingly used to make automotive parts, particularly in Body-In-White, to reduce weight as well as to improve passive safety. Nevertheless, a major problem of cold-stamped parts made from such high strength steels is the large springback value. Springback occurred in a formed part needs to be considered in the process design due to that springback is variably sensitive to materials and process parameters [34], [229]. In subsequent section, a uniaxial tension test of DP780 steel which is presented.

2.2.1 Uniaxial tension test

The measured engineering stress-strain curve in the rolling direction for DP780 steel is shown in Figure 2.4.

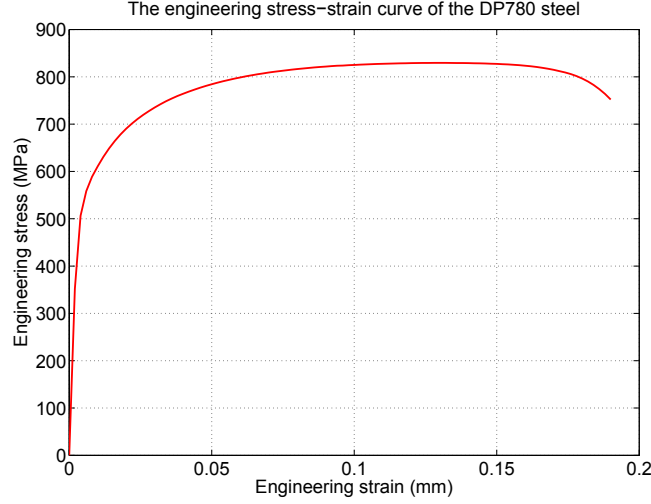


Figure 2.4: Engineering stress-strain curve of DP780 steel [75].

The initial yield stress is defined as

$$(\sigma_f)_0 = \frac{P_y}{A_0} \quad (2.1)$$

where P_y is the initial yielding load at which plastic deformation commences.

The maximum engineering stress called the ultimate tensile strength (UTS) is calculated as

$$UTS = \frac{P_{max}}{A_0} \quad (2.2)$$

However, it can be seen from Figure 2.4 the transition from elastic to plastic deformation is not sharp and it is difficult to establish a precise yield stress. Therefore, yield stress called yield strength (YS) is determined by drawing a line parallel to the elastic loading line which is offset by the specified amount of 0.2%. In tensile test of DP780 steel, the properties are different in directions so that some anisotropy exists. The state of anisotropy is usually indicated by the R-value which is defined as the ratio of width strain to thickness strain. As for anisotropic plastic behavior, the sheet sample was characterized along three directions: the rolling, 45 degree and transverse directions. Uniaxial tension test data of the DP780 steel is shown in Table 2.1.

2.2.2 The true stress-strain curve

Since the engineering stress-strain curve is calculated based on the initial cross-sectional area of the sample and the original gauge length, it is not suitable for

Table 2.1: Uniaxial tension test data [75].

Direction	Rolling direction
E [GPa]	198.8
YS [MPa]	527
UTS [MPa]	831.5
Uni. elongation [%]	13.1
Total elongation [%]	19.8
R-value	0.781
Poisson's ratio	0.3
Friction coefficient	0.1

use in the analysis of forming process. To overcome these disadvantages, the study of sheet metal forming processes is based on the true stress-strain curve. The true stress-strain curve can be calculated from the engineering stress-strain diagram using the relationships as follows:

$$\sigma = \frac{P}{A} = \frac{P}{A_0} \frac{A_0}{A} = \sigma_{eng} \frac{l}{l_0} = \sigma_{eng} \left(1 + \frac{e_{eng}}{100}\right) \quad (2.3)$$

$$\varepsilon = \ln \left(1 + \frac{e_{eng}}{100}\right) \quad (2.4)$$

The true stress-strain curve calculated from the engineering stress-strain curve is shown in Figure 2.5. The true stress-strain curve in Figure 2.5 cannot be calculated

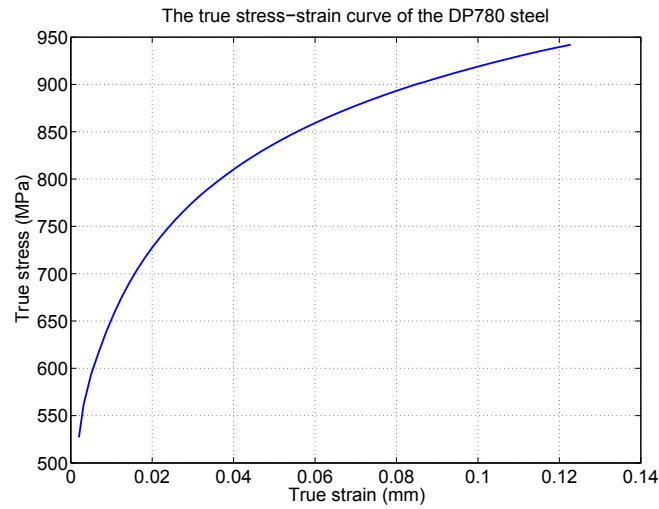


Figure 2.5: True stress-strain curve of DP780 steel.

beyond a strain corresponding to maximum load. This strain is called the maximum uniform strain defined as:

$$\varepsilon_u = \ln \left(1 + \frac{E_u}{100}\right) \quad (2.5)$$

2.3 Deformation of sheet in plane stress

2.3.1 Strain diagram

In a typical sheet process most elements will deform under membrane stresses σ_1 and σ_2 , which are both non-zero. The third stress, σ_3 , perpendicular to the surface of the sheet is usually quite small as the contact pressure between the sheet and the tooling is generally very much lower than the yield stress of the material. It is assumed that normal stress is zero, such a process is called plane stress deformation. It is convenient to describe the deformation of an element as shown in Figure 2.6 in terms of either the strain ratio β or the stress ratio α . The usual convention is to define the principal directions so that $\sigma_1 > \sigma_2$ and the third direction is perpendicular to the surface where $\sigma_3 = 0$. The deformation mode is thus:

$$\varepsilon_1; \varepsilon_2 = \beta \varepsilon_1; \varepsilon_3 = -(1 + \beta) \varepsilon_1 \quad (2.6)$$

$$\sigma_1; \sigma_2 = \alpha \sigma_1; \sigma_3 = 0 \quad (2.7)$$

The sum of natural strains is zero:

$$\varepsilon_1 + \varepsilon_2 + \varepsilon_3 = 0 \quad (2.8)$$

The sheet metals are very sensitive to modes of deformation to which they are

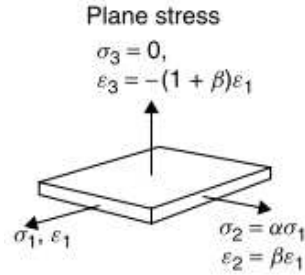


Figure 2.6: A general plane stress sheet process.

applied. For a given material, the necessary efforts as well as the capacity of deformation can differ greatly from one mode to another. Therefore, the study of the formability of the sheet metal by the definition of the different deformation modes is vital. In the study of any sheet metal forming process, it is first necessary to determine the strain over the part. This can be done by measuring a grid marked on the sheet metal which is shown in Figure 2.7. By convention, the major principal direction 1 is assigned to the direction of the greatest principal stress and consequently greatest principal strain. The minor principal direction 2 is considered as perpendicular to the direction 1. Figure 2.8 indicates the strain distribution of different modes.

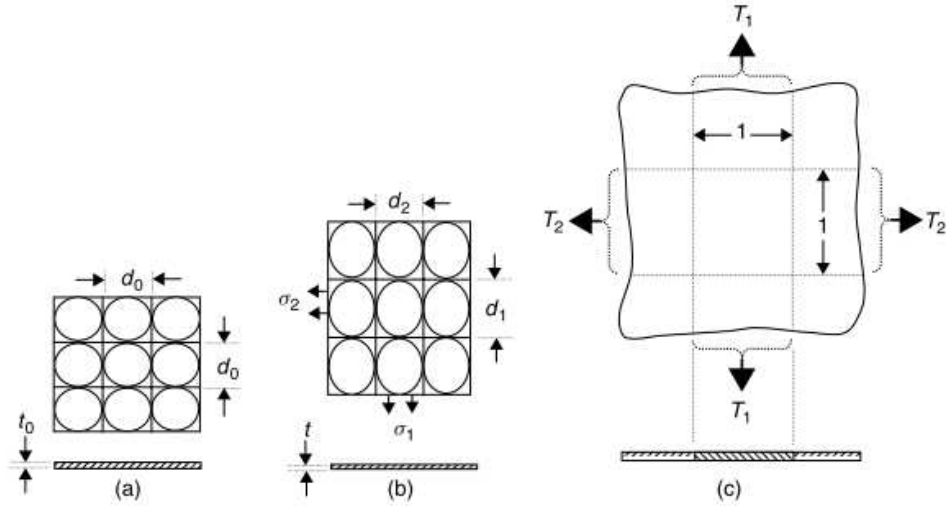


Figure 2.7: An element of a sheet showing: (a) the undeformed state with circle and square grids marked on it; (b) the deformed state with the grid circles deformed to ellipses of major diameter d_1 and minor diameter d_2 and (c) the tractions, T , or forces transmitted per unit width [83].

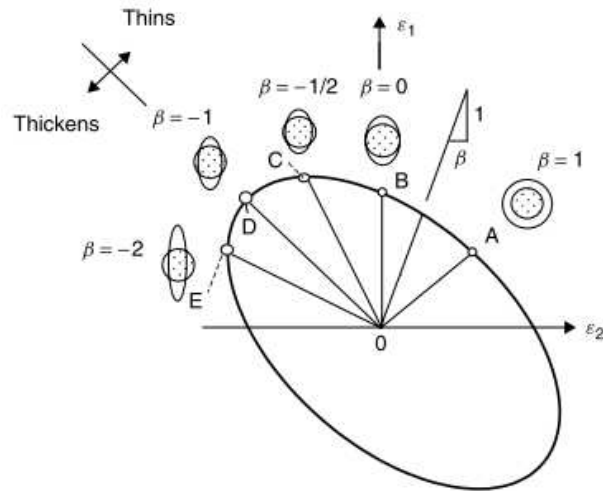


Figure 2.8: Strain distributions of different modes [83].

Table 2.2: Modes of deformation of sheet metal forming

Mode	Deformation	Stresses
Equal biaxial tension, $\beta=1$	$\varepsilon_1 > 0; \varepsilon_2 > 0; \varepsilon_3 < 0; \varepsilon_1 + \varepsilon_2 = -\varepsilon_3; \varepsilon_1 = \varepsilon_2 = -\frac{\varepsilon_3}{2}$	$\sigma_1 > 0; \sigma_2 > 0; \sigma_3 = 0;$
Plane strain, $\beta=0$	$\varepsilon_1 > 0; \varepsilon_2 = 0; \varepsilon_3 < 0; \varepsilon_1 = -\varepsilon_3$	$\sigma_1 > 0; \sigma_2 > 0; \sigma_3 = 0; \sigma_2 = \frac{\sigma_1}{2}$
Uniaxial tension, $\beta=-1/2$	$\varepsilon_1 > 0; \varepsilon_2 < 0; \varepsilon_3 < 0; \varepsilon_2 + \varepsilon_3 = -\varepsilon_1; \varepsilon_2 = \varepsilon_3 = -\frac{\varepsilon_1}{2}$	$\sigma_1 > 0; \sigma_2 = 0; \sigma_3 = 0$
Pure shear, $\beta=-1$	$\varepsilon_1 > 0; \varepsilon_2 < 0; \varepsilon_3 = 0; \varepsilon_2 = -\varepsilon_1$	$\sigma_1 > 0; \sigma_2 < 0; \sigma_3 = 0; -\sigma_2 = \sigma_1$
Uniaxial compression, $\beta=-2$	$\varepsilon_1 > 0; \varepsilon_2 < 0; \varepsilon_3 \geq 0; \varepsilon_3 + \varepsilon_1 = -\varepsilon_2; \varepsilon_1 = \varepsilon_3 = -\frac{\varepsilon_2}{2}$	$\sigma_1 = \sigma_3 = 0$

2.3.2 Effective stress-strain laws

The next step in study of sheet metal forming processes is to determine the stress state associated with strain at each point. As mentioned previously, the engineering stress-strain curve is characterized by an elastic part and a plastic part. In order to model the isotropic hardening behaviour, empirical effective stress-strain laws are necessarily used. The constitutive laws are commonly used as:

- Power law: A power law or law of Hollomon is defined as

$$\bar{\sigma} = K\bar{\varepsilon}^n \quad (2.9)$$

where $\bar{\sigma}$ is effective or equivalent stress; $\bar{\varepsilon}$ is effective or equivalent plastic strain; K is the strength coefficient and n is the strain-hardening index. The power law is described as in Figure 2.9. The constants K and n are obtained by linear regression. The slope of this curve give the exponent of strain-hardening. By fitting the power law to two points, a point, A, and the maximum stress point, the exponent of strain-hardening, n , is determined as:

$$n = \frac{\ln \sigma_{max} - \ln \sigma_A}{\ln \varepsilon_u - \ln \varepsilon_A} \quad (2.10)$$

By substitution, the coefficient of strain-hardening K is defined as

$$K = \frac{\sigma}{\varepsilon_u^n} \quad (2.11)$$

The disadvantage of this law is that at zero strain, it predicts zero stress and an infinite slope to the curve. It does not indicate the actual initial yield stress.

- Law of Swift or law of Krupkowski is defined as:

$$\bar{\sigma} = K(\varepsilon_0 + \bar{\varepsilon})^n \quad (2.12)$$

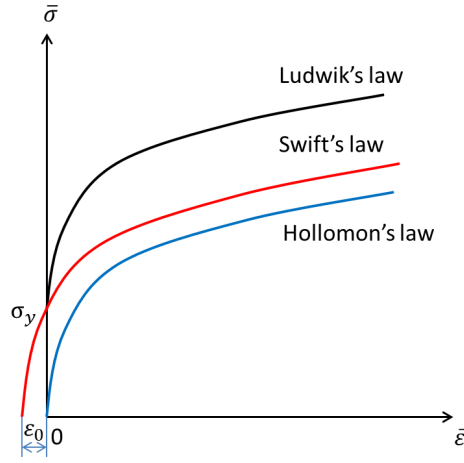


Figure 2.9: Law of Hollomon.

where the constant ϵ_0 is termed a pre-strain or offset strain constant. The Swift law is represented as in Figure 2.9.

In materials which are very nearly fully annealed and for which ϵ_0 is small, this relation can be obtained by first fitting Equation 2.9 and then, using the same values of K and n , to determine the value of ϵ_0 by fitting the curve to the experimentally determined initial yield stress using the equation:

$$\sigma_y = K\epsilon_0^n \quad (2.13)$$

- Law of Ludwik is defined as:

$$\bar{\sigma} = \sigma_y + K\bar{\epsilon}^n \quad (2.14)$$

where σ_y is initial yield stress. The law of Ludwik is described as in Figure 2.9.

In order to describe the strain-hardening of DP780 steel, it is essential to give a constitutive law which well characterized its behavior in FE numerical simulation. Three material laws are compared with experimental data of DP780 steel as shown in Figure 2.10. It has been found that the Swift law is the best fit to the experimental data. Therefore, it is used in numerical analysis in next sections.

2.4 State-of-the-art of FEM simulation in sheet metal forming

2.4.1 Role of finite element simulation applied in automotive industry

The automotive industry faces world-wide serious challenges: fierce market competition and strict governmental regulations on environment protection. The strate-

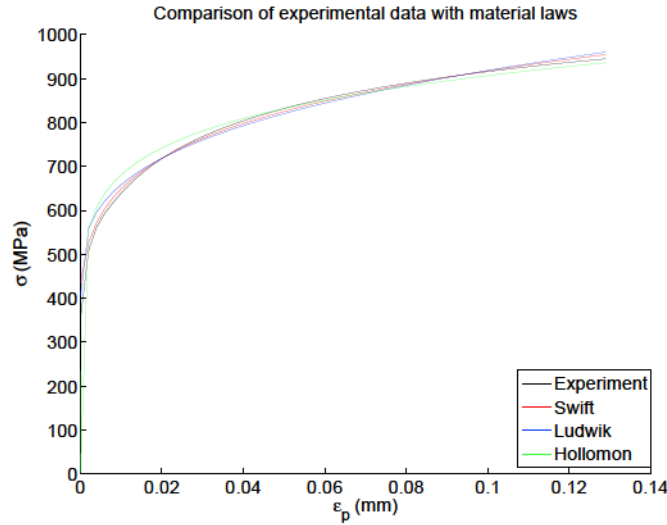


Figure 2.10: Comparison of experimental data with material laws.

gies of the automakers to meet these challenges is sometimes called the 3R Strategy: Reduction in time-to-market, reduction in development costs to gain competitiveness, and reduction in the vehicle weight to improve fuel efficiency. The solutions to achieve this triple goal are essentially based on the implementation of CAD/CAE/CAM technologies in product development and process design. A very significant component of this endeavour is focused on the reduction of the tooling costs and the lead-time related to the stamping of autobody panels, even under increasing technological difficulties such as the use of aluminum alloys and high-strength steels, and requirements for higher geometrical accuracy of stamped parts. To deal with the problems brought about by these trends, which are beyond past experience, numerical methods for sheet forming simulation become more and more important, replacing the physical tryout of stamping dies by a computer tryout. The success of numerical simulation depends mainly on the advances in forming simulation codes, but progress in other related technologies is also important. Examples of related technology are the CAD systems that rapidly construct and modify tool surfaces, modern mesh generators to, more or less automatically, create FE- meshes on CAD surfaces, visualization hardware and software, which enables users to grasp the huge data, and, finally, the computer hardware, which makes it possible to perform large scale simulations within reasonable time [129].

At present, the role of finite element simulation in design and manufacturing of stamping tools is illustrated as in Figure 2.11. This process is begun with the concept and style design of a new car and ended up with the commencement of production. Simulation may be effectively performed at five different stages in Figure 2.11 for the purpose of helping decision making in design and modification of parts and tools. The first simulation is at the production process design stage <1>. Purpose of the simulation at the stage is to make a rough estimation whether panels of

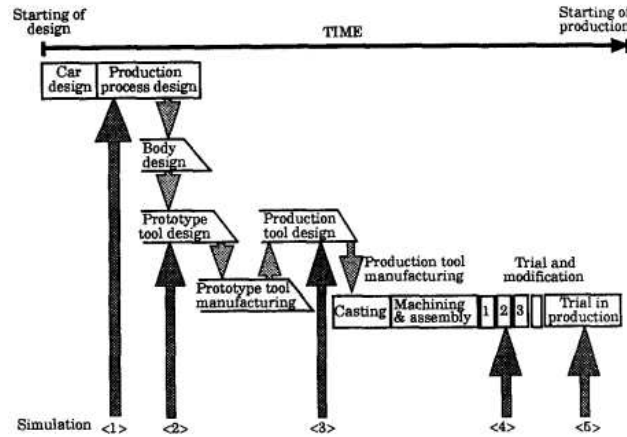


Figure 2.11: Design and manufacturing process of stamping tools in automobile industry at present [128].

new designed car can be formed or not. If answer is "no", the ear design must be modified. However, at this stage geometry of body parts are not fully described in CAD system and no tool data exists, thus it is not possible to make full simulation. The precise simulation is achieved at stage <3> to determine number of stamping steps, such as first drawing, second drawing, trimming, edge bending, and to design die face geometry used at each stamping step. At this stage die face geometry is modeled by CAD surface description and thus modification of die face data is made rather easily according to the simulation results on same CAD system. The performance of integrated CAD and simulation system is crucial for obtaining well optimized stamping steps and die face shape in very limited time allocated to the production tool design. The simulation is also required at the tryout stage <4>, to find a solution to avoid the forming defects appeared during tryout. In order to study the mechanism of origination and propagation of defects, the systematic series of simulation can be taken place after production started <5>, and obtained information is efficiently made use of in the next new model [128].

Ideally, the finite element simulation is powerful enough to predict all the forming defects and provide optimum stamping tools and conditions. The prototype tools from the design and manufacturing procedure are eliminated and number of trial and modification operations is reduced. Thus, the design and manufacturing process of stamping tools might be shorten dramatically as is illustrated in Figure 2.12[128].

2.4.2 Literature review on FEM simulation of sheet metal forming process for springback prediction

Using FEM simulation for predicting defects in sheet metal forming design is very common. One of these dominant defects is geometrical defects due to the springback. Several research works assessed how springback prediction capability depends on the utilized numerical approaches. Mattiasson et al. [134], Wagoner et al. [228] and Li

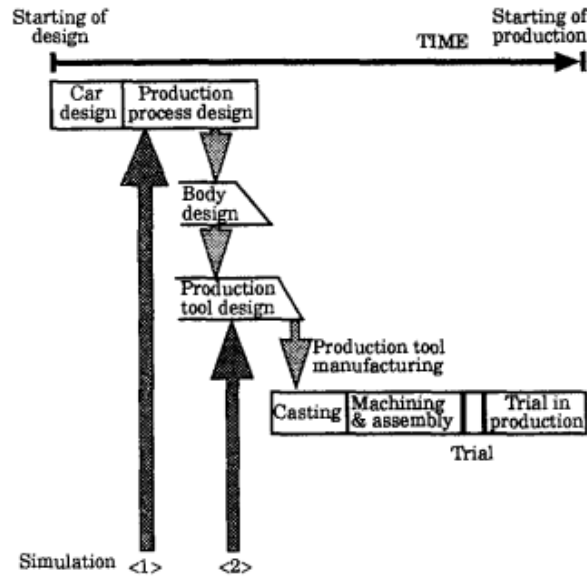


Figure 2.12: Design and manufacturing process of stamping tools in automobile industry in the future [128].

et al. [121] FEM simulations of springback are much more sensitive to numerical tolerances than forming simulations are. Li et al. [121] investigated the effects of element type on the springback simulation. Yuen [244] and Tang [214] found that different unloading scheme will affect the accuracy of the springback prediction. Similarly, Focellese et al. [60] and Narasimhan and Lovell [150] pointed out that different integration scheme will also influence the result of springback simulation. Park et al. [165] and Valente and Traversa [223] attempted to link dynamic explicit simulations of forming operations to static implicit simulations of springback. He and Wagoner investigated the impact of the finite element mesh system of the blank on springback results using the same benchmark problem [76]. The effect of the dynamic term on springback was evaluated by Chung et al. [35]. Numerical factors affecting springback including contact damping parameter, penalty parameter, blank element size, number of corner elements were investigated by Lee and Yang [116]. For the last few years, a couple of investigations in relation to the effectiveness of numerical models have been also taken into consideration making comparison between numerical predictions and experimental results. Particularly, the influence of numerical parameters comprising the type of the utilized element, the number of integration points, the hardening rule and so forth, with the aim to improve the effectiveness and reliability of the numerical results [120]. Xu et al. analyzed the effect of sensitivity factors in a U-bending process of Numisheet'93 benchmark problem using a fully explicit solution scheme in which the impact of integration points number, blank element size and punch velocity is researched [240]. Li et al. [120] explored a variety of issues in the springback simulations. *They concluded that (1) typical forming simulations are acceptably accurate with*

5-9 through thickness integration points for shell/beam type elements, whereas springback analysis within 1% numerical error requires up to 51 points, and more typically 15-25 points, depending on R/t (R :tool radius and t : sheet thickness), sheet tension and friction coefficient. (2) More contact nodes are necessary for accurate springback simulations than for forming simulation, approximately one node per 5 [°] of turn angle versus 10 [°] recommended for forming. (3) Three-dimensional shell and non-linear solid elements are preferred for springback prediction even for large w/t ratios because of the presence of persistent anticlastic curvature. For $R/t > 5.6$, shell elements are preferred since solid elements are too computation-intensive. For $R/t < 5.6$, nonlinear 3D solid elements are required for accurate springback prediction.

It has been found that the reliability of a numerical simulation depends both on material behavior modeling (yield condition and hardening model) and on typical numerical parameters (mesh dimension, element type, number of integration points, integration scheme, punch velocity, and so on). Oliveira et al. [158] evaluated the influence of work-hardening modeling in springback prediction in the first phase of the Numisheet2005, Benchmark 3: the U-shape Channel Draw. Several work-hardening constitutive models are used in order to allow the different materials' mechanical behavior to be better described: the Swift law or a Voce type saturation law[227] to describe the classical isotropic work-hardening; a Lemaitre and Chaboche[118] type law to model the non-linear kinematic hardening, which can be combined with the previous two; and Teodosiu's microstructural work-hardening model [217]. They found that the differences in springback prediction are not significantly higher than those previously reported for components with lower equivalent plastic strain levels. It is shown that these differences can be related to the predicted through-thickness stress gradients [158]. Taherizadeh et al. [212] predicted the springback of Numisheet2005 Benchmark 3 with different material models using the commercial finite element code ABAQUS. ***They concluded that the isotropic hardening model cannot accurately predict springback of sheet metal parts when the forming process leads to cyclic deformations..*** While the mixed isotropic-nonlinear kinematic hardening model is able to capture the main cyclic hardening phenomena and therefore is more appropriate for simulating the springback. Li et al.[122] investigated Effect of the material-hardening mode on the springback simulation accuracy of V-free bending. They found that the material-hardening mode directly affects the springback simulation accuracy, and the greater the veracity of the hardening mode, the greater the springback accuracy. Geng and Wagoner [64] evaluated springback prediction accuracy in comparing four different yield functions: von Mises, Hill quadratic, Barlat three parameter, and Barlat 1996. They found that Simulations utilizing Barlat's 1996 yield function showed remarkable agreement with all measurements, in contrast to simulations with the other three yield functions.

Many authors investigated the effect of material anisotropy on springback amount. Gomes et al. [71] analyzed the variability of springback of an anisotropic high strength steel, comparing numerical and experimental investigations of a benchmark

U-shape stamping process (NUMISHEET 93). Springback variations comparing the results along rolling direction 0 [°] and along transverse one 90 [°] were considerable: springback increases at the increasing of the angle from the rolling direction. The role of anisotropy on the springback occurrence was also assessed by Ragai et al. [176] They studied stainless steel 410 draw-bend specimens at the varying of blank holder force and noticed differences on springback at 0 [°], 45 [°], and 90 [°] from the rolling direction. In particular, such differences proved that the effect on the process results is different for different restraining forces levels. Verma et al. [225] developed both FE and analytical models to analyze effect of normal anisotropy, concluding that higher anisotropy gives higher springback, so that springback is minimum for an isotropic material. They also analyzed by analytical models the effects of sheet thickness and strain hardening exponent observing that both parameters increase implies a springback lowering.

Another parameter to be considered in springback investigation is Young modulus E . Some researchers have pointed out that most of the metallic materials are characterized by an inelastic recovery behavior after plastic deformation since the elastic modulus decreases with plastic strain [144]. Yu [243] compared the effect of varied elastic modulus and constant elastic modulus on springback. He concluded that Springback angles simulated with varied elastic modulus are larger than those simulated with constant elastic modulus. And the simulated profile for U-channel with varied modulus is closer to the experimental result than that with constant elastic modulus. The effect of inelastic recovery on springback needs to be considered so as to get a more precise springback simulation.

2.5 State-of-the-art of metamodeling techniques for computer based engineering design

Since several thousand evaluations are required for a probabilistic evaluation, the FE model of the sheet metal forming process can not directly be used. There is a need to use an approximation, a metamodel, of the numerical model.

2.5.1 Role of metamodeling in support of engineering design

Metamodels are widely used to replace the actual expensive computer analyses in engineering design optimization. Engineering analyses using complex computer codes supplying a vector of design variables and computing a vector of responses can take many hours to run. Even though the computing power is improved, the expense of running many analysis codes remains significant. To solve such a challenge, approximation or metamodeling techniques are often employed. It has been obvious that metamodeling provides a decision-support role for design engineers. Metamodeling and its role in support of engineering design optimization are shown in Figure 2.13. The supporting functions that metamodeling can provide as follows [232]:

- Model approximation. Approximation of computation-intensive processes

across the entire design space, or global approximation, is used to reduce computation costs.

- Design space exploration. The design space is explored to enhance the engineers' understanding of the design problem by working on a cheap-to-run metamodel.
- Problem formulation. Based on an enhanced understanding of a design optimization problem, the number and search range of design variables may be reduced; certain ineffective constraints may be removed; a single objective optimization problem may be changed to a multi-objective optimization problem or vice versa. Metamodel can assist the formulation of an optimization problem that is easier to solve or more accurate than otherwise.
- Optimization support. Industry has various optimization needs, e.g., global optimization, multi-objective optimization, multidisciplinary design optimization, probabilistic optimization, and so on. Each type of optimization has its own challenges. Metamodeling can be applied and integrated to solve various types of optimization problems that involve computation-intensive functions.

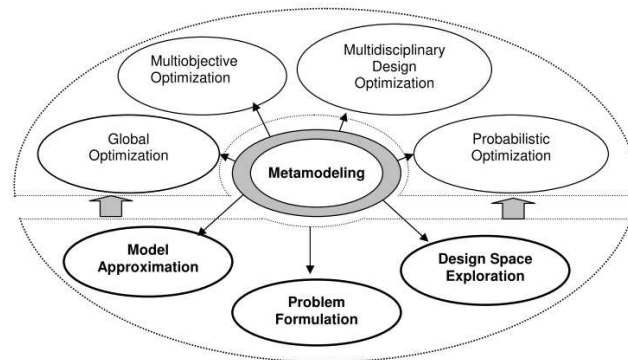


Figure 2.13: Metamodeling and its role in support of engineering design optimization [232].

2.5.2 Metamodeling process

A metamodel is an approximation of the input/output (I/O) transformation that is implied by the simulation model [103]. The principle of metamodeling is presented as in Figure 2.14. This shows that the FE model is an approximation of the physical process and the metamodel is an approximation of the FE model. Due to this "double approximation", there is a risk that the physical process is not well-represented by the metamodel.

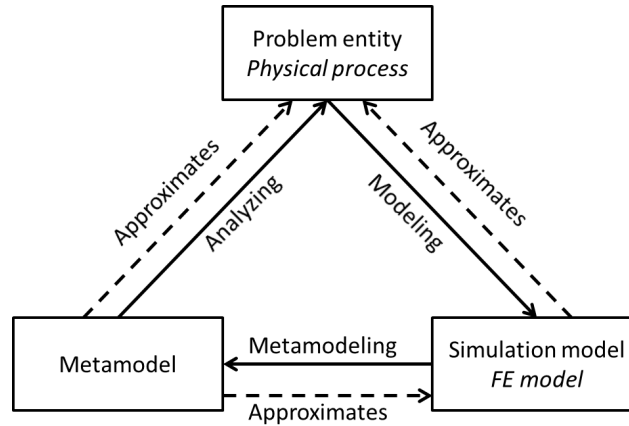


Figure 2.14: Principle of metamodeling [103].

2.5.3 Literature review of metamodeling techniques

Metamodeling is mainly conducted involving three basic steps (a) choosing an experimental design for generating data, (b) choosing a model to represent the data, and then (c) fitting the model to the observed data [200]. The commonly used metamodeling techniques categorized according to sampling, model types and model fitting are shown in Table 2.3 [200].

2.5.3.1 Design of Experiments

In engineering, traditionally a single parameter is varied (perturbed) and the effects are observed. Experimental design techniques which were developed for physical experiments are being applied to the design of computer experiments to increase the efficiency of the analyses. An experimental design represents a sequence of experiments to be performed, expressed in terms of factors (design variables) set at specified levels (predefined values). An experimental design is represented by a matrix X where the rows denote experiment runs, and the columns denote particular factor settings [200]. Classic experimental designs are widely used including factorial or fractional factorial [142], central composite design (CCD) [142], Box-Behnken [142], alphabetical optimal [140] and Plackett-Burman designs [142]. These classic methods tend to spread the sample points around boundaries of the design space and leave a few at the center of the design space. The most basic experimental design is a full factorial design. The number of design points dictated by a full factorial design is the product of the number of levels for each factor. The most common are 2^k (for evaluating main effects and interactions) and 3^k designs (for evaluating main and quadratic effects and interactions) for k factors at 2 and 3 levels, respectively. A 2^3 full factorial design is shown in Figure 2.15 (a).

The size of a full factorial experiment increases exponentially with the number of factors; this leads to an unmanageable number of experiments. Fractional factorial designs are used when experiments are costly, and many factors are required. A

DOE	Classic methods	Space-filling methods	Hybrid methods
	(Fractional) factorial	Space-filling methods	Random or human selection
	Central composite	Simple Grids	Importance sampling
	Box-Behnken	Latin Hypercube	Directional simulation
	Alphabetical optimal	Orthogonal Arrays	Discriminative sampling
	Plackett-Burman	Hammersley sequence	Sequential or adaptive methods
		Uniform designs Minimax and Maximin	
Metamodel Choice	Polynomial (linear, quadratic, or higher)		
	Splines (linear, cubic, NURBS)		
	Multivariate Adaptive Regression Splines (MARS)		
	Gaussian Process		
	Kriging		
	Radial Basis Functions (RBF)		
	Least interpolating polynomials		
	Artificial Neural Network (ANN)		
	Knowledge Base or Decision Tree		
	Support Vector Machine (SVM)		
	Hybrid models		
Model Fitting	(Weighted) Least squares regression		
	Best Linear Unbiased Predictor (BLUP)		
	Best Linear Predictor		
	Log-likelihood		
	Multipoint approximation (MPA)		
	Sequential or adaptive metamodeling		
	Back propagation (for ANN)		
	Entropy (inf.-theoretic, for inductive learning on decision tree)		

Table 2.3: Commonly used metamodeling techniques [200].

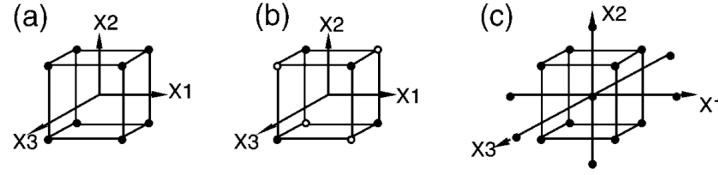


Figure 2.15: Basic three-factor designs. (a) 2^3 full factorial; (b) 2^{3-1} fractional factorial; (c) composite design [200].

fractional factorial design is a fraction of a full factorial design; the most common are $2^{(k-p)}$ designs. A half fraction of the 2^3 full factorial design is shown in Figure 2.15(b). The reduction of the number of design points in a fractional factorial design is not without a price. The 2^3 full factorial design shown in Figure 2.15(a) allows estimation of all main effects (x_1, x_2, x_3) all two factor interactions (x_1x_2, x_1x_3 and x_2x_3), as well as the three factor interaction ($x_1x_2x_3$). For the $2^{(3-1)}$ fractional factorial indicated by the solid dots in Figure 2.15(b), the main effects are aliased (or biased) with the two factor interactions. The most common second order designs, configured to reduce the number of design points, are central composite and Box-Behnken designs. A Central Composite Design (CCD) is a two level ($2^{(k-p)}$ or 2^k) factorial design, augmented by n_c center points and two star points positioned at $\pm\alpha$ for each factor. This design, shown for three factors in Figure 2.15(c) consists of $2^{(k-p)} + 2^k + n_c$ total design points. For three factors, setting $\alpha = 1$ locates the star points on the centers of the faces of the cube, giving a face-centred central composite (CCF) design; note that for values of α other than 1, each factor is evaluated at five levels. Often it is desirable to use the smallest number of factor levels in an experimental design. One common class of such designs is the Box-Behnken designs [19]. These are formed by combining 2^k factorials with incomplete block designs. They do not contain points at the vertices of the hypercube defined by the upper and lower limits for each factor. This is desirable if these extreme points are expensive or impossible to test. Besides CCD, alphabetical optimal designs, especially D-optimal designs, are also widely used [67], [140]. Myers and Montgomery [142] identified the pitfalls of the D-optimality designs, which have only model-dependent D-efficiency and do not address prediction variance. Moreover, for second-order models, the D-criterion often does not allow any (or many) center runs. This often leaves large variance in the design center.

As computer experiments involve mostly systematic error rather than random error as in physical experiments, Sacks et al. [183] stated that in the presence of systematic rather than random error, a good experimental design tends to fill the design space rather than to concentrate on the boundary. They also stated that classic designs, e.g. CCD and D-optimality designs, can be inefficient or even inappropriate for deterministic computer codes. Simpson et al. [89] confirmed that a consensus among researchers was that experimental designs for deterministic computer analyses should be space filling. For sampling deterministic computer experiments, the

use of space-filling designs which treat all regions of the design space equally [195]. Simpson et al. [196] and Palmer [163] also recommend the use of space filling designs in the early stages of design when the form of the metamodel cannot be pre-specified. As discussed by Booker et al. [16], in the 'classical' design and analysis of physical experiments (i.e. using central composite and factorial designs) random variation is accounted for by spreading the sample points out in the design space, and by taking multiple data points (replicates) (see Figure 2.16(a)). Sacks et al. [183] state that the 'classical' notions of experimental blocking, replication and randomization are irrelevant when it comes to deterministic computer experiments; thus, sample points in DACE (Design and Analysis of Computer Experiments also referred to as kriging) should be chosen to fill the design space. They suggest minimising the Integrated Mean Squared Error (IMSE) over the design region by using IMSE-optimal designs; the 'space filling' design illustrated in Figure 2.16(b) is an IMSE optimal design.

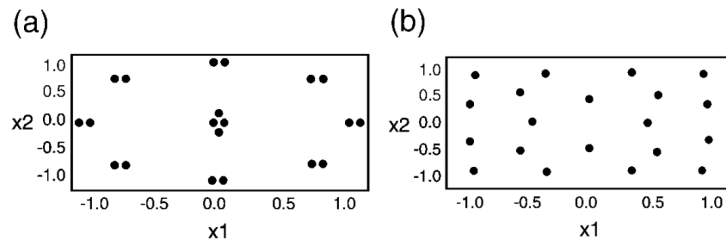


Figure 2.16: (a) "Classical" Design and (b) "Space filling" Design [17].

Koch [108] investigates the use of a modified central composite design which combines half fractions of a CCI and a CCF to more evenly distribute the points throughout the design space. Koehler and Owen [109] described several Bayesian and Frequentist "Space Filling" designs, including maximum entropy design [39], mean squared-error designs, minimax and maximin designs [93], Latin Hypercube designs, randomized orthogonal arrays, and scrambled nets. Minimax and maximin designs were originally proposed by Johnson et al. [93], specifically for use with computer experiments. Sherwy and Wynn [193] and Currin et al. [39] use the maximum entropy principle to develop designs for computer experiments. Tang [213] describes orthogonal array-based Latin hypercubes, which he asserts are more suitable for computer experiments than general Latin hypercubes. Park [167] discusses optimal Latin hypercube designs for computer experiments which either minimize IMSE or maximise entropy, spreading the points out over the design region. Morris and Mitchell [145] propose maximin distance designs found within the class of Latin hypercube arrangements, since they offer a compromise between the entropy/maximin criterion, and good projective properties in each dimension. Owen [160] advocates the use of orthogonal arrays as suitable designs for computer experiments, numerical integration and visualisation; a collection of orthogonal array generators is available over the Internet [159]. A review of Bayesian experimental designs for linear and nonlinear regression models is given in Chaloner and Verdinelle [25]. Hammersley sequences and uniform designs belong to a more general group called low discrep-

any sequences are relatively more often used in the literature [28]. Hammersley sampling is found to provide better uniformity than Latin Hypercube designs. It is found that the Latin Hypercube design is only uniform in 1-D projection while the other methods tend to be more uniform in the entire space. Also found is that the appropriate sample size depends on the complexity of the function to be approximated. In general, more sample points offer more information of the function, however, at a higher expense. For low-order functions, after reaching a certain sample size, increasing the number of sample points does not contribute much to the approximation accuracy. Moreover, when certain optimality criteria are used to generate samples, these optimality criteria such as maximum entropy are concerned with the sample distribution and are independent to the function. While the approximation accuracy depends on whether sample points capture all the features of the function itself. Therefore those optimality criteria are not perfectly consistent with the goal of improving approximation, due to which the additional computational cost of searching for the optimal sample is often not well justified [198].

The Monte Carlo Simulation (MCS) method, which is a random sampling method, is still a popular sampling method in industry, regardless of its inefficiency. It is probably because the adequate and yet efficient sample size at the outset of metamodeling is unknown for any blackbox function. Improved from the Monte Carlo simulation method, the importance sampling (IS) bears the potential of improving its efficiency while maintain the same level of accuracy as MCS [255]. Zou and colleagues developed a method based on an indicator response surface, in which IS was performed in a reduced region around the limit state [255], [254], [106]. Another variation of MCS is directional simulation [48], [230], [155]. A new discriminative sampling method has been developed when the sampling goal was for optimization instead of global metamodeling [235], [234]. With its original inspiration from [62], this sampling method is space filling and reflects the goal of sampling; it is a more aggressive MCS method. Comparatively, these MCS-rooted methods are less structured but offer more flexibility. If any knowledge of the space is available, these methods may be tailored to achieve higher efficiency. They may also play a more active role for iterative sampling-metamodeling processes.

Mainly due to the difficulty of knowing the appropriate sampling size a priori, sequential and adaptive sampling has gained popularity in recent years. Lin [124] proposed a sequential exploratory experiment design (SEED) method to sequentially generate new sample points. Jin et al. [91] applied simulated annealing to quickly generate optimal sampling points. Sasena et al. [187] used the Bayesian method to adaptively identify sample points that gave more information. Wang [231] proposed an inheritable Latin Hypercube design for adaptive metamodeling. Samples are repetitively generated fitting a Kriging model in a reduced space [233]. Jin et al. [90] compared a few different sequential sampling schemes and found that sequential sampling allows engineers to control the sampling process and it is generally more efficient than one-stage sampling. One can custom design flexible sequential sampling schemes for specific design problems.

2.5.3.2 Metamodeling

After the experimental design is appropriately selected and the computer runs are performed, the next step is to choose an approximating model and fitting method. Metamodeling evolves from classical Design of Experiments (DOE) theory, in which polynomial functions are used as response surfaces, or metamodels. Given a response, y , and a vector of independent factors x influencing y , the relationship between y and x is:

$$y = f(x) + \varepsilon \quad (2.15)$$

where ε represents random error which is assumed to be normally distributed with mean zero and standard deviation σ . Since the true response surface function $f(x)$ is usually unknown, a response surface $g(x)$ is created to approximate $f(x)$. Predicted values are then obtained using $\hat{y} = g(x)$. The most widely used response surface approximating functions are low-order polynomials. For low curvature, a first order polynomial can be used as in Equation 2.16; for significant curvature, a second order polynomial which includes all two-factor interactions is available as represented in Equation 2.17:

$$\hat{y} = \beta_0 + \sum_{i=1}^k \beta_i x_i \quad (2.16)$$

$$\hat{y} = \beta_0 + \sum_{i=1}^k \beta_i x_i + \sum_{ii} x_i^2 + \sum_{i=1}^k \sum_{j=1, i < j}^k \beta_{ij} x_i x_j \quad (2.17)$$

The parameters of the polynomials in Equations 2.16 and 2.17 are usually determined by least squares regression analysis by fitting the response surface approximations to existing data. These approximations are normally used for prediction within Response Surface Methodology (RSM). RSM was first developed by Box and Wilson [20]. A more complete discussion of response surfaces and least squares fitting is presented in Myers and Montgomery [142].

Besides the commonly used polynomial functions, Sacks et al. [183], [182] proposed the use of a stochastic model, called Kriging [38], to treat the deterministic computer response as a realization of a random function with respect to the actual system response. Neural networks have also been applied in generating the response surfaces for system approximation [164]. Other types of models include Radial Basis Functions (RBF) [52],[57], Multivariate Adaptive Regression Splines (MARS) [61], Least Interpolating Polynomials [41], and inductive learning [111]. A combination of polynomial functions and artificial neural networks has also been archived in [224]. So far there is no conclusion about which model is definitely superior to the others. Among various models, Kriging and second-order polynomials are the most intensively studied.

In general the Kriging models are more accurate for nonlinear problems but difficult to obtain and use because a global optimization process is applied to identify the maximum likelihood estimators. Kriging is also flexible in either interpolating the sample points or filtering noisy data. On the contrary, a polynomial model is

2.6. Identification of sensitivity threshold of a FEM numerical model 33

easy to construct, clear on parameter sensitivity, and cheap to work with but is less accurate than the Kriging model [89]. However, polynomial functions do not interpolate the sample points and are limited by the chosen function type.

Recently, a new model called Support Vector Regression (SVR) was used and tested [36]. SVR achieved high accuracy over all other metamodeling techniques including Kriging, polynomial, MARS, and RBF over a large number of test problems. It is not clear, however, what are the fundamental reasons that SVR outperforms others. The Least Interpolating Polynomials use polynomial basis functions and also interpolate responses. They choose a polynomial basis function of "minimal degree" as described by [41] and hence are called "least interpolating polynomials". This type of metamodel deserves more study. In addition, Pérez et al. [168] transformed the matrix of second-order terms of a quadratic polynomial model into the canonical form to reduce the number of terms. Messac and his team developed an extended RBF model [146] by adding extra terms to a regular RBF model to increase its flexibility, based on which an optimal model could be searched for. It is claimed that this extended RBF applies to almost all problems.

Each metamodel type has its associated fitting method. For example, polynomial functions are usually fitted with the (weighted) least square method; the kriging method is fitted with the search for the Best Linear Unbiased Predictor (BLUP). Building a neural network involves fitting a network of neurons by means of back-propagation to data which is typically hand selected.

It can be concluded that there are many metamodeling methods to use as a surrogate model for FEM simulations. However, it depends on the accuracy of metamodels which is used to fit given data. Comparing the accuracy between metamodels needs to carry out. The metamodel which has the best accuracy is chosen. In addition, the confidence of results obtained from FEM numerical simulations is very important. The subsequent section will discuss a novel approach to detect the sensitivity threshold of FEM numerical models.

2.6 Identification of sensitivity threshold of a FEM numerical model

2.6.1 Problem statement

Recently, much research has exploited FEM simulation-based computer experiments with DOE methods to design engineering system in the presence of uncertainty. Marreta and Lorenzo [131] used the integration of central composite design (CCD) in which the experiments are placed in the design variables hypercube, FEM numerical simulation and Monte Carlo to evaluate the influence of material properties variability on springback and thinning in sheet metal stamping processes. Chen and Koç [27] adopted the DOE of Box-Behnken RSM with random number generation combined with FE analysis to identify the effects of BHF, material and friction on springback variation of DP steel channel. Computer experiments based on the

Box-Behnken method are placed in the design variables hypercube as in the center of each edge and in the center of the hypercube. Jansson et al. [88] applied D-optimality criterion (DOPT) in which it uses a Genetic Algorithm to filter the set of current designs and mark a D-optimal subset, as the DOE with FE model to assess reliability of a sheet metal forming process using the Monte Carlo analysis and metamodels. Central composite design was utilized to create input data for FE numerical simulation of sheet metal stamping process for searching optimal stamping tools configuration, punch travel and blank holder force (BHF) in research work of Ledoux et al. [113]. To design sheet metal forming process in the presence of uncertainties, Zhang [249] adopted a DOE of Box-Behnken method, FEM model of sheet metal forming process and probabilistic design approach to execute uncertainty propagation. Souza and Rolfe [42] considered the inherent variability in material, sheet thickness and process conditions in sheet metal forming by using the full factorial DOE, FEM simulation and multivariate probabilistic models. In order to have robust design, Aspenberg and Kini also used the combination of the DOE, FEM deterministic numerical simulation, surrogate model and Monte Carlo analysis in the design of automotive body and production systems [10], [101].

However, these FEM numerical simulation-based computer experiments lack a step to qualify the FEM models before building the DOE as shown in Figure 2.17. The computer experiments show that FEM numerical simulation has finite precision due to errors introduced by the numerical solution methods used (resolution of meshing, contact/friction, discretization error, approximation error, convergence problems, etc) [204]. Therefore, a method which determine the input parameters' tolerance range at which FEM numerical models can give confident results is required.

2.6.2 Sensitivity in FEM analysis: illustrating sensitivity threshold

The notion of sensitivity threshold in this research work derives from the observation of the responses of FEM numerical simulations which show unconfident results. Sensitivity threshold is understood to be a threshold at which a response of FE numerical model is chaotic to very small variation of an input parameter.

2.6.2.1 Illustration on a simple FE numerical beam bending model in 1D

To illustrate this sensitivity threshold of FEM numerical simulation, consider a linear elastic (E) cantilever beam shown in Figure 2.18 subjected to a point load (F) at its free end and with the solution of the deflection of the free end Δ [88]:

$$\Delta = \frac{12FL^3}{3Ea^4} \quad (2.18)$$

The values of the variables in the beam bending application are given in Table 2.4. The side length of the beam considered as an input variable which is changed from $\pm 5\%$ down to $\pm 10^{-8}\%$ around its nominal value. The reason why step variation of

2.6. Identification of sensitivity threshold of a FEM numerical model35

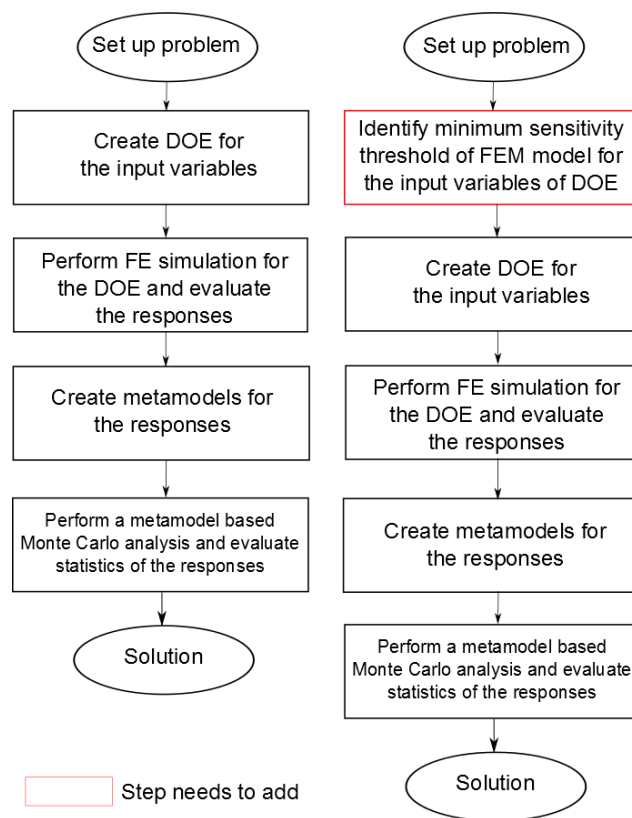


Figure 2.17: A typical FEM simulation-based uncertainty propagation approach.

input parameter in percent is that percentage can express any quantity with any unit as well as any scale.

Table 2.4: Beam bending data

Force F [N]	Young's modulus E [GPa]	Beam length L [mm]	Side length a [mm]
1000	210	100	10

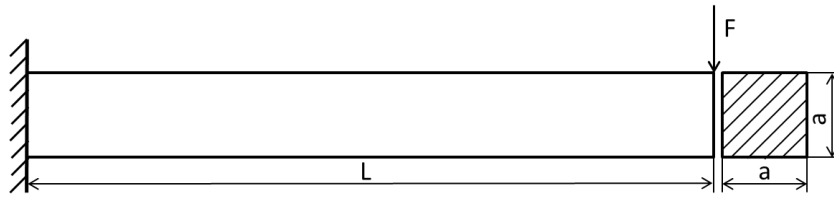


Figure 2.18: Cantilever beam problem.

Modeling and simulation of beam bending are carried out in 1D in Abaqus/Standard. Euler-Bernoulli beam element is used to model the beam. Comparison of deflection calculated by analytic formula (2.18) and FE numerical analysis in 1D is shown in Figure 2.19.

It can be seen from Figure 2.19 that once the side length varies around its nominal values from -5% to $+5\%$, the response calculated by the analytic formula (2.18) and that of FE numerical analysis in 1D are coincident. The responses are smooth and sharp. However, when zooming in the local zone of $\pm 0.02\%$ around the nominal value of 10 [mm], the responses calculated by the FE numerical analysis in 1D with different element sizes have leaps corresponding to the side length values of $10 \pm 0.01\%$. While the analytic formula of the deflection gives a smooth and sharp response. Even this problem is also observed when the element size decreases. This shows finite precision of FE numerical simulation.

2.6.3 Elaboration of numerical model of sheet metal draw bending

Prior to illustrating the sensitivity threshold on a complex application of sheet metal forming process, benchmark problem description and modeling are presented.

2.6.3.1 Benchmark problem of draw bending process

A case study investigated in this paper is a benchmark problem of Numisheet 2011 International conference [75]. The main problem of this benchmark which needs to take into account is to evaluate the springback behavior of advanced high strength steels such as DP780 steel. A schematic view of die, punch, blank and their dimensions for the draw bending process is shown in Figure 2.20.

2.6. Identification of sensitivity threshold of a FEM numerical model³⁷

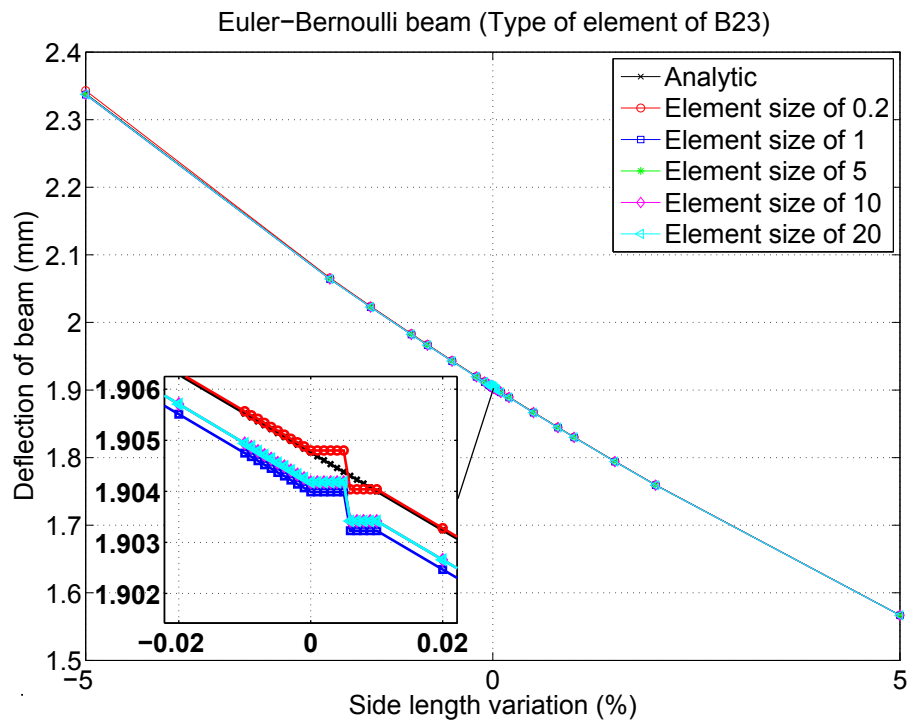


Figure 2.19: Comparison of deflection calculated by analytic formula and FE numerical analysis in 1D with different element sizes enlarged.

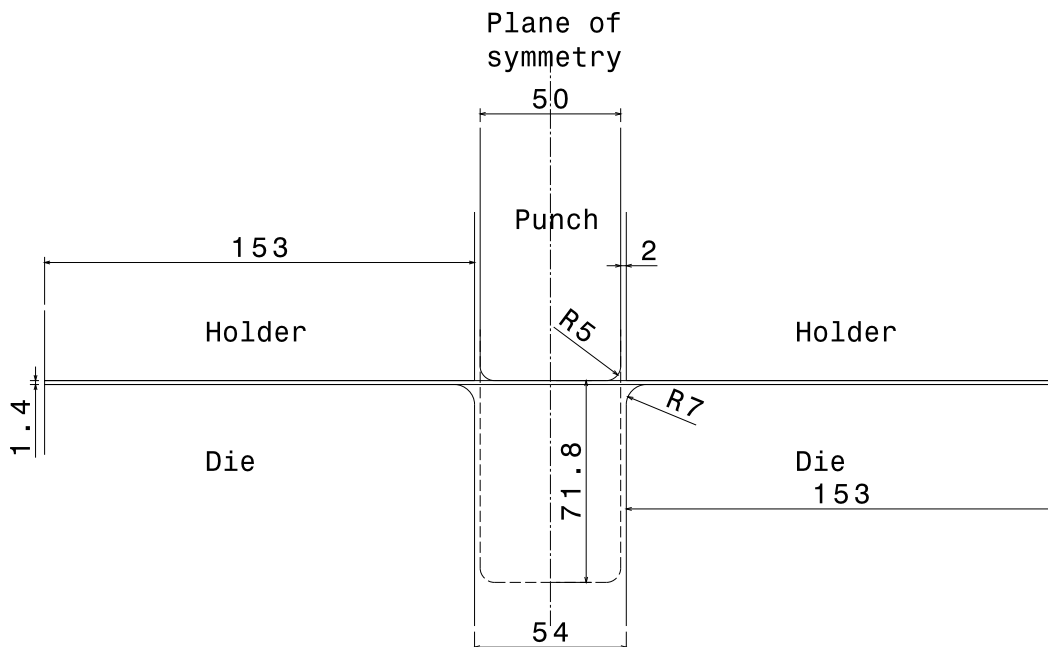


Figure 2.20: A schematic view of tools and dimensions for the open-channel.

The blank is obtained from DP780 steel sheet of 1.4 mm thick, 360 mm long and 30 mm wide. Details on material properties are shown in Table 2.1 and Table 2.5.

With respect to machine and tooling specifications, blank holding force of 2.94 KN is maintained by the blank holder. For lubrication, P-340N is applied on the tool surfaces and the blank. The punch speed is 1 mm/s and the punch stroke is 71.8 mm after initial contact between the punch and the blank.

Table 2.5: Material constant for yield function Hill 48 [75].

Sample	F	G	H	L	M	N
DP780	0.4640	0.5615	0.4385	1.5000	1.5000	1.5926

2.6.3.2 Springback and side wall curl determination

In order to represent shape defect due to the springback, three measurements including the springback of wall opening angle β_1 , the springback of flange angle β_2 and sidewall curl radius ρ are shown in Figure 2.21. They describe the variation of the part's cross-sectional shape obtained before and after removing the tools. The springback in the direction orthogonal to the cross-section is not considered in this case.

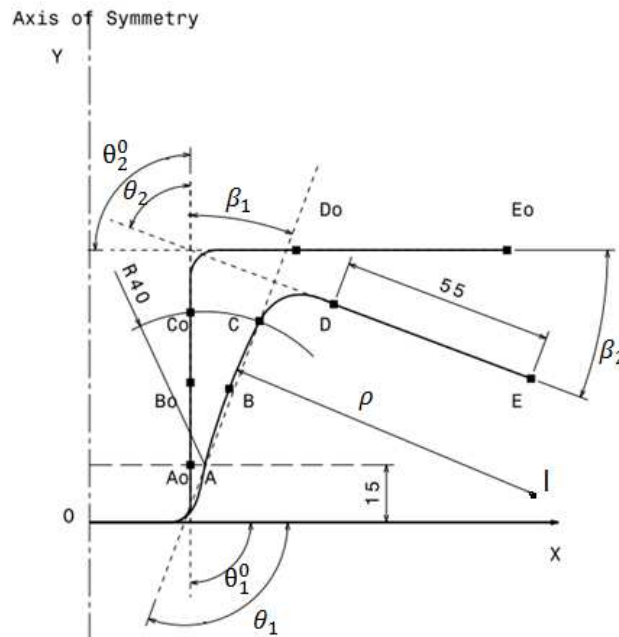


Figure 2.21: A schematic view of springback profile and parameters proposed by Numisheet 2011.

For calculating the springback parameters, it is necessary to determine the measurements before and after springback. To do so, the least square method is applied

2.6. Identification of sensitivity threshold of a FEM numerical model 39

to identify the points of Ao, Bo, Co, Do and Eo on the formed part's profile according to given x and y coordinates. Based on the known point coordinates, the wall angle (θ_1^0) and the flange angle (θ_2^0) before springback are computed. Similarly, other points of A, B, C, D and E are defined on the part's profile which the tools have been removed. They are then used to calculate the wall angle (θ_1) and the flange angle (θ_2) after springback. The side wall curl radius is estimated by a curve fitting technique through three points A, B and C to construct a circular arc.

The equations for calculating the springback and the side wall curl radius are presented in Appendix A.1 .

2.6.3.3 Numerical modeling of draw bending process

FEM modeling

Observations from experimental measurements have shown that the part profiles remains symmetric during the manufacturing process [75], so only half of the draw bending model in 3D is illustrated as in Figure 2.22. Thus, the blank sheet is discretized by 2709 elements with element size of 1.4 mm. Also, the blank sheet is modeled by using one layer of four nodes shell element (4-node doubly curved shell, reduced integration, hourglass control and finite membrane strains). The blank thickness is modeled by 7 integration points through thickness with Simpson's rule. The punch, die and blank holder are modeled as analytical rigid surfaces. Boundary conditions applied on the tools are shown in Figure 2.22. Displacement of punch and blank holder is translation along axis Z, the remaining degrees of freedom (DOF) are blocked. The die is blocked all the DOF. Symmetrical boundary condition is applied on the half of the part profile in which the translation along axis X, rotation around axis Y and Z are blocked. The blank holder force remains constant during the draw bending process.

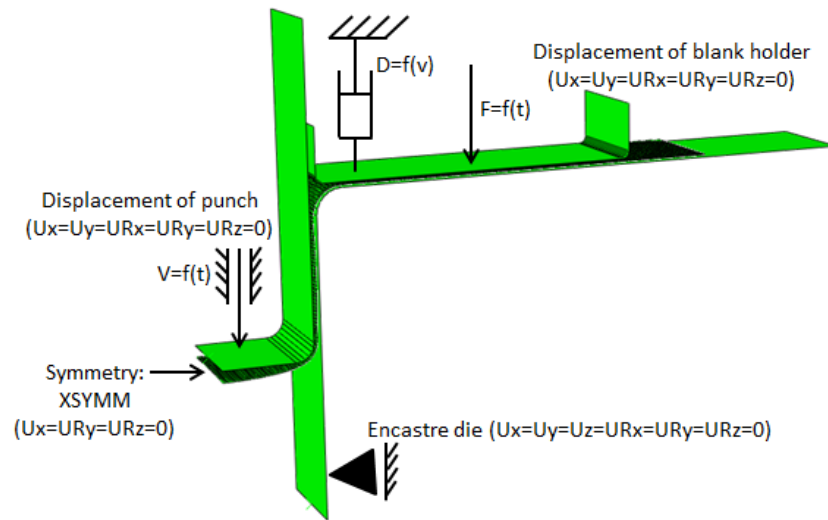


Figure 2.22: A schematic modeling of draw bending process.

For contact interaction, contact constraint enforcement method for modeling sheet metal forming operation is penalty contact enforcement in which type of contact of surface-to-surface is applied between blank surface and tools' surfaces. The pure master-slave contact pair is used with tools' surfaces being assigned as master surfaces while blank's surface being considered as slave surface. Friction formulation used between the blank and the tools is basic Coulomb friction model. In the basic form of the Coulomb friction model, two contacting surfaces can carry shear stresses up to a certain magnitude across their interface before they start sliding relative to one another. The Coulomb friction model is defined:

$$\tau_{crit} = \mu p \quad (2.19)$$

where τ_{crit} is critical shear stress at which sliding of the surfaces starts as a fraction of the contact pressure p between the surfaces; the fraction μ is known as the coefficient of friction.

Constitutive modeling

The relationship between the yield stress and the plastic strain for the material used in this case study follows the Swift law [207]:

$$\bar{\sigma} = K (\varepsilon_0 + \bar{\varepsilon}_p)^n \quad (2.20)$$

where ε_0 is a pre-strain or offset strain constant; ε_p is effective plastic strain; K and n are strain hardening coefficients. Where

$$\bar{\varepsilon}_p = \int_0^t \bar{\varepsilon}_p dt \quad (2.21)$$

The anisotropic characteristics of the sheet metal are described according to the quadratic Hill yield criterion [78] has the form:

$$\sigma_{11}^2 + \frac{R_0(1 + R_{90})}{R_{90}(1 + R_0)} \sigma_{22}^2 - \frac{2R_0}{1 + R_0} \sigma_{11} \sigma_{22} + \frac{(1 + 2R_{45})(R_0 + R_{90})}{R_{90}(1 + R_0)} \sigma_{12}^2 - \bar{\sigma}^2 = 0 \quad (2.22)$$

where R_0 , R_{45} , and R_{90} are Lankford's coefficients for describing the material anisotropy; σ_{11} , σ_{22} , and σ_{12} are stress components.

Modeling and numerical simulation of draw bending process are carried out by Finite Element Method using the ABAQUS® software. Process simulations are executed through two different steps. The first step is to simulate forming operation via dynamic explicit procedure. Simulation of springback behavior is performed in the second step through static implicit procedure. The details of two procedures are dicussed in Appendix A.2.

2.6. Identification of sensitivity threshold of a FEM numerical model 41

2.6.3.4 Discussion on different results between Abaqus versions

The values of springback parameters obtained from FEM simulations with three versions of Abaqus (6.9-1, 6.11-2 and 6.12-2) are different despite using the same input file. A comparison of springback results obtained by using three different versions of Abaqus is shown in Table 2.6. It shows that there is uncertainty between Abaqus versions.

Table 2.6: A comparison of springback results obtained by using three different versions of Abaqus.

Parameters	Values	Abaqus version	β_1 [°]	β_2 [°]	ρ [mm]
F_{BHF} [kN]	38.235	6.9-1	-7.8796	-9.4804	186.895
R_d [mm]	2				
R_p [mm]	2	6.11-2	-7.9531	-9.2680	187.725
R_e [MPa]	550				
R_m [MPa]	840				
μ	0.13	6.12-2	-8.0313	-9.3651	189.42
t [mm]	1.5				

2.6.3.5 Sensitivity threshold in FEM numerical simulation of sheet metal draw bending

Sensitivity threshold analysis of FEM numerical simulation in sheet metal draw bending is executed as illustrated in Figure 2.23. The input data used in numerical

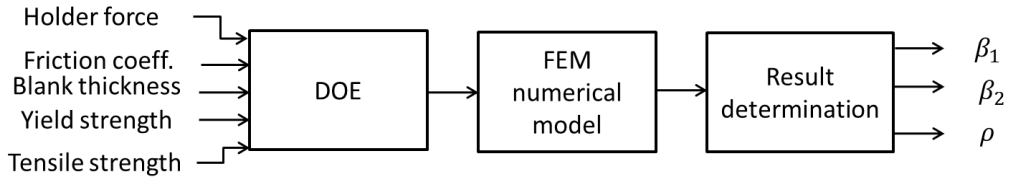


Figure 2.23: Sensitivity threshold analysis of FEM numerical simulation in sheet metal draw bending.

model of draw bending for comparison with experimental result is shown in Table 2.7. In order to be able to take into account the sensitivity threshold when having the variation of material properties, it is essential to transform the yield strength R_e , tensile strength R_m and uniform elongation E_u into the coefficients of Swift's model encompassing K , n , and ε_0 .

The pre-strain ε_0 is defined as:

$$\varepsilon_0 = \frac{R_e}{E} \quad (2.23)$$

where E is Young's modulus of material.

The maximum uniform strain ε_u is defined as:

$$\varepsilon_u = \ln \left(1 + \frac{E_u}{100} \right) \quad (2.24)$$

The true yield strength and true tensile strength are calculated as follows:

$$R_e^{true} = R_e(1 + \varepsilon_0) \quad (2.25)$$

$$R_m^{true} = R_m(1 + \varepsilon_u) \quad (2.26)$$

The strain-hardening index n and the strength coefficient K are defined as:

$$n = \frac{\ln R_m^{true} - \ln R_e^{true}}{\ln(\varepsilon_0 + \varepsilon_u) - \ln \varepsilon_0} \quad (2.27)$$

$$K = \frac{R_m^{true}}{(\varepsilon_0 + \varepsilon_u)^n} \quad (2.28)$$

Table 2.8 shows a comparison between experimental results provided by Numisheet 2011 [75] and our numerical results. Figure 2.24 shows the true stress-strain curve of DP780 steel which is fitted by the Swift law with different values of R_e and R_m .

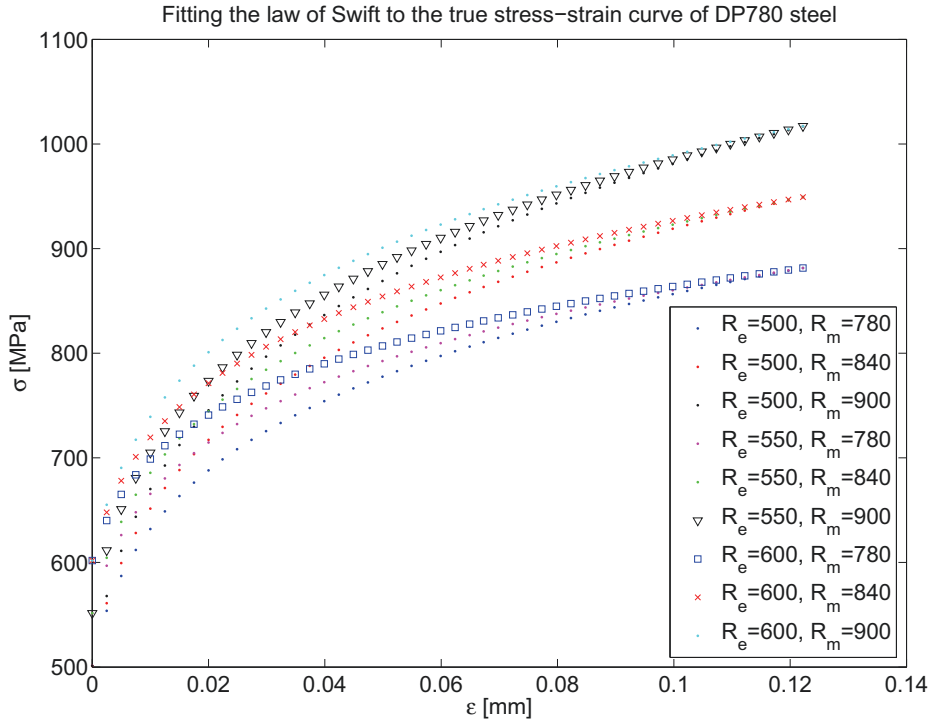


Figure 2.24: Representation of Swift's law with different values of R_e and R_m .

On the other hand, in order to analyze the sensitivity threshold of FEM numerical model, the nominal values of input parameters of draw bending are given as

2.6. Identification of sensitivity threshold of a FEM numerical model 43

Table 2.7: Input data for comparison with experimental results of Numisheet 2011.

Input parameters	
Blank thickness [mm]	1.4
Yield strength [MPa]	527
Tensile strength [MPa]	831.5
Friction coefficient	0.1
Blank holder force [N]	2940
Die radius [mm]	7
Punch radius [mm]	5

Table 2.8: Numerical and experimental comparison of Numisheet 2011.

Springback parameters	θ_1 [°]	θ_2 [°]	ρ [mm]
Numerical results	108.32	75.228	137.02
Experimental results	110.62-118.3425	77.61-80	118.36-120
[75]			

Table 2.9: Nominal values of input parameters for sensitivity threshold analysis

Input parameters	
Blank thickness [mm]	1.4
Yield strength [MPa]	550
Tensile strength [MPa]	840
Friction coefficient	0.1
Blank holder force [N]	2940
Die radius [mm]	7
Punch radius [mm]	5

Table 2.10: Output parameters

Springback parameters	θ_1 [°]	θ_2 [°]	ρ [mm]
Before springback	90.2001	90.1709	N/A
After springback	108.674	75.1115	135.048

shown in Table 2.9. As a result, springback measurements obtained from numerical results are shown in Table 2.10.

Consider springback responses of β_1 , β_2 and ρ with respect to blank thickness variation $\pm 5\%$ to $\pm 0.01\%$ around the nominal value from 1.1 [mm] to 1.6 [mm] as shown in Figure 2.25, 2.26, 2.27.

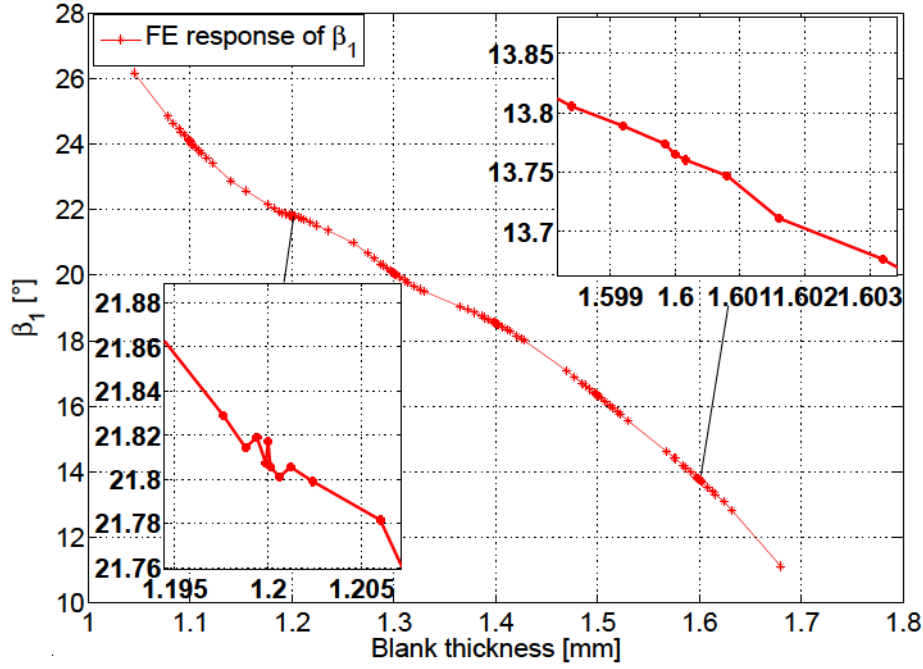


Figure 2.25: Evolution of blank thickness with respect to the wall opening angle β_1 .

Preliminarily, it can be seen that the springback responses are smooth, sharp and shows clear trend in the global variation range from 1.1 [mm] to 1.6 [mm]. The responses of β_1 and β_2 gradually decrease with increasing blank thickness. While the response of ρ increases when the blank thickness augments.

Nevertheless, it is found that there are noises on the springback responses in the local variation range around nominal values of blank thickness. To illustrate for this, consider the springback responses with respect to blank thickness of 1.2 [mm] and 1.6 [mm] in which thickness values are decreasingly varied from $\pm 5\%$ to $\pm 0.01\%$ around their nominal values. When zooming in the local zone around the nominal value of 1.2 [mm] and 1.6 [mm], observation shows that it appears the noises on the springback responses. The closer to nominal value the thickness values are, the more significant the amplitude of noises is. As a consequence, it makes the results inaccurate. Similar problem is also observed on the springback responses with respect to the other nominal values.

From these results, it is worth noting here that there is indeed a sensitivity threshold below which the variations around a nominal value are not correctly prop-

2.6. Identification of sensitivity threshold of a FEM numerical model45

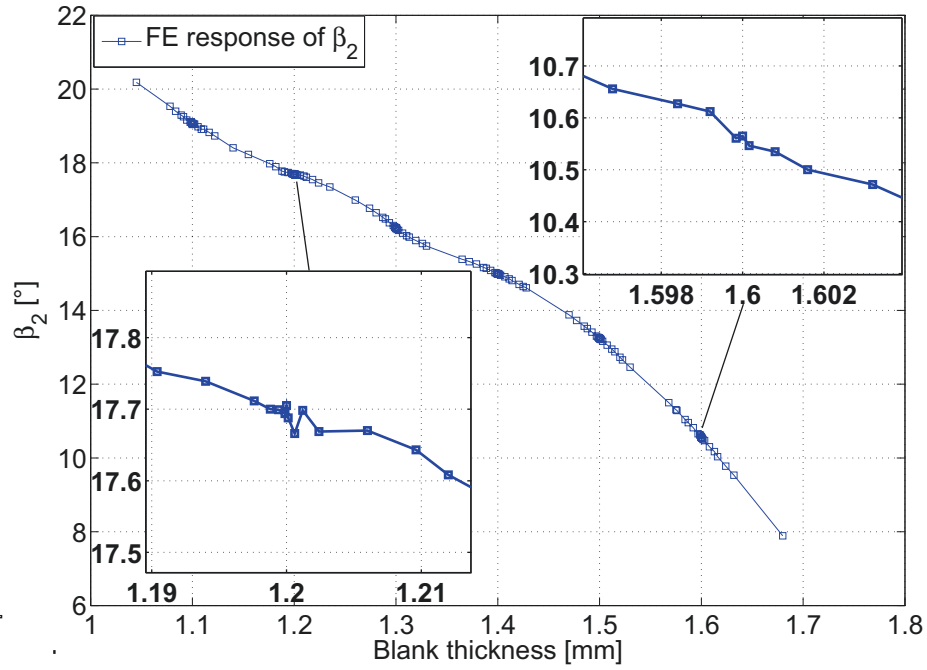


Figure 2.26: Evolution of blank thickness with respect to the flange angle β_2 .

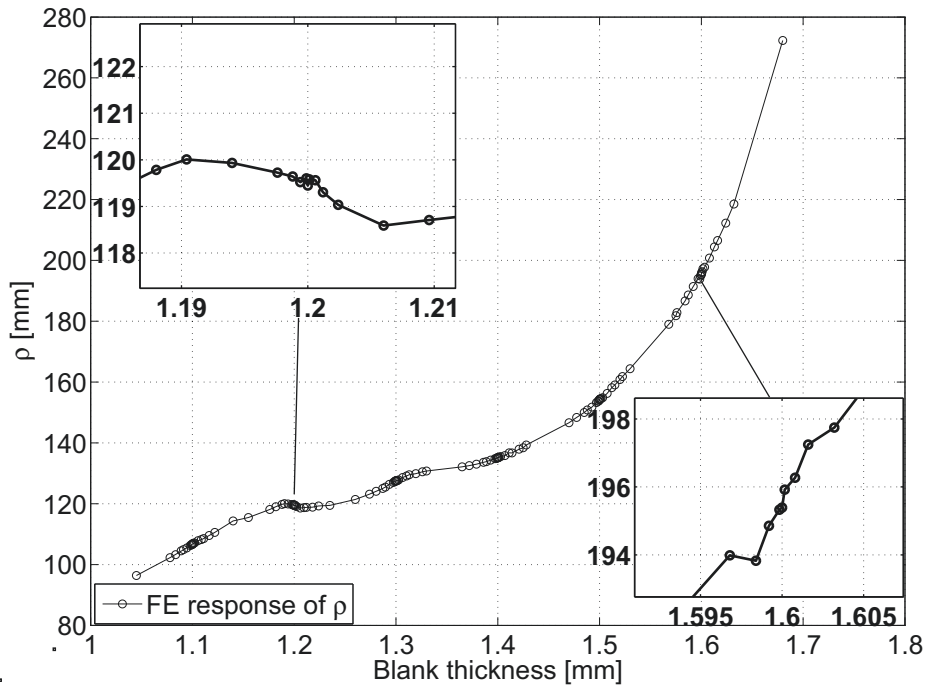


Figure 2.27: Evolution of blank thickness with respect to the side wall curl ρ .

agated by the numerical model.

2.7 Finite Difference Method (FDM)-based sensitivity threshold identification of FEM numerical simulation

2.7.1 Sensitivity analysis method

Sensitivity analysis is of fundamental importance to design based on computational approaches. Sensitivity analysis consists in computing derivatives of one or more quantities (outputs) with respect to one or several independent variables (inputs). It allows the use of gradient descent methods, reveals when optimal designs have been produced and indicates which variables are of most importance at any stage in the design process [99].

Finite-difference formulae are very commonly used to estimate sensitivities. Finite-difference approximations for a derivative are derived by truncating a Taylor series expansion of the function $y = f(x)$ about a point x . To outline the derivation of finite-difference approximations, consider the Taylor series expansion of a scalar function $f(x + h)$

$$f(x + h) = f(x) + h \frac{df}{dx} + \frac{h^2}{2!} \frac{d^2f}{dx^2} + \frac{h^3}{3!} \frac{d^3f}{dx^3} + \dots \quad (2.29)$$

The forward finite-difference approximation for the first derivative can then be obtained by solving the preceding equation for $\frac{df}{dx}$, which gives

$$\frac{df}{dx} \approx \frac{f(x + h) - f(x)}{h} + O(h) \quad (2.30)$$

where h is called the finite-difference interval. The truncation error is $O(h)$, and hence this is a first-order approximation. To reduce the truncation error, an additional set of equations can be attained by writing down the Taylor series expansion of $f(x - h)$ as follows:

$$f(x - h) = f(x) - h \frac{df}{dx} + \frac{h^2}{2!} \frac{d^2f}{dx^2} - \frac{h^3}{3!} \frac{d^3f}{dx^3} + \dots \quad (2.31)$$

The backward finite-difference approximation for the first derivative can then be obtained by solving the preceding equation for $\frac{df}{dx}$, which gives

$$\frac{df}{dx} \approx \frac{f(x) - f(x - h)}{h} + O(h) \quad (2.32)$$

Subtracting Equation (2.31) from Equation (2.29) and solving for $\frac{df}{dx}$ gives the following central difference approximation

$$\frac{df}{dx} = \frac{f(x + h) - f(x - h)}{2h} + O(h^2) \quad (2.33)$$

It can be seen that the central difference scheme is second-order accurate since the truncation error is $O(h^2)$. It is similarly possible to construct higher-order finite-difference formulae. Finite-difference approximations for the higher-order derivatives can be derived by nesting lower-order formulae. For example, the central difference approximation in Equation (2.33) can be used to estimate the second-order derivative as follows:

$$\frac{d^2 f}{dx^2} = \frac{df(x+h)/dx - df(x-h)/dx}{2h} + O(h^2) \quad (2.34)$$

Substituting central difference approximations for $df(x-h)/dx$ and $df(x+h)/dx$ into the preceding equation gives

$$\frac{d^2 f}{dx^2} = \frac{f(x+2h) - 2f(x) + f(x-2h)}{4h^2} + O(h^2) \quad (2.35)$$

In theory, one can use an arbitrarily small step-size h without any significant loss of accuracy [99]. Consequently, when estimating sensitivities of an analytic function using finite-difference formulae, the finite-difference approximations are different at large step sizes and converge with decreasing step size. In particular, as depicted in Figure 2.28 the first-order forward, backward and central difference approximation converge at the same limit as the step size h approaches asymptotically zero.

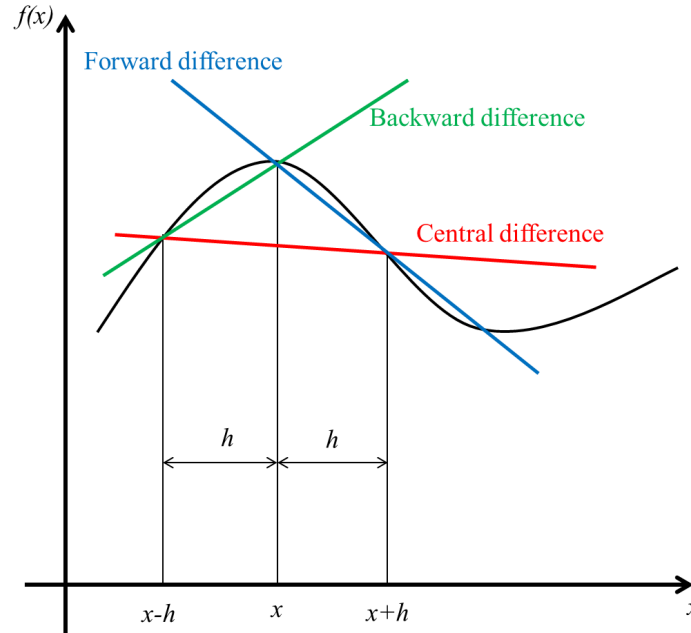


Figure 2.28: Different geometric interpretations of the first-order finite difference approximation related to forward, backward and central difference approximation.

In practice, however, because of finite precision arithmetic (round-off errors), the accuracy of the approximations critically depends on the step size h . Therefore,

when estimating sensitivities of an analytic function using finite-difference formulae, we are faced with the step-size dilemma, that is the desire to choose a small step size to minimize truncation error while avoiding the use of a step so small that errors due to subtractive cancellation become dominant [99]. More specifically, the subtractive cancellation errors arises because of the term $f(x + h) - f(x)$ in the numerator of forward finite differences. It is difficult to accurately evaluate the difference between two terms that are similar in magnitude using finite precision arithmetic, particularly for small values of h .

2.7.2 Illustration of analytic function

To illustrate the influence of the step size in the finite-difference method on the sensitivity estimation, consider the following analytic function [133]:

$$f(x) = \frac{e^x}{\sqrt{\sin^3 x + \cos^3 x}} \quad (2.36)$$

The variation of nominal value of $x = 1.5$ in percentage is decreasingly varied from 10% down to $10^{-13}\%$. Calculation is performed by Matlab.

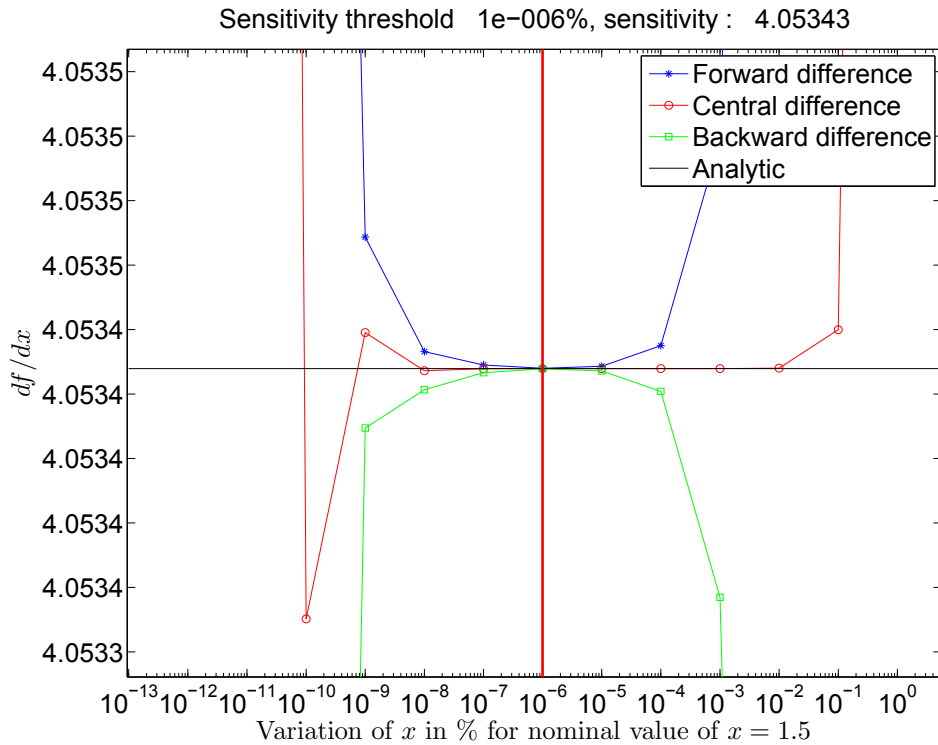


Figure 2.29: Sensitivity of $f(x)$ at $x = 1.5$ using the finite difference approximations.

As can be seen from Figure 2.29, the first-order forward, backward, central difference approximations have large differences at the greater variation step sizes on the right side and then asymptotically converge at the smaller step size in the

middle. More specifically, they asymptotically converge at the variation size of $10^{-6}\%$ which is marked by a vertical line in red. However, as the variation size is reduced below a value of $10^{-7}\%$, subtractive cancellation errors become significant at which the derivatives diverge and as a consequence, the estimates are unreliable. When the variation step h is so small that no difference exists in the numerator of finite difference approximations (for steps smaller than 10^{-16}), the finite-difference estimates yields zero. This results from finite precision of numerical tools.

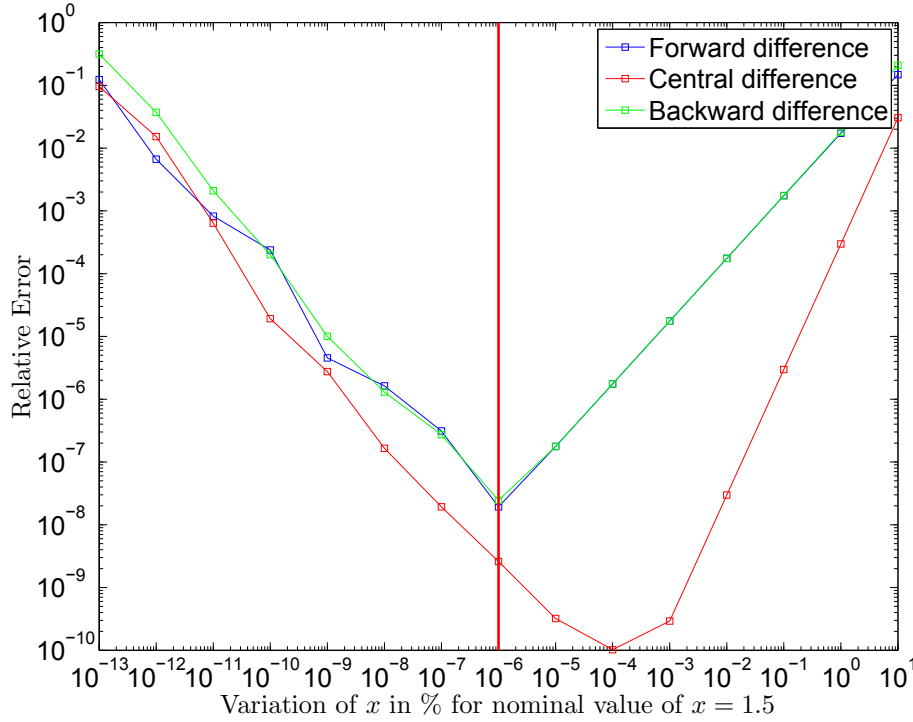


Figure 2.30: Comparison of ε relative error in the first derivative computed using FDM with respect to analytical derivative.

Relative error in the sensitivity estimates given by finite-difference method with the analytic result as the reference $\varepsilon = \frac{|f'(x) - f'(x)_{ref}|}{|f'(x)_{ref}|}$ [133]. Figure 2.30 shows the dependence on the step size h of the accuracy of the derivative approximations for the forward finite difference, central difference and the backward difference. It can clearly be seen that as the step size is reduced, the accuracy of the finite-difference approximations degrades significantly because of subtractive cancellation errors. In particular, when the variation step size is less than or equal to $10^{-6}\%$, the relative error in the derivative approximations increases substantially. Beyond that, once the variation of x is too small to have the difference in the output, smaller than $10^{-16}\%$, the finite-difference estimates eventually yields zero and then relative error $\varepsilon = 1$.

It is concluded that the Matlab can give confident results when the variation step size is larger than or equal to $10^{-6}\%$. In other words, the minimum sensitivity threshold of the Matlab in this case study reaches to the variation step size of $10^{-6}\%$.

2.7.3 Illustration of FE numerical beam bending model in 1D

Sensitivity threshold analysis by FDM of the FE numerical beam bending model in 1D is shown in Figure 2.31. In particular, the sensitivity threshold analysis of

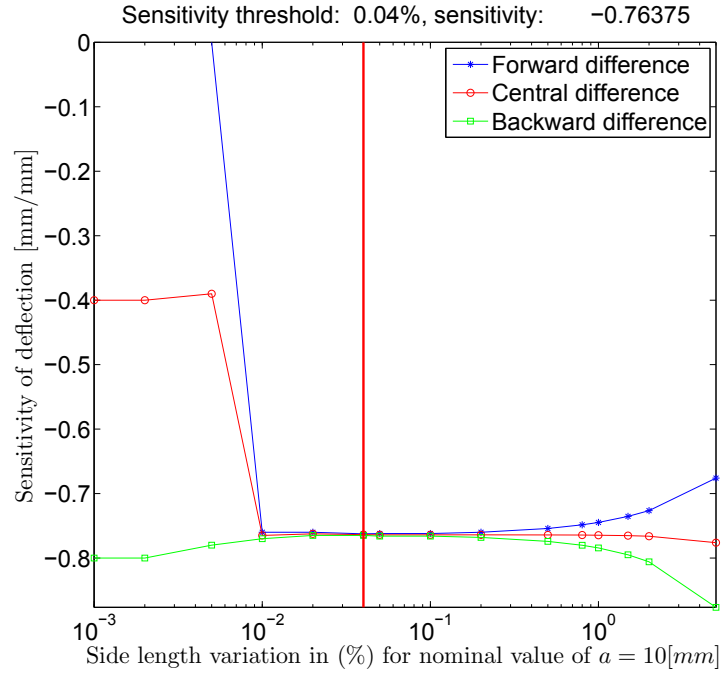


Figure 2.31: Sensitivity threshold of FE numerical beam bending model in 1D with element size of 0.2.

FEM numerical simulation when having the cross-sectional side length variation of the beam is calculated as follows:

The variation step h of side length determined from the variation percentages of nominal value is defined as:

$$h = \frac{\delta_j^{percent} \times Val_{Nom}}{100} \quad (2.37)$$

where $\delta_j^{percent}$ is the j th side length variation in percentage and Val_{Nom} is the nominal value of side length ($a = 10$ [mm])

The forward finite-difference approximation is calculated as follows:

$$\frac{df}{da} = \frac{f(\Delta + h) - f(\Delta)}{h} \quad (2.38)$$

where $f(\Delta)$ is the deflection value of the free end of the beam at $a = 10$ [mm] and $f(\Delta + h)$ is the deflection value of the free end of the beam at $a = 10 + h$ [mm].

The backward finite-difference approximation is determined as:

$$\frac{df}{da} = \frac{f(\Delta) - f(\Delta - h)}{h} \quad (2.39)$$

where $f(\Delta - h)$ is the deflection value of the free end of the beam at $a = 10 - h$ [mm].

The central finite-difference approximation is defined as:

$$\frac{df}{da} = \frac{f(\Delta + h) - f(\Delta - h)}{2h} \quad (2.40)$$

It is found that initially the first-order forward, central and backward finite-difference approximations have large difference at the variation step size of 5% and asymptotically converges at the variation step size of 0.04%. Below this point, the approximations diverges at the smaller variation step sizes. It can be claimed that the minimum sensitivity threshold of the FE numerical beam bending model in 1D reaches to the variation step size of 0.04% corresponding to the side length $a = 10 \pm 0.004$ [mm].

On another hand, the relative error in the estimates using FDM with respect to theoretical result is calculated and represented in Figure 2.32. It is found that the minimum sensitivity threshold of the FE numerical beam bending model corresponds to minimum difference between the relative errors in the estimates by FDM with respect to theoretical result.

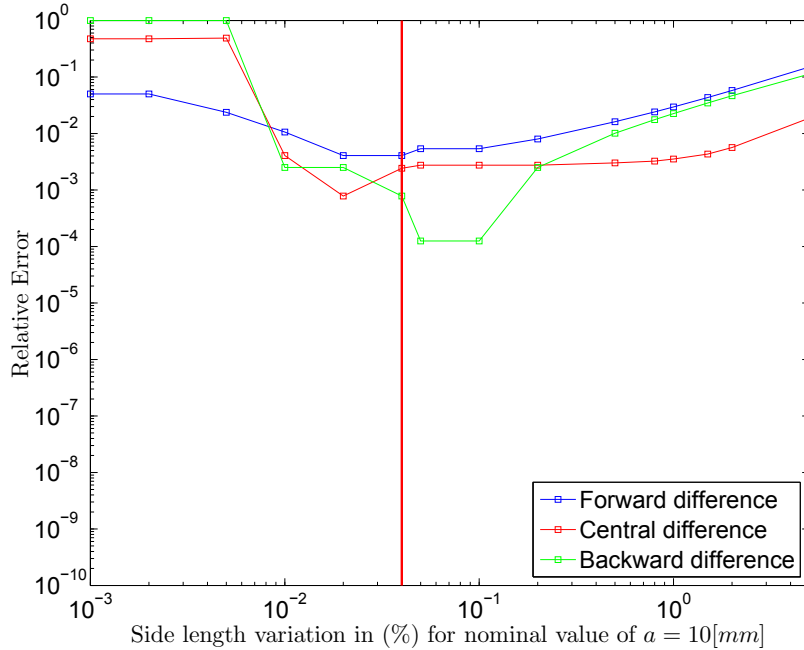


Figure 2.32: Relative error in the estimates using FDM with respect to theoretical result.

Whether the minimum sensitivity threshold can be improved or not, the analysis is tested with different element sizes encompassing element size of 20, 10, 5, 1 and 0.2.

The results of sensitivity threshold analysis are shown in Table 2.11. Surprisingly, however, the sensitivity threshold augments with the number of elements in this case.

Table 2.11: Synthesis of sensitivity threshold of FE numerical beam bending model in 1D with different element sizes

Element size [mm]	Sensitivity threshold [%]	Corresponding side length [mm]
20	0.01	10 ± 10^{-4}
10	0.01	10 ± 10^{-4}
5	0.01	10 ± 10^{-4}
1	0.02	$10 \pm 2 \times 10^{-3}$
0.2	0.04	$10 \pm 4 \times 10^{-3}$

2.7.4 Proposed methodology for identifying sensitivity threshold of FE numerical simulation

To investigate the minimum sensitivity threshold of a FE non-linear numerical model to the input's variations, an approach based on the sensitivity analysis of finite-difference method (FDM) is proposed. The procedure of proposed approach includes steps as shown in Figure 2.33. A problem is set up with variation of input parameters. Design of experiments is used for sampling the input variables' values which they are then used as inputs in FE numerical simulation. The output responses are determined and used in identification of sensitivity threshold based on finite-difference method. As a result, these sensitivity threshold results are considered as a reminder when entering the variation interval of the input parameters in the DOE of computer experiments.

In order to run numerical experiments conveniently and identify the sensitivity threshold automatically, simulating draw bending process by Abaqus software and determining the springback responses with Matlab are integrated under the workflow of ModeFrontier.

To reduce the analysis time, parallel calculation technique is applied by connecting several computers in a network server instead of only using one computer with the Cygwin in the ModeFrontier. The input files of Abaqus in which the variables' values have been updated from DOE are sent to the calculation server to run the numerical experiments in parallel. Subsequently, the result files will be returned to a local computer to determine the springback measurements as well as to calculate the sensitivity.

The technique for detecting the minimum sensitivity threshold:

The minimum sensitivity threshold of FE numerical model is identified at a value of variation step where the forward, backward and central difference approximation converge.

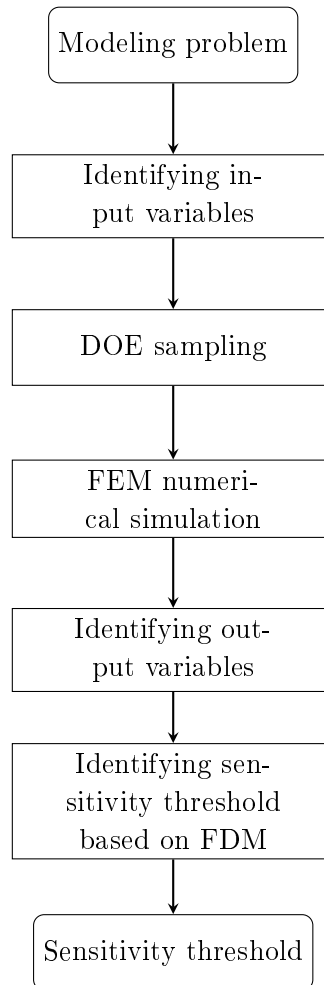


Figure 2.33: Proposed methodology for identifying sensitivity threshold of FE numerical simulation.

2.8 Example of application

To validate the proposed method for identification of minimum sensitivity threshold, a complex case of numerical simulation of sheet metal draw bending process is considered in this section.

2.8.1 Identification of minimum sensitivity threshold

In order to identify the minimum sensitivity threshold of FEM numerical simulation of the draw bending process, the h variation step of the input variables including sheet thickness, material properties, friction coefficient, blank holder force and tooling geometry is gradually decreased from 20% to 0.01% of their nominal values. Input data for identifying the minimum sensitivity threshold is shown in Table A.1.

The springback responses including β_1 , β_2 and ρ are considered as the response functions. They are respectively computed according to the finite difference method as shown in Section 2.7.1.

The minimum sensitivity threshold results of FE numerical sheet metal draw bending when having variation step of sheet thickness from 20% to 0.01% determined from 25 computer runs are shown in Figure 2.34, 2.35, 2.36.

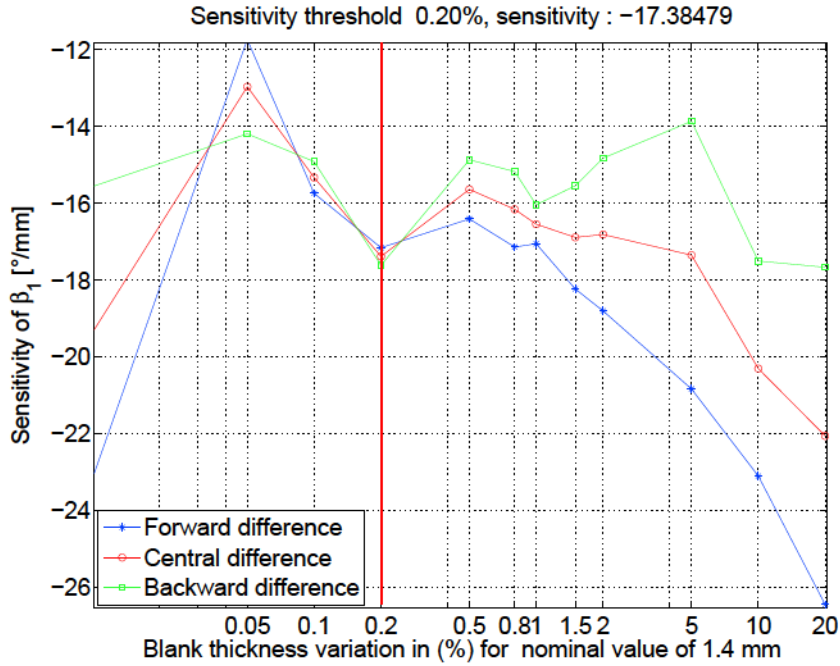


Figure 2.34: The minimum sensitivity threshold of FE numerical sheet metal draw bending regarding β_1 when having the blank thickness variations from 20% to 0.01%.

It can be seen from the Figure 2.34 that three forward, backward and central difference approximations regarding the springback angle of β_1 are different at the point of 20%. Subsequently, they are gradually close to together at the point of 1%

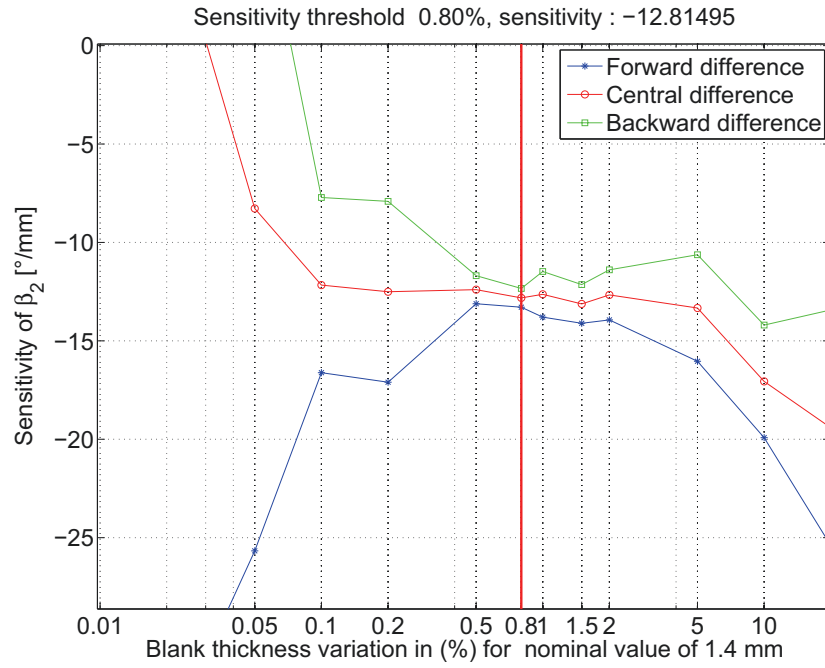


Figure 2.35: The minimum sensitivity threshold of FE numerical sheet metal draw bending regarding β_2 when having the blank thickness variations from 20% to 0.01%.

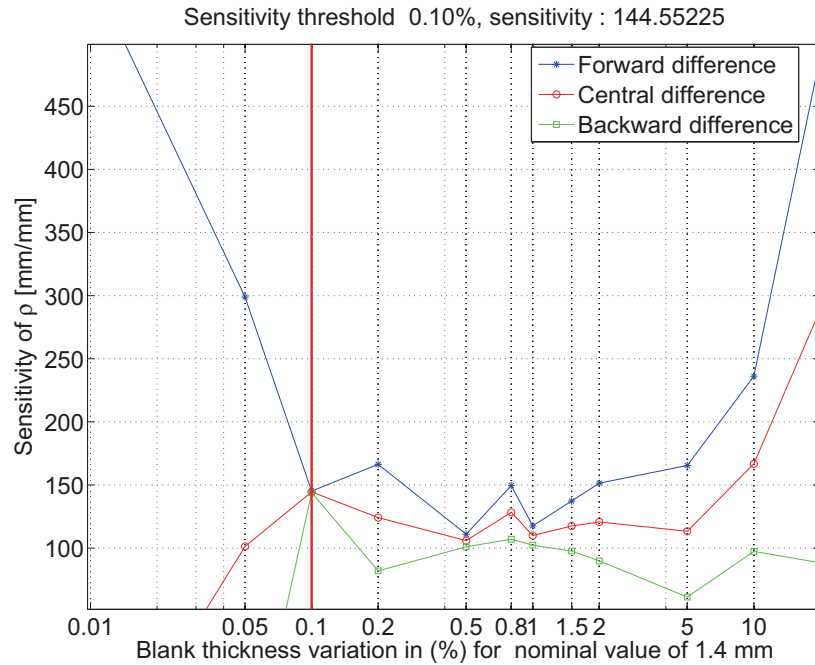


Figure 2.36: The minimum sensitivity threshold of FE numerical sheet metal draw bending regarding ρ when having the blank thickness variations from 20% to 0.01%.

and converge at the point of 0.2%. Below this point, they diverge at the point of 0.1%, they continue diverging at the point of 0.05% and then changing according to arbitrary direction. It is claimed that the minimum sensitivity threshold of FE numerical model regarding β_1 when having uncertainty of blank thickness is 0.2%. Similarly, the difference approximations of the angle β_2 in Figure 2.35 converge at the point of 0.8%, afterwards they diverge from this point till the point of 0.01%. It is said that the minimum sensitivity threshold regarding β_2 reaches to 0.8%. In the similar detecting technique, the sensitivity threshold of side wall curl radius ρ is at 0.1% as shown in Figure 2.36. The derivatives of springback responses with respect to blank thickness variation steps are initially different from the point of 20% and comes close to together at 1% as well as at 0.5%. They converge at the point of 0.1%. The sensitivity curves of springback responses are not smooth and sharp due to the behaviour of non-linear response functions of FE numerical models as well as scatter due to errors of numerical methods.

According to the proposed approach, this shows that FEM numerical simulation is not sensible to very small variation step of blank thickness, in particular variation step of nominal values smaller than 0.2%, 0.8% and 0.1% respectively corresponding to the angles of β_1 , β_2 and side wall curl radius ρ . As a consequence, numerical responses of this FEM model are unstable when the interval of blank thickness variation are smaller than 0.8% around its nominal value. Meaning that the FEM numerical simulation does not get confident responses with blank thickness of 1.4 ± 0.0112 [mm] in this case study. Furthermore, the local sensitivity of springback responses in terms of blank thickness variation is also inferred from these sensitivity results. As can be seen from Figure 2.34, 2.35, 2.36 that the local sensitivity of wall opening angle β_1 , the flange angle β_2 and the side wall curl radius ρ is 17.38479 [$^\circ \text{ mm}^{-1}$], 12.81495 [$^\circ \text{ mm}^{-1}$] and 144.55225 [mm mm^{-1}] when blank thickness is 1.4 [mm]. It shows that the blank thickness influence significantly on the springback responses.

With similar detection, the minimum sensitivity threshold of seven parameters including blank thickness (t), yield strength (R_e), ultimate tensile strength (R_m), blank holder force (F_{BHF}), friction coefficient (μ), die radius (R_d) and punch radius (R_p) is synthesized in Table 2.12.

Sensitivity results are listed in Table 2.13.

2.8.2 Sensitivity analysis of sheet metal draw bending

In order to identify the influence of individual input parameter on springback, sensitivity analysis can be conducted from the results of the proposed method to predict the influence of individual input parameter on the springback responses by using sensitivity functions as follows:

- For the wall opening angle β_1 :

$$S_i = \frac{d\beta_1}{dx_i} \xi x_i^{nom} \quad (2.41)$$

Table 2.12: Synthesis of the seven input parameters' minimum sensitivity threshold

Parameters	Sensitivity threshold regarding $\beta 1$ [%]	Sensitivity threshold regarding $\beta 2$ [%]	Sensitivity threshold regarding ρ [%]	General sensitivity threshold [%]	Corresponding variation range
t	0.2	0.8	0.1	0.8	1.4 ± 0.0112 [mm]
R_e	1	5	5	5	550 ± 27.5 [MPa]
F_{BHF}	1.5	5	1.5	5	2940 ± 147 [N]
μ	1.5	5	5	5	0.1 ± 0.005
R_d	0.2	5	1	5	7 ± 0.35 [mm]
R_p	1	5	10	10	5 ± 0.5 [mm]
R_m	2	5	2	5	840 ± 42 [MPa]

Table 2.13: Sensitivity of springback responses with respect to the input parameters

Parameters	Sensitivity of $\beta 1$	Sensitivity of $\beta 2$	Sensitivity of ρ
t	17.3848 [$^\circ \text{ mm}^{-1}$]	12.8150 [$^\circ \text{ mm}^{-1}$]	144.5523 [mm mm^{-1}]
R_e	0.0072 [$^\circ \text{ MPa}^{-1}$]	0.00027 [$^\circ \text{ MPa}^{-1}$]	0.0285 [mm MPa^{-1}]
F_{BHF}	0.00044 [$^\circ \text{ N}^{-1}$]	0.00056 [$^\circ \text{ N}^{-1}$]	0.00534 [mm N^{-1}]
Fric. coeff.	26.4348	5.3282	145.9892
R_d	0.0639 [$^\circ \text{ mm}^{-1}$]	0.2547 [$^\circ \text{ mm}^{-1}$]	6.07191 [mm mm^{-1}]
R_p	0.7132 [$^\circ \text{ mm}^{-1}$]	0.1225 [$^\circ \text{ mm}^{-1}$]	1.1378 [mm mm^{-1}]
R_m	0.0188 [$^\circ \text{ MPa}^{-1}$]	0.0139 [$^\circ \text{ MPa}^{-1}$]	0.1622 [mm MPa^{-1}]

- For the flange angle β_2 :

$$S_i = \frac{d\beta_2}{dx_i} \xi x_i^{nom} \quad (2.42)$$

- For the side wall curl radius ρ :

$$S_i = \frac{d\rho}{dx_i} \xi x_i^{nom} \quad (2.43)$$

where x_i is the i th input parameter; ξ is the variation percentage and x_i^{nom} is the i th input parameter at nominal value.

Sensitivity analysis results of the input variables contributing to the springback responses of β_1 , β_2 , and ρ are presented in Figure (2.37, 2.38, 2.39).

Sensitivity result of input variables contributing to β_1 at their nominal value

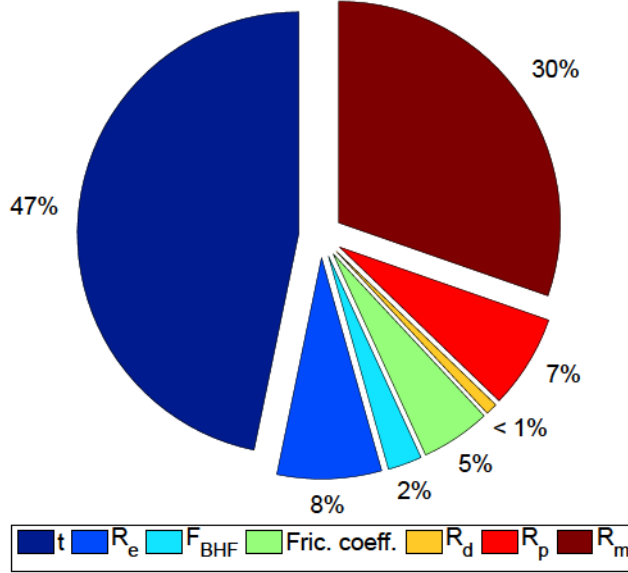
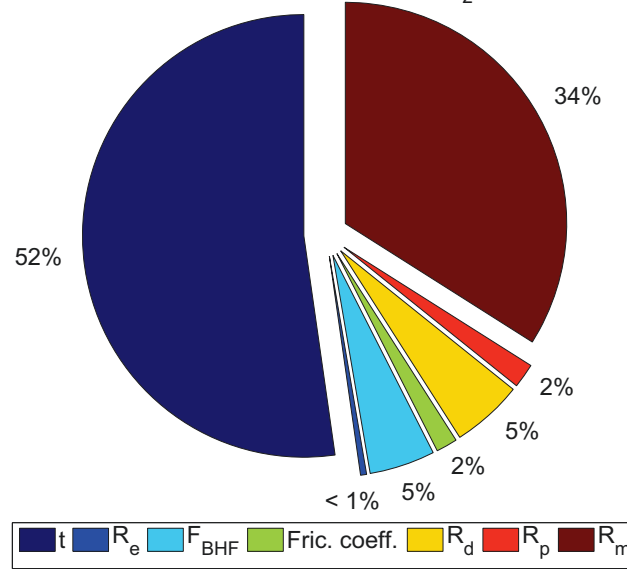
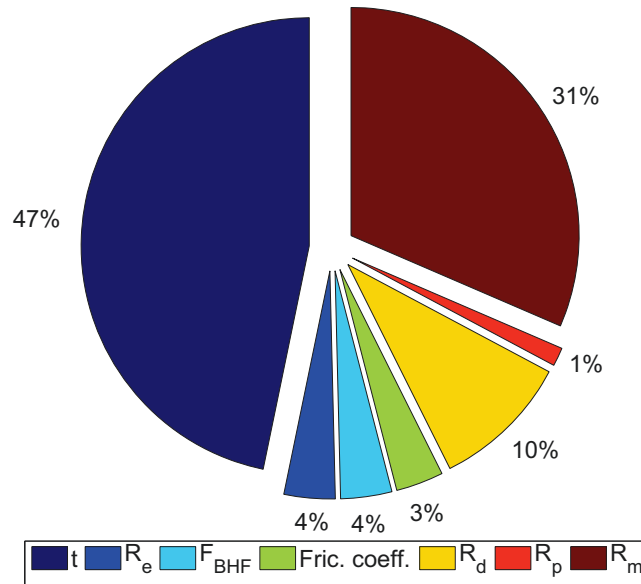


Figure 2.37: Sensitivity analysis result of the input variables contributing to β_1 at their nominal value

As can be clearly seen from Figure 2.37 blank thickness and ultimate tensile strength are pointed out as two parameters having the greatest influence on the wall opening angle β_1 , followed by yield strength, punch radius, friction coefficient, blank holder force and die radius in which the effect of die radius is quasi-null. Also, the influence of blank thickness accounts for 52% of the overall variation of the flange angle β_2 , followed by UTS with 34%, BHF and die radius with 5%. Whereas the effect of friction, punch radius and YS is trivial. The variation of the side wall curl ρ is significantly contributed by blank thickness, UTS and

Sensitivity result of input variables contributing to β_2 at their nominal valueFigure 2.38: Sensitivity analysis result of the input variables contributing to β_2 at their nominal valueSensitivity result of input variables contributing to ρ at their nominal valueFigure 2.39: Sensitivity analysis result of the input variables contributing to ρ at their nominal value

die radius with 47%, 31% and 10% respectively. While the influence of YS, BHF, friction and punch radius is quite low in this case. Overall, it is found that taking the uncertainty of blank thickness and material properties scatter (YS and UTS) into account in the early process design for controlling their influences on formed part performance contributes significantly to reduction of scrap rate. In order to reduce the effects of inherent variability of the sheet, material properties and tooling geometry, searching optimal configurations of controllable variables consisting of BHF and friction condition should be done.

2.9 Building surrogate-models for computer experiments

As previously mentioned, in addition to reducing computation costs in time-consuming FEM simulation-based design process, applying metamodeling in uncertainty propagation and optimization brings many benefits including [232]:

- The efficiency of optimization is greatly improved with metamodels;
- Parallel computation is supported because the approximation is based on sample points, which could be obtained independently;
- Sensitivity analysis can obtain that this helps the relationship between input variables and output variables;
- Metamodeling can handle both continuous and discrete variables.

Hence, in this section a strategy for building metamodels is proposed that will also be used in uncertainty propagation in Chapter 3 and optimization in Chapter 4.

2.9.1 Proposed strategy

Metamodels are built according to the flowchart as shown in Figure 2.40. This strategy consists of 5 stages in which the first stage of modeling encompasses the first 6 steps as mentioned in Section 2.5.2. More specifically, the goals of the metamodels in this thesis are understanding and prediction of variations in sheet metal forming process. Subsequently, executing optimization algorithms on the metamodels to search for optimal designs for the process. The input and output variables were specified in modeling of the sheet metal forming process. The range of accuracy of the metamodels depends on the goals of the metamodel. A metamodel used for prediction should be very accurate, whereas for a metamodel used for understanding, it will be sufficient if only a trend is visible. The accuracy required for metamodels utilised for optimisation purposes will lie somewhere in between. The ranges of accuracies may be specified via the validity measures such as the Root Mean Square Error (RMSE), Maximum Absolute Error (MAE) and the R^2 -value. Secondly, prior to sampling for the input variables based on DOE methods, it is crucial to identify the minimum sensitivity threshold of FE model to obtain confident results from

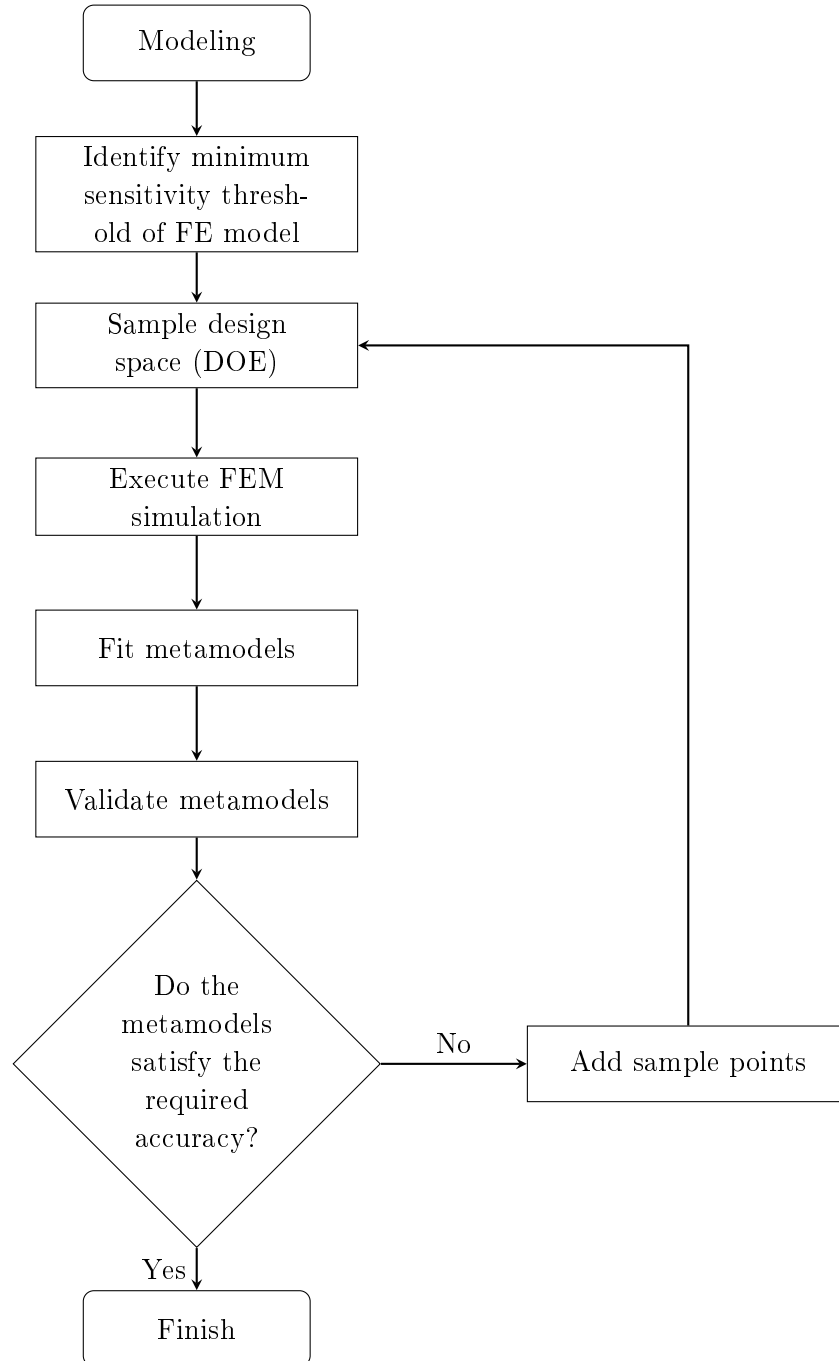


Figure 2.40: Flowchart of metamodeling process

FEM simulation. The method for identifying the minimum sensitivity threshold of FE model has been proposed in previous section. As a result of this method, the intervals of the input variables for DOE are properly given.

Next stage, the input variables are sampled based on DOE methods, followed by running FEM simulations. Afterwards, the metamodels are fitted through the response values. The validity measures are calculated to compare the metamodel's accuracy to the required accuracy. If the metamodel does not satisfy the accuracy demands, one may return to the DOE stage to add more experimental points and subsequently fit the metamodel with the additional information. This process is repeated until the required accuracy demands are met.

2.9.2 Metamodeling for sheet metal forming process

One FEM simulation of sheet metal forming process usually takes several hours to complete. In order to have a probabilistic evaluation (i.e. mean and variance of the outputs) in uncertainty propagation of sheet metal forming process, several thousands evaluations are required. Furthermore, for obtaining the best solution in optimization, several thousands sample points are demanded. Therefore, it is impractical to run the input/output FEM simulations directly. Instead of that there is a need to use a surrogate-model for these purposes. The workflow of metamodeling

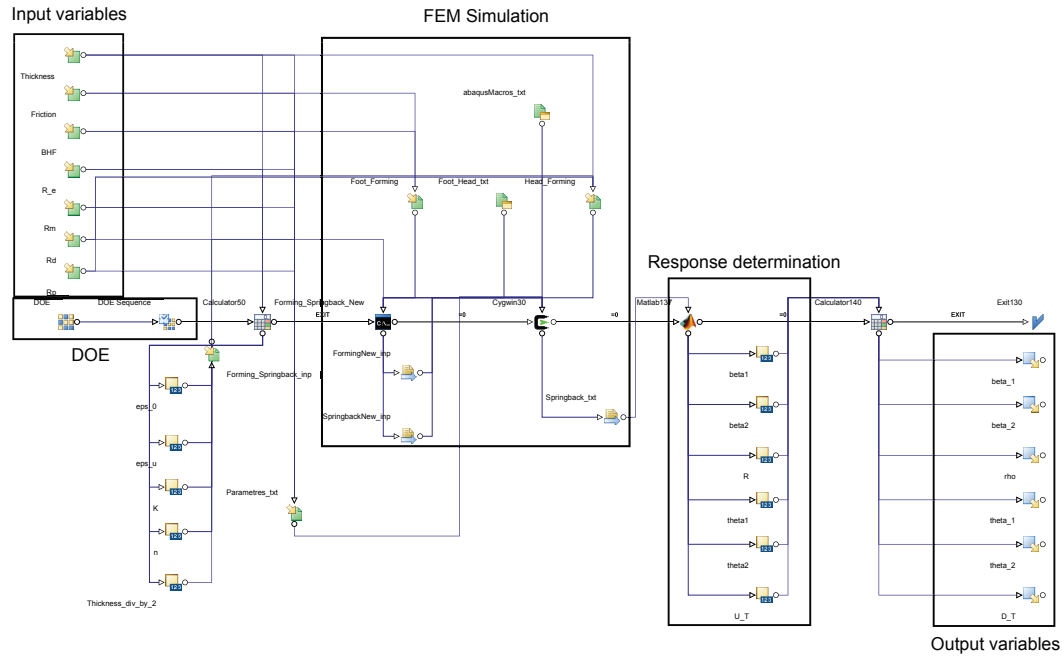


Figure 2.41: Workflow of metamodeling for sheet metal forming process

for sheet metal forming process, which is modeled by modeFRONTIER™, is shown in Figure 2.41. The input variables include sheet thickness t , blank holder force F_{BHF} , friction coefficient μ , yield strength R_e , tensile strength R_m , punch radius R_p , and die radius R_d . Input data for DOE strategy is given in Table 2.14, in which

material properties are referred from Arcelormittal [7]. Design of experiments based

Table 2.14: Input data for DOE strategy

Factors	Levels		
t [mm]	1	1.5	2
F_{BHF} [kN]	2.94	26.47	50
μ	0.04	0.1	0.16
R_e [MPa] [7]	500	550	600
R_m [MPa] [7]	780	840	900
R_p [mm]	2	6	10
R_d [mm]	2	6	10

on a multi level Full-Factorial sequence is utilized to sample. This method works best with less than 8 variables and less than 4 levels. In this case, 7 factors are assigned 3 levels as shown in Table 2.14. Hence, they are combined as $3^7 = 2187$ initial sampling points are generated.

The output variables are springback parameters including the flange angle β_2 , the wall opening angle β_1 and the side wall curl radius ρ . We need to build a metamodel for each output variable:

$$\beta_1 = f_1(t, F_{BHF}, \mu, R_e, R_m, R_p, R_d) \quad (2.44)$$

$$\beta_2 = f_2(t, F_{BHF}, \mu, R_e, R_m, R_p, R_d) \quad (2.45)$$

$$\rho = f_3(t, F_{BHF}, \mu, R_e, R_m, R_p, R_d) \quad (2.46)$$

The aim of a metamodel \hat{y} is to accurately approximate a true response model y . In this work, the true response model y is the FEM simulation responses. An expression which shows the relationship between the FEM simulation responses and the metamodel as follows:

$$y = \hat{y} + \varepsilon \quad (2.47)$$

where ε is a random error term.

Metamodeling techniques are used to build the metamodel \hat{y} in this work encompassing Response Surface Methodology (RSM), Kriging and Radial Basis Functions (RBF). The detailed description of the metamodeling techniques is represented in Appendix A.5.

2.9.2.1 Metamodel validation

The fitness of the metamodel is assessed using a variety of techniques. As shown in previous sections, least squares regression analysis is used with Response Surface Methodology(RSM) [142], the Kriging method is fitted with the search for the Best Linear Unbiased Predictor (BLUP) [200]. Metamodels are to be validated before being thereafter used as a surrogate in uncertainty propagation and optimization processes. According to Jin et al. [92] two metrics , namely, R-square and Relative

Maximum Absolute Error (RMAE) are used to measure the accuracy of metamodels. While R-square indicates overall accuracy (the larger the better), RMAE indicates local errors (the smaller the better). A good overall accuracy does not necessarily means a good local accuracy. The RMAE, Maximum Absolute Error (MAE) and the R^2 -value, defined below:

$$RMAE = \frac{\max(|y_1 - \hat{y}_1|, |y_2 - \hat{y}_2|, \dots, |y_n - \hat{y}_n|)}{\sqrt{\frac{1}{n} \sum_{i=1}^n (y_i - \bar{y})^2}} \quad (2.48)$$

$$MAE = \max|y_i - \hat{y}_i|, i = 1, \dots, m \quad (2.49)$$

$$R^2 = 1 - \frac{\sum_{i=1}^m (y_i - \hat{y}_i)^2}{\sum_{i=1}^m (y_i - \bar{y})^2} \quad (2.50)$$

where m is the number of validation points; \hat{y}_i is the predicted value for the observed value y_i . \bar{y} is the mean of the observed values at the validation points. It is to be noted that the lower the value of $RMSE$ and/or MAX , the more accurate the metamodel. $RMSE$ is used to gauge the overall accuracy of the model, while MAX is used to gauge the local accuracy of the model.

2.9.2.2 Results of Metamodels

As discussed above, the Full Factorial Design (FFD) of 7 factors with 3 levels is used as the DOE. Initially, 2187 designs are sampled, after FEM simulation, 2128 correct simulations get. There are 59 fails due to the numerical problems between the input values and meshing problem resulting in excessive distortions. Hence, it should complement DOEs to improve the accuracy of metamodels. There are 972 DOEs added by the FFD of 7 factors in which 5 factors are assigned 3 levels and 2 factors are assigned 2 levels with the input data as shown in Table 2.15. Totally, there are 3100 designs used to build the metamodels. Figure 2.42a, 2.42b show

Table 2.15: Input data for DOE strategy

Factors	Levels		
t [mm]	1	1.5	2
F_{BHF} [kN]	14.705	N/A	38.235
μ	0.07	N/A	0.13
R_e [MPa] [7]	500	550	600
R_m [MPa] [7]	780	840	900
R_p [mm]	2	6	10
R_d [mm]	2	6	10

graphical representation of the FFD of F_{BHF} , R_d , R_p and R_e , R_m , t respectively.

Metamodels for sheet metal draw bending process are built based on two methods of polynomial RSM and Kriging.

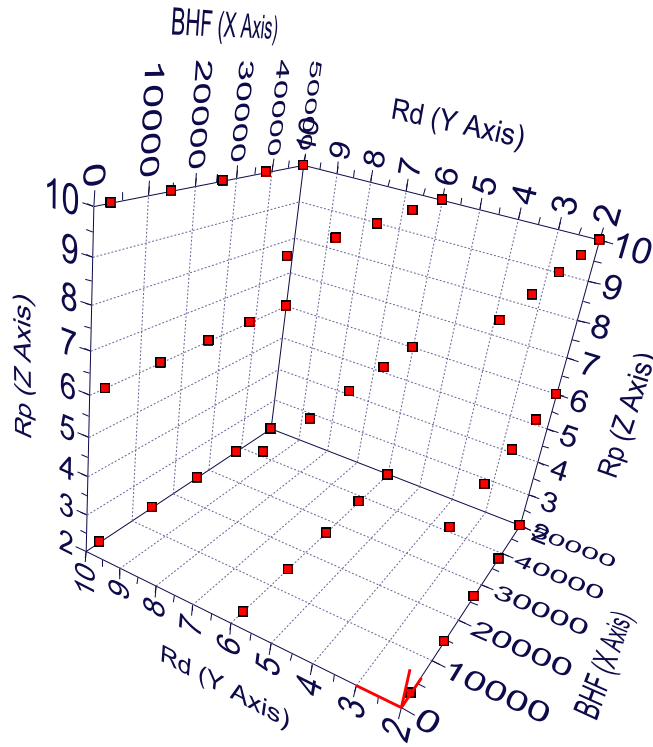
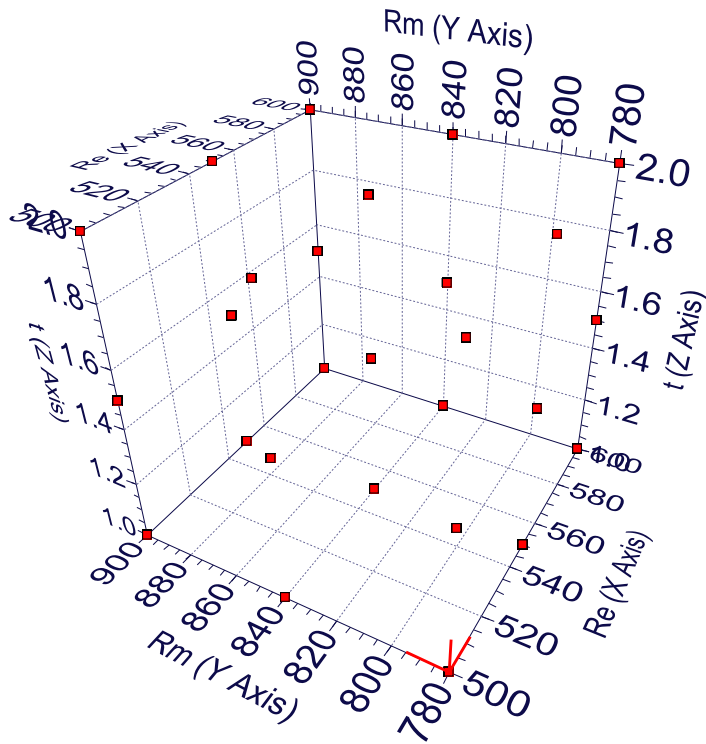
(a) F_{BHF}, R_d, R_p .(b) R_e, R_m, t .

Figure 2.42: Graphical representation of the FFD of the factors.

Polynomial RSM

The relationship between the output variables of β_1, β_2, ρ and the input variables of $t, F_{BHF}, \mu, R_e, R_m, R_p, R_d$ using the polynomial of degree of 2 is represented as follows:

$$\begin{aligned}\beta_1 = & 0.2 + 0.2F_{BHF} + 1.3R_d + 0.1R_p - 0.3t - 0.1F_{BHF}^2 - 0.1F_{BHF}R_d - 0.6R_d^2 \\ & + 0.1R_dR_m + 0.1F_{BHF}R_p - 0.1R_p^2 - 0.2F_{BHF}f - 0.1R_df + 0.2F_{BHF}t - 0.4R_dt \\ & - 0.1R_mt + 0.2ft - 0.1t^2\end{aligned}\quad (2.51)$$

$$\begin{aligned}\beta_2 = & 0.7 + 0.7R_d - 0.1f - 0.2t - 0.1F_{BHF}^2 - 0.4R_d^2 - 0.2F_{BHF}f + 0.3F_{BHF}t \\ & - 0.2R_dt - 0.1R_mt + 0.2ft - 0.2t^2\end{aligned}\quad (2.52)$$

$$\begin{aligned}\rho = & 0.01 - 0.01F_{BHF} - 0.03R_d - 0.01f - 0.04t + 0.01F_{BHF}R_d + 0.02R_d^2 \\ & - 0.01R_dR_e - 0.01R_dR_m + 0.01R_eR_m - 0.01R_df + 0.01R_ef + 0.01R_mf + 0.01f^2 \\ & + 0.02F_{BHF}t + 0.03R_dt - 0.01R_et + 0.03t^2\end{aligned}\quad (2.53)$$

Graphically, it is impossible to represent the responses associated with all the inputs in 3D. Therefore, metamodels are graphically represented between β_1, β_2, ρ and design variables of F_{BHF}, R_d as follows:

$$\beta_1 = f(F_{BHF}, R_d) \quad (2.54)$$

$$\beta_2 = f(F_{BHF}, R_d) \quad (2.55)$$

$$\rho = f(F_{BHF}, R_d) \quad (2.56)$$

These metamodels built by using Multivariate Polynomial Interpolation based on the Singular Value Decomposition (SVD) with polynomial degree of 2 are presented in Figure 2.43.

Kriging

The outputs of springback in function of the inputs variables can be rewritten based on Kriging as follows:

$$y = X\beta + Z(x) \quad (2.57)$$

where $Z(x)$ is assumed to be a Gaussian stochastic process with zero mean. Metamodels built by using Kriging between β_1, β_2, ρ and design variables F_{BHF}, R_d are shown in Figure 2.44.

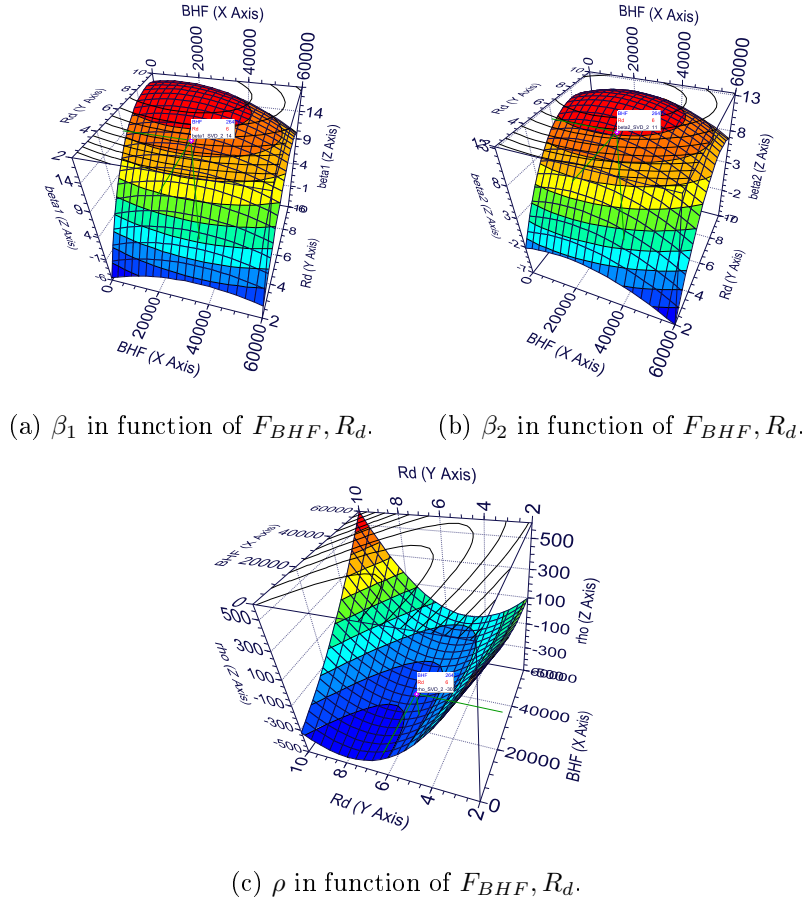
Figure 2.43: Metamodels of β_1 , β_2 and ρ in function of F_{BHF}, R_d built by RSM.

Table 2.16: Comparison of accuracy between radial functions of RBF

Radial Functions	Responses	MAE	R-square
Inverse MultiQuadrics	β_1	9.0596×10^{-11}	1
	β_2	3.2892×10^{-10}	1
	ρ	6.0101×10^{-7}	1
Gaussians	β_1	3.8164×10^{-7}	0.9999
	β_2	2.3661×10^{-6}	0.9999
	ρ	1.3626×10^{-3}	0.9999
Duchon's Polyharmonic Splines	β_1	2.1150×10^{-9}	1
	β_2	3.0074×10^{-9}	1
	ρ	1.1064×10^{-5}	1
Hardy's MultiQuadrics	β_1	1.7401×10^{-9}	1
	β_2	7.7675×10^{-9}	1
	ρ	1.8937×10^{-5}	1

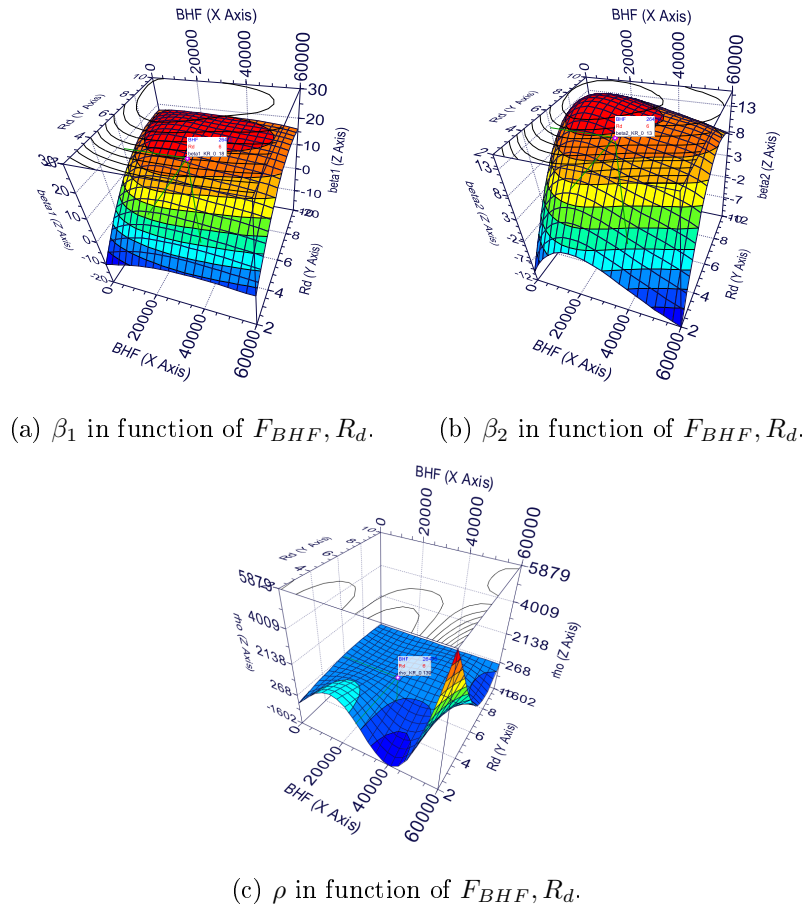


Figure 2.44: Metamodels of β_1, β_2, ρ in function of F_{BHF}, R_d built by Kriging.

Radial Basis Functions

As discussed in Section A.5.3, there are five different radial functions available in the ModeFRONTIER. Each kind of radial functions results in different accuracy of metamodels. In order to have the best accuracy of metamodels built by the RBF, comparison of accuracy between radial functions of the RBF is presented in Table 2.16. It can be seen that the RBF with radial function of Inverse MultiQuadrics has the best accuracy. Therefore, it is used for fitting the responses. Metamodels built by the RBF with radial function of the IMQ between β_1 , β_2 , ρ and design variables F_{BHF} , R_d are shown in Figure 2.45.

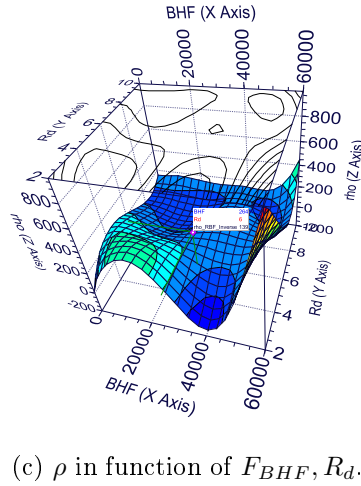
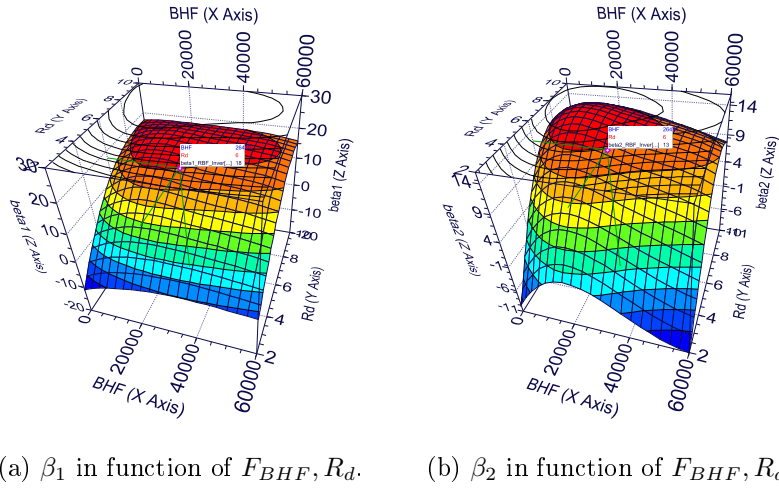


Figure 2.45: Metamodels of β_1 , β_2 , ρ in function of F_{BHF} , R_d built by Radial Basis Functions.

Neural Networks

NN are a very efficient and powerful interpolation tool. Inspired by the brain structure and functions, NN can learn from training data: in this way NN can model any generic non-linear relationship between input and output variables. This response surface method based on classical feedforward Neural Networks, with one hidden layer, and with an efficient Levenberg-Marquardt back propagation training algorithm. The initialization of the network's parameters is based on the proper initialization approach by Nguyen and Widrow [153]. Metamodels built by NN between β_1 , β_2 , ρ and design variables F_{BHF} , R_d are shown in Figure 2.46.

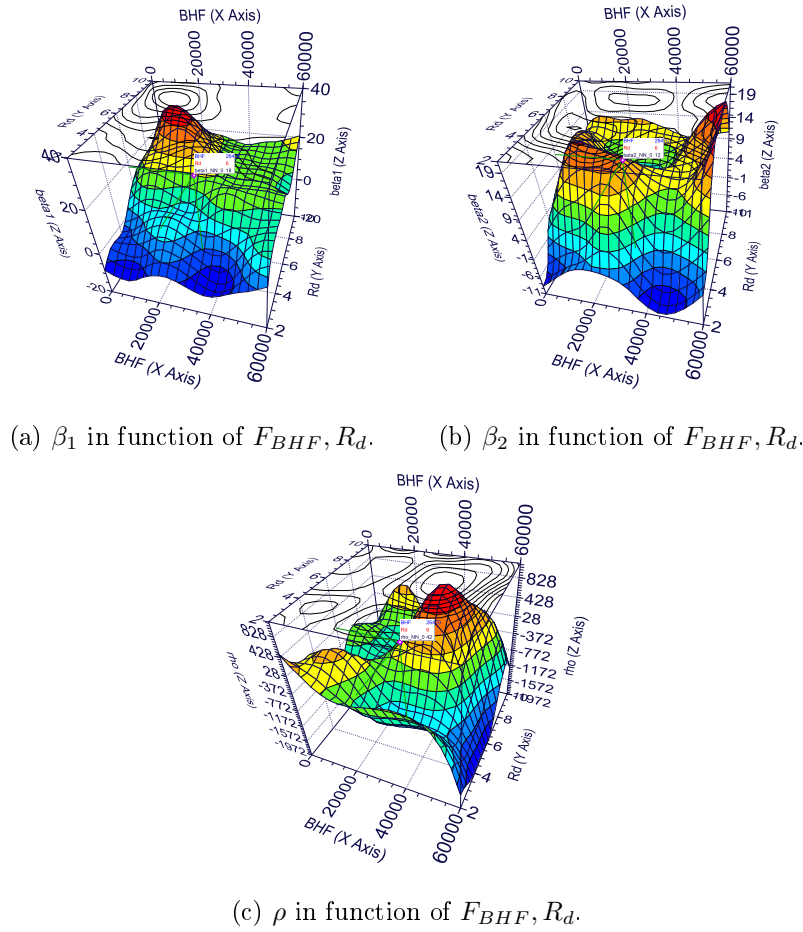


Figure 2.46: Metamodels of β_1, β_2, ρ in function of F_{BHF}, R_d built by Neural Networks.

2.9.2.3 Accuracy of Metamodels

As discussed above, in order to use the metamodels as surrogate models of time-consuming FEM numerical simulations, it is vital to evaluate the accuracy of the metamodels. The two metrics which are used to measure the metamodels' accuracy

are the R-square and the MAE. Table 2.17 shows the accuracy of each kind of metamodels.

Table 2.17: Comparison of accuracy of metamodels

RSM	Responses	MAE	R-square
Kriging	β_1	7.4591×10^{-5}	0.9999
	β_2	5.6535×10^{-3}	0.9999
	ρ	4.2752×10^{-6}	1
SVD2	β_1	12.0715	0.8727
	β_2	30.8179	0.8829
	ρ	96665.8	0.0768
SVD3	β_1	9.9122	0.9724
	β_2	29.4869	0.9651
	ρ	92667.0694	0.1431
RBF	β_1	9.0596×10^{-11}	1
	β_2	3.2892×10^{-10}	1
	ρ	6.0101×10^{-7}	1
NN	β_1	0.8783	0.9999
	β_2	12.1686	0.9982
	ρ	21912.8576	0.9154

It is found that the accuracy of RBF is the best both in terms of R-square and in terms of MAE. Thus, the metamodels built by using RBF will be used in next steps of this thesis.

2.10 Summary of the chapter

This chapter has been dedicated to numerical approaches applied for design of computer experiments based on FEM numerical simulation. Several main points in this chapter are synthesized as follows:

- The widely used sheet metal forming processes have been reviewed. In particular, the sheet metal bending has been introduced exhaustively and has been used as a case study in this thesis. Comparison between constitutive equations used to model material behavior has been also done.
- The state-of-the-art of FEM numerical simulation in sheet metal forming process design has been reviewed. It has been addressed that there is a sensitivity threshold of FEM numerical simulation below which the responses are insensitive to very small variations of input parameters. ***A FDM-based method has been proposed to detect the sensitivity threshold.*** As a result of this method, the intervals of input parameters are given, and thus when carrying out design of computer experiments using FEM numerical models, the values

of the input parameters must be outside the detected intervals to have good results.

- Shape variation due to springback of formed part is taken into account and determined. Sensitivity analysis has been performed to identify the effects of seven input parameters on the response. It has been found that blank thickness is the most influenced parameter on shape variation due to springback in the sheet metal bending.
- Design of computer experiments with full factorial of FEM numerical model of U-shaped sheet metal bending has been executed. Since running the experiments directly with FEM numerical model is impossible, a strategy based on metamodels for computer experiments are introduced. Observation from comparison between the RSM methods has shown that metamodels built by RBF with radial function of inverse multiquadratics have the best accuracy. It will be used as surrogate model in uncertainty propagation and optimization in next chapters.

Uncertainty and geometric dispersion

Contents

3.1 State-of-the-art	73
3.1.1 Uncertainty definition, categorization and propagation	73
3.1.2 Uncertainty modeling, representation and propagation	77
3.1.3 Sampling techniques	84
3.1.4 Determination of sheet metal part variations	86
3.1.5 Quality evaluation of sheet metal part with multiple characteristics	90
3.2 Uncertainty propagation in sheet metal forming process design	93
3.2.1 Uncertainty classification	93
3.2.2 Strategy for uncertainty propagation	95
3.2.3 Analysis of the effects of uncertainties on the product performance	98
3.3 Summary of the chapter	110

3.1 State-of-the-art

3.1.1 Uncertainty definition, categorization and propagation

3.1.1.1 Uncertainty definition

The concept of uncertainty has been around for a much longer time; starting with Socrates and Plato, philosophers doubted whether scientific knowledge, no matter how elaborate, sufficiently reflected reality. They realized that the more we gain insight into the mysteries of nature, the more we become aware of the limits of our knowledge about how 'things as such' are [215].

A fundamental definition of uncertainty is "liability to chance or accident", "doubtfulness or vagueness", "want of assurance or confidence; hesitation, irresolution", and "something not definitely known or knowable" [194], [218].

Although the term is used in various ways among the general public, many specialists in decision theory, statistics and other quantitative fields have defined uncertainty as: *"Uncertainty: The lack of certainty. A state of having limited knowledge where it is impossible to exactly describe the existing state, a future outcome, or more than one possible outcome"*.

Uncertainty can be viewed as the difference between the present state of knowledge and the complete knowledge as shown in Figure 3.1. It is classified into aleatory and epistemic types [79].

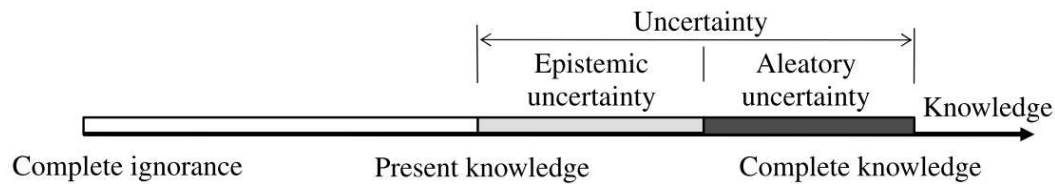


Figure 3.1: Uncertainty types [74]

Uncertainty is ubiquitous in any engineering system, at any stage of product development, and throughout a product life cycle. Examples of uncertainty are manufacturing imprecision, usage variations, imperfect knowledge, and variability associated with loading, material properties, and geometric dimensions. Such uncertainties have a significant impact on product performance. A small variation in environment or design variables may lead to a significant quality loss. The ignorance of uncertainty may cause erroneous decision making, low robustness and reliability, costly warranty, low customer satisfaction, and even catastrophe [74], [157], [51], [247], [85]. With the intensive requirement of high product quality and reliability, understanding, identifying, and managing various uncertainties have become imperative [74].

3.1.1.2 Uncertainty categorization

There are different possibilities to classify uncertainties which the engineer has to encounter during the design process. One way to categorize the sources of uncertainty proposed by Kennedy et al. [100] is to consider:

- Parameter uncertainty, which comes from the model parameters that are inputs to the computer model (mathematical model) but whose exact values are unknown to experimentalists and cannot be controlled in physical experiments. Examples are the local free-fall acceleration in a falling object experiment, and various material properties in a finite element analysis for engineering.
- Parametric variability, which comes from the variability of input variables of the model. For example, the dimensions of a work piece in a process of manufacture may not be exactly as designed and instructed, which would cause variability in its performance.

- Structural uncertainty, also known as model inadequacy, model bias, or model discrepancy, which comes from the lack of knowledge of the underlying true physics. It depends on how accurately a mathematical model describes the true system for a real-life situation, considering the fact that models are almost always only approximations to reality. One example is when modeling the process of a falling object using the free-fall model; the model itself is inaccurate since there always exists air friction. In this case, even if there is no unknown parameter in the model, a discrepancy is still expected between the model and true physics.
- Algorithmic uncertainty, also known as numerical uncertainty, which comes from numerical errors and numerical approximations per implementation of the computer model. Most models are too complicated to solve exactly. For example the finite element method or finite difference method may be used to approximate the solution of a partial differential equation, which, however, introduces numerical errors. Other examples are numerical integration and infinite sum truncation that are necessary approximations in numerical implementation.
- Experimental uncertainty, also known as observation error, which comes from the variability of experimental measurements. The experimental uncertainty is inevitable and can be noticed by repeating a measurement for many times using exactly the same settings for all inputs/variables.
- Interpolation uncertainty, which comes a lack of available data collected from computer model simulations and/or experimental measurements. For other input settings that do not have simulation data or experimental measurements, one must interpolate or extrapolate in order to predict the corresponding responses.

Another way of categorization is to classify uncertainty into two categories, aleatory uncertainty and epistemic uncertainty [79], [156], [40].

- Aleatory uncertainty is defined in the literature as irreducible uncertainty, inherent uncertainty, variability and stochastic uncertainty. Aleatory uncertainty is generally quantified by a probability or frequency distribution when sufficient information is available to estimate the distribution. Examples of this category include the dimensions of manufacturing parts and material properties.
- On the other hand, epistemic uncertainty is due to the lack of knowledge or the incompleteness of information. Epistemic uncertainty is also referred to in the literature as reducible uncertainty, subjective uncertainty, and cognitive uncertainty. Epistemic quantities are sometimes referred to as quantities which have a fixed value in an analysis, but we do not know that fixed value. For example, the elastic modulus for the material in a specific component is presumably fixed but unknown or poorly known.

3.1.1.3 Uncertainty propagation

There are two major types of problems in uncertainty quantification: one is the forward propagation of uncertainty and the other is the inverse assessment of model uncertainty and parameter uncertainty. In this research work, we focus on the forward uncertainty propagation which is the quantification of uncertainties in system outputs propagated from uncertain inputs. It focuses on the influence on the outputs from the parametric variability listed uncertainty categorization. The targets of uncertainty propagation analysis can be:

- To evaluate low-order moments of the outputs, i.e. mean and variance.
- To evaluate the reliability of the outputs. This is especially useful in reliability engineering where outputs of a system are usually closely related to the performance of the system.
- To assess the complete probability distribution of the outputs. This is useful in the scenario of utility optimization where the complete distribution is used to calculate the utility.

The illustration of the methodologies for uncertainty propagation and distribution propagation is shown in Figure 3.2 [37].

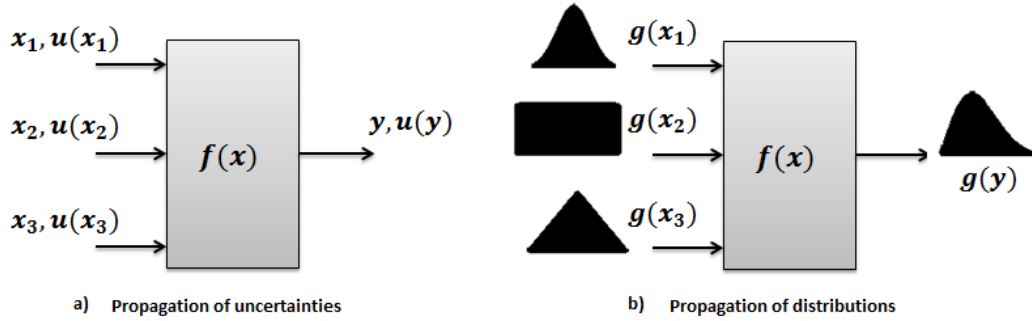


Figure 3.2: Methodologies for uncertainty propagation and distribution propagation [37]

Figure 3.2a shows an illustration representing the propagation of uncertainties. In this case, three input quantities are presented x_1, x_2 and x_3 along with their respective uncertainties $u(x_1), u(x_2)$ and $u(x_3)$. The measurand and its uncertainty are respectively y and $u(y)$. As can be noted, only the main moments (expectation and standard deviation) of the input quantities are used in the propagation and thus a certain amount of information is lost. When propagating distributions however, see Figure 3.2b, no approximations are made and the whole information contained on the input distributions are propagated to the output [37].

3.1.2 Uncertainty modeling, representation and propagation

As mentioned previously, uncertainties can be broadly classified into two types of aleatory and epistemic. The main reason why classifying uncertainties in engineering systems is that the strategy and methods for modeling and representing uncertainty in design depend on the types of uncertainty. Aleatory uncertainty is commonly modeled by random variables or stochastic processes by probability theory if information is sufficient to estimate probability distributions. Epistemic uncertainty can be handled by probability theory and nonprobability theories including evidence theory [192], possibility theory [105], [104], fuzzy set theory [245] and interval analysis [143]. The first step for robust design is to characterize and quantify uncertainty in a system. Uncertainty analysis methods can be classified into the types as probabilistic and non-probabilistic methods as presented in Table 3.1. Hence, in this section, several approaches for representing and propagating uncertainty are reviewed.

3.1.2.1 Probabilistic approaches

Probabilistic methods are the most popular ones for representing parameter uncertainty because of their universality. Three types of probabilistic models are commonly used to represent uncertainty in design: random variable, random field and time-dependent stochastic processes. Probabilistic models are appropriate when sufficient experimental or field data exists on the quantities of interest. To illustrate, consider an uncertain scalar ξ . Given a sufficient number of realizations of this scalar, kernel density estimation techniques can be employed to fit a probability density function (PDF) $\mathcal{P}(\xi)$ to the data. Alternatively, the structure of the PDF can be assumed (e.g., Gaussian, log-normal, beta, etc.) and its parameters can be estimated from the data. However, in practice, it is often the case that sufficient data may not exist for accurately estimating the joint pdf of the uncertain parameters. In such situations, it is necessary to invoke simplifying assumptions or perhaps solicit expert opinion. For example, when modeling uncertainties arising from manufacturing tolerances on an engineering component, a Gaussian model is often used. The use of a Gaussian uncertainty model can sometimes be justified on the basis of data/experience generated from previous studies or in some cases by virtue of the central-limit theorem. In practice, the Gaussian assumption is often made for the sake of mathematical convenience since a Gaussian distribution can be specified uniquely by its first two moments. However, when representing uncertainty in the Young's modulus of a component say, a Gaussian model cannot be justified. This is because the support of a Gaussian distribution is $[-\infty, +\infty]$, so with nonzero probability, the Young's modulus can turn out to be negative. This is of course not physically permissible. Hence, recourse has to be made to nonnegative distributions such as the log-normal or uniform distributions [99].

The probabilistic methods are further classified as statistical and non-statistical approaches.

Approach	Probabilistic		Non-probabilistic
	Simulation-based methods	Monte Carlo Simulation	Interval analysis [143]
		Latin Hypercube Sampling	Fuzzy set theory [245]
		Importance Sampling [137],[54]	Possibility theory [152]
		Adaptive Sampling [24]	Evidence theory [192]
		Surrogate models	Convex modeling [13]
	Local expansion-based methods	Taylor series	
	Most probable point-based methods [58]	First-order reliability method	
		Second-order reliability method	
	Functional expansion-based methods	Neumann expansion	
		Polynomial chaos expansion	
	Numerical integration-based methods [56],[191],[117]	Dimension reduction [177],[242]	

Table 3.1: Methodologies for uncertainty propagation

Simulation-based methods

Simulation methods are nonintrusive and can be applied to virtually any uncertainty propagation problem. The most popular simulation method is the Monte Carlo simulation (MCS) technique. The procedure of the basic Monte Carlo method involves [33]:

- generating a set of values by randomly sampling the known or assumed probability density function for each input variable,
- executing an experiment and collecting the data for each of the generated samples,
- employing statistics for the output data set to define its probability density function.

When probabilistic models with specified statistics are used to represent uncertainty, the uncertainty propagation problem essentially involves computing the statistical moments of the output and its complete probability distribution. Given the joint probability density function $\mathcal{P}(\xi)$ of the uncertain parameters, the MCS technique can be applied to compute the complete statistics of the response quantities of interest with an arbitrary level of accuracy, provided sufficient number of samples is used. Consider the multidimensional integral given below:

$$I = \langle \phi(\xi) \rangle = \int_{\mathcal{E}} \phi(\xi) \mathcal{P}(\xi) d\xi \quad (3.1)$$

where $\phi(\xi)$ is a function calculated by running an expensive computer model. The above integral arises, for example, when computing the k th statistical moment of an output function $f(\xi)$, in which case we set $\phi(\xi) = f^k(\xi)$. Multidimensional integrals of this form can rarely be evaluated analytically. The basic idea of simulation techniques is to numerically approximate the above multidimensional integral. In Monte Carlo integration, $\phi(\xi)$ is evaluated at various points generated by drawing samples from the distribution $\mathcal{P}(\xi)$, say $\xi^{(1)}, \xi^{(2)}, \dots, \xi^{(m)}$. Subsequently, the integral is approximated by an average of the realizations of ϕ , that is:

$$\langle \phi(\xi) \rangle \approx \tilde{\phi} = \frac{1}{m} \sum_{i=1}^m \phi(\xi^{(i)}) \quad (3.2)$$

$\tilde{\phi}$ is referred to as the Monte Carlo estimate of I , that is, an approximation to $\langle \phi(\xi) \rangle$. The strong law of large numbers states that, if ϕ is integrable over \mathcal{E} , then $\tilde{\phi} \rightarrow I$ almost surely as $m \rightarrow \infty$. The variance of the Monte Carlo estimate is given by

$$Var(\tilde{\phi}) = \frac{\sigma_{\phi}^2}{m} \quad (3.3)$$

where $\sigma_{\phi}^2 = \frac{1}{(m-1)} \sum_{i=1}^m (\phi(\xi^{(i)}) - \tilde{\phi})^2$ is the sample estimate of the variance of $\phi(\xi)$. The variance computed using Equation 3.3 can be used to judge the accuracy of the

Monte Carlo estimate. It follows from Equation 3.3 that the standard error of $\tilde{\phi}$ is given by σ_{ϕ}/\sqrt{m} . Note that the error estimate is independent of the dimension of ξ . It is important to know that, even if the Monte Carlo method converges to the exact statistic solution as the number of samples goes to infinity, the convergence of the mean error estimate is slow. Hence, thousands or millions of data samples may be required to get enough accuracy. Since the convergence rate of the Monte Carlo estimate is $O(1/\sqrt{m})$, to improve accuracy by one decimal place, around 100 times more samples will be required [99].

Since the basic Monte Carlo method is computationally expensive, modifications of the Monte Carlo method have been developed to improve the efficiency of uncertainty analysis. One of the most popular modified Monte Carlo methods is the Latin Hypercube sampling method [135]. In the Latin Hypercube sampling method, the selection of sample points is highly constrained. For a single random variable, instead of randomly sampling from a complete PDF, the range of random values is partitioned into several segments of equal probability. Each segment corresponds to an equal area under the PDF curve. In each segment, a point is sampled with respect to the complete PDF. In the case of multiple random variables, the values picked in the segments of each random variable are randomly combined with the values in the segments of other random variables without duplicating [33].

Using a surrogate model of the black-box simulation code in uncertainty analysis has been widely used in the last few years. The approach involves first constructing a polynomial model of the simulation code which is then used as a surrogate of the original computationally expensive model during MCS.

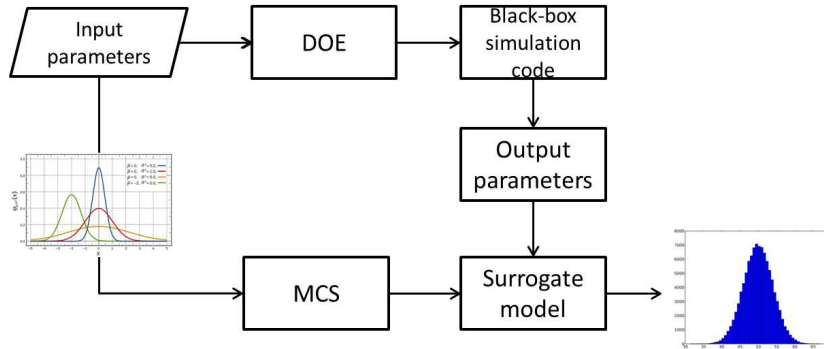


Figure 3.3: Uncertainty analysis using surrogate models.

Local expansion-based methods

For improving computational efficiency, non-statistical methods have been developed. The most widely used non-statistical uncertainty analysis method is local expansion-based methods. In local expansion-based methods, Taylor series expansions can be employed to approximate the statistical moments of the outputs of

interest. Consider the second-order Taylor series approximation of the function $\phi(\xi)$ at the point ξ^0 :

$$\hat{\phi}(\xi) = \phi(\xi^0) + \sum_{i=1}^{p\xi} \frac{\partial \phi}{\partial \xi_i} (\xi_i - \xi_i^0) + \frac{1}{2} \sum_{i=1}^{p\xi} \sum_{j=1}^{p\xi} \frac{\partial^2 \phi}{\partial \xi_i \partial \xi_j} (\xi_i - \xi_i^0) (\xi_j - \xi_j^0) \quad (3.4)$$

The mean and standard deviation of $\phi(\xi)$ can be approximated using Equation 3.4 as follows:

$$\hat{\mu}_\phi = \hat{\phi}(\xi^0) + \frac{1}{2} \sum_{i=1}^{p\xi} \frac{\partial^2 \phi}{\partial \xi_i^2} \sigma_{\xi_i}^2, \quad (3.5)$$

$$\hat{\sigma}_\phi = \sqrt{\sum_{i=1}^{p\xi} \left(\frac{\partial \phi}{\partial \xi_i} \right)^2 \sigma_{\xi_i}^2 + \frac{1}{2} \sum_{i=1}^{p\xi} \sum_{j=1}^{p\xi} \left(\frac{\partial^2 \phi}{\partial \xi_i \partial \xi_j} \right)^2 \sigma_{\xi_i}^2 \sigma_{\xi_j}^2}. \quad (3.6)$$

Neglecting the second-order terms in Equation 3.5 and Equation 3.6 results in first-order approximations for the mean and standard deviation of $\phi(\xi)$. The knowledge of the first two statistical moments of the input uncertainties is required to approximate the mean and standard deviation of $\phi(\xi)$. This is in contrast to simulation methods, which require the joint PDF of ξ [99]. The local expansion-based methods are very simple, convenient and very useful for exploration of a design space. However, the methods are good for Gaussian probability distribution, and it is very hard to apply to other types of probability distributions in input parameters. Also, the result can be inaccurate since these are approximate methods.

Functional expansion-based methods

In order to deal with the problem that if the probability distributions of the input parameters are not normal distributions, the approximate methods could be inaccurate, Polynomial Chaos expansions are proposed. The idea of polynomial chaos (PC) representations of stochastic processes was introduced by Wiener [237] as a generalization of Fourier series expansion. More specifically, Wiener used multidimensional Hermite polynomials as basis functions for representing stochastic processes. The basic idea is to project the process under consideration onto a stochastic subspace spanned by a set of complete orthogonal random polynomials. A general second-order stochastic process $h(\theta)$ can be represented as

$$h(\theta) = \sum_{i=0}^{\infty} h_i \varphi_i(\xi) \quad (3.7)$$

where $\varphi_i(\xi)$ are orthogonal polynomials and h_i are the PC coefficients. Since $\varphi_i(\xi)$, $i = 0, 1, 2, \dots, \infty$ form an orthogonal basis in the L_2 space of random variables

$$\langle \varphi_i(\xi) \varphi_j(\xi) \rangle = \langle \varphi_i^2(\xi) \rangle \delta_{i,j}, \quad (3.8)$$

where $\delta_{j,k}$ is the Kronecker delta operator and $\langle . \rangle$ defined as

$$\langle f(\xi)g(\xi) \rangle = \int f(\xi)g(\xi)W(\xi)d\xi \quad (3.9)$$

where $W(\xi)$ is the weight function corresponding to the PC basis. The weight function is chosen to correspond to the distribution of the elements of ξ [239]. For example, when Hermite polynomials are used as basis functions, the weight function is given by the multidimensional Gaussian distribution.

More recently, Xiu and Karniadakis [239] proposed a generalized PC approach that employs basis functions from the Askey family of orthogonal polynomials. The Hermite chaos expansion appears as a special case in this generalized approach, which is referred to as Wiener-Askey chaos [9]. The motivation for this generalization arises from the observation that the convergence of Hermite chaos expansions can be far from optimal for non-Gaussian inputs. In such cases, the convergence rate can be improved by replacing Hermite polynomials with other orthogonal polynomials that better represent the input. For instance, when the elements of ξ have a uniform distribution, then an expansion in Legendre basis functions converges faster compared to Hermite polynomials. This finding opens the possibility of representing stochastic processes with different orthogonal polynomials according to the property of the processes as shown in Table 3.2 [239].

Table 3.2: Relations between probability distributions and orthogonal polynomials

Distribution	Probability Density	Orthogonal Polynomials	Support Range
Normal	$\frac{e^{-\frac{x^2}{2}}}{\sqrt{2\pi}}$	Hermite $He_n(x)$	$(-\infty, +\infty)$
Uniform	$1/2$	Legendre $P_n(x)$	$(-1, +1)$
Beta	$\frac{(1-x)^\alpha(1-x)^\beta}{2^{\alpha+\beta+1}B(\alpha+1, \beta+1)}$	Jacobi $P_n^{(\alpha, \beta)}(x)$	$(-1, +1)$
Exponential	e^{-x}	Laguerre $L_n(x)$	$(0, +\infty)$
Gamma	$\frac{x^\alpha e^{-x}}{\Gamma(\alpha+1)}$	Generalized Laguerre $L_n^{(\alpha)}(x)$	$(0, +\infty)$

3.1.2.2 Non-probabilistic approaches

In this section, only interval analysis and fuzzy set are briefly reviewed. The others are advanced topics which are not considered in this thesis.

Interval analysis

Interval analysis [143] has been widely used for uncertainty analysis. Interval analysis is based on using algebraic procedures to propagate intervals of possible values for variables through to an interval of possible values for a function of these variables. The uncertainty in each element x_i of X would be represented by an interval.

$$X = [x_{min}, x_{max}] = x \in R | x_{min} \leq x \leq x_{max} \quad (3.10)$$

The interval bounds are then propagated through the analysis model to arrive at bounds on the output variables of interest which can be conservatively wide. All values within the interval are equally likely - this is in contrast to probabilistic representations where the extremes occur with much lower frequency than the average value. Interval analysis is a representation that requires very little information about variability of a parameter because it is not necessary to know how a parameter X is distributed between its two bounds. Furthermore, interval analysis does not infer an uncertainty structure on $f(X)$ based on an uncertainty structure assumed for X . Thus, the uncertainty representation for $f(X)$ obtained with interval analysis lacks the structure obtained with the other uncertainty representations such as probability, evidence, and possibility theory.

Fuzzy set

Fuzzy set theory proposed by Zadeh [245] also provides a powerful approach for modeling parameter uncertainty based on inexact or incomplete knowledge. Fuzzy sets are sets whose elements have degrees of membership. In classical set theory, the membership of elements in a set is assessed in binary terms according to a bivalent condition - an element either lies inside a set or outside it. In fuzzy set theory, classical bivalent sets are usually called crisp sets, since the degree of membership of a point is either 1 if it is inside the set or 0 if outside the set.

A fuzzy set is a pair (U, m) where U is a set and $m: U \rightarrow [0, 1]$.

For each $x \in U$, the value $m(x)$ is called the grade of membership of x in (U, m) . For a finite set $U = \{x_1, \dots, x_n\}$, the fuzzy set (U, m) is often denoted by $\{m(x_1)/x_1, \dots, m(x_n)/x_n\}$.

Let $x \in U$. Then x is called not included in the fuzzy set (U, m) if $m(x) = 0$, x is called fully included if $m(x) = 1$, and x is called a fuzzy member if $0 < m(x) < 1$. The set $\{x \in U | m(x) > 0\}$ is called the support of (U, m) and the set $\{x \in U | m(x) = 1\}$ is called its kernel. The function m is called the membership function of the fuzzy set (U, m) .

In fuzzy modeling, uncertainty is represented using sets with fuzzy boundaries. In other words, a membership function is associated with a fuzzy set, which indicates the degree of membership of a given point. The degree of membership can vary from 0 to 1.

Possibility theory is an extension of theory of fuzzy set and fuzzy logic [152].

3.1.3 Sampling techniques

As mentioned in simulation-based methods Section 3.1.2.1, there are two commonly used sampling techniques: Random Sampling (RS) (also known as Monte Carlo Sampling) and Latin Hypercube Sampling (LHS).

3.1.3.1 Random sampling

The random sampling, also known as Monte Carlo Sampling (MCS), is widely used for stochastic analysis [180]. Given the stochastic properties of one or more random variables, a sample average approximation problem is constructed. Assume that N samples of the random vector $X = [X_1, X_2, \dots, X_n]^T$ are needed. If each variable X_i ($i = 1, 2, \dots, n$) follows a CDF (Cumulative Distribution Function) P_{X_i} , the N samples x_i^j ($j=1, 2, \dots, N$) are independently generated using Quantile-Quantile transformation from the N samples ν_i^j , which are uniformly distributed on $[0, 1)$,

$$x_i^j = P_{X_i}^{-1}(\nu_i^j) (i = 1, 2, \dots, n; j = 1, 2, \dots, N), \quad (3.11)$$

where $P_{X_i}^{-1}(\cdot)$ is the inverse CDF of X_i .

Then, the following N samples of X are obtained.

$$x^j = [x_1^j, x_2^j, \dots, x_n^j] (j = 1, 2, \dots, N). \quad (3.12)$$

An example of MCS input generation of 10000 sample points is given in Figure 3.4.

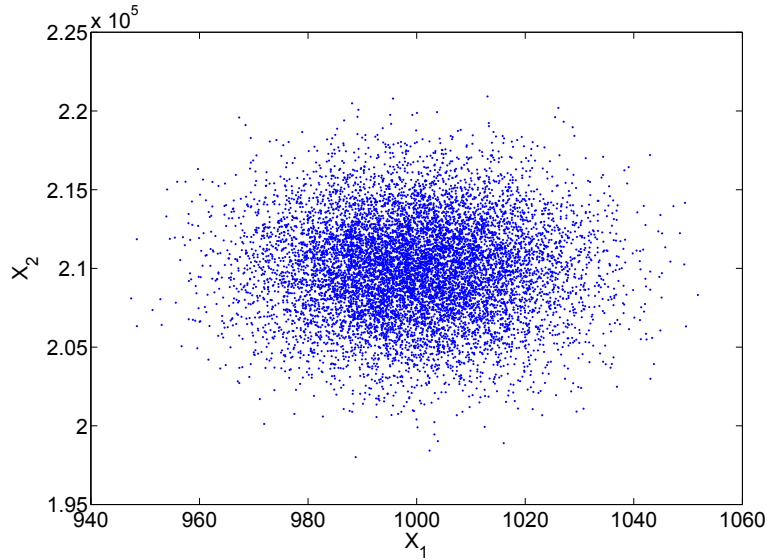


Figure 3.4: Monte Carlo Sampling generation based on Gaussian distribution.

3.1.3.2 Latin Hypercube Sampling

Latin Hypercube Sampling (LHS) which was introduced by McKay et al. [136] is a stratified sampling technique in which the uniformly distributed samples $\nu_i^j (j = 1, 2, \dots, N)$ are drawn by

$$\nu_i^j = \frac{\pi_i(j-1) + w_i^j}{N} (i = 1, 2, \dots, n; j = 1, 2, \dots, N) \quad (3.13)$$

where π_i is a uniform permutation of $0, \dots, N-1$, and w_i^j is a random observation from $U[0, 1)$. ν_i^j can also be obtained by the widely used median version of Equation 3.13,

$$\nu_i^j = \frac{\pi_i(j-1) + 0.5}{N} (i = 1, 2, \dots, n; j = 1, 2, \dots, N). \quad (3.14)$$

Then,

$$x_i^j = P_{X_i}^{-1}(\nu_i^j) (i = 1, 2, \dots, n; j = 1, 2, \dots, N). \quad (3.15)$$

The N samples of X_1 are paired at random without replacement with the N samples

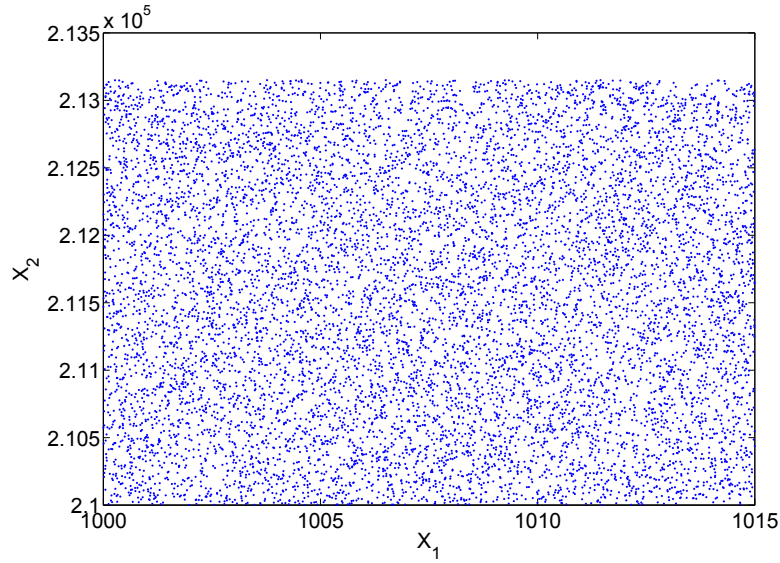


Figure 3.5: Latin Hypercube Sampling generation based on Uniform distribution.

of X_2 . These N pairs are combined in a random manner without replacement with the N samples of X_3 to form N triplets. This process continues until Nn -tuplets are formed. The Nn -tuplets may be contained in an $N \times n$ sample matrix in which each row corresponds to one sample of X . Totally, there are N samples of X in the matrix [84]. An example of LHS input generation of 10000 sample points is given in Figure 3.5.

Since LHS exhaustively stratifies across the whole range of each sampled variable, it mitigates the problem that important intervals with low probability but high

consequences are likely to be missed [161]. Compared to RS, LHS requires fewer samples for a similar accuracy. It is more efficient for estimating statistical moments (mean, variance, etc.) and produces more stable results than RS [77]. However, the main shortcoming of LHS stratification scheme is one-dimensional and does not provide good uniform properties on a multidimensional unit hypercube [49]. If the performance function is highly nonlinear, LHS provides no significant practical advantage over RS [130], [68].

Hence, in this thesis, the sampling mode of LHS for uncertainty propagation is used

3.1.4 Determination of sheet metal part variations

3.1.4.1 NUMISHEET benchmark

Springback variation is one of the main causes which influence on the performance of stamped parts. Springback arises due to elastic strain recovery of material after reloading deformation loads. Therefore, its magnitude is significantly dependent on the residual stresses in the workpiece after the forming tools are released. Springback cannot be eliminated but it can be controlled and minimized. In this section, several methods for determination of springback variations are reviewed.

In order to represent shape defect due to springback in the U-draw bending process, the NUMISHEET conference [127], [75] proposed the benchmark measurements of springback includes the wall angle θ_1 , flange angle θ_2 and sidewall curl radius ρ are shown in Figure 3.6. The parameters β_1 , β_2 and ρ are introduced to

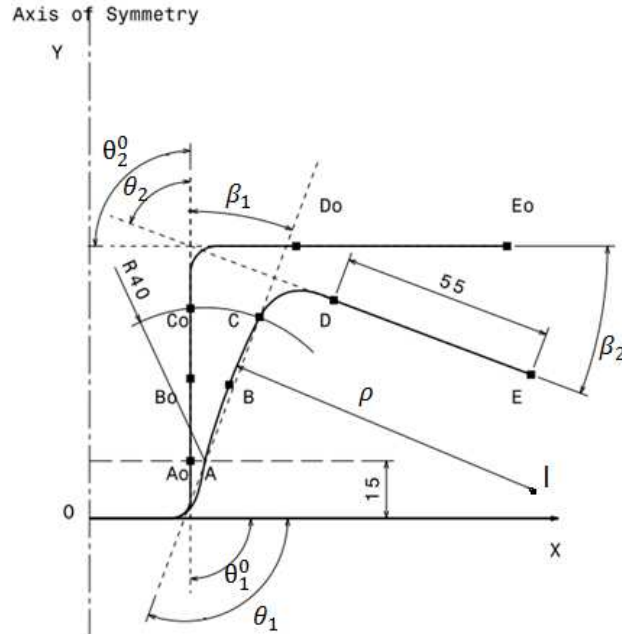


Figure 3.6: A schematic view of springback profile and parameters.

estimate the variation of part shape before and after springback. More specifically, they describe the variation of the part' cross-sectional shape obtained before and after removing the tools. The springback in the direction orthogonal to the cross-section is not considered in this case. Marretta et al. [132] utilized the relative displacement between deformed blank after load removing and final stamped part as springback indicator. Such indicator was calculated in terms of three dimensional nodal displacement taking into account the maximum value of such displacement. Springback values obtained from simulations via sections shown in Figure 3.7.

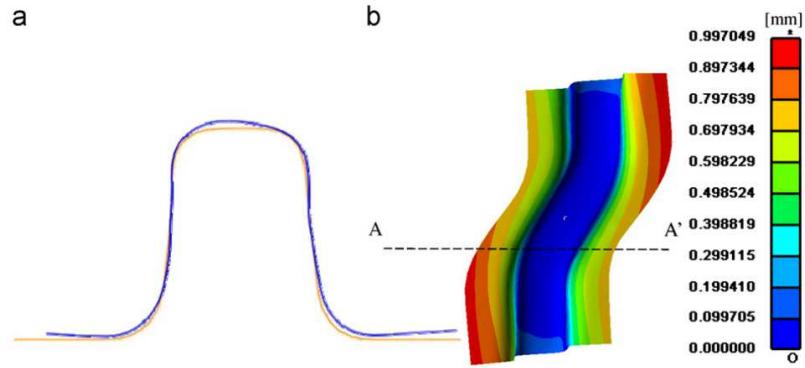


Figure 3.7: Springback map and its section [132].

3.1.4.2 Geometric defects based on modal analysis

Ledoux et al. [112] proposed a method to represent geometric defects of stamped part based on a discrete modal decomposition. This method enable to decompose size, position and form defects based on model basis which is generated by the natural vibration of forms. Geometric defects of stamped part are represented by different modes as illustrated in Figure 3.8.

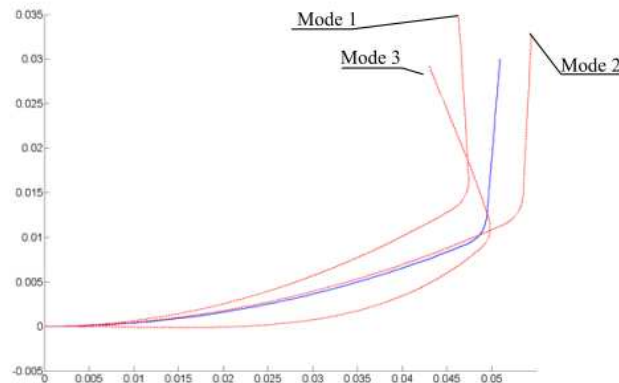


Figure 3.8: Shapes of the modes of stamped part [112].

3.1.4.3 Geometric deviations description using Principal Component Analysis (PCA)

Starting from the idea that how to visualize the Pareto optimal front in multi-objective optimization for 3 output variables (β_1, β_2, ρ) in which each one has 2 objectives to optimize. This leads to using 6-dimensional hypersurface. To overcome this problem, PCA is proposed. The PCA can transform the high-dimensional problems into lower-dimensional problems and provide sufficient information. The PCA is a statistical procedure that uses an orthogonal transformation to convert a set of observations of possibly correlated variables into a set of values of linearly uncorrelated variables called principal components. The idea of using the PCA to describe the part's geometric deviation is to transform the coordinate of nodes representing the part shape after springback from higher dimension into lower dimension. The advantages of this are able to represent any part shape and to reduce the dimension of the output if the output variables have relationship and dependence to each other. Particularly, instead of determining 3 springback parameters (β_1, β_2, ρ) via the cross-sections, the part performance is represented by its node coordinates. This idea is illustrated in Figure 3.9. Where $[1 \times n_i]$ is row matrix of node coordinates of the i th design, n_i is number of node of the i th design.

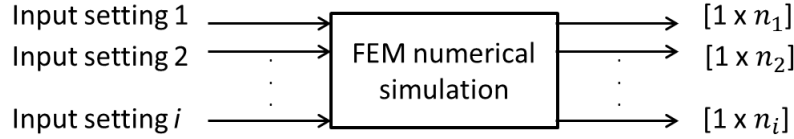


Figure 3.9: Approach of geometric deviation determination based on the sheet metal part's node coordinates.

The aim of PCA is to introduce a new set of m orthogonal axes in such a way that our original data will show the highest variance on the principal axis 1, the second highest variance along the principal axis 2, and so on, with the least variance being shown along the principal axes m . These axes are referred to as principal component axes. Each principal component is a linear combination of the original variables. The procedure of PCA is shown in Figure 3.10. In the application of sheet metal draw bending process, 2187 designs (3 levels and 7 factors) are executed, each output has 2860 nodes in 3-dimensions. Data set from FEM simulation is a matrix which has a size of $[2187 \times 8580]$.

However, through analysis of deformation modes of the part, it has been found that it requires at least 3 modes of deformation to represent the formed part shape properly. Meaning that there are still 3 output dimensions which are not our interest.

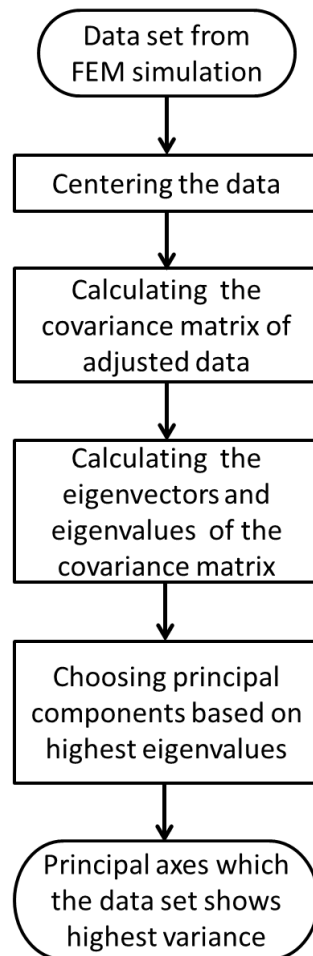


Figure 3.10: Procedure of the principal component analysis.

3.1.5 Quality evaluation of sheet metal part with multiple characteristics

3.1.5.1 Definition of process capability index

A process capability index is a numerical summary that compares the behaviour of a product or process characteristics to engineering specifications [202]. These measures are also often called the process capability indices or process capability ratio which is a statistical measure of process capability. A process capability is the ability of a process to produce output within specification limits. A process where almost all the measurements fall inside the specification limits is a capable process. This can be represented as shown in Figure 3.11.

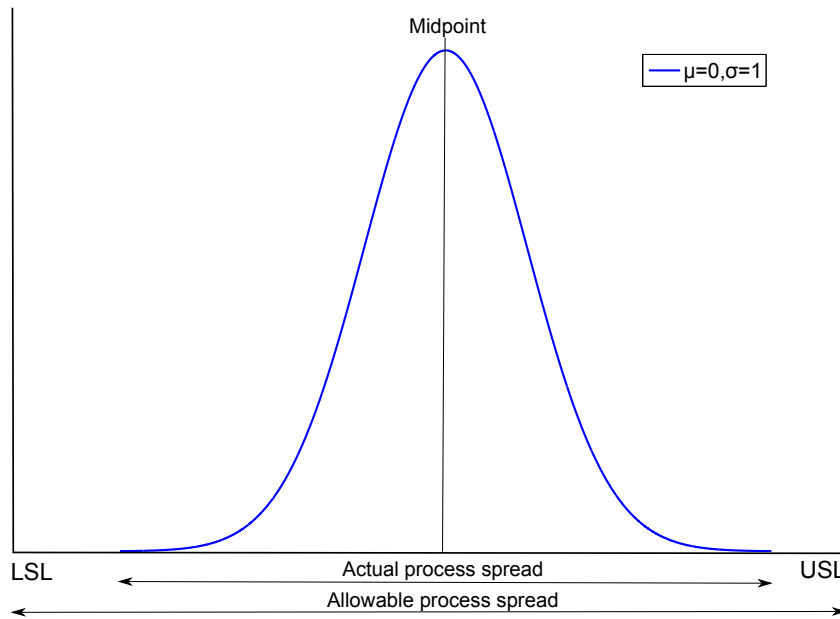


Figure 3.11: Graphical illustration of process capability.

There are several commonly accepted process capability indices that can be used to measure the capability of a process such as C_p , C_{pk} , C_{pm} , and C_{pmk} .

3.1.5.2 The C_p index

The C_p index is defined by the following formula [94], [206], [96]:

$$C_p = \frac{USL - LSL}{6\sigma} = \frac{IT}{6\sigma} \quad (3.16)$$

where IT is tolerance interval defined by upper specification limit (USL) and lower specification limit (LSL) and σ is standard deviation of product batch.

Under the usual assumption of normality of the distribution law of the batch and a process centered in the middle of the tolerance range, the rate of non-conforming

parts can be calculated [2]:

$$NCR_{ppm} = 2\Phi(1 - 3C_p)10^6 \quad (3.17)$$

where Φ is the function of a standard normal distribution law [110] and NCR is non-conformity rate. Due to its simplicity, however, the index of C_p only compares the batch dispersion with respect to the tolerance zone and it does not take into account the mean shift of the batch compared to the target.

3.1.5.3 The C_{pk} index

On the other hand, the index C_{pk} takes both the magnitude of process variance and the mean shift into consideration. The C_{pk} index is defined by the following formula:

$$C_{pk} = \min \left\{ \frac{USL - \mu}{3\sigma}, \frac{\mu - LSL}{3\sigma} \right\} = \frac{\frac{IT}{2} - |\delta|}{3\sigma} \quad (3.18)$$

where δ represents the mean shift of the batch compared to the target.

As mentioned above, the C_{pk} index was developed because the C_p index does not adequately deal with cases where process mean μ is not centered (the mean does not equal to the midpoint) as illustrated in Figure 3.12. However, C_{pk} by itself still

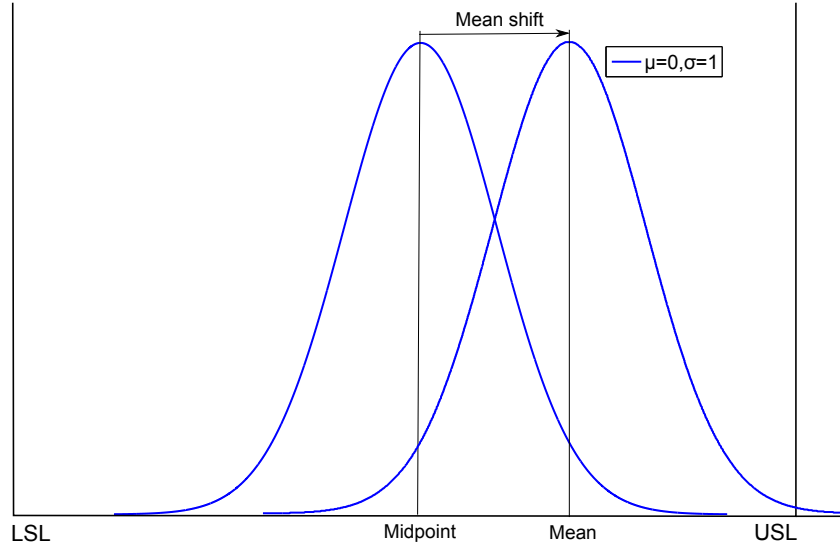


Figure 3.12: Normal distribution with a mean shift causes an increase in rejects.

cannot provide an adequate measure of process centering. That is, a large value of C_{pk} does not provide information about the location of the mean in the tolerance interval $USL - LSL$. The C_p and C_{pk} indices are appropriate measures of progress for quality improvement situations when reduction of variability is the guiding factor and process yield is the primary measure of a success. However, they are not related to the cost of failing to meet customers' requirement of the target [238].

By respecting an index C_{pk} greater than 1 means ensuring that the batch is in the range of tolerance [Min, Max].

Boyles [21] presented the application of C_{pk} on the normal distribution and the variations of reject rate for different values of the index C_{pk} in terms of the mean shift of the batch. Two limits are defined on the rate of non-conformity in terms of C_{pk} of the batch.

The lower bound is defined by [2]:

$$NCR_{ppm}^{lower} = (1 - \Phi(3C_{pk}))10^6 \quad (3.19)$$

The upper bound is defined by [2]:

$$NCR_{ppm}^{upper} = 2(1 - \Phi(3C_{pk}))10^6 \quad (3.20)$$

Relationship between the C_{pk} index and process yield and process fallout is shown in Table 3.3.

Table 3.3: Relationship between C_{pk} and process yield and process fallout

C_{pk}	Sigma level (σ)	Area under the probability den- sity function	Process yield [%]	Process fallout (DPMO/PPM)
0.33	1	0.6826894921	68.27	317311
0.67	2	0.9544997361	95.45	45500
1.00	3	0.9973002039	99.73	2700
1.33	4	0.9999366575	99.99	63
1.67	5	0.9999994267	99.9999	1
2.00	6	0.9999999980	99.999998	0.002

3.1.5.4 The C_{pm} index

Hsiang and Taguchi [82] introduced the C_{pm} index which was also later proposed independently by Chan et al. [26]. The C_{pm} index is based on the loss function of Taguchi. The C_{pm} index is defined by the following formula [21]:

$$C_{pm} = \frac{USL - LSL}{6\sqrt{\sigma^2 + (\mu - T)^2}} = \frac{IT}{6\sqrt{\sigma^2 + \delta^2}} \quad (3.21)$$

This index is oriented towards measuring the ability of a process to cluster around the target, and reflects the degrees of process targeting.

3.1.5.5 The C_{pmk} index

Pearn et al. [169] proposed the process capability index of C_{pmk} , which combines the features of the three earlier indices of C_p , C_{pk} and C_{pm} . The C_{pmk} index alerts

the user whenever the process variance increases and/or the process mean deviates from its target value [238]. The C_{pmk} index is defined as [169]:

$$C_{pmk} = \min \left\{ \frac{USL - \mu}{3\sqrt{\sigma^2 + \delta^2}}, \frac{\mu - LSL}{3\sqrt{\sigma^2 + \delta^2}} \right\} = \frac{\frac{IT}{2} - |\delta|}{3\sqrt{\sigma^2 + \delta^2}} \quad (3.22)$$

An expression of upper bound of non-conformity rate in terms of the C_{pmk} index is expressed in Pearn et al. [170] derived from the relation which was presented by Boyles [21] between the C_{pk} index and the upper bound of non-conformity rate:

$$NCR_{ppm}^{upper} = 2(1 - \Phi(3C_{pmk}))10^6 \quad (3.23)$$

3.1.5.6 The inertia criterion

Starting from the definition of the loss function Taguchi, Pillet proposes a new criterion called the inertia criterion which is defined by [2]

$$I = \sqrt{\delta^2 + \sigma^2} \quad (3.24)$$

This criterion represents the quality loss due to the off-centering and spread of a batch.

3.2 Uncertainty propagation in sheet metal forming process design

3.2.1 Uncertainty classification

A classical classification is the separation of uncertainty into the two types: aleatory and epistemic. Aleatory uncertainties are of intrinsically irreducible stochastic nature. Aleatory uncertainties in sheet metal forming include stochastic variabilities in material properties, blank thickness and friction. These aleatory uncertainties are regarded as parametric variabilities. On the other hand, epistemic uncertainty is due to the lack of knowledge or the incompleteness of information and it is subjective and reducible. Epistemic uncertainties include uncertainties about the model used to describe the reality, its boundary and operation conditions, also referred to as model form errors [125], and also the errors introduced by the numerical solution methods used (e.g., discretization error, approximation error, convergence problems) [14].

In the sheet metal forming process design based on FEM numerical simulation, both kind of uncertainties are present. The classification of the uncertainties is shown in Figure 3.13. In terms of aleatory uncertainties, the variation of blank thickness and material properties emanates from batch-to-batch variation and/or coil-to-coil variation, even within batch and part-to-part variation. They are inherent irreducible uncertainties in the sheet metal forming process. They are random variations and uncontrollable variables. While friction variation between tool surfaces within batch is derived from lubrication variation, however, it is controllable

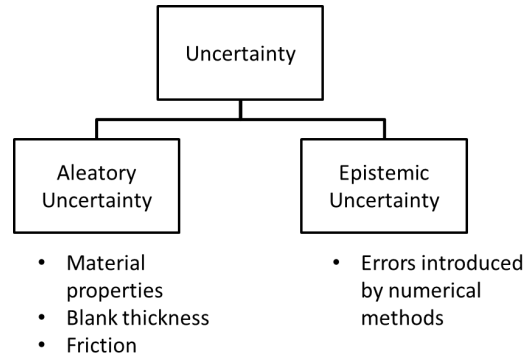


Figure 3.13: Taxonomy of uncertainty in sheet metal forming process design based on FEM numerical simulation.

variable. On the other hand, the accuracy of a mathematical model to describe an actual physical system of interest depends on the model uncertainty which is referred to as model form and numerical method errors is a form of epistemic uncertainty. Due to FEM numerical model considered as a black box, the errors introduced by the numerical solution methods are unavoidable uncertainties. To reduce these errors due to finite precision of FEM numerical simulation, we have proposed a method to point out "a prohibited interval" where the values of input parameters should not be inside when propagating uncertainties based on FEM simulation to get reliable responses.

On the other hand, on the basis of the original idea proposed by Taguchi, the parameters in any design problem may be classified into two groups [30]: (1) control factors composed of the inputs that the designer is free to manipulate and (2) noise factors, which are the inputs that are difficult or expensive to control.

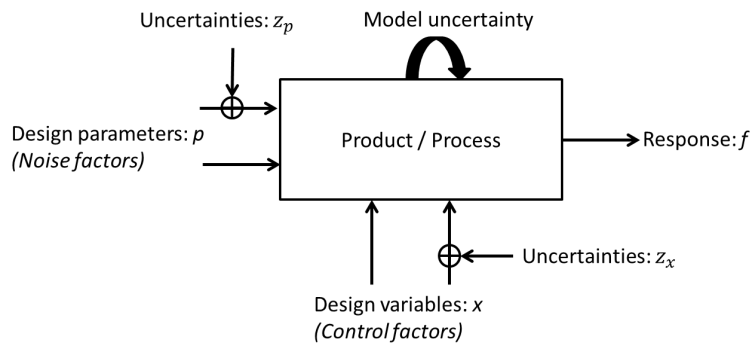


Figure 3.14: P-Diagram.

Figure 3.14 depicts a P-diagram of a numerical model used to describe the real physical product or process. It represents the schematic relationship between the

input of the model and the response. A sheet metal forming process or product has an output or response f which depends on the input. The input can be divided into design variables x and design parameters p . The design parameters or noise factors can be categorized as material properties (e.g. yield strength, tensile strength), blank thickness and friction between surfaces of tools and blank. The output behavior of the system can be controlled by the design variables such as process settings (e.g. blank holder force), tooling geometry (e.g. die and punch radii). This can be described by the following mathematical formulation:

$$f = f(x, p) \quad (3.25)$$

When uncertainties exist, the response f can be rewritten as follows:

$$f = f(x + z_x, p + z_p) \quad (3.26)$$

Moreover, model uncertainty arises when using numerical techniques to describe the real physical process, thus the designer has to deal with model uncertainties like numerical noise [216]. The resulting model uncertainty depends on the input of the system. The presence of this type of uncertainty is represented in Figure 3.14 by an arrow coming out of the system and entering the system again since it can be seen as an internal error of the model itself.

3.2.2 Strategy for uncertainty propagation

As discussed in Chapter 2, before carrying out uncertainty propagation, it is very necessary to build metamodels which are thereafter used to estimate probabilistic moments of the responses. Since several thousand, even million evaluations are required for a probabilistic evaluation, the FE model of the sheet metal forming process can not directly be used. Therefore, an approach for uncertainty propagation based on metamodel is proposed as shown in Figure 3.15.

After the input variables have been distinguished, the uncertainty of input parameters is modeled and represented by probabilistic approach. In particular, the inputs in sheet metal forming process design are modeled and represented by probabilistic approaches in which a Gaussian distribution is used.

More specifically, the idea here is to represent the input parameters by the nominal value, i.e. the mean or average value, the interval $[x_i^-, x_i^+]$, where x_i^- and x_i^+ denote the lower and upper bound respectively. Afterwards, probabilistic models are used to represent the uncertain parameters as continuous random variables. Modeling uncertainties arising from manufacturing tolerances of sheet thickness, variations in material properties, friction variation between tooling surfaces is by probabilistic distributions. Monte Carlo Sampling or Latin Hypercube Sampling is then used to sample values of the uncertain parameters. These sampling points are propagated through the metamodels to obtain statistical moments of the responses.

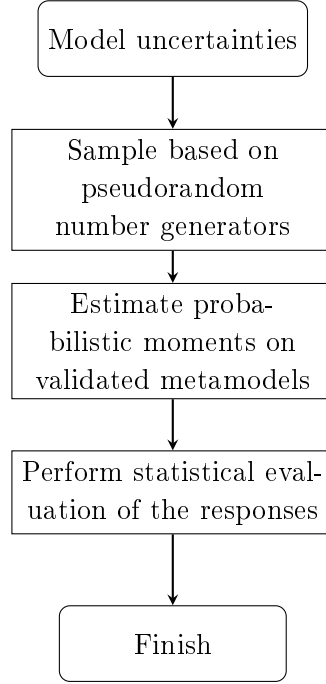


Figure 3.15: An proposed approach for uncertainty propagation.

3.2.2.1 Probabilistic description of uncertainty

In the practical engineering problems, randomness of the uncertain parameters are often modeled as a set of discretized random variables. Suppose X is a random variable and n observations of X are given. The samples of X are given by x_1, x_2, \dots, x_n . The statistical description of a random variable X can be completely described by a cumulative distribution function (CDF) or a probability density function (PDF), denoted by $P_X(x)$ and $p_X(x)$ respectively. To calculate the probability $Pr[\cdot]$ of X having a value between x_1 and x_2 , the area under the PDF between these two limits is calculated as follows:

$$Pr[x_1 \leq X \leq x_2] = \int_{x_1}^{x_2} p_X(x) dx = P_X(x_2) - P_X(x_1) \quad (3.27)$$

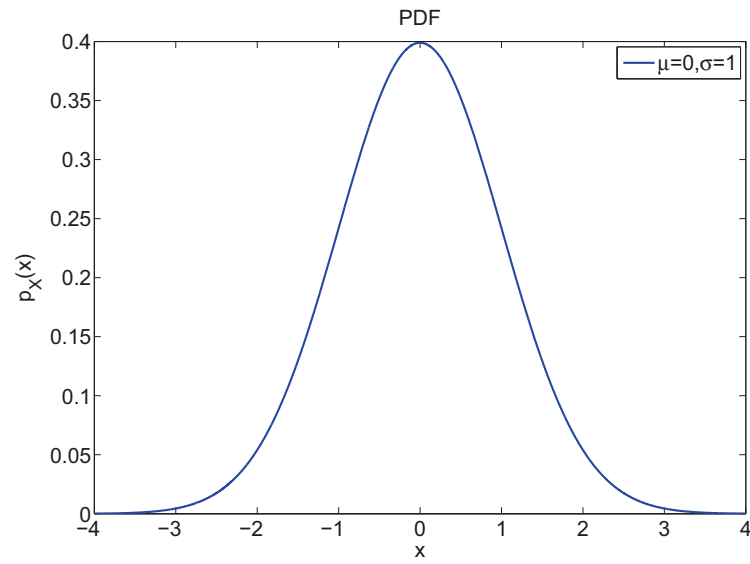
The PDF is the first derivative of the CDF, that is:

$$p_X(x) = \frac{dP_X(x)}{dx} \quad (3.28)$$

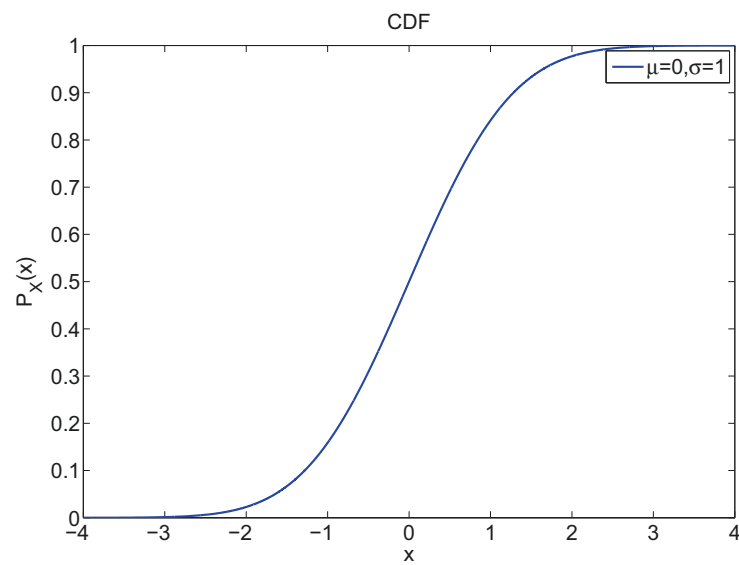
The PDF and CDF for a normal or Gaussian distribution with $\mu_X = 0$ and standard variation $\sigma_X = 1$ are given in Figure 3.16.

The expected value $E(X)$ and variance $Var(X)$ of the random variable are given by:

$$E(X) = \mu_X = \int_{-\infty}^{+\infty} x p_x(x) dx \quad (3.29)$$



(a) PDF



(b) CDF

Figure 3.16: Probability density function and cumulative distribution function for a normal distribution

$$Var(X) = \sigma_X^2 = \int_{-\infty}^{+\infty} (x - \mu_X)^2 p_X(X) dx \quad (3.30)$$

In sheet metal forming process, there are several variables being taken into account. Uncertainty modeling and representation of input parameters are shown in Table 3.4. Modeling uncertainties of the input parameters is represented by Gaussian dis-

Table 3.4: Probabilistic modeling and representation of uncertainties in the input parameters

Parameters	Distribution	Interval bounds	Mean	Stdev.	IT
F_{BHF} [kN]	Normal	[2.94,50]	26.47	0.6667	± 2
R_d [mm]	Normal	[2,10]	6	0.0167	± 0.05
R_p [mm]	Normal	[2,10]	6	0.0167	± 0.05
R_e [MPa]	Normal	[500,600]	550	16.667	± 50
R_m [MPa]	Normal	[780,900]	840	20	± 60
μ	Normal	[0.04, 0.16]	0.1	0.0033	± 0.01
t [mm]	Normal	[1,2]	1.5	0.0167	± 0.05

tribution since a Gaussian model can be specified uniquely by its first two moments.

3.2.2.2 Propagation of distribution

Uncertainties in the input parameters are modeled by Gaussian distribution and propagated based on the RBF metamodels as built in Section 2.9. Illustration of methodology of distribution propagation in the sheet metal draw bending process is demonstrated in Figure 3.17. The input parameters are sampled by LHS. The input parameters are assumed as continuous random variables. This represents aleatory uncertainties in the input parameters of sheet metal draw bending process.

One of the purposes of uncertainty propagation is to evaluate the statistical moments of the outputs. Figure 3.18 and Table 3.5 show probability density as well as the mean and standard deviation of β_1 , β_2 and ρ .

Table 3.5: The two first statistical moments of β_1 , β_2 and ρ

Parameters	β_1 [°]	β_2 [°]	ρ [mm]
Mean	17.823	12.7535	150.854
Standard deviation	0.9693	0.745	66.7696

It can be seen that the distribution shape of β_1 and β_2 is almost Gaussian, whereas that of ρ is not Gaussian. This shows strong nonlinearity of the model.

3.2.3 Analysis of the effects of uncertainties on the product performance

Depending on the part's functional requirements, the part performance can be represented in different ways. In this section, several geometric descriptions of perfor-

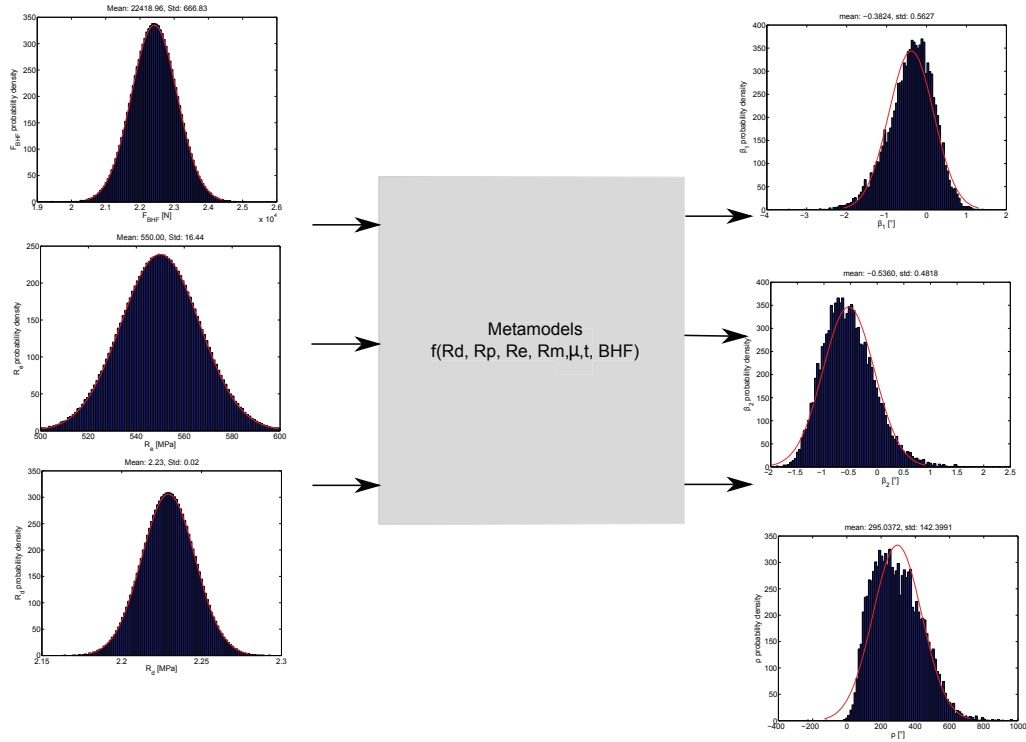


Figure 3.17: Illustration of proposed approach for distribution propagation.

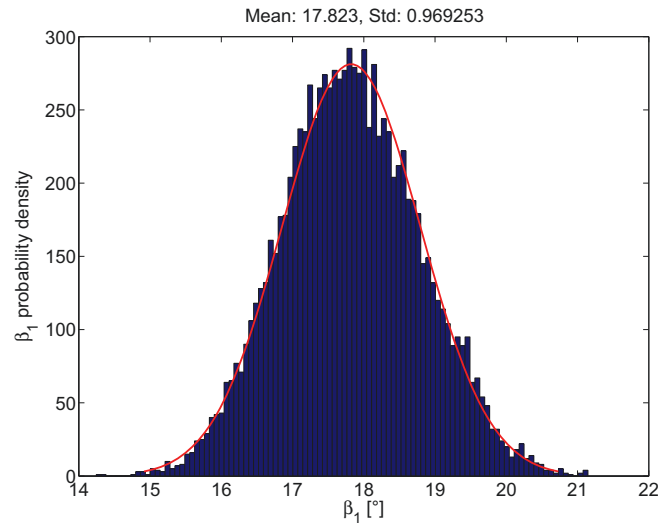
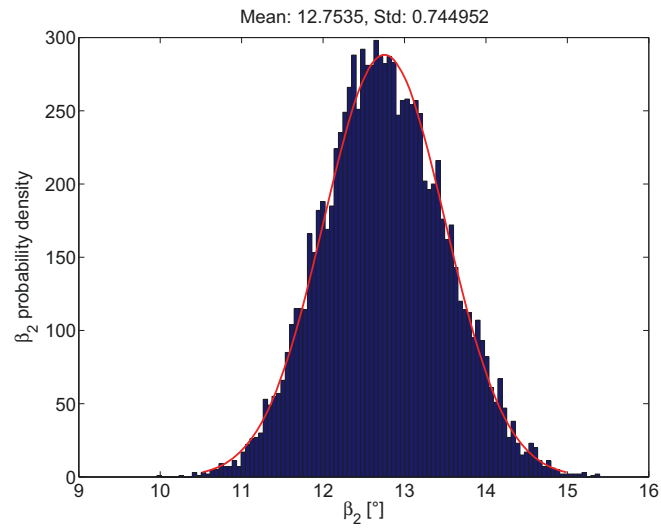
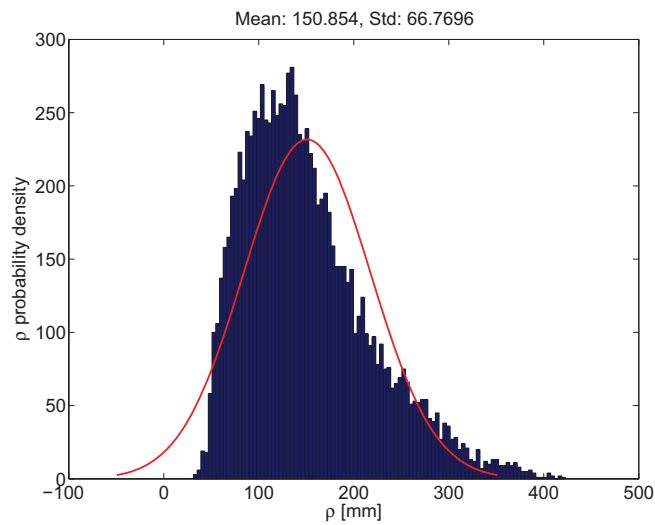
mance variations are presented.

3.2.3.1 Geometric tolerance analysis for the sheet metal part

Traditionally, initial design tolerances for mechanical parts are often selected from tolerance chart, which describes the natural variation of the processes by which parts are made. This chart indicates the range of variation achievable by each process. Also, the range of variation depends on the nominal size of the part dimension. However, these tolerance values are used as a estimate, since no parts have been made. In addition, the aleatory uncertainties are unavoidable in the manufacturing process, they result in the part performance variations.

In order to overcome these problems, an arbitrary geometric tolerance analysis for the sheet metal parts in the presence of uncertainty is suggested. Geometric tolerances of the sheet metal part under consideration are presented in Figure 3.19. In particular, flatness, parallelism, position and perpendicularity tolerances are required to represent the performance variations due to manufacturing imprecisions. These geometric tolerances' values are determined through nodal coordinates of the formed part which have been obtained from FEM numerical simulation.

Analysis of geometric tolerances for the sheet metal part is carried out on the basis of uncertainty propagation. Figure 3.22 and 3.23 show the probability density of geometric tolerances obtained by propagating the uncertainties of input param-

(a) β_1 probability density(b) β_2 probability density(c) ρ probability densityFigure 3.18: The probability density of β_1 , β_2 and ρ

3.2. Uncertainty propagation in sheet metal forming process design 101

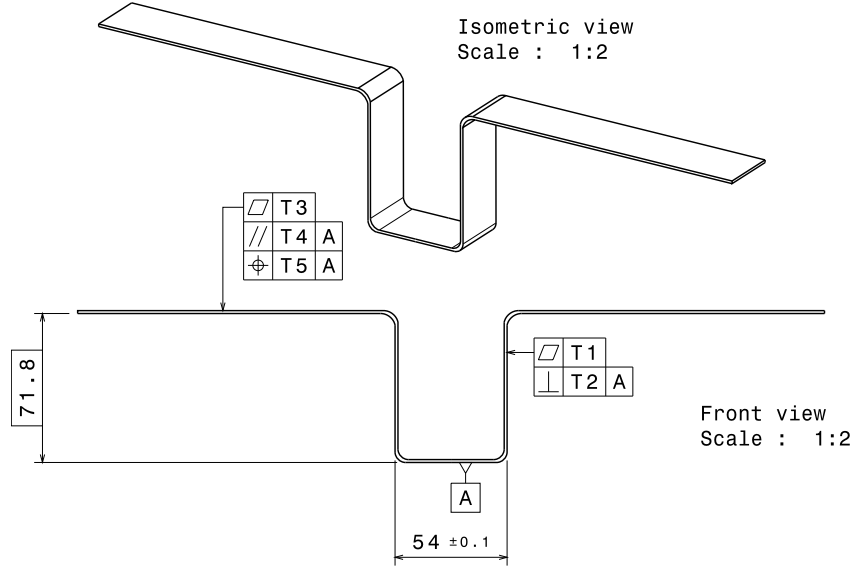


Figure 3.19: Geometric tolerances of the sheet metal part.

ters on metamodels of the geometric tolerances. The metamodels of the geometric tolerances with respect to F_{BHF} and R_d are shown in Figure 3.20 and 3.21.

As can be seen from Figure 3.22 and 3.23, it is found that due to the uncertainties in the inputs, the variations in performance are quite large. This can lead to troubles in the assembly process. In order to tackle this problem, process design optimization will be carried out in Chapter 4.

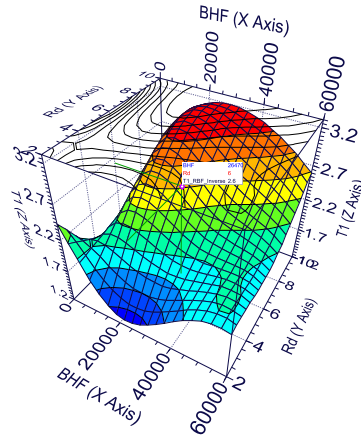
3.2.3.2 An example of determination of performance variations based on functional requirement

According to the part's functional requirement, it is subsequently assembled with other components as illustrated in Figure 3.24. It is assumed that the components are assembled each other by rivets. To ensure that there is no problem in the assembly process, the components need to work properly as functioned. Hence, the holes' position variation on the components due to the springback should be taken into account.

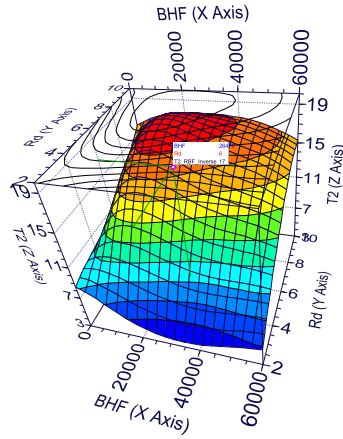
Figure 3.25 shows cross-sections of the components in the assembly system.

In order to determine the variability of hole position due to the springback, the cross-section 5 through the part 1 is considered as shown in Figure 3.25. Hole position, marked by point T, before and after springback with a half of the part 1 is demonstrated in Figure 3.26. The functional requirement of the hole on the part includes:

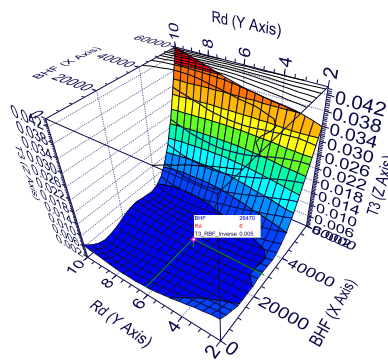
- The position of the hole from the reference point in the horizontal axis is 100 [mm].



(a) $T1$ flatness tolerance with respect to F_{BHF} and R_d

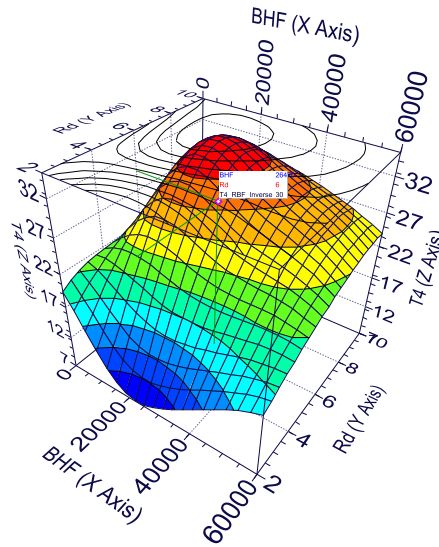


(b) $T2$ perpendicularity tolerance with respect to F_{BHF} and R_d

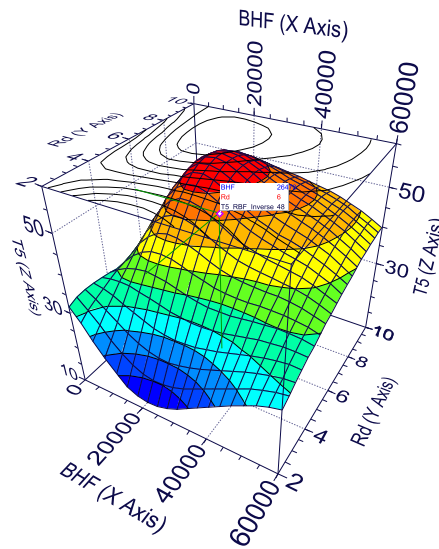


(c) $T3$ flatness tolerance with respect to F_{BHF} and R_d

Figure 3.20: Probability density of geometric tolerances of $T1$, $T2$, $T3$

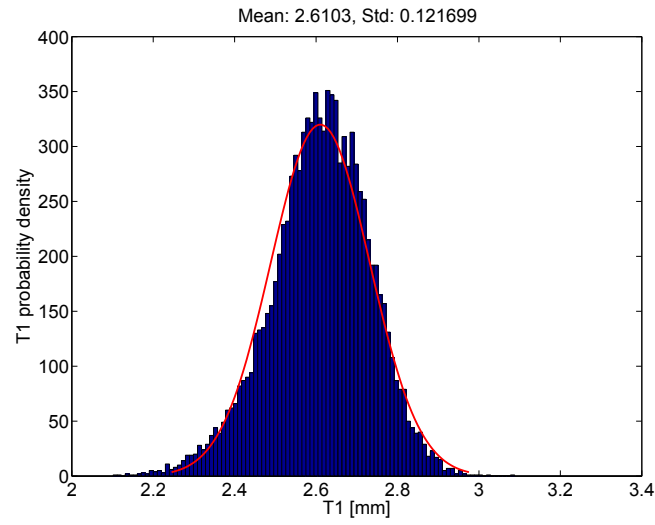
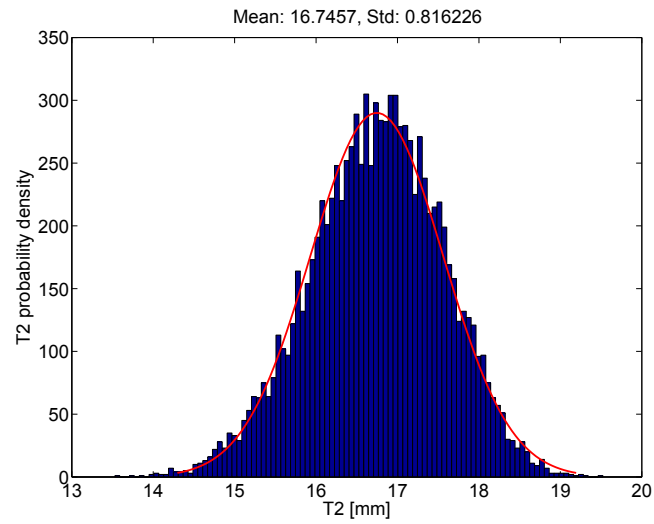
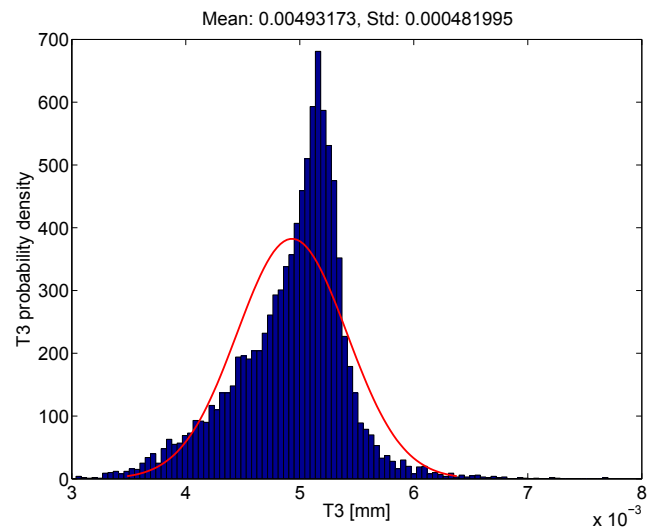


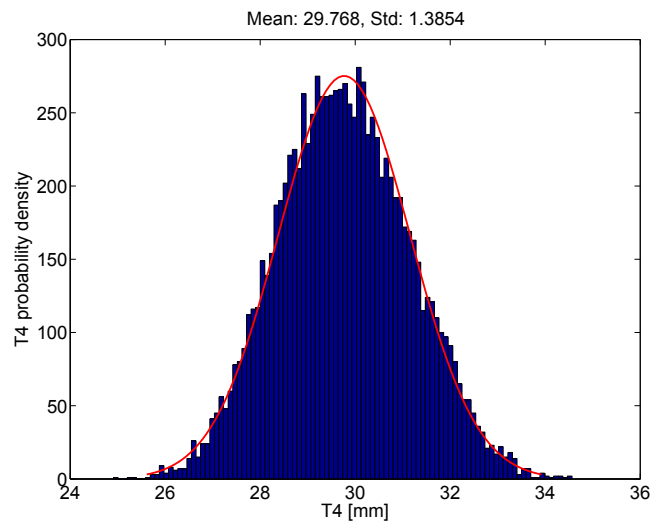
(a) $T4$ parallelism tolerance with respect to F_{BHF} and R_d



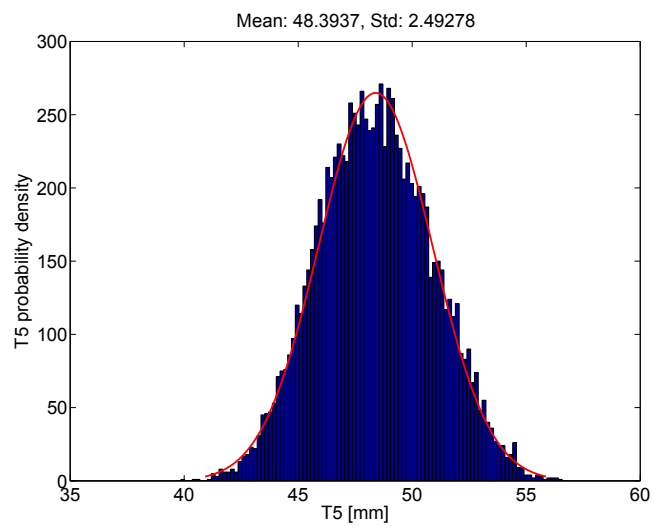
(b) $T5$ position tolerance with respect to F_{BHF} and R_d

Figure 3.21: Probability density of geometric tolerances of $T4$ and $T5$

(a) Probability density of $T1$ flatness tolerance(b) Probability density of $T2$ perpendicularity tolerance(c) Probability density of $T3$ flatness toleranceFigure 3.22: Probability density of geometric tolerances of $T1$, $T2$, $T3$



(a) Probability density of $T4$ parallelism tolerance



(b) Probability density of $T5$ position tolerance

Figure 3.23: Probability density of geometric tolerances of $T4$ and $T5$

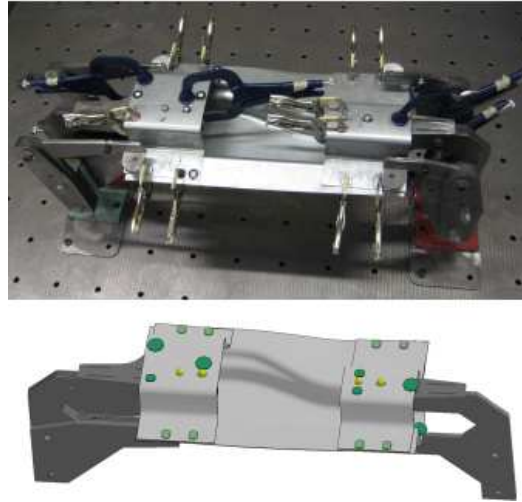


Figure 3.24: Components assembled in the system [72].

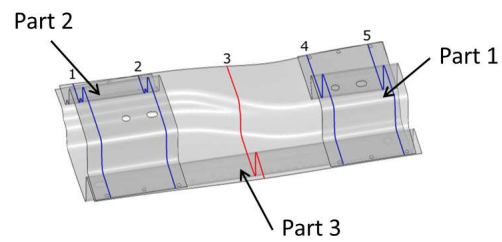


Figure 3.25: Cross-sections in the assembly system [72].

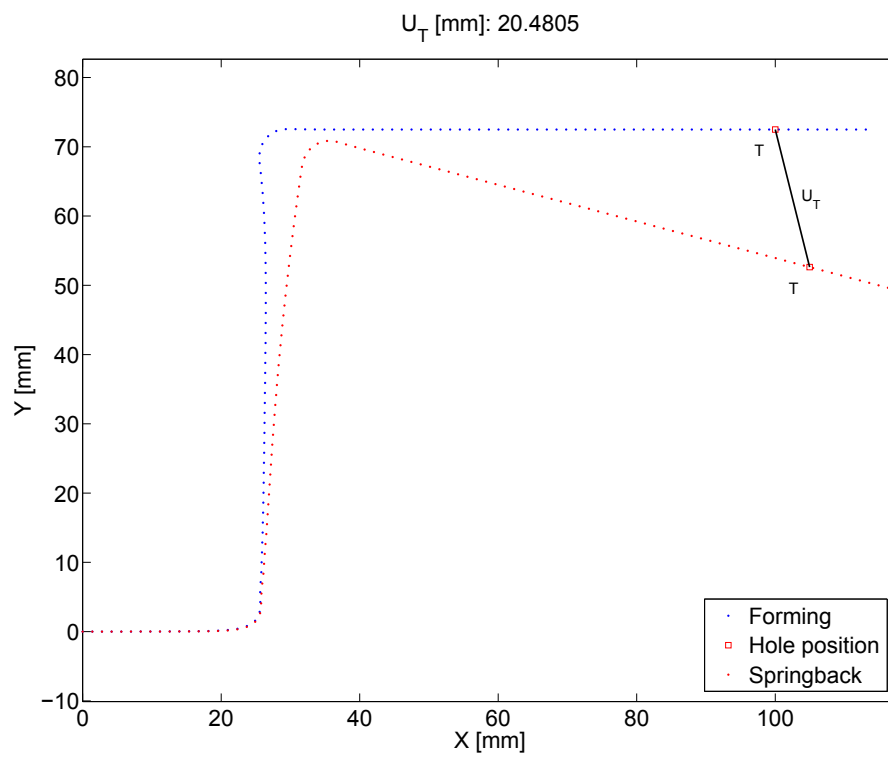


Figure 3.26: The variability of hole position before and after springback.

- The magnitude of the hole's displacement should be in allowable tolerance interval.

However, the sheet metal components used in this semi-industrial case study usually have large shape defects due to the springback. Thus, taking into account the components' performance variations caused by the uncertainties of input parameters in the early design process is required.

In short, the magnitude of hole displacement after springback is considered as an output variable in this case study. Instead of taking into account the effect of uncertainties on the springback measurements of β_1 , β_2 and ρ , the effect of uncertainties on the magnitude of hole displacement U_T is investigated. The magnitude of hole displacement is defined by:

$$U_T = \sqrt{(x_T - x_T^0)^2 + (y_T - y_T^0)^2} \quad (3.31)$$

where (x_T^0, y_T^0) is coordinate of point T before springback and (x_T, y_T) is coordinate of point T after springback.

3.2.3.3 Metamodel and uncertainty analysis for U_T

In order to figure out which RSM is best fit for the results of U_T from the DOE, comparison between the accuracy of the metamodels is investigated as shown in Table 3.6. As can be seen from Table 3.6, the RBF has the best accuracy for fitting

Table 3.6: Comparison of accuracy of metamodels for U_T

RSM	Responses	MAE	R-square
Kriging	U_T	1.0258×10^{-4}	0.9999
SVD2	U_T	36.6112	0.8268
SVD3	U_T	38.6366	0.9370
RBF	U_T	5.7494×10^{-10}	1
NN	U_T	16.9244	0.9988

the U_T . Therefore, it is used to build metamodel. Figure 3.27 shows metamodel of U_T with respect to F_{BHF} and R_d . With the same input parameters as presented in Table 3.4, Figure 3.28 shows the probability density as well as mean and standard deviation of hole displacement U_T . It can be seen that the variation of hole position is significant due to aleatory uncertainties in the inputs. Also, the hole displacement is quite large, thus reducing its displacement and variation is necessary. As a solution of this problem, the MORDO will be proposed in the Chapter 4.

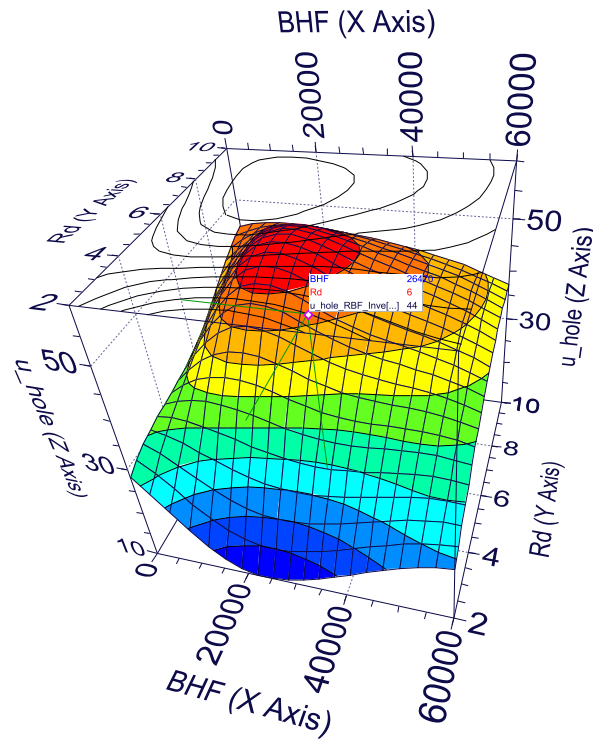


Figure 3.27: Metamodel of U_T with respect to F_{BHF} and R_d .

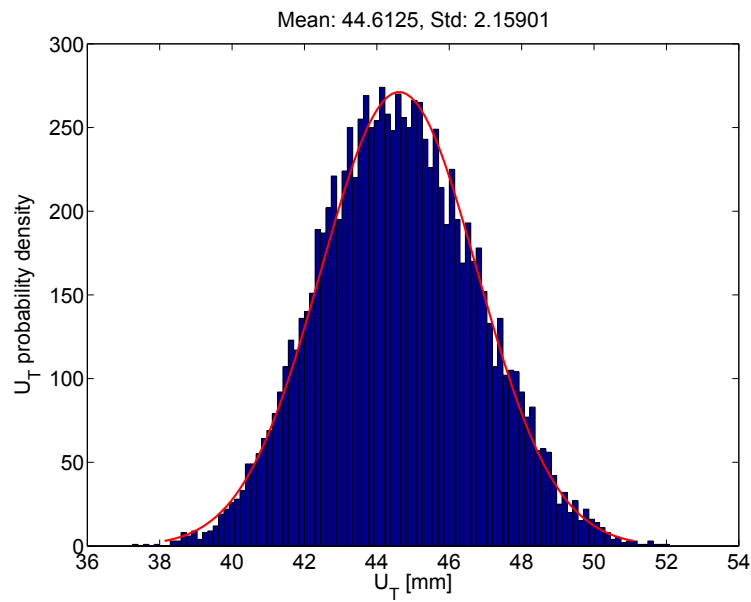


Figure 3.28: The probability density of hole displacement U_T .

3.2.3.4 Prediction of process capability based on C_{pk}

In contrast of tolerance analysis as mentioned above, prediction of process capability is carried out based on customer requirements which are defined by specification limits. Process capability is the ability of a process to produce output within specification limits [151]. In other words, measures of process fallout are estimated. Process fallout quantifies how many defects a process produces and is measured by Defects Per Million Opportunities (DPMO) or Parts Per Million (PPM). If the process output is approximately normally distributed, the relationships between the process capability index C_{pk} and process yield as well as process fallout are shown in Table 3.3. From the geometric tolerance limits are given by the customer requirements, the process capability index C_{pk} is subsequently calculated and compared with the parameters in Table 3.3 to evaluate the process capability. The index C_{pk} is defined by the following formula as reviewed in Section 3.1.5.3:

$$C_{pk} = \frac{\frac{IT}{2} - |\delta|}{3\sigma} \quad (3.32)$$

Moreover, with given values of C_{pk} as shown in Table 3.3, the IT values are determined as follows:

$$IT = 6\sigma C_{pk} + 2|\delta| \quad (3.33)$$

3.3 Summary of the chapter

This chapter focuses on uncertainty propagation and analysis of the effects of uncertainties on the output parameters. The methods for modeling, representing and propagating uncertainties have been reviewed. Uncertainty classification in modeling and simulating sheet metal bending process is given, in particular uncertainties in material properties, blank thickness and friction condition are considered as aleatory uncertainties which are uncontrollable factors. The aleatory uncertainties are modeled by Gaussian distribution. Errors introduced by numerical methods in FEM numerical model of the process are regarded as epistemic uncertainties. In order to reduce the effects of epistemic uncertainties in FEM numerical model, an approach for detecting the sensitivity threshold has been proposed as presented in Chapter 2.

The criteria for evaluating the product quality and process capability has been also reviewed. Uncertainty propagation based on metamodels built by RBF is carried out. Geometric tolerance analysis based on geometric variations caused by uncertainties in the inputs and based on the C_{pk} index is introduced. It is found that due to the uncertainties in the inputs, the variation in performance of the formed part is quite large.

In order to investigate the effects of geometric variation of the formed part due to uncertainties on the assembly process, the displacement of a hole on the part has been taken into account. Observation from uncertainty analysis for the hole displacement shows that the performance of hole position varies significantly.

Prediction of process yield based on the C_{pk} index shows that the process design being subjected to uncertainties of input parameters gives significant changes in production and non-conform parts.

It is required to optimize the process to meet the tolerances specifications.

Optimization under uncertainty of sheet metal forming

Contents

4.1 State-of-the-art	113
4.1.1 Robust design and Reliability-based design	113
4.1.2 Optimization under uncertainty	127
4.1.3 Multi-objective optimization and Pareto optimality	134
4.1.4 Algorithms for multi-objective optimization	137
4.2 Multi-objective optimization strategy under uncertainty for sheet metal forming process	140
4.2.1 Deterministic process design optimization	141
4.2.2 Uncertainty analysis	147
4.2.3 Multi-objective robust design optimization (MORDO)	149
4.2.4 Pareto multiple objective criteria decision-making support based on capability indices	153
4.2.5 Synthesis of results	164
4.3 Summary of the chapter	166

4.1 State-of-the-art

4.1.1 Robust design and Reliability-based design

Various non-deterministic methods have been developed to deal with design uncertainties. These methods can be classified into two approaches, namely reliability-based methods and robust design based methods.

4.1.1.1 Robust design

A robust design is a design which is insensitive to variations. The term *Robust Design* was originally introduced by the Japanese engineer Genichi Taguchi in the 1950s and early 1960s, also known as Taguchi method, as a way of improving the quality of product and processes by reducing their sensitivity to variations resulting from uncertainty, thereby reducing the effects of variability without eliminating its sources [208], [211], [4] [115].

According to Taguchi, product design is a more cost-conscious and effective way to realize robust, high quality products than by tightly controlling manufacturing processes. Taguchi noticed that there are two ways a product may prove to be unsatisfactory - the product may not meet target performance specifications or the variability in the product's performance may be unacceptably large. From Taguchi's perspective, tolerance design which involves tightening tolerances on product or process parameters is expensive and should be utilized only when robustness cannot be "designed in" by selecting parameter levels that are least sensitive to variations [4]. Taguchi's approach to the product design process may be divided into three stages [208]:

(1) *System design*: is the conceptual design stage where the system configuration is developed. This stage determines the basic performance parameters of the product and its general structure.

(2) *Parameter design*: sometimes called robust designs identifies factors that reduce the system sensitivity to noise, thereby enhancing the system's robustness.

(3) *Tolerance design*: specifies the allowable deviations in the parameter values, loosening tolerances if possible and tightening tolerances if necessary.

Robust design occurs during the parameter design stage that precedes tolerance design but follows the system design in which a preliminary layout is specified for the product or process. Taguchi notes that too many tolerance-driven engineers skip directly from system design to tolerance design and ignore the critically important parameter design stage.

Instead of measuring quality by means of tolerance ranges, Taguchi proposed a quality loss function in which the quality loss L is proportional to the square of the deviation of performance y from a target T as Figure 4.1. The quality loss function is defined as:

$$L = k(y - T)^2 \quad (4.1)$$

The quality loss function represents Taguchi's Philosophy of striving to deliver on-target products and processes rather than those that barely satisfy a corporate limit or tolerance level. Figure 4.2 shows the different types of performance variations, where the large circles denote the target and the response distribution is indicated by the dots and the associated probability density function. The aim of robust design is to make the system response close to the target with low variations, without eliminating the noise factors in the system, as illustrated in Figure 4.2(d). In the robust design, there are three categories of information [4]: control factors, noise factors, and responses as shown in Figure. Control factors, also known as design variables, are parameters that a designer adjusts to reach a desired product. Noise factors are exogenous parameters that affect the performance of a product or process but are not under a designer's control. Responses are performance measures for the product or process.

Robust design is classified differently according to various viewpoints. Synthesis of classification of robust design is shown in Table 4.1. Park et al. [166] classified robust design into three methods: (1) the Taguchi method, (2) robust optimization

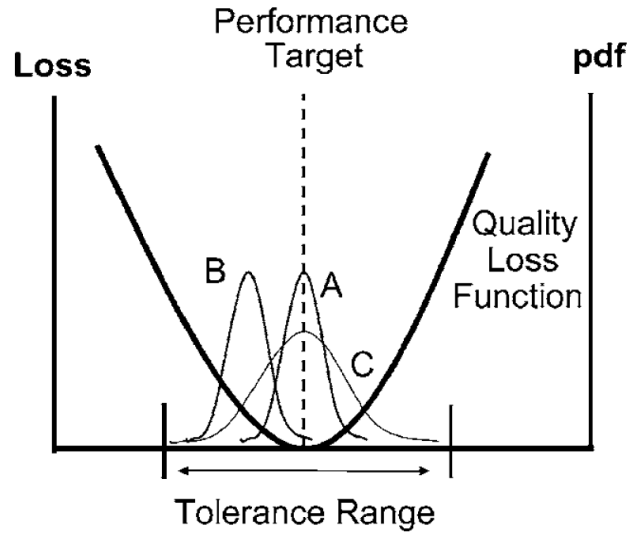


Figure 4.1: The quality loss function and performance target for three manufactured products whose performance varies through different ranges and whose values of mean performance may or may not coincide with the desired performance [4]

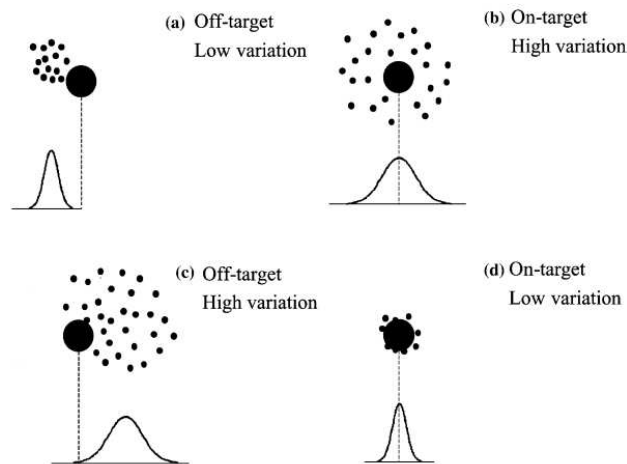


Figure 4.2: Different types of performance variations [246].

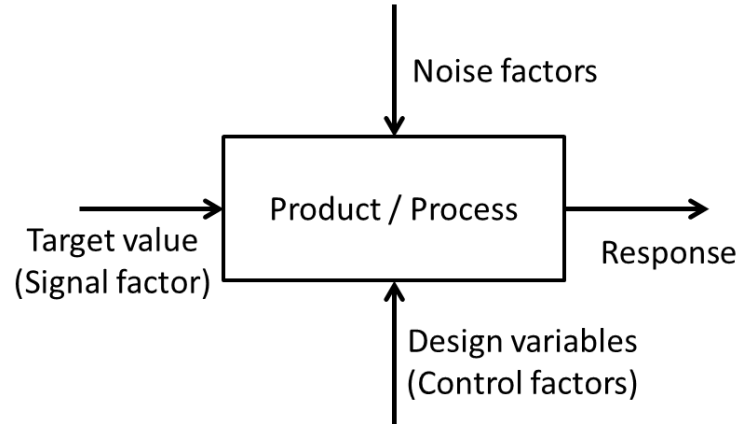


Figure 4.3: A *P*-diagram showing information input and response in a product or process model [4].

Table 4.1: Synthesis of classification of robust design

Classification of Robust Design			
Zang et al. 2005 [246]	Park et al. 2006 [166]	Choi 2006 [33] and Allen et al. 2006 [4]	
Taguchi method	Taguchi method	Type I - Taguchi method	
Optimization method	Robust optimization	Type II - Managing uncertainty in controllable parameters	
Stochastic optimization method	Robust design with the axiomatic approach	Type III - Managing uncertainty embedded in system functions	
		Type IV - Managing propagated uncertainty in a design and analysis process chain	

(3) robust design with the axiomatic approach. According to Zang et al. [246] robust design is classified into three categories including Taguchi, optimization and stochastic optimization methods. However, Choi et al. [33] and Allen et al. [4] distinguish four main types of robust design based on the source of variability, namely as follows:

- Type I - Managing uncertainty in uncontrollable parameters: Robust design aims to identify design variables that satisfy the design requirements despite variation in noise factors (aleatory uncertainty). Type I robust design was proposed by Taguchi.

Suppose that y is a function of control factors x and noise factors z , then:

$$y = f(x, z) \quad (4.2)$$

where the function f can be a detailed simulation model, a surrogate model, or a physical system. Taguchi's robust design evaluates the mean performance and its variation by crossing two arrays: an inner array, designed in the control variables, and an outer array, designed in the noise variables. Figure 4.4 a two

		Noise Array									
						Z ₂					
						Z ₁					
		x ₁	x ₂	x ₃	.		1	2	3	4	.
Control Array	1	+	+	+	.		Y ₁₁	Y ₁₂	Y ₁₃	.	.
	2	-	+	+	.		Y ₂₁	Y ₂₂	Y ₂₃	.	.
	3	+	-	+	.		Y ₃₁	Y ₃₂	Y ₃₃	.	.
	4	-	-	+	.		Y ₄₁	Y ₄₂	Y ₄₃	.	.

							μ _{y1}	σ _{y1}	S/N _{y1}	L _{y1}	
							μ _{y2}	σ _{y2}	S/N _{y2}	L _{y2}	
							μ _{y3}	σ _{y3}	S/N _{y3}	L _{y3}	
							μ _{y4}	σ _{y4}	S/N _{y4}	L _{y4}	

Figure 4.4: Taguchi robust design matrix [248].

level factorial design is adopted for both the inner and outer array. For each row of the inner array, response values are generated for each noise variables combination. For example, inner array row 1 with outer column 1 leads to the response value y_{11} , inner row 1 with outer column 2 leads to response value y_{12} , and so on. This design then leads to multiple response values for each combination of control variables, from which a response mean, μ , and variance or standard deviation, σ , can be computed [248].

Given the mean and variance for each inner array row, the experiments can be compared to determine which set of control settings best achieves "mean on target" and "minimized variation" performance goals.

The Mean Square Deviation (MSD) measures the deviation of y from the desired target value T :

$$MSD := \frac{1}{n} \sum_{i=1}^n (y_i - T)^2 \quad (4.3)$$

Taguchi proposed the signal-to-noise ratio (SNR):

$$SNR = -10\log_{10}(MSD) = -10\log_{10} \left(\frac{1}{n} \sum_{i=1}^n (y_i - T)^2 \right) \quad (4.4)$$

as measure of the MSD in the performance. The use of SNR in system analysis provides a quantitative value for response variation comparison. Taguchi used the SNR as an optimization criterion. Maximizing the SNR results in the minimization of the response variation and more robust system performance is obtained. There are many different SNR. However, there are four primary ones suggested by Taguchi. Specific SNR depend on the goal of the experiment. Only three is considered here. *The smaller the better*: Taguchi treats this case as if there is a target value of zero for the response. Thus

$$SNR = -10\log_{10}(MSD) = -10\log_{10} \left(\frac{1}{n} \sum_{i=1}^n y_i^2 \right) \quad (4.5)$$

The larger the better: This case is treated in the same fashion as the smaller the better case, but y_i is replaced by $1/y_i$. As a result, the SNR is given by

$$SNR = -10\log_{10}(MSD) = -10\log_{10} \left(\frac{1}{n} \sum_{i=1}^n \frac{1}{y_i^2} \right) \quad (4.6)$$

The target is best: In this case, we are attempting to determine values of x that achieve a target value for the response. Deviations in either direction are undesirable. If the control parameters are chosen such that $\bar{y} = T$ (the population mean is the target value), then the MSD is just the population variance. If the population standard deviation is related to the mean, then the MSD may also be scaled by the mean to give

$$SNR = -10\log_{10}(MSD) = -10\log_{10} \left(\frac{S^2}{\bar{y}^2} \right) = 10\log_{10} \left(\frac{\bar{y}^2}{S^2} \right) \quad (4.7)$$

In general, there are two goals in performing robust design. One is to minimize the variability produced by the noises factors. The other is to make the mean value close to the target value. The design to attain one goal is not usually consistent with the one to attain the other goal. To meet the two goals, Taguchi developed a two-step optimization strategy. The first step is to reduce the variation, and the second step is to adjust the mean on the target. The procedure is shown in Figure 4.5. The first step, shown in Figure 4.5(a),

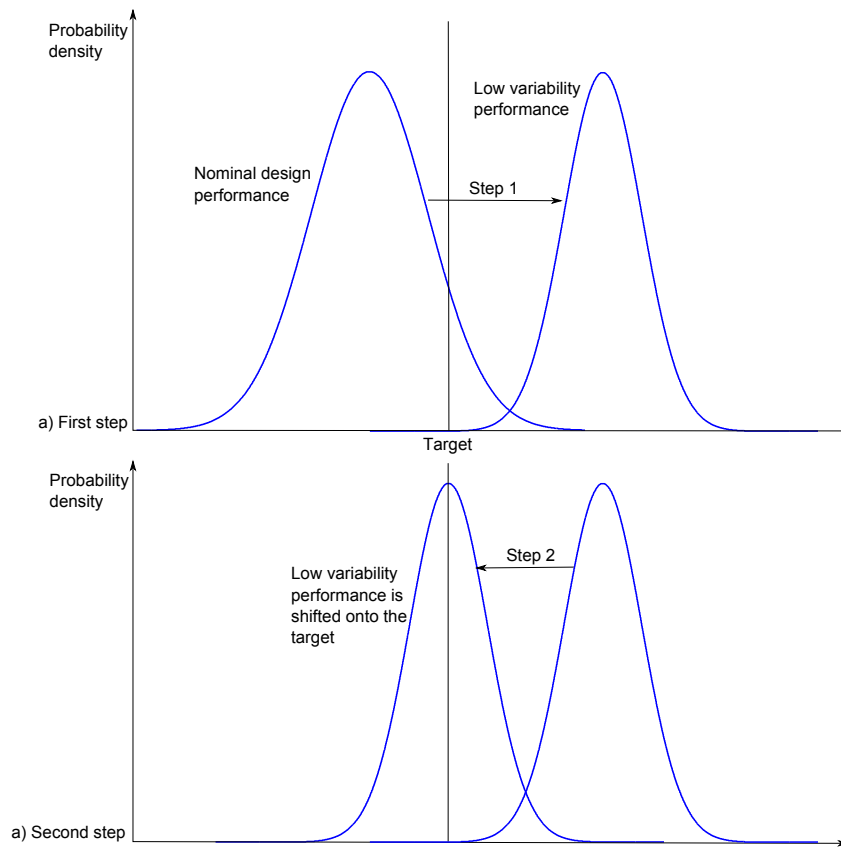


Figure 4.5: Two steps of Taguchi method [166].

concentrates on minimization of the variation, while the mean is ignored. In the second step (Figure 4.5(b)), the mean is moved to the target value while sacrificing the improved variation somewhat [208], [209] [171],[210], [166].

The principle of the Taguchi method is easy to understand and does not require a strong background in statistics [166]. However, the Taguchi method has several drawbacks. First of all, the SNR is criticized since it combines the mean and variance of the response and hence, mean and variance are confounded. This means that one cannot distinguish which variables affect the mean and which variables affect the variance. Other drawbacks of the Taguchi method are the many function evaluations required for the crossed array design and the impossibility of taking into account interaction effects between design variables [221], [97], [236].

Although Taguchi's contributions to the Philosophy of robust design are almost unanimously considered to be of fundamental importance, there are certain limitations and inefficiencies associated with his methods [246]. Taguchi's techniques were based on direct experimentation. However, designers often use a computer to simulate the performance of a system instead of actual experiments. On the other hand, Box and Fung [63] pointed out that the orthogonal array method does not always yield the optimal solution and suggested that non-linear optimisation techniques should be employed when a computer model of the design exists. Box [18] pointed out that there are various mathematical difficulties/requirements associated with the use of signal-to-noise ratio. Montgomery [141] demonstrated that the inner array used for the control factors in the Taguchi's approach and the outer array used for noise factors, is often unnecessary and results in a large number of experiments. Tsui [220] showed that the Taguchi method does not necessarily find an accurate solution for design problems with highly non-linear behaviour.

- Type II - Managing Uncertainty in Controllable Parameters: Robust design aims to identify the design variables that satisfy the design requirements despite the variations (aleatory uncertainty) in the design variables themselves. Type II robust design was proposed by Chen et al. [30] as shown in Figure 4.6. Type II robust design is different from Type I in that its input does not include a noise factor. The variation in performance is caused solely by variations in control factors or design variables [30]. In Type II robust design, designers search for means of control factors that satisfy a set of performance requirement targets despite variation in control factors. For example, in the early stages of design, it is clear that design variable values will change as the design evolves; therefore it is preferable to identify starting values which, if they change, have the least possible effect on the system performance and thus require minimal iteration as the design process proceeds [4].

A method combining Types I and II robust design in the early stages of product development, namely, the Robust Concept Exploration Method (RCEM)

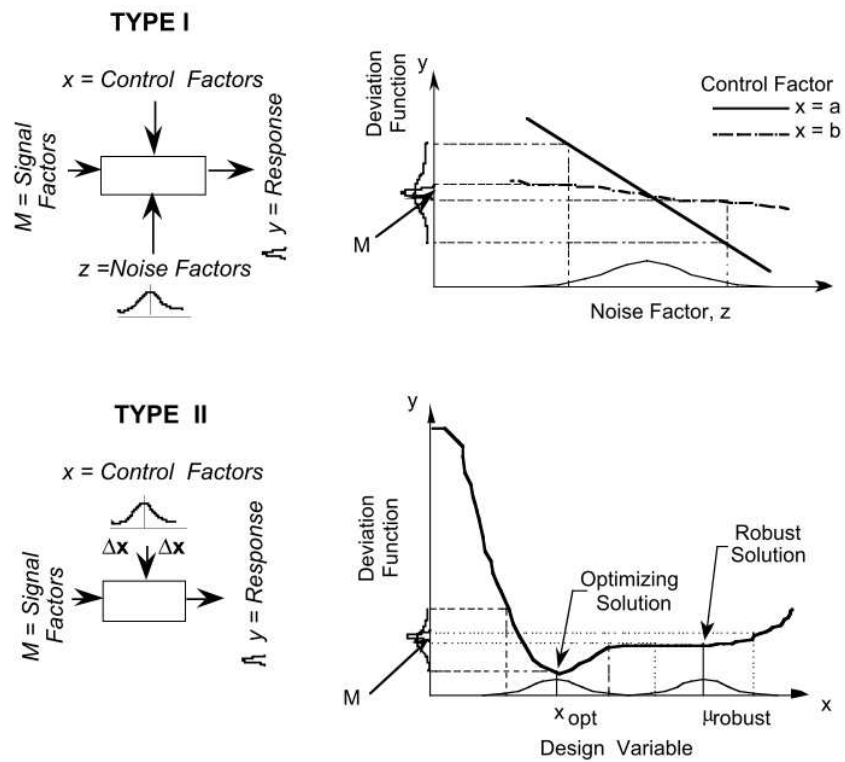


Figure 4.6: A comparison of two types of robust design [30].

[31] has been developed. RCEM is a domain-independent approach for generating robust, multidisciplinary design solutions. RCEM has been employed successfully for a simple structural problem and design of a solar powered irrigation system [31], a High Speed Civil Transport [29], a General Aviation Aircraft [197], product platforms [199], and other applications.

- Type III - Managing Uncertainty Embedded in System Functions: Robust design identifies the adjustable ranges for design variables that satisfy the set of performance requirement targets and are insensitive to variability (epistemic uncertainty) within the system model. For example, a model may incorporate simplifying assumptions or random factors (e.g., random realizations of a micro-structure in materials design) that affect the accuracy and precision of its predictions [4]. Figure 4.7 illustrates Type III Robust design.

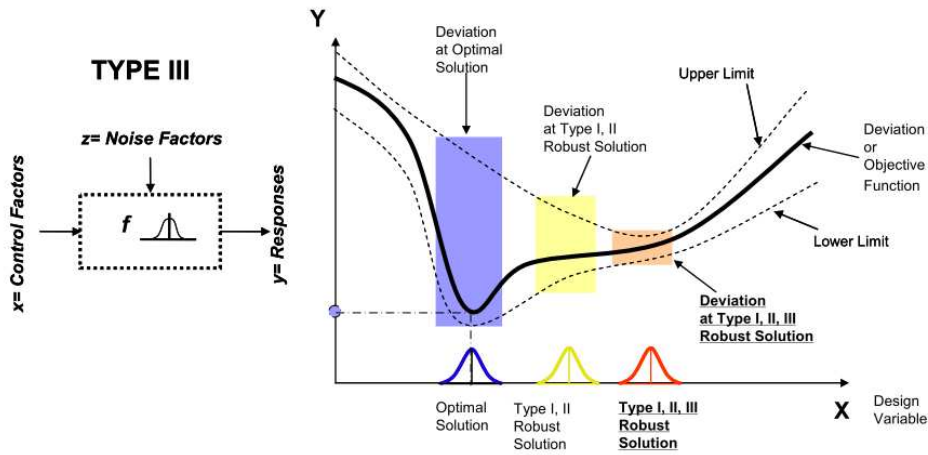


Figure 4.7: Type III Robust design [33].

- Type IV - Managing Propagated Uncertainty in a Design and Analysis Process Chain: Robust design identifies the adjustable ranges of design variables under potential uncertainty (aleatory and epistemic uncertainty) and uncertainty propagation in a design and analysis process chain; accounts for uncertainty in downstream activities and uncertainty propagation. Type IV robust design is focused on uncertainty associated with the design process chain as shown in Figure 4.8 [33].

4.1.1.2 Reliability-based design

Reliability-based design was developed based on reliability analysis. Reliability analysis is essentially concerned with calculating the probability that a system may fail given a statistical model of the uncertain parameters affecting its response. To illustrate, consider the case when the criterion governing failure of the system under

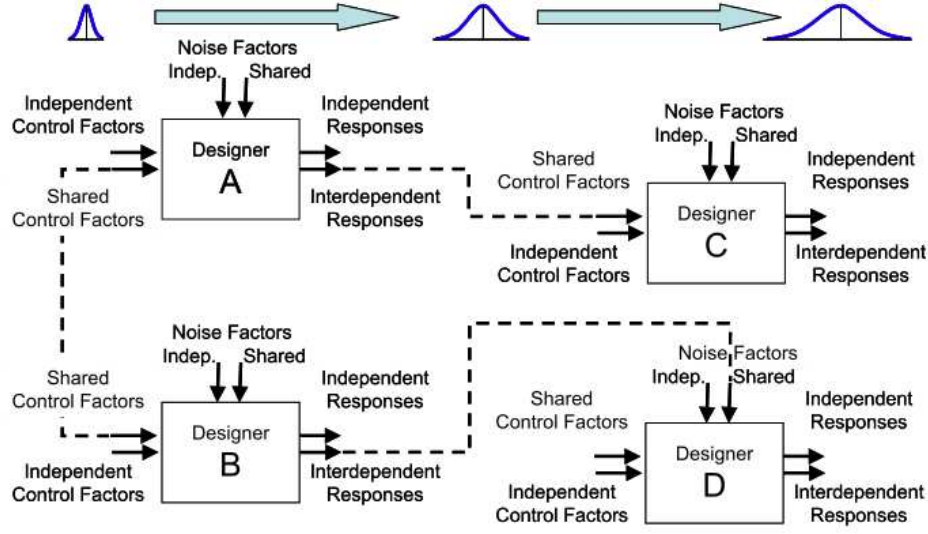


Figure 4.8: Type IV Robust design [33].

consideration can be written as $g(X) \leq 0$, where $X \in R^{pX}$ is a set of random variables whose statistics are known. The equation $g(X) = 0$ is commonly referred to as the limit state function or the equation of the failure surface. Figure 4.9 depicts how the limit state function partitions the uncertainty space into the failure domain and the safety domain [99]. The central focus of reliability analysis is the development of efficient numerical methods for calculating the probability of failure P_f that $g(X) \leq 0$, that is,

$$P_f = P[g(X) \leq 0] = \int_{g(X) \leq 0} p(X) dX \quad (4.8)$$

where $p(X)$ is the joint PDF of X . The reliability of the system under consideration is then given by $(1 - P_f)$ or $100(1 - P_f)\%$. Reliability-based design method is illustrated in Figure 4.10.

The integral in Equation 4.8 is difficult to evaluate in practice for the following reasons [99]:

- (1) the domain of integration $g(X) \leq 0$ is usually not available in analytical form and is often computed by running a computationally expensive computer model,
- (2) in practice, pX can be large and hence direct numerical evaluation of the multidimensional integral is often computationally prohibitive,
- (3) in many situations, only the first two statistical moments of X are available and hence assumptions have to be made regarding the structure of the joint pdf $p(X)$.

The probability of failure can be approximated by the Monte Carlo estimate [99]:

$$P_f \approx \frac{1}{m} \sum_{i=1}^m I[g(X^i) \leq 0] \quad (4.9)$$

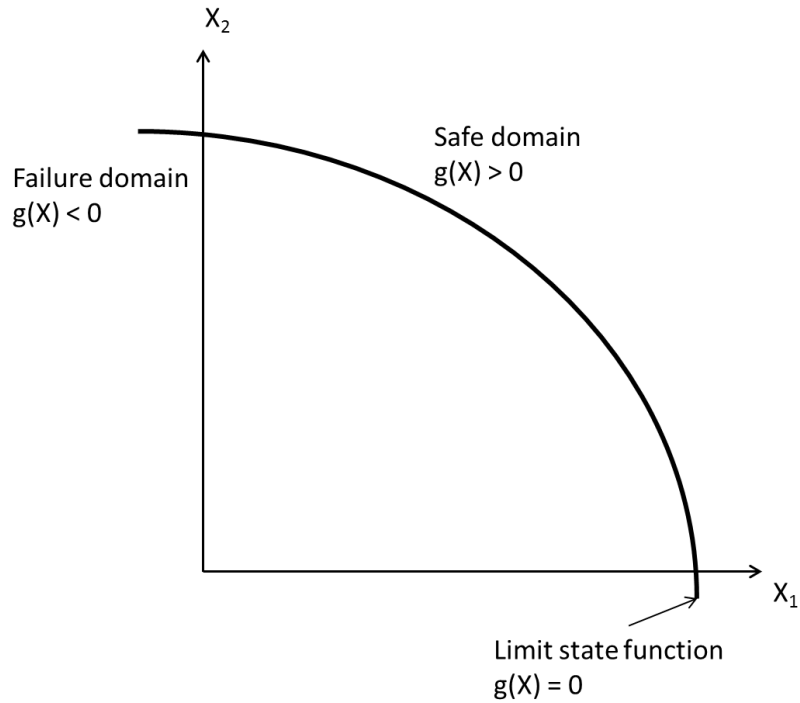


Figure 4.9: Limit state function in reliability analysis. The region where $g(X) < 0$ is the failure domain whereas the region where $g(X) > 0$ is the safe domain [99].

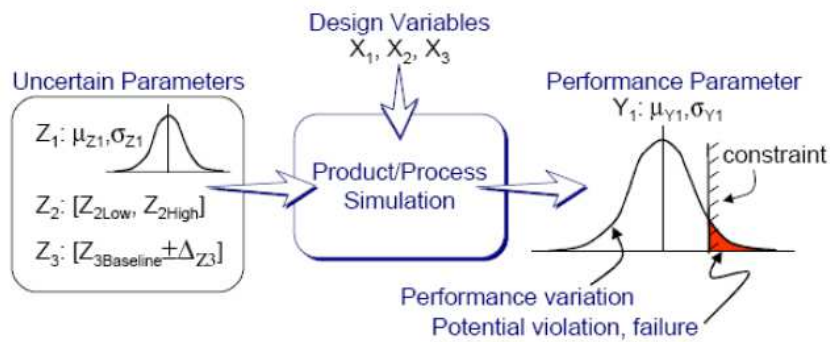


Figure 4.10: Reliability-based design [249].

where I is the indicator function which returns the value 1 if $g(X^i) \leq 0$ and 0 if the converse is true. The reliability of the system R can be calculated as:

$$R = 1 - P_f = 1 - \left(\frac{\#SimulationsInFailureRegion}{Total\#SystemSimulations} \right) = \left(\frac{\#SimulationsInSafeRegion}{Total\#SystemSimulations} \right) \quad (4.10)$$

This calculation is executed by the following steps [249]: (1) Model and represent random variables by appropriate distributions in which their properties are indicated.

(2) Specify the number of simulations to be executed.

(3) Generate uniformly distributed random numbers for each random variable.

(4) Convert each uniform random number to a random variable value corresponding to appropriate distribution.

(5) Evaluate failure function(s) using random variable values, and determine whether simulation point is a success ($g(X) > 0$) or failure ($g(X) < 0$) for each failure function $g(X)$.

(6) Repeat step 3 through step 5 for the number of simulations specified in step 2.

(7) Compute reliability R for each failure function.

Moreover, the first-order reliability method (FORM) and second-order reliability method (SORM) are two popular methods which were developed based on reliability analysis.

- First Order Reliability Method (FORM):

The FORM [80] linearizes $g(X)$ at the MPP (Most Probable Point) in the transformed U-space, which consists of independent standard normal variables U that are transformed from independent random variables X . The transformation is given by [179]:

$$F_{X_i}(X_i) = \Phi(U_i) \quad (4.11)$$

where F_{X_i} and Φ are the cumulative distribution functions (CDF) of X_i and U_i respectively.

$$U_i = \Phi^{-1}F_i(X_i) \quad (4.12)$$

If X_i ($i=1, \dots, n$) are dependent, the transformation is given by the Nataf transformation [179],

$$\begin{aligned} U_1 &= \Phi^{-1}F_{X_1}(X_1) \\ U_2 &= \Phi^{-1}F_{X_2|X_1}(X_2|X_1) \\ U_3 &= \Phi^{-1}F_{X_3|X_1, X_2}(X_3|X_1, X_2) \\ &\dots \end{aligned} \quad (4.13)$$

where $F_{X_2|X_1}(X_2|X_1)$ and $F_{X_3|X_1, X_2}(X_3|X_1, X_2)$ are conditional CDFs of X_2 and X_3 respectively

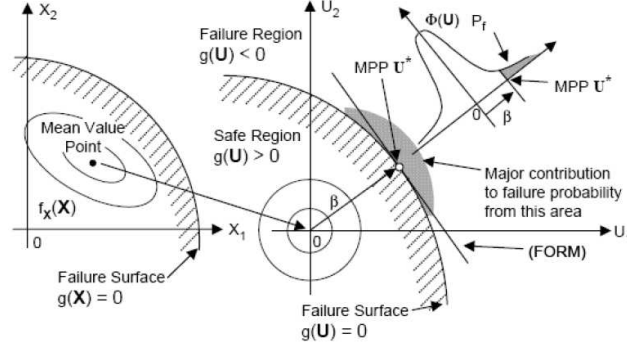


Figure 4.11: FORM reliability analysis method.

The MPP u^* is found by solving

$$\min \|u\| = \sqrt{\sum_{i=1}^n u_i^2} \quad (4.14)$$

subject to $\hat{g}(u) = 0$

where $\hat{g}(u)$ is the limit-state function in the U -space. Then the reliability index is calculated by

$$\beta = \|u^*\| = \left[\sum_{i=1}^n (u_i^*)^2 \right]^{1/2} \quad (4.15)$$

When $P_f < 0.5$, P_f computed by [123]

$$P_f = \Phi(-\beta) \quad (4.16)$$

A most probable point (MPP) search algorithm may need the derivative of $\hat{g}(U)$ [251]. If the derivative are evaluated numerically, the number of function calls will be linearly proportional to the number of random variables n . If the forward finite difference algorithm is used, the number of limit-state function calls N_{FORM} is

$$N_{FORM} = k(n + 1) \quad (4.17)$$

where k is the number of iterations of the MPP search. Because N_{FORM} is linear in terms of n , the FORM is first-order efficient.

- Second Order Reliability Method (SORM):

If $\hat{g}(U)$ is highly nonlinear, the FORM will be inaccurate. Then the SORM may be used. Breitung's formulation [23] for the SORM is given by

$$P_f = \Phi(-\beta) \prod_{i=1}^{n-1} (1 + \beta v_i)^{1/2} \quad (4.18)$$

where $v_i (i = 1, \dots, n-1)$ are the principal curvatures of $\hat{g}(U)$ at the MPP. The other popular SORM formulation is given by Tvedt [222], which is considered more accurate than the Breitung's formulation [252].

The SORM is more expensive than the FORM because second derivatives are required. If the forward finite difference formula is used for the derivative evaluation, the number of function calls by the SORM is

$$N_{SORM} = k(n+1) + \frac{n(n+1)}{2} = N_{MPP} + \frac{n(n+1)}{2} \quad (4.19)$$

The SORM is second-order efficient because N_{SORM} is quadratic in terms of n .

4.1.2 Optimization under uncertainty

Optimization under uncertainty is referred to combination of optimisation techniques and uncertainties in order to optimise robust manufacturing processes. Two approaches to Optimisation Under Uncertainty are often distinguished: robust optimisation and reliability based optimisation. Before discussing the two approaches, the approach of deterministic optimization will be described.

4.1.2.1 Deterministic optimization (DO)

A traditional optimisation problem is often formulated as [8]:

$$\text{Find} \quad x \quad (4.20a)$$

$$\text{to minimize} \quad f(x) \quad (4.20b)$$

$$\text{subject to} \quad g_i(x) \leq 0 (i = 1, 2, \dots, k) \quad (4.20c)$$

$$x_L \leq x \leq x_U \quad x \in R \quad (4.20d)$$

where the vector x denotes the vector of all input variables that one wants to choose in an optimal way. The variables are subjected to types of constraints, the functions g_i , that represent constraints on some given responses, and the second group of constraints which represents limits for the variables themselves. In a deterministic design optimization, the basic idea is to optimize a merit function subject to deterministic constraints and input variable bounds.

The functions can be evaluated by two methods. One is to use experiments when the function is not mathematically defined. The other is to use mathematical expression that are directly calculated or approximated by numerical approaches. This thesis is mainly focused on the latter method.

The aim of deterministic optimisation is to minimise objective function f subject to constraint $g \leq 0$. The input variables in this strategy can be exactly controlled. Running the FEM simulation for selected values of the input variables yields one value for each response. The deterministic optimum lies exactly on the constraint (the shaded area is the infeasible region) as shown Figure 4.12(a). This implies the

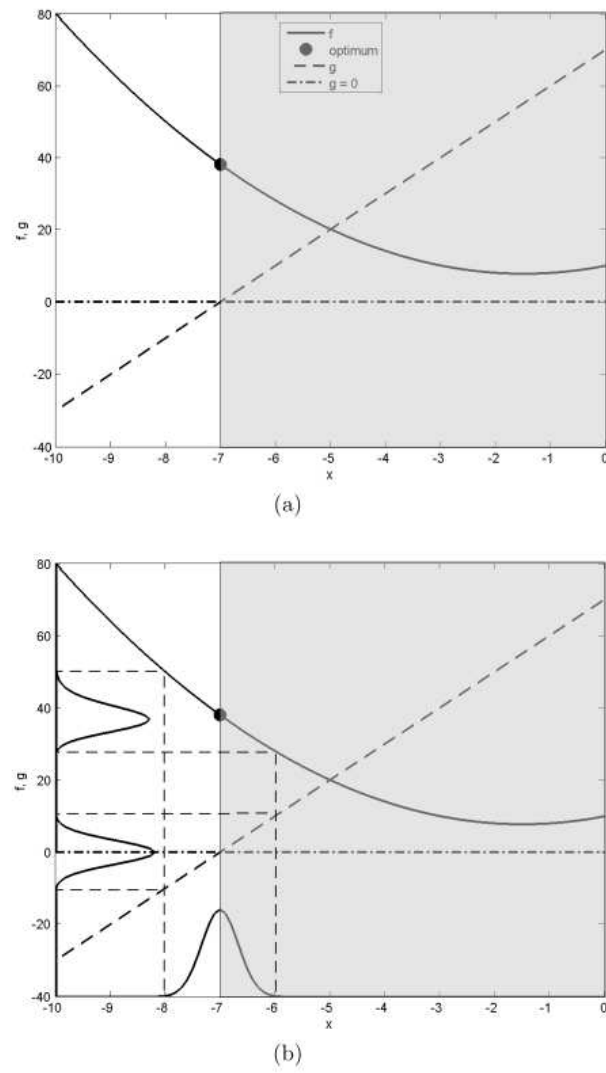


Figure 4.12: (a) Deterministic constrained optimisation; (b) Robustness and reliability of a deterministic constrained optimum where noise is present [15].

process is feasible, at least in a deterministic situation [15]. Unfortunately, in a real manufacturing environment, input variables cannot be controlled exactly. Moreover, some variables cannot be controlled at all, but show a large degree of variation. This variation is subsequently translated to the response quantities, which will display a probability distribution instead of one value only as illustrated in Figure 4.12(b). The deterministic constrained optimum input variable setting is now subject to noise. This causes response distributions of both objective function f and constraint g . The obtained response variation implies that the products violating the constraint will not satisfy demands after the process, which will result in scrap [15].

Large variations in response quantities will deteriorate product quality and a high scrap rate significantly contributes to the costs. Therefore, taking account of variation during optimisation in order to achieve a robust sheet metal forming process is very important. The DO of metal forming processes can be found in many research works, see e.g. [22], [87], [149], [15], [174].

4.1.2.2 Reliability Based Design Optimization (RBDO)

Due to the existence of uncertainties in either engineering simulations or manufacturing processes, RBDO is required to deal with the uncertainties as soon as in the design process. Reliability analysis and optimization are two essential components of RBDO: (1) Reliability Analysis focuses on analyzing the probabilistic constraints to ensure the reliability levels are satisfied; (2) Optimization is seeking for the optimal performance subject to the probabilistic constraints. The RBDO approach handles noise variables in a probabilistic way. The goal of RBDO is to minimize an objective function defined in terms of the nominal performance and its variability subject to a target reliability on the constraint functions. In other words, an original inequality constraint of the form $g \leq 0$ is replaced with a reliability constraint of the form $P[g \leq 0] \leq R_g$, where R_g is the specified reliability target and $P[\cdot]$ is the probability of failure. The probability that the inequality constraint is not satisfied is hence given by $1 - R_g$ [99].

When noise or perturbations exist, the objective and the constraint functions are modified as follows:

$$f(x) \rightarrow f(x, z) \quad (4.21)$$

$$g_i(x) \rightarrow g_i(x, z) \quad (4.22)$$

where x and z denote the design variables and noise factors respectively.

The reliability-based design optimization formulation can be formally given as follows [99]:

$$\text{Find } x \quad (4.23a)$$

$$\text{to minimize } l[f(x, z)] \quad (4.23b)$$

$$\text{subject to } P[g_i(x, z)] \leq R_{gi} \quad (4.23c)$$

$$x_L \leq x \leq x_U \quad (4.23d)$$

where the function $l[f(x, z)]$ is the new objective function that ensures that the mean and variance of $f(x, z)$ are simultaneously minimized, and R_{gi} is the reliability target for the i th constraint.

As can be seen from 4.23 that at each function evaluation (i.e., at each given x) we need to calculate the probability of every constraint value at this point being greater or less than specified threshold values. The inequality 4.23c can be expressed by a multi-dimensional integral as follows:

$$P[g_i(x, z)] = Pr[g_i(x, z_x, z_p) \leq 0] = \int_{g_i(x, z_x, z_p) \leq 0} p_i(z_x, z_p) dz_x dz_p \leq R_{gi} \quad (4.24)$$

where $p(z_x, z_p)$ is the joint probability density function of uncertain variables z_x and z_p . These probabilities are dictated by the tails of the probability distributions of the constraint functions. The probability that a manufacturing process fails equals the area below the probability density function outside the specification limits for a 3σ -process as shown in Figure 4.13. The predefined reliability level is achieved by

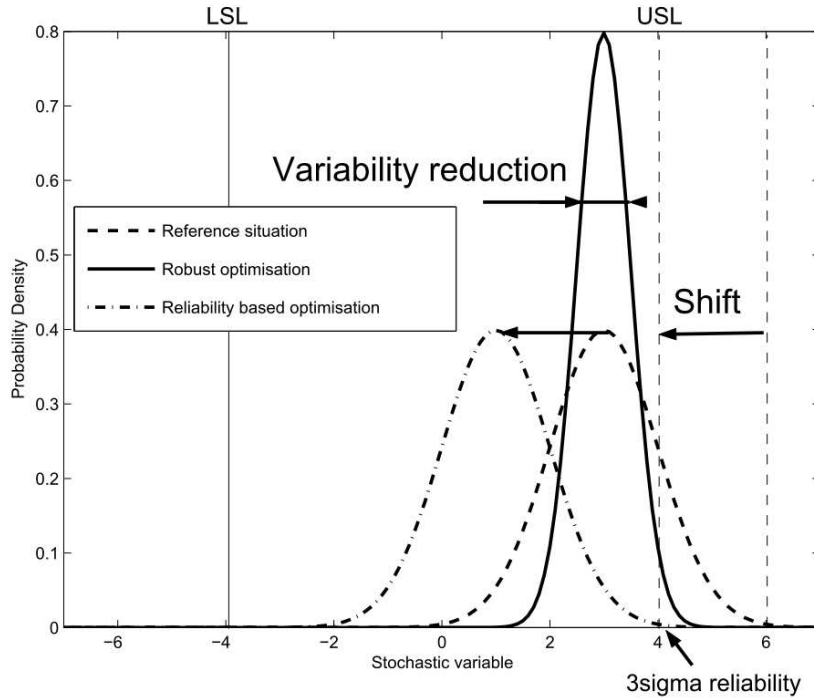


Figure 4.13: Robust and reliability based optimization[15].

shifting the probability density function of the response, rather than reducing its variability as was the case for robust optimisation. Shifting the response distribution by reliability-based optimisation differs from shifting the response by deterministic optimisation. Deterministic optimisation can be seen as shifting the mean of an unknown response distribution. Reliability-based optimisation aims at shifting the distribution by explicitly and accurately determining the area in the tail of the

distribution that is outside the specification limits [15]. The RBDO problems in metal forming were discussed in [88], [102], [178], [184], [205], [250].

4.1.2.3 Robust Design Optimization (RDO)

A robust design is a design insensitive with respect to uncertainties. The task of robust design optimization is to minimize the variability of the performance, while meeting the requirements of optimum performance and constraint conditions. Similar to the RBDO approach, uncertainties are handled in a probabilistic way. An illustration of the principle of RDO is shown in Figure 4.14 which design variable setting x_2 is selected instead of x_1 due to that the x_2 yield a narrower response and thus a more robust design. Less variation implies a higher product quality and lower costs. The RDO techniques aim at reducing the variability in the response by influencing control variables given a certain input noise. While it can be seen

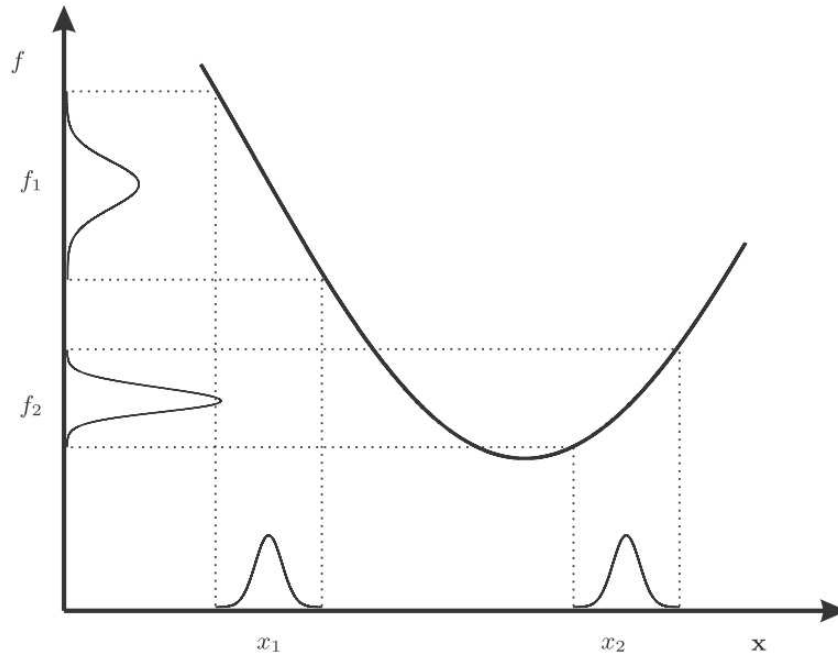


Figure 4.14: The principle of robust design optimization [15], [236].

from Figure 4.13 that the RBDO approach focuses on the area in the tail of the distribution outside the specification limit [15], [236].

Lee et al. [114] and Doltsinis et al. [50] presented the mathematical formulation of RDO where the variations of the design variables and the structural performance are introduced into the objective functions as well as the constraint conditions. The

RDO formulation is given as follows [50], [10]:

$$\textbf{Find} \quad x \quad (4.25a)$$

$$\textbf{to minimize} \quad [E(f(x, z)), \sigma(f(x, z))] \quad (4.25b)$$

$$\textbf{subject to} \quad E(g_i(x, z)) + \beta_i \sigma(g_i(x, z)) \leq 0 (i = 1, 2, \dots, k) \quad (4.25c)$$

$$\sigma(h_j(x, z)) \leq \sigma_j^+ (j = 1, 2, \dots, l) \quad (4.25d)$$

$$x_L \leq x \leq x_U \quad (4.25e)$$

This formulation indicates that both the expected value of the performance function $E(f)$, and its standard deviation $\sigma(f)$ are minimized. The notation $h_j(x, z)$ represents the structural performances to which constraints on standard deviations are applied. In other words, the j th structural performance function has an upper limit on the standard deviation that is given by σ_j^+ . The variable boundaries and optimal design values now refer to the choice of the mean value if x is stochastic. The quantity β_i is a prescribed feasibility index for the i th original constraint. Thus, the constraint will not always be fulfilled. Depending on the different choices of β_i , the probability that constraint is fulfilled will vary. Assuming that the function $g_i(x)$ is normally distributed and β_i is set to be 3, the probability that the original constraint condition will be satisfied is 0.9987 [50], [10].

Doltsinis et al. [50] take one further step in formulating a robust design optimisation problem, by introducing a weighting factor α for the tradeoff between minimising the mean performance and its standard deviation.

$$\textbf{Find} \quad x \quad (4.26a)$$

$$\textbf{to minimize} \quad \tilde{f} = (1 - \alpha)E(f(x, z))/\mu^* + \alpha\sigma(f(x, z))/\sigma^* \quad (4.26b)$$

$$\textbf{subject to} \quad E(g_i(x, z)) + \beta_i \sigma(g_i(x, z)) \leq 0 (i = 1, 2, \dots, k) \quad (4.26c)$$

$$\sigma(h_j(x, z)) \leq \sigma_j^+ (j = 1, 2, \dots, l) \quad (4.26d)$$

$$x_L \leq x \leq x_U \quad (4.26e)$$

$$0 \leq \alpha \leq 1 \quad (4.26f)$$

This is the simplest form of introducing weights to the objectives, namely by making them linearly weighted. $\alpha = 0$ corresponds to a pure mean value minimisation problem and $\alpha = 1$ a pure standard deviation minimisation problem. This particular formulation can be useful when investigating the tradeoff situation, simply by using different values of α from zero to one. All the different choices of the parameter α constitutes the Pareto optimal set. The basic idea here is that the problem will have a different optimal solution depending on what variances of the objective performance we tolerate. This, of course, is the designers choice. Levi et al. [119] give one example on how to choose α , where the choice depends on the desired objective for the objective function f . There was only a few reasearch works using the RDO in metal forming processes that it can be found in [248], [15], [236].

4.1.2.4 A comparison between DO, RBDO and RDO

For deterministic optimization, uncertainties are not taken into account during optimization. The goal of DO is to increase the reliability of a process by optimizing towards a point as far away as possible from the failure constraints. In other words, shifting the mean of the response to a location far away from the specification limits gives a more reliable process in this case. However, the probability distribution of response is not known, as a consequence, the variation of the response is not known either. Therefore, it cannot conclude on the robustness or reliability of the obtained optimal process. Nevertheless, after having obtained the deterministic optimum, one can validate the process capability (process robustness and reliability) by performing a Monte Carlo Analysis (MCA). More specifically, the noise variables are sampled randomly according to a normal distribution, while the design variables values are the ones of the obtained deterministic optima. As a result, the process mean μ and variation σ can be calculated for each response by running the FEM simulations for varying values of the noise variables. Comparing the response distributions to the LSL and USL of each response yields the scrap rate. Nonetheless, it is impractical to perform MCA using FEM simulations due to its extremely time-consuming process.

Reliability-based design optimization takes into account noise variables and response distributions. The RBDO estimates the probability distribution of the response based on the known probability distributions of the random parameters, and thus, the estimation of probability of failure of a product or process is also obtained by determining the tail of the response distribution that is outside the specification limit. Compared with the DO, the RBDO can shift the whole of the probability density function of the response to achieve a certain reliability level, while the DO can only shift the mean of response due to the distribution being unknown.

Robust design optimization presents a good compromise between deterministic and reliability based optimisation. It not only takes uncertainties into account but also minimize the effects of uncertainty without eliminating their causes. The objective is different from the RBDO, and is to optimize the mean performance and minimize its variation, while maintaining feasibility with probabilistic constraints. The response distribution is described by a mean μ and standard deviation σ , which makes it possible to increase process robustness in a quantitative way. Even the process reliability can be quantified by calculating the process capability index (e.g. C_{pk} , C_{pm} , C_{pkm}). This is based on the assumption that the response distribution is normally distributed. If the response is not normally distributed, the quantified reliability level is just an approximation.

According to Park et al. [166], the RBDO is similar to the RDO. Both approaches aim at incorporating uncertainty into the optimization study. Whereas Zang et al. [246] discussed that there is a conceptual difference between RDO and RBDO. The RDO rather aims at reducing the variability of structural performance caused by fluctuations in parameters than to avoid a catastrophe in an extreme event. In the case of RBDO, it can make a design that displays large variations as long as there are safety margins failure in the design, i.e. the variability is not minimized.

Furthermore, the two approaches differ in some aspects [236]. The choice for using the RDO approach or the RBDO approach depends on the objective of the optimization study. In the RDO, insensitiveness of the objective function is emphasized. In the RBDO, reliability of constraints is important [166]. Thus, both approaches will obviously lead to different optimization outcomes.

The optimization objectives in an industrial setting are the minimization the number of scrap products or costs of a production process. Purely minimizing the objective function (instead of the variance) favors the use of RBDO [5]. Moreover, this approach is able to give a quantification of the reliability of the found optimum. However, the accuracy of the RBDO approach depends on several factors:

- The prediction of the probability of failure is affected significantly by mean errors. When using FEM simulations to simulate a process, many assumptions are being made, it leads to a large mean shift of the simulated response. For instance, the impact of material modeling on the response of a stamping process is studied in [11], [12]. Del et al. [47] showed that there is a bias in the mean predicted by stochastic FEM simulations of a drawing operation and measured experimental values. From this point of view, using the RBDO approach would result in erroneous results.
- The RBDO approach focuses on the tail of the response distribution to calculate the probability of failure or reliability. Accuracy at low probabilities require more objective function evaluations compared to a robustness analysis [189], [205]. If only a limited number of FE simulations can be performed (which is generally the case because of time reasons), care must be taken in interpreting the resulting reliability of the RBDO approach.
- The RBDO approach is more sensitive to inadequate assumptions on the probabilistic distribution compared to the robust optimization approach. In this sense, the RBDO might be of less practical value if information about the statistical distribution is limited available and not sufficient to permit a reliability analysis.

On the other hand, the RDO is less sensitive to model errors, inadequate stochastic input data and more efficient compared to the RBDO approach [101], [97], [115], [81]. This is because the mean of the objective function is of interest in this case, for which statistics are less costly to compute and more reliable for small sample sizes and limited stochastic input data [53]. If the focus of an optimization problem is on minimizing the response variance, the RDO approach is most suitable. However, this approach can also be used to simultaneously minimize the mean of the response.

4.1.3 Multi-objective optimization and Pareto optimality

The design scope is frequently defined by multiple and sometimes conflicting design objectives, along with a substantial number of design variables. The simultaneous optimization of competing objectives is considered as multi-objective optimization.

The presence of multi objectives in a problem gives rise to a set of optimal solution, known as Pareto optimal solutions, instead of a single optimal solution [139], [46], [69]. The terms in multi-objective optimization are reviewed in the following [139], [43], [148], [203]:

4.1.3.1 Search space

Search space or design space is the set of all possible combinations of the design variables. If all design variables are real, the design space is given as $x \in R^N$ (N is the number of design variables). The feasible domain S is the region in design space where all constraints are satisfied.

4.1.3.2 Multi-objective optimization problem formulation

Multi-objective optimization problem is formulated as

$$\begin{aligned} &\text{Minimize } F(x), \text{ where } F = f_j : \forall j = 1, M; x = x_i : \forall i = 1, N \\ &\text{Subject to :} \\ &C(x) \leq 0, \text{ where } C = c_p : \forall p = 1, P, \\ &H(x) = 0, \text{ where } H = h_k : \forall k = 1, K. \end{aligned}$$

4.1.3.3 Domination criteria

A feasible design $x^{(1)}$ dominates another feasible design $x^{(2)}$ (denoted as $x^{(1)} < x^{(2)}$), if both of the following conditions are true:

The design $x^{(1)}$ is no worse than $x^{(2)}$ in all objectives, i.e., $f_j(x^{(1)}) \not\geq f_j(x^{(2)})$ for all $j = 1, 2, \dots, M$ objectives

$$x^{(1)} \not\leq x^{(2)} \Rightarrow \forall j \in M f_j(x^{(1)}) \not\geq f_j(x^{(2)}) \quad (4.27a)$$

$$\text{or} \quad \forall j \in M f_j(x^{(1)}) \leq f_j(x^{(2)}) \quad (4.27b)$$

The design $x^{(1)}$ is strictly better than $x^{(2)}$ in at least one objective, or $f_j(x^{(1)}) < f_j(x^{(2)})$ for at least one $j \in \{1, 2, \dots, M\}$

$$x_{(1)} < x^{(2)} \Rightarrow \wedge j \in M f_j(x^{(1)}) < f_j(x^{(2)}) \quad (4.28)$$

4.1.3.4 Non-dominated solutions

If two designs are compared, then the designs are non-dominated with respect to each other *if* neither design dominates the other.

A design $x \in S$ (S is the set of all feasible designs) is non-dominated with respect to a set $A \subseteq S$, if $\nexists a \in A : a < x$.

Such design in function space are called non-dominated solutions. Moreover, any design x is Pareto optimal if x is non-dominated with respect to S [70].

4.1.3.5 Pareto optimal set

All the designs x ($x \in S$) which are non-dominated with respect to any other design in set S , comprise a set known as Pareto optimal set.

4.1.3.6 Pareto optimal front (POF)

The function space representation of the Pareto optimal set is the Pareto optimal front. When there are two objectives, the Pareto optimal front is a curve, when there are three objectives, the Pareto optimal front is represented by a surface and if there are more than three objectives, it is represented by a hyper-surface. A generic Pareto front is illustrated in Figure 4.15.

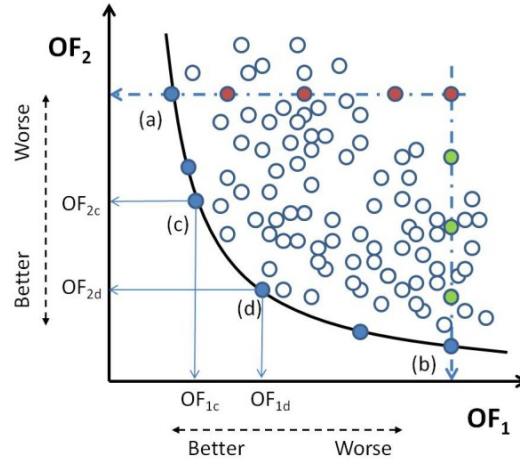


Figure 4.15: Generic Pareto front. Full blue points indicate members of the Pareto set. Point (a) is the optimum for objective function for a given value of (red points). Point (b) minimizes for another value of (compared to green points). For a member of the Pareto set, say (c), any attempt to improve a goal involves worsening the other, point (d) for comparison. Empty blue points are other possible solutions that are worse than those in the Pareto set [175].

4.1.3.7 Trade-offs between multiple objectives

The aim of multi-objective optimization is to determine a single best design that satisfies designer's requirement for each objective. One way is to find a solution based on a trade-off that determined empirically or interactively by designers. Another way is to first find trade-offs between multiple objectives and then designers select the best solution based on a suitable criterion. In the latter case, the trade-offs are represented by non-dominated solutions, which are solutions that are not dominated by any other solutions as shown in Figure 4.16. To select the best solution from a set of non-dominated solutions, it would be better to sample many non-dominated solutions. Ideally, Pareto solutions, which mean global non-dominated solutions that form global trade-offs, should be obtained [186]. In multi-objective optimization, the RDO objectives including the deviation from the mean and standard deviation are to vary in the antagonistic way.

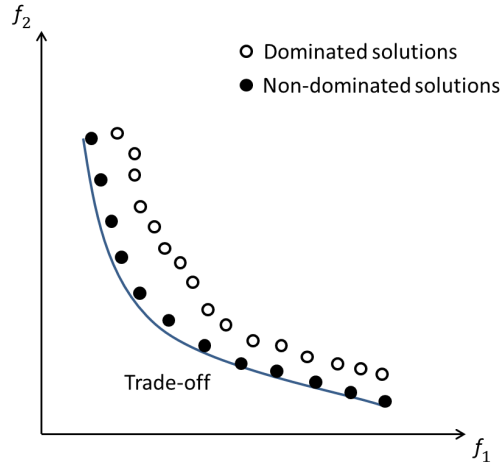


Figure 4.16: Trade-off of two-objective minimization problem, which is represented by non-dominated solutions [186].

4.1.4 Algorithms for multi-objective optimization

There are a number of different methods available for solving multi-objective optimization problems. These problems can be tackled by stochastic (genetic algorithms, simulated annealing) and deterministic (sequential quadratic programming) optimization methods. One popular approach is condensing multiple objectives into a single, composite objective function by methods like using a weighted sum of multiple objective functions to combine them into a scalar fitness function [147], geometric mean, perturbation, Tchybeshev, min-max, goal programming, and physical programming [139], [138], [190]. Another approach is to optimize one objective while treating other objectives as constraints [226]. These approaches give one Pareto optimal solution in each simulation. On the other hand, there numerous multi-objective evolutionary algorithms (MOEAs) that can be made to find multi Pareto optimal solutions in a single simulation run. Some of the latest ones include strength Pareto evolutionary algorithm proposed by Zitzler and Thiele [253], Pareto archived evolutionary strategies (PAES) by Knowles and Corne [107], elitist non-dominated sorting genetic algorithm (NSGA-II) by Deb et al. [44], and controlled elitist non-dominated sorting genetic algorithm by Deb and Goel [45].

4.1.4.1 Evolutionary algorithms

Evolutionary algorithms (EAs) are based on the principle of biological evolution, i.e. survival of the fittest. Unlike classical methods, they do not use a single search point but a population of points called individuals. Each individual represents a potential solution to the problem. In these algorithms, the population evolves toward increasingly better regions of the search space by undergoing statistical transformations called recombination, mutation and selection[66]. The typical evolutionary

algorithms are genetic algorithms which have been mainly applied to single objective optimization problems.

Multi-objective optimization problems (MOPs) are more complex than single-objective optimization problems (SOPs) because they involve optimization of several objectives. This yields not a single optimal solution but a set of equally important optima, called the Pareto front. In multi-objective optimization it is important to guide the search process toward the Pareto front and at the same time maintain adequate population variety to capture as many diverse optimal solutions as possible [173].

Most of the popular evolutionary algorithms are based on the concept of Pareto dominance and involve a finite size of population at each generation [43]. One of the multi-objective evolutionary algorithms (MOEAs) that has been effective in finding the Pareto optimal solutions is the elitist non-dominated sorting genetic algorithm (NSGA-II) developed by Deb et al. [44]. The algorithm is described as follows [43]:

Elitist non-dominated sorting genetic algorithm (NSGA-II)

The flowchart of NSGA-II is given as shown in Figure 4.17. The algorithm is described as follows:

1. Randomly initialize population (designs in the variable space) of size $npop$.
2. Compute objectives and constraints for each design.
3. Rank the population using non-domination criteria (many individuals can have same rank and rank-1 is the best).
4. Compute crowding distance (this distance finds the relative closeness of a solution to other solutions in the function space and is used to differentiate between the solutions on same rank).
5. Employ genetic operators - selection, crossover and mutation - to create intermediate population of size $npop$.
6. Evaluate objectives and constraints for this intermediate population.
7. Combine the two (parent and intermediate) populations, rank them and compute the crowding distance.
8. Select new population of $npop$ best individuals based on the rank and crowding distance.
9. Go to step 3 and repeat till termination criteria is reached, which in the current study is chosen to be the number of generations.

The NSGA-II is a fast and elitist multi-objective evolutionary algorithm. Its main features are:

- A fast non-dominated sorting procedure is implemented. Sorting the individuals of a given population according to the level of non-domination is a complex task: non-dominated sorting algorithms are in general computationally expensive for large population sizes. The adopted solution performs a clever sorting strategy.
- NSGA-II implements elitism for multi-objective search, using an elitism-preserving

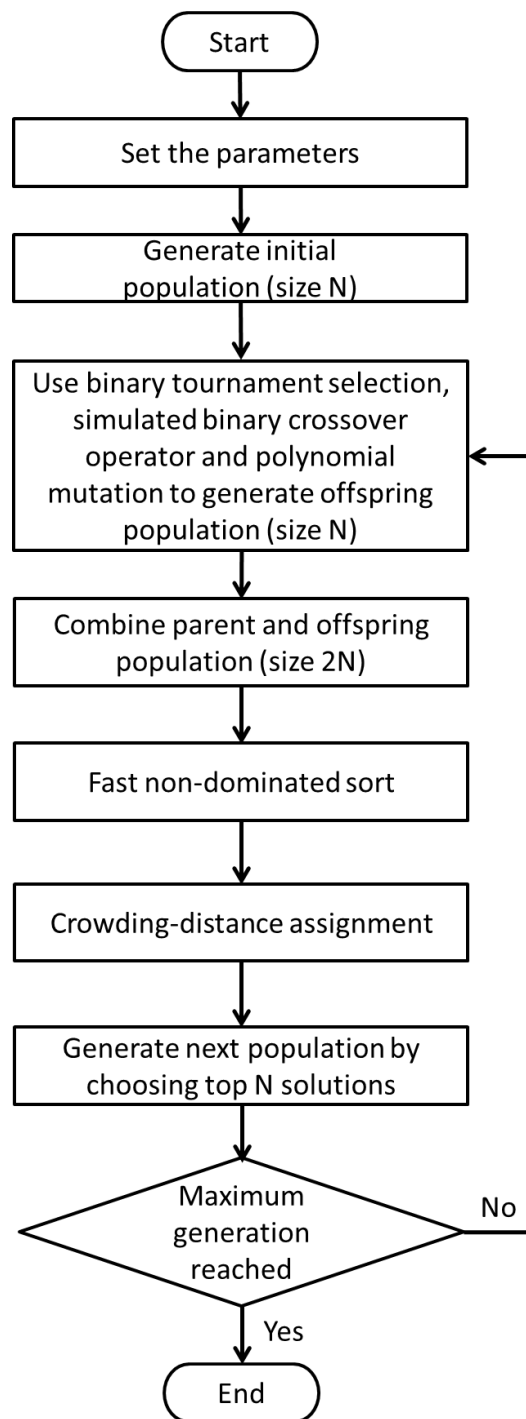


Figure 4.17: NSGA-II flowchart.

approach. Elitism is introduced storing all non-dominated solutions discovered so far, beginning from the initial population. Elitism enhances the convergence properties towards the true Pareto-optimal set.

- A parameter-less diversity preservation mechanism is adopted. Diversity and spread of solutions is guaranteed without use of sharing parameters, since NSGA-II adopts a suitable parameter-less niching approach. It is used the crowding distance, which estimates the density of solutions in the objective space, and the crowded comparison operator, which guides the selection process towards a uniformly spread Pareto frontier.
- The constraint handling method does not make use of penalty parameters. The algorithm implements a modified definition of dominance in order to solve constrained multi-objective problems efficiently.
- NSGA-II allows both continuous ("real-coded") and discrete ("binary-coded") design variables. The original feature is the application of a genetic algorithm in the field of continuous variables.

4.2 Multi-objective optimization strategy under uncertainty for sheet metal forming process

The focus of this thesis is to propose a robust design optimization strategy for sheet metal forming process. Prior to performing the RDO strategy, deterministic process design optimization is conducted in order to investigate whether we can vary the springback parameters acting on the design variables. In this section, optimization strategies for the benchmark problem of sheet metal draw bending process as presented in Section 2.6.3.1 will be deployed.

As discussed in Section 3.2.1, the input variables of the process are distinguished into two types: design variables (control factors) and design parameters (noise factors). In particular, the design variables include three parameters:

- Blank holder force F_{BHF}
- Die radius R_d
- Punch radius R_p

Noise factors consist of 4 parameters:

- Blank thickness t
- Yield strength R_e
- Ultimate tensile strength R_m
- Friction coefficient μ

Suppose that the target values of springback parameters β_1, β_2, ρ and hole displacement U_T are respectively $0[^\circ]$, $0[^\circ]$, $+\infty$ and $0[\text{mm}]$.

4.2.1 Deterministic process design optimization

As reviewed in Section 4.1.2.1, the basic idea of deterministic process design optimization is to optimize a merit function subject to deterministic constraints and design variable bounds. However, uncertainties in noise factors are not taken into account. A deterministic process design optimization strategy is shown in Figure 4.18. The deterministic process design optimization is formulated depending on the

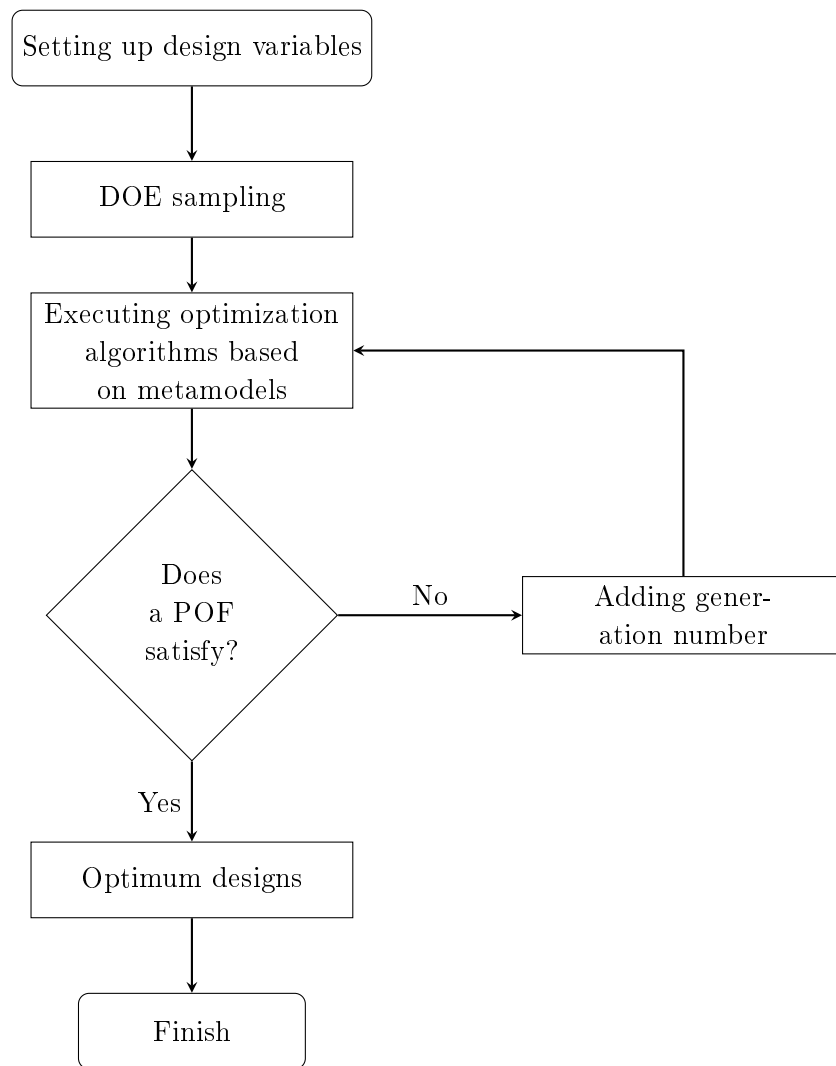


Figure 4.18: A deterministic process design optimization strategy

output variables of the sheet metal draw bending process under consideration.

4.2.1.1 Springback parameters of β_1, β_2, ρ

In the case that the output variables consist of three parameters (β_1, β_2, ρ) . Multi-objective optimization problem is formulated as follows:

$$\text{Find } x \quad (4.29a)$$

$$\text{to minimize} \quad (4.29b)$$

$$F_{obj1}(x) = (E[\beta_1(x)])^2 \quad (4.29c)$$

$$F_{obj2}(x) = (E[\beta_2(x)])^2 \quad (4.29d)$$

$$F_{obj3}(x) = \left(\frac{1}{E[\rho(x)]} \right)^2 \quad (4.29e)$$

where the vector x denotes the vector of seven input variables (F_{BHF} , R_p , R_d , t , R_e , R_m , μ). $E[\cdot]$ is expected value of output variables.

The values of design variables are randomly generated in the interval bounds as presented in Table 4.2, while the design parameters are assigned by their nominal value. The sampling points of the design variables are graphically represented in Figure 4.20.

Table 4.2: The interval bounds of input variables

Input variables	Interval bounds	Nominal values
F_{BHF} [kN]	[2.94, 50]	N/A
R_d [mm]	[2, 10]	N/A
R_p [mm]	[2, 10]	N/A
R_e [MPa]	N/A	550
R_m [MPa]	N/A	840
μ	N/A	0.1
t [mm]	N/A	1.5

The optimization algorithm used in this strategy is NSGA-II. More specifically, the input parameters of NSGA-II are presented in Table 4.3. The NSGA-II has

Table 4.3: Parameters of NSGA-II

Parameters	Values
Population size	1000
Number of Generations	100
Crossover Probability	0.9
Mutation Probability for Real-Coded Vectors	1.0
Mutation Probability for Binary Strings	1.0
Distribution Index for Real-Coded Crossover	20
Distribution Index for Real-Coded Mutation	20

found 23822 POF designs. The obtained POFs are shown in Figure 4.21.

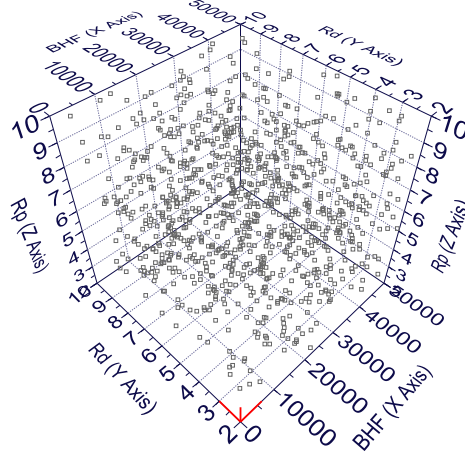


Figure 4.19: 1000 random designs for R_d , R_p and F_{BHF}

Figure 4.20: Design of experiments based on a random sequence for the design variables.

4.2.1.2 Weighted Sum Method

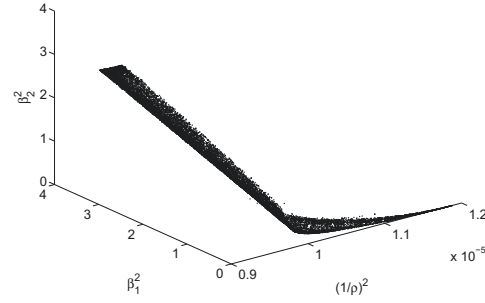
Multi-objective optimization problems have many optimal solutions. Therefore, after the Pareto optimal solutions are obtained, there is still a need to further search among them to find one or a few good compromise solutions.

The Weighted Sum Method (WSM) is one of the multi-criteria decision making methods which is widely used for evaluating a number of alternatives in terms of a number of decision criteria [59], [219]. The WSM is based on weights given by a decision maker. Suppose that a given multi-criteria decision analysis problem is defined on m alternatives and n decision criteria, the best alternative is the one that satisfies the following expression [59]:

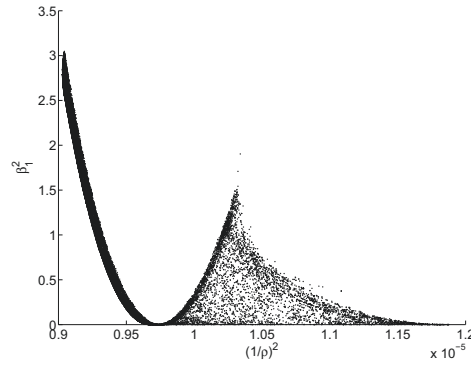
$$A_{WSM-score}^* = \sum_{i=1}^n w_j f_{ij}, j = 1, 2, 3, \dots, m. \quad (4.30)$$

where $A_{WSM-score}^*$ is the WSM score of the alternative A_i , w_j denotes the weight defining the importance of the i th criterion and f_{ij} is the performance value of the alternative A_i . For the maximization case, the best alternative is the one that yields the maximum total performance value [219].

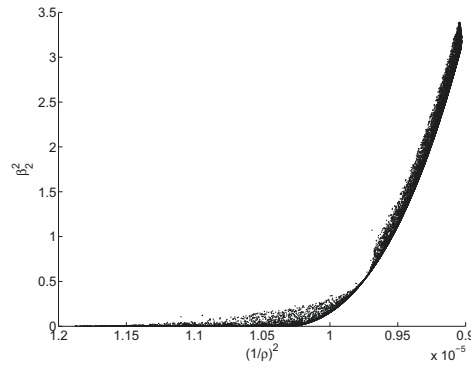
It is crucial to state here that it is applicable only when all the data are expressed in exactly the same unit. The criteria vectors $f_i^*(i = 1, n)$ are often non-commensurable among themselves, with possibly large numerical differences in their entries. These incompatibilities are overcome by normalizing the entries of each vector over the positive unit range $[0, 1]$, without changing their ordinal positions. In general, for a vector f^* with entries $f_j^*(j = 1, m)$, this is accomplished through the



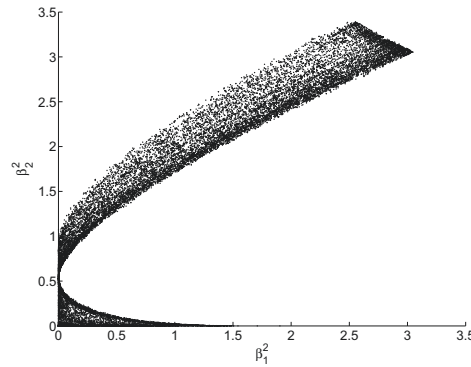
(a) 3D view



(b) 2D view along the z -axis



(c) 2D view along the y -axis



(d) 2D view along the x -axis

Figure 4.21: The POF obtained by NSGA-II.

normalization calculation [73]:

$$X_j = \frac{(f_j^* - f^{min})}{(f^{max} - f^{min})} \quad (4.31)$$

where f^{min} and f^{max} are the minimum and maximum entry values for the original vector f^* . Note that the minimum and maximum entry values for the normalized vector $X = [X_1, \dots, X_m]^T$ are $X^{min} = 0$ and $X^{max} = 1$. The normalization applies regardless of whether the individual vector entries f_j^* are positive, negative or zero valued.

For the multi-objective optimization problem of three springback parameters, 23822 Pareto-optimal design alternatives have been found by NSGA-II. The WSM method is applied to find the best compromise solution on the POF surfaces. With the weights $w_{\beta_1} = w_{\beta_2} = w_{1/\rho} = 0.3333$, the best compromise solution is presented in Table 4.4.

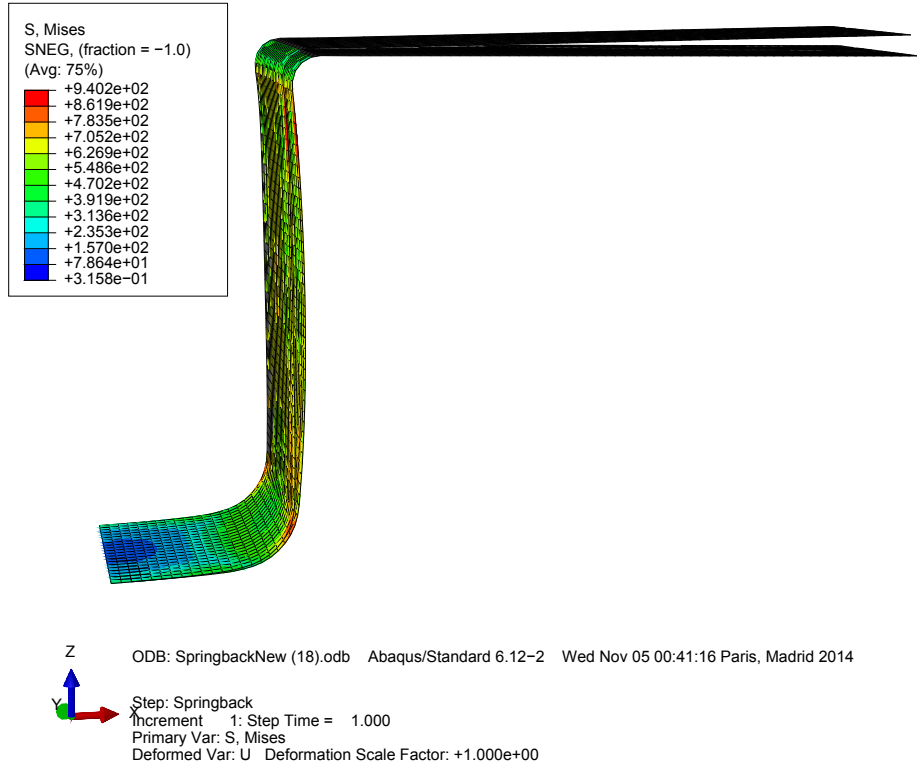
Table 4.4: The best compromise solution obtained by the WSM.

Parameters		NSGA-II
F_{BHF} [kN]		22.419
R_d [mm]		2.2292
R_p [mm]		8.0641
R_e [MPa]		550
R_m [MPa]		840
μ		0.1
t [mm]		1.5
Predicted results	β_1 [°]	9.9412×10^{-2}
	β_2 [°]	-6.2576×10^{-1}
	ρ [mm]	319.0607

4.2.1.3 POF verification

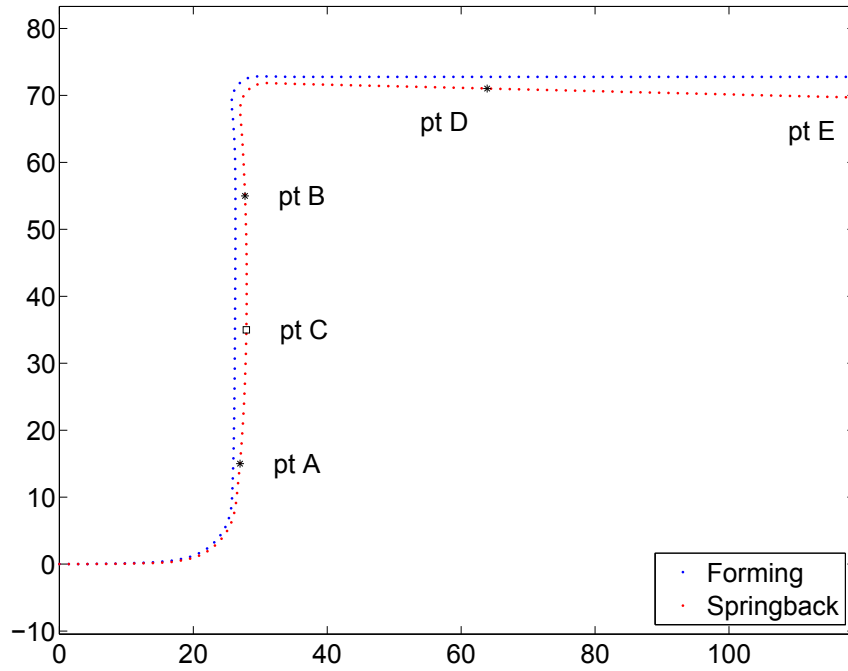
In the case of optimization of springback parameters β_1 , β_2 and ρ , a best compromise solution has been obtained by the WSM. In order to verify the feasibility of this optimal design, the optimal design configuration is tested to the FEM numerical model of the process. The verified results are shown in Table 4.5 Numerical illustration of the optimal design solutions in multi-objective optimization of springback parameters β_1 , β_2 , ρ is shown in Figure 4.22.

As can be seen from Table 4.5, the verified results obtained from optimal configurations with respect to the springback parameters β_1 , β_2 , ρ are consistent.



(a) The formed part in 3D with an optimal design solution obtained by NSGA-II

beta1 [°]: 0.621803, beta2 [°]: 0.781355, rho [mm]: 349.222



(b) The formed part's cross-section in 2D with an optimal design solution obtained by NSGA-II

Figure 4.22: Numerical illustration of the optimal design solution obtained when optimizing the springback parameters β_1, β_2, ρ by NSGA-II.

Table 4.5: The best compromise solution obtained by the WSM for springback parameters β_1 , β_2 , ρ .

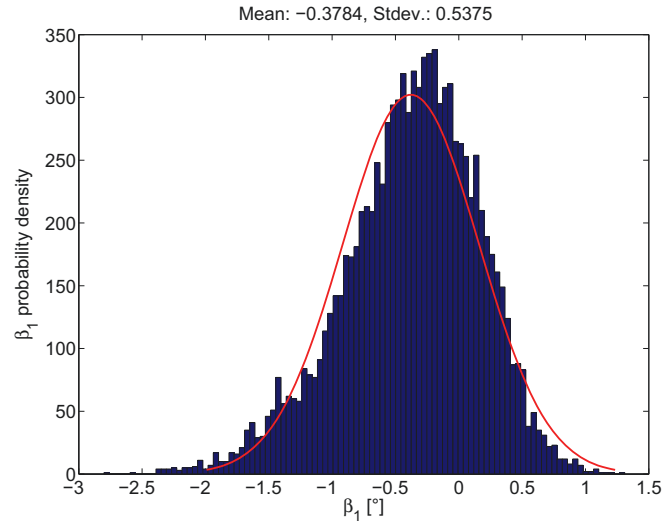
Parameters		NSGA-II
F_{BHF} [kN]		22.419
R_d [mm]		2.2292
R_p [mm]		8.0641
R_e [MPa]		550
R_m [MPa]		840
μ		0.1
t [mm]		1.5
Predicted results	β_1 [°]	9.9412×10^{-2}
	β_2 [°]	-6.2576×10^{-1}
	ρ [mm]	319.0607
Numerical verification	β_1 [°]	6.2180×10^{-1}
	β_2 [°]	7.8136×10^{-1}
	ρ [mm]	349.22
Difference	β_1 [°]	5.224×10^{-1}
	β_2 [°]	1.556×10^{-1}
	ρ [mm]	30.1593

4.2.2 Uncertainty analysis

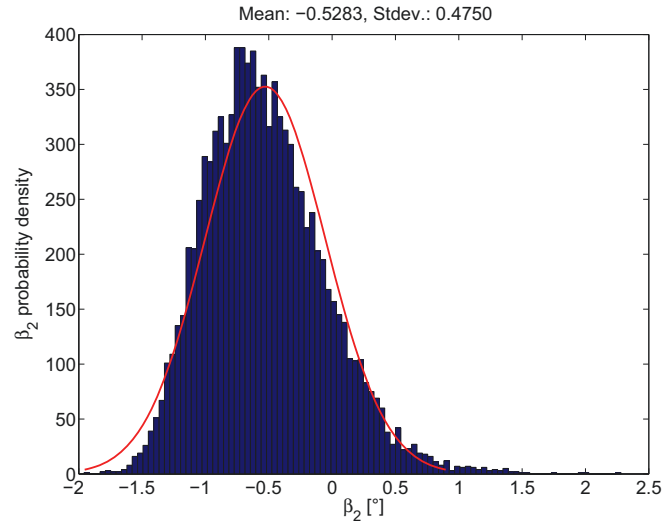
By using the DO, it has obtained the deterministic results as shown in Table 4.5. However, as mentioned previously uncertainties are inherent in material properties, sheet dimension and friction condition. Consequently, they lead to variation in formed parts' performance. In order to show this problem, uncertainty analysis on the basis of the obtained deterministic results is carried out. It is assumed that uncertainties in material properties, sheet dimension and friction condition are represented by Gaussian distribution. Note that this analysis is effected for the optimal configurations obtained by NSGA-II. Distributions of uncertainty analysis of the springback parameters β_1 , β_2 , ρ are shown in Figure 4.23.

It can be seen that there is the deviation in the mean value and the variance in the responses caused by aleatory uncertainties in the uncontrollable parameters as shown in Table 4.6. a

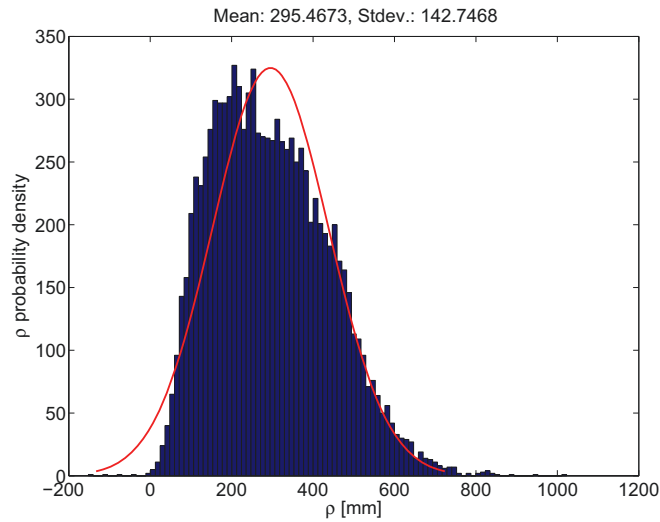
As a consequence, this optimal configuration of design variables is not robust. To overcome this problem, robust design approach is proposed in next section.



(a) β_1 probability density



(b) β_2 probability density



(c) ρ probability density

Figure 4.23: Results of uncertainty analysis of β_1 , β_2 and ρ

Table 4.6: Analysis results of the effects of aleatory uncertainties in uncontrollable parameters on the output parameters of β_1, β_2, ρ

	Deterministic design optimization	Uncertainty analysis	
Output variables	β_1, β_2, ρ	β_1, β_2, ρ	
Parameters	Nominal value	Mean	Stdev
F_{BHF} [kN]	22.419	22.419	N/A
R_d [mm]	2.2292	2.2292	N/A
R_p [mm]	8.0641	8.0641	N/A
R_e [MPa]	550	550	16.6667
R_m [MPa]	840	840	20
μ	0.1	0.1	0.0033
t [mm]	1.5	1.5	0.0167
β_1 [°]	9.9412×10^{-2}	-3.784×10^{-1}	5.375×10^{-1}
β_2 [°]	-6.2576×10^{-1}	-5.283×10^{-1}	4.75×10^{-1}
ρ [mm]	319.0607	295.467	142.747

4.2.3 Multi-objective robust design optimization (MORDO)

According to Choi et al. [33] and Allen et al. [4], there are four types of robust design as reviewed in Section 4.1.1.1. A proposed approach of robust design in this thesis is combined both the type I and type II. In the type I, the variance in response is caused by variations in the noise factors. While the type II robust design is different from type I that the variation in performance is caused by solely by variations in control factors or design variables [30]. The proposed approach for MORDO takes both uncertainties in control factors and uncertainties in noise factors into account.

Robust design optimization is to minimize both the deviation in the mean value $\delta = |\mu_f - T|$, and the variance σ_f^2 , of the performance function, subject to the constraints. The multi-objective design strategy using robust design optimization is demonstrated in Figure 4.24. Suppose that x is vector of the control factors of F_{BHF}, R_d, R_p and z is vector of the noise factors of t, R_e, R_m, μ . Probabilistic modeling and representation of uncertainties in the factors are presented in Table 4.8. Modeling uncertainties of blank thickness, material properties, friction coefficient is represented by Gaussian distribution for the sake of mathematical convenience since a Gaussian model can be specified uniquely by its first two moments.

The MORDO optimization is also carried out by NSGA-II algorithm with input parameters as shown in Table 4.7.

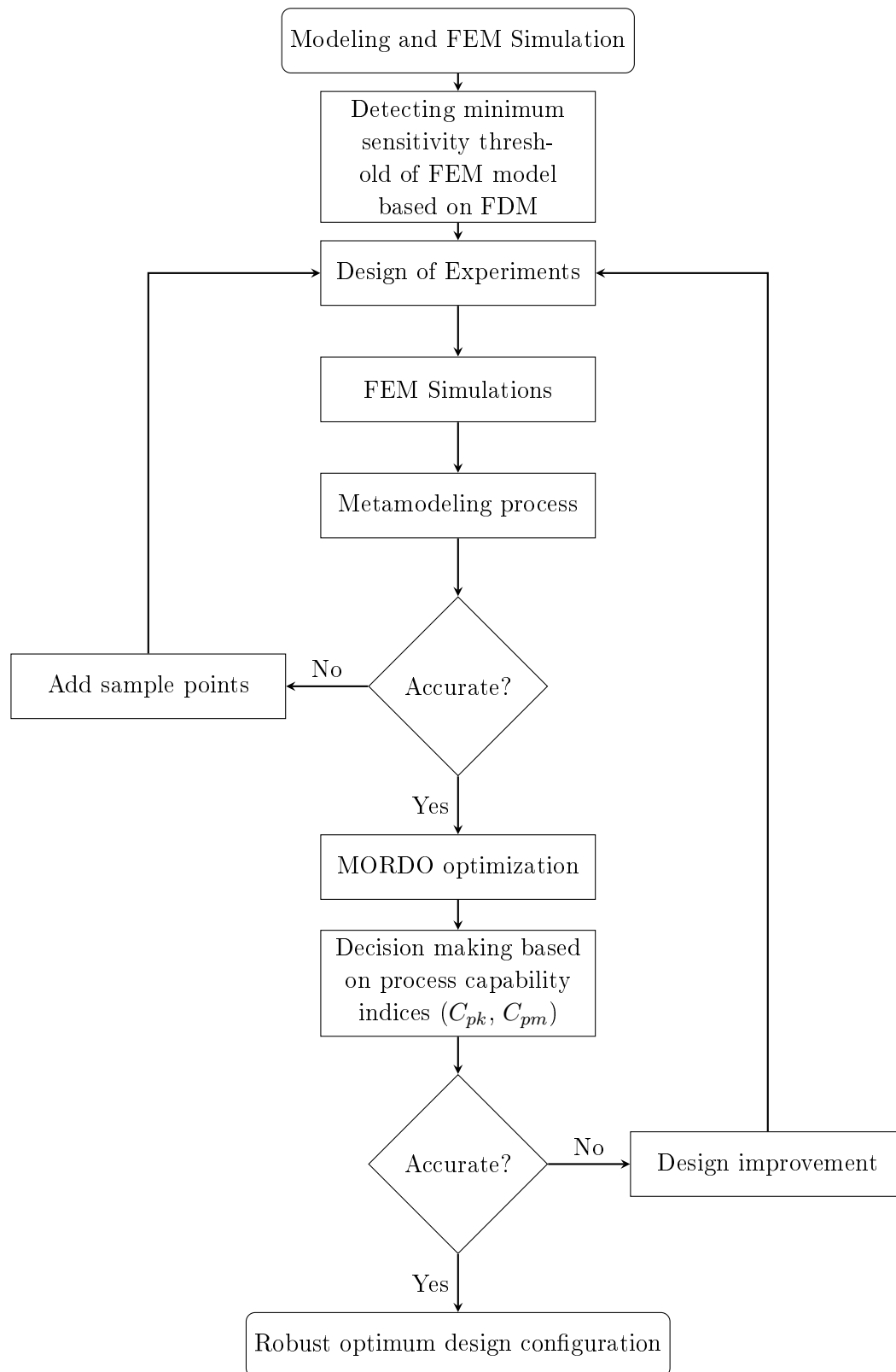


Figure 4.24: Robust design strategy applied for sheet metal forming process design.

Table 4.7: Parameters of NSGA-II

Parameters	Values
Population size	125
Number of Generations	20
Crossover Probability	0.9
Mutation Probability for Real-Coded Vectors	1.0
Mutation Probability for Binary Strings	1.0
Distribution Index for Real-Coded Crossover	20
Distribution Index for Real-Coded Mutation	20

4.2.3.1 MORDO of hole displacement of U_T

In the case that the performance function of the problem is hole displacement U_T , the MORDO formulation is represented as follows:

$$\text{Find } x \quad (4.32a)$$

$$\text{to minimize} \quad (4.32b)$$

$$F_{obj1}(x) = E[U_T(x, z)] - U_T^{Target} \quad (4.32c)$$

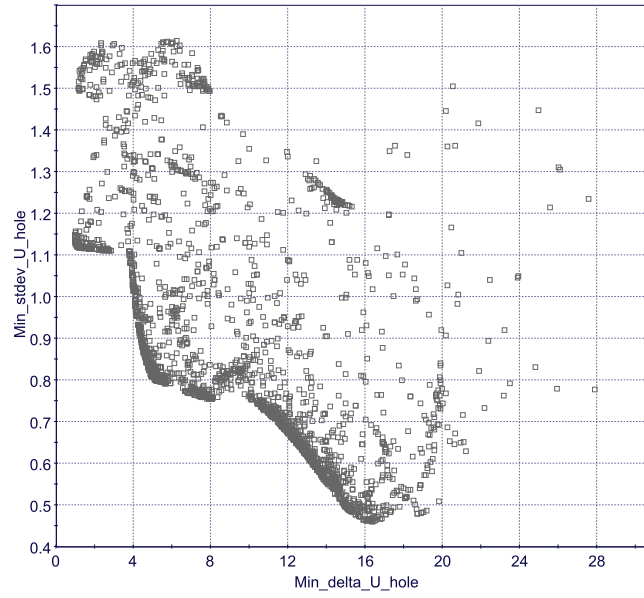
$$F_{obj2}(x) = \sigma(U_T(x, z)) \quad (4.32d)$$

The noise factors are assumed to be stochastic, whereas the control factors are used to optimise the process. The factors are assumed to be continuous random variables in which uncertainties are represented by probabilistic distributions as presented in Table 4.8.

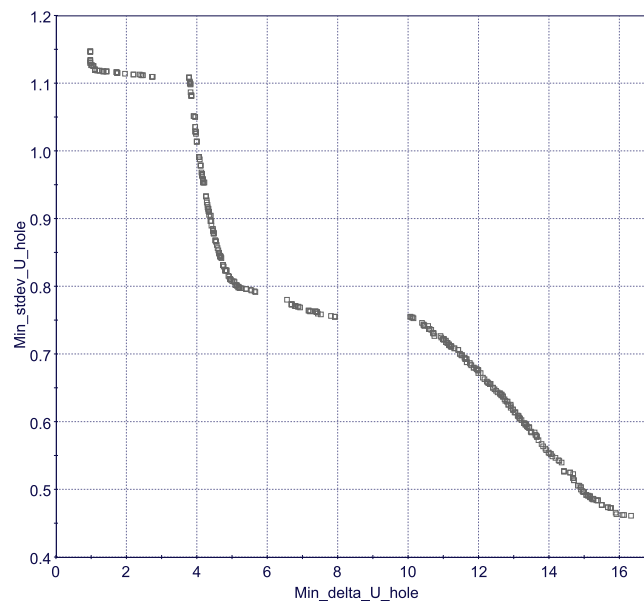
Table 4.8: Probabilistic modeling and representation of uncertainties in the parameters for the case of hole displacement U_T

Parameter	Distribution	Mean	Stdev.	Interval bounds of mean
F_{BHF} [kN]	Normal	N/A	0.6667	[4.940, 48]
R_d [mm]	Normal	N/A	0.0167	[2.05, 9.95]
R_p [mm]	Normal	N/A	0.0167	[2.05, 9.95]
R_e [MPa]	Normal	550	16.6667	N/A
R_m [MPa]	Normal	840	20	N/A
μ	Normal	0.1	0.0033	N/A
t [mm]	Normal	2	0.0167	N/A

The NSGA-II algorithm is used in this MORDO optimization with input parameters as shown in Table 4.7. This algorithm has been found 425 optimal design solutions graphically represented by Pareto optimal front (POF) as shown in Figure 4.25.



(a) Total designs (2500 points)



(b) 425 optimal designs on POF

Figure 4.25: Pareto optimal front obtained from MORDO of hole displacement of U_T

4.2.3.2 MORDO of springback parameters of β_1 , β_1 , ρ

The multi-objective robust design optimization formulation with the three output variables is represented as follows:

$$\text{Find } x \quad (4.33a)$$

$$\text{to minimize} \quad (4.33b)$$

$$F_{obj1}(x) = E[\beta_1(x, z)] - \beta_1^{Target} \quad (4.33c)$$

$$F_{obj2}(x) = E[\beta_2(x, z)] - \beta_2^{Target} \quad (4.33d)$$

$$F_{obj3}(x) = E\left[\frac{1}{\rho(x, z)}\right] - \frac{1}{\rho^{Target}} \quad (4.33e)$$

$$F_{obj4}(x) = \sigma(\beta_1(x, z)) \quad (4.33f)$$

$$F_{obj5}(x) = \sigma(\beta_2(x, z)) \quad (4.33g)$$

$$F_{obj6}(x) = \sigma\left(\frac{1}{\rho(x, z)}\right) \quad (4.33h)$$

Similarly, the uncertainties in controllable and uncontrollable parameters are modeled by Gaussian distribution as shown in Table 4.9.

Table 4.9: Probabilistic modeling and representation of uncertainties in the parameters for the case of three output variables of β_1 , β_1 , ρ

Parameter	Distribution	Mean	Stdev.	Interval bounds
F_{BHF} [kN]	Normal	N/A	0.6667	[4.940, 48]
R_d [mm]	Normal	N/A	0.0167	[2.05, 9.95]
R_p [mm]	Normal	N/A	0.0167	[2.05, 9.95]
R_e [MPa]	Normal	550	16.6667	N/A
R_m [MPa]	Normal	840	20	N/A
μ	Normal	0.1	0.0033	N/A
t [mm]	Normal	1.5	0.0167	N/A

Since there are 6 objective functions, Pareto optimal solutions are represented by a hypersurface of 6-dimensions. However, it may not be graphically represented in this case.

4.2.4 Pareto multiple objective criteria decision-making support based on capability indices

Results of multi-objective robust design optimization are Pareto optimal solutions. One of the problems in MORDO is to address a good compromise design which is governed by multiple conflicting criteria. To solve this, a Pareto multiple objective criteria decision making based on capability indices of C_{pk} , C_{pm} and I is proposed. Where, the indices of C_{pm} and I are the same, so only the C_{pm} index is used to identify an IT 's value with the Taguchi criterion. Firstly, this approach is introduced

for the case of design governed by objective criteria of 2 when optimizing the hole displacement U_T . Afterwards, it is extended to design governed by objective criteria of more than 2, particularly applied for 6 objective criteria (3 means and 3 standard deviations) in MORDO of springback parameters of β_1 , β_2 , $1/\rho$.

4.2.4.1 Decision-making support in 2-D criteria space

The idea is started from graphical representation of capability indices of C_{pk} and C_{pm} in which the C_{pk} index is represented by linear form, whereas the C_{pm} index are represented by quadratic form.

The C_{pk} index is defined by the following formula:

$$C_{pk} = \min \left\{ \frac{USL - \mu}{3\sigma}, \frac{\mu - LSL}{3\sigma} \right\} = \frac{\frac{IT}{2} - |\delta|}{3\sigma} \quad (4.34)$$

Where σ is standard deviation; δ is deviation from target; IT is interval of tolerance.

The index C_{pm} is defined by the following formula:

$$C_{pm} = \frac{IT}{6\sqrt{\delta^2 + \sigma^2}} \quad (4.35)$$

The graphical representation of the C_{pk} and C_{pm} indices with a Pareto front is shown in Figure 4.26. Depending on which capability index used by a designer, a best compromise solution is figured out. Graphically, the best solution is a tangent point between the representations of indices and the Pareto front.

As the target value of U_T is assumed to be 0 [mm], the specification of U_T is represented as $U_T = 0 \pm IT/2$ [mm].

The C_{pk} index

To support decision making in design process, a proposal based on the C_{pk} index is performed. Tolerance intervals (IT) of the design are indicated corresponding to values of C_{pk} in the following expression:

$$IT_i = 2 \times |\delta_{U_T}^i| + 6 \times \sigma_{U_T}^i \times C_{pk}^i \quad (4.36)$$

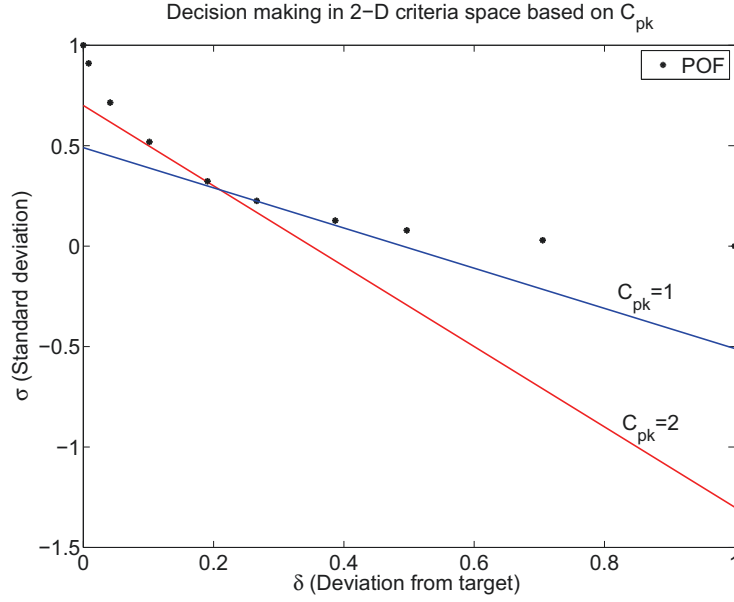
Where i denotes the i -th Pareto optimal design, $i = 1, 2, \dots, 425$ in this case. Table 4.10 and Figure 4.27 show the synthesis of relationship between the values of C_{pk} and the IT and design ID.

The C_{pm} index

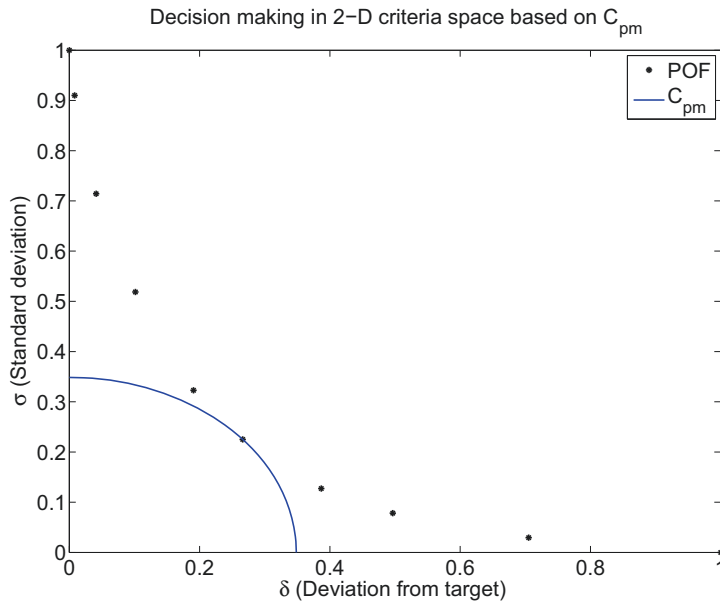
Identification of the best solution based on the C_{pm} index is started from the following expression:

$$IT = 6C_{pm}^i \times \sqrt{(\delta_{U_T}^i)^2 + (\sigma_{U_T}^i)^2} \quad (4.37)$$

However, it is different from the C_{pk} index that the value of IT does not influence on determining the best design configuration. More specifically, whatever the value



(a) Decision making in 2-D criteria space based on C_{pk}



(b) Decision making in 2-D criteria space based on C_{pm}

Figure 4.26: Pareto multiple-objective criteria decision making based on capability indices in 2-D space.

Table 4.10: Relationship between the values of C_{pk} and the IT and design ID

C_{pk}	Process yield [%]	Process fallout (PPM)	IT [mm]	Design ID
0.33	68.27	317311	4.16	2270 (Table 4.11)
0.67	95.45	45500	6.48	1112 (Table 4.12)
1.00	99.73	2700	8.72	1112 (Table 4.12)
1.33	99.99	63	11	1112 (Table 4.12)
1.67	99.9999	1	13.3	2388 (Table 4.13)
2.00	99.9999998	0.002	15.5	2388 (Table 4.13)

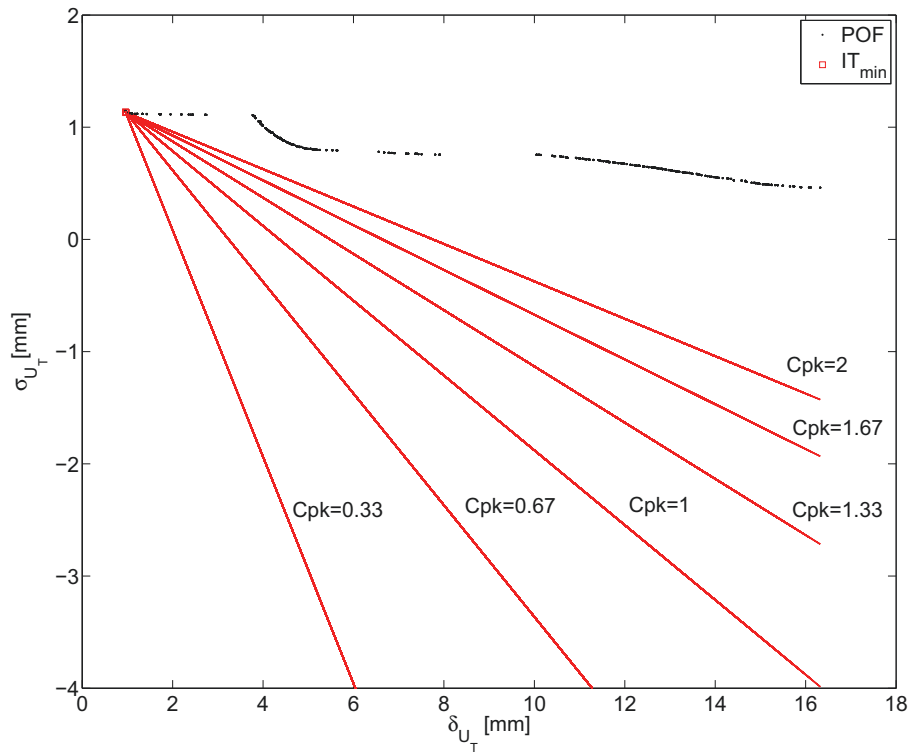


Figure 4.27: Graphical representation of different values of the C_{pk} with respect to the POF

Table 4.11: The best solution when $C_{pk}^i = 0.33$

C_{pk} values	$C_{pk} = 0.33$			
IT values [mm]	$IT = 4.16$			
Solution ID	2270			
Parameters	Mean	Stdev	Min	Max
F_{BHF} [N]	4.7469×10^4	6.6530×10^2	4.5398×10^4	4.9590×10^4
R_d [mm]	9.95	1.6686×10^{-2}	9.8977	1.0003×10^1
R_e [MPa]	5.4999×10^2	1.6703×10^1	4.8229×10^2	6.0456×10^2
R_m [MPa]	8.4001×10^2	20	7.7752×10^2	9.1239×10^2
R_p [mm]	2.5346	1.6709×10^{-2}	2.4716	2.5875
μ	0.1	3.3052×10^{-3}	8.8856×10^{-2}	1.1199×10^{-1}
t [mm]	2	1.6682×10^{-2}	1.9476	2.0518
U_T [mm]	9.5861×10^{-1}	1.1350	-2.2866	4.6162

Table 4.12: The best solution when $C_{pk} = 0.67$, $C_{pk} = 1.00$ and $C_{pk} = 1.33$

C_{pk} values	$C_{pk} = 0.67$; $C_{pk} = 1.00$; $C_{pk} = 1.33$			
IT values [mm]	$IT = 6.48$; $IT = 8.72$; $IT = 11$			
Solution ID	1112			
Parameters	Mean	Stdev	Min	Max
F_{BHF} [N]	4.7778×10^4	6.6530×10^2	4.5707×10^4	4.9898×10^4
R_d [mm]	9.95	1.6686×10^{-2}	9.8977	1.0003×10^1
R_e [MPa]	5.4999×10^2	1.6703×10^1	4.8229×10^2	6.0456×10^2
R_m [MPa]	8.4001×10^2	20	7.7752×10^2	9.1239×10^2
R_p [mm]	2.5346	1.6709×10^{-2}	2.4716	2.5875
μ	0.1	3.3052×10^{-3}	8.8856×10^{-2}	1.1199×10^{-1}
t [mm]	2	1.6682×10^{-2}	1.9476	2.0518
U_T [mm]	9.5960×10^{-1}	1.1340	-2.2829	4.6259

Table 4.13: The best solution when $C_{pk} = 1.67$ and $C_{pk} = 2.00$

C_{pk} values	$C_{pk} = 1.67$; $C_{pk} = 2.00$			
IT values [mm]	$IT = 13.3$ and $IT = 13.5$			
Solution ID	2388			
Parameters	Mean	Stdev	Min	Max
F_{BHF} [N]	4.8000×10^4	6.6530×10^2	4.5929×10^4	5.0120×10^4
R_d [mm]	9.95	1.6686×10^{-2}	9.8977	1.0003×10^1
R_e [MPa]	5.4999×10^2	1.6703×10^1	4.8229×10^2	6.0456×10^2
R_m [MPa]	8.4001×10^2	20	7.7752×10^2	9.1239×10^2
R_p [mm]	2.4464	1.6709×10^{-2}	2.3834	2.4993
μ	0.1	3.3052×10^{-3}	8.8856×10^{-2}	1.1199×10^{-1}
t [mm]	2	1.6682×10^{-2}	1.9476	2.0518
U_T [mm]	9.7356×10^{-1}	1.1306	-2.2787	4.6392

of C_{pm} , the IT changes but the design solution is still the same. Table 4.14 shows the synthesis of relationship between the values of C_{pm} and the IT and design ID. Figure 4.28 illustrates graphical representation of the C_{pm} of 1.33 with respect to the POF.

Table 4.14: Relationship between the values of C_{pm} and the IT and design ID

C_{pm}	Process yield [%]	Process fallout (PPM)	IT [mm]	Design ID
0.33	68.27	317311	2.94	1112 (Table 4.15)
0.67	95.45	45500	5.97	1112 (Table 4.15)
1.00	99.73	2700	8.91	1112 (Table 4.15)
1.33	99.99	63	11.85	1112 (Table 4.15)
1.67	99.9999	1	14.89	1112 (Table 4.15)
2.00	99.9999998	0.002	17.83	1112 (Table 4.15)

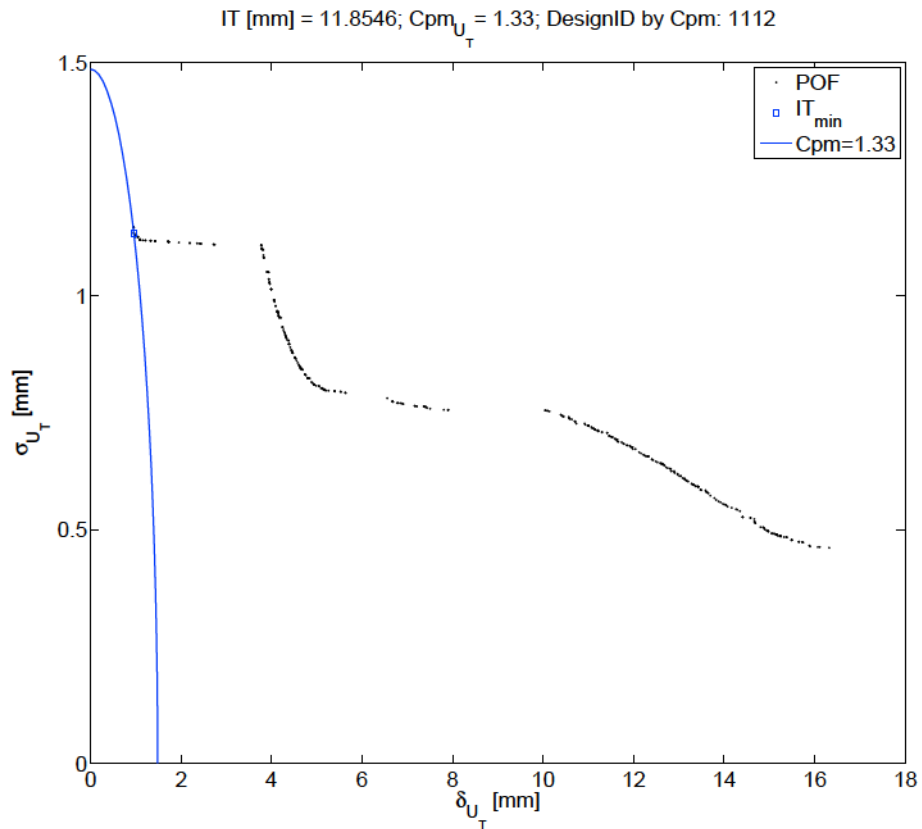


Figure 4.28: Graphical representation of the C_{pm} of 1.33 with respect to the POF

Table 4.15: The best solution found by using the C_{pm} index

Criteria	C_{pm}			
Solution ID	1112			
Parameters	Mean	Stdev	Min	Max
F_{BHF} [N]	4.7778×10^4	6.6530×10^2	4.5707×10^4	4.9898×10^4
R_d [mm]	9.95	1.6686×10^{-2}	9.8977	1.0003×10^1
R_e [MPa]	5.4999×10^2	1.6703×10^1	4.8229×10^2	6.0456×10^2
R_m [MPa]	8.4001×10^2	20	7.7752×10^2	9.1239×10^2
R_p [mm]	2.5346	1.6709×10^{-2}	2.4716	2.5875
μ	0.1	3.3052×10^{-3}	8.8856×10^{-2}	1.1199×10^{-1}
t [mm]	2	1.6682×10^{-2}	1.9476	2.0518
U_T [mm]	9.5960×10^{-1}	1.1340	-2.2829	4.6259

Comparison of the IT values between using C_{pk} and C_{pm}

It can be seen from Table 4.16 that when the values of capability indices are larger than or equal to 1, the IT values found by the C_{pk} index is less than the ones by the C_{pm} index in this case study.

Table 4.16: Comparison of the IT values between using C_{pk} and C_{pm}

Values of capability indices	IT by C_{pk} [mm]	IT by C_{pm} [mm]
0.33	4.16	2.94
0.67	6.48	5.97
1.00	8.72	8.91
1.33	11	11.85
1.67	13.3	14.89
2.00	15.5	17.83

4.2.4.2 Decision making in 6-D criteria space

The proposed approach is extended to design governed by objective criteria of more than 2, particularly applied for 6 objective criteria in MORDO of springback parameters of β_1 , β_2 , and $1/\rho$. Since there are 6 given objective functions, Pareto optimal solutions are represented by a hypersurface of 6-dimensions of σ_{β_1} , σ_{β_2} , $\sigma_{1/\rho}$, δ_{β_1} , δ_{β_2} , $\delta_{1/\rho}$. Thus, finding a best compromise solution from Pareto optimal solutions in 6-D will be carried out by combining used capability indices from higher dimensions into lower dimensions.

As mentioned above, the target values of β_1 , β_2 , and $1/\rho$ are supposed to be 0 [°] and 0 [mm] respectively, the specifications of these three variables are represented as $\beta_1 = 0 \pm IT/2$ [°], $\beta_2 = 0 \pm IT/2$ [°] and $1/\rho = 0 \pm IT/2$ [mm].

The C_{pk} index

In order to find a best compromise solution from Pareto optimal solutions, combining C_{pk}^i of multi-objective is proposed as follows [172]:

$$MC_{pk} = \left(\prod_{i=1}^m C_{pk}^i \right)^{(1/m)} \quad (4.38)$$

Where, i is the number of output variables.

In the case of three springback parameters of β_1 , β_2 , $1/\rho$, the best solution is the one that is a maximum value of the following expression:

$$MC_{pk} = (C_{pk}^{\beta_1} \times C_{pk}^{\beta_2} \times C_{pk}^{1/\rho})^{(1/3)} \quad (4.39)$$

Where, the C_{pk}^i for three output variables of β_1 , β_2 , $1/\rho$ is represented by the following expressions:

- $C_{pk}^{\beta_1}$ is defined as follows:

$$C_{pk}^{\beta_1} = \frac{IT/2 - |\delta_{\beta_1}|}{3\sigma_{\beta_1}} \quad (4.40)$$

- $C_{pk}^{\beta_2}$ is defined as follows:

$$C_{pk}^{\beta_2} = \frac{IT/2 - |\delta_{\beta_2}|}{3\sigma_{\beta_2}} \quad (4.41)$$

- $C_{pk}^{1/\rho}$ is defined as follows:

$$C_{pk}^{1/\rho} = \frac{IT/2 - |\delta_{1/\rho}|}{3\sigma_{1/\rho}} \quad (4.42)$$

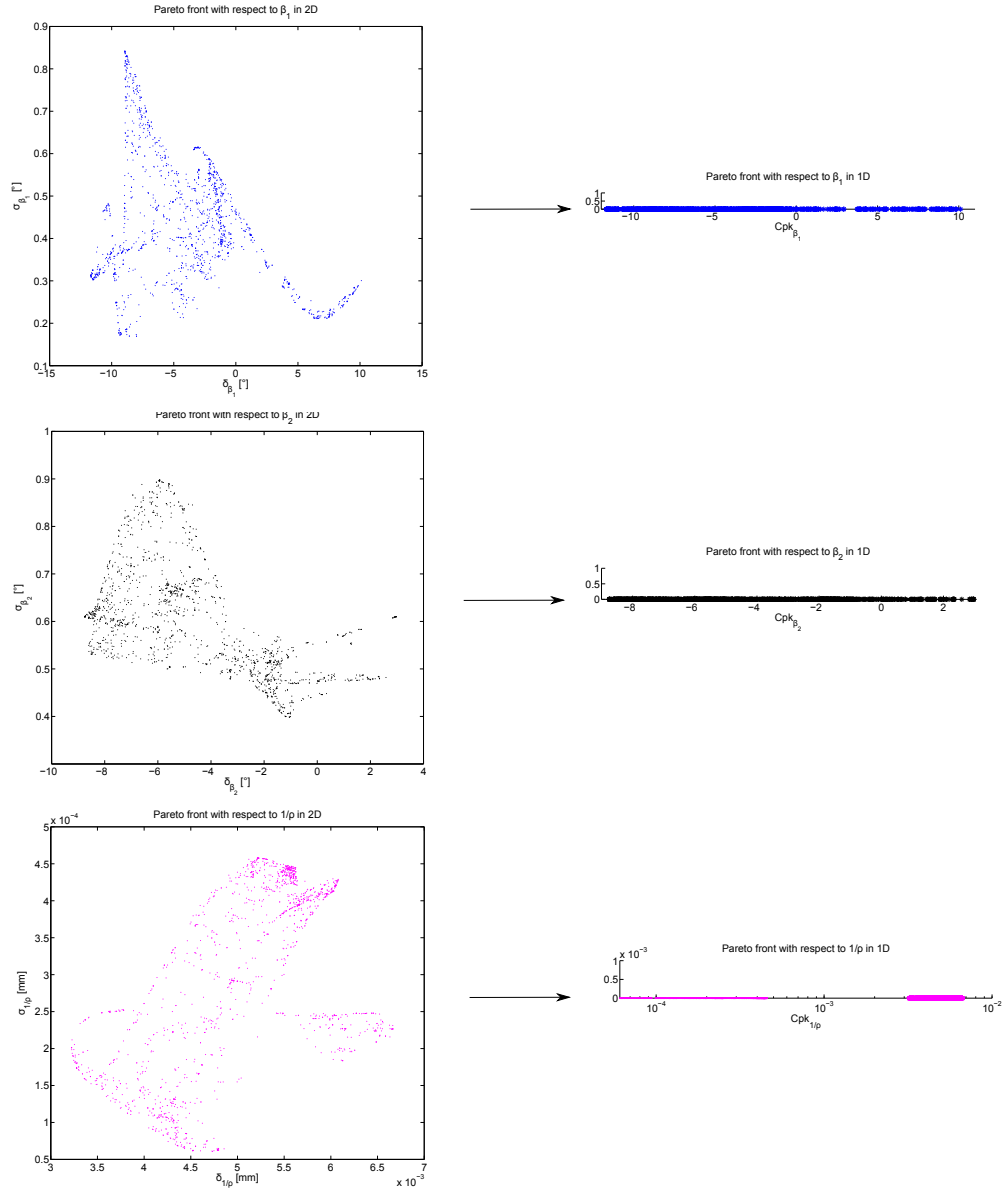


Figure 4.29: The principle of the proposed approach in decision-making support in higher dimensions

The principle of the proposed approach is to combine the standard deviation (σ) and the deviation from the mean (δ) of an output parameter from 2-dimensions into 1-dimension as represented in Figure 4.29.

As mentioned above, the best solution is the one that the value of MC_{pk} is maximum and with different values of IT , the best solution is different. However, in order to ensure that the process yield is at least of 99.99%, the value of the C_{pk} is larger or equal to 1.33. Thus, it needs to find the best design configuration which satisfies both these requirements.

- With $0 < IT \leq 8$, the best alternative obtained corresponding to the maximum value of MC_{pk} is as shown in Table 4.17. However, it is found that the values of $C_{pk}^{\beta_1}$ and $C_{pk}^{\beta_2}$ are less than 1.33 as illustrated in Figure 4.30. It should be noted that the cluster of points on the Figure 4.30 is not the POF, but it is the result of reducing the dimensions by the indices. In addition to this, the values of output variables are fairly large. This design configuration does not meet the required tolerance interval.

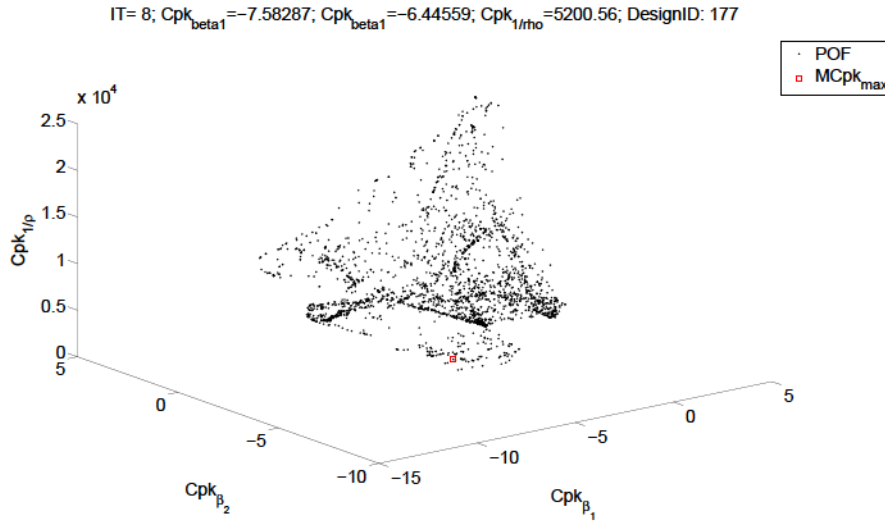


Figure 4.30: The best compromise solution found by finding maximum value of MC_{pk} with $IT = 8$

- With $9 \leq IT \leq 502$, the best alternative is obtained as shown in Table 4.18.

The C_{pm} index

The best solution in the C_{pm} index case is a maximum value of the following expression [172]:

Table 4.17: The best compromise solution found by finding maximum value of MC_{pk} of three springback parameters β_1 , β_2 , $1/\rho$

C_{pk} values	$C_{pk}^{\beta_1} = -7.58287; C_{pk}^{\beta_2} = -6.44559; C_{pk}^{\rho} = 5200.56$			
IT values	$IT = 8$			
Solution ID	177			
Parameters	Mean	Stdev	Min	Max
F_{BHF} [N]	8.9333×10^3	6.6530×10^2	6.8621×10^3	1.1054×10^4
R_d [mm]	9.95	1.6686×10^{-2}	9.8977	1.0003×10^1
R_e [MPa]	5.4999×10^2	1.6703×10^1	4.8229×10^2	6.0456×10^2
R_m [MPa]	8.4001×10^2	20	7.7752×10^2	9.1239×10^2
R_p [mm]	7.9776	1.6709×10^{-2}	7.9147	8.0306
μ	0.1	3.3052×10^{-3}	8.8856×10^{-2}	1.1199×10^{-1}
t [mm]	1.5	1.6682×10^{-2}	1.4476	1.5518
β_1 [°]	1.9099×10^1	6.6373×10^{-1}	1.6715×10^1	2.1122×10^1
β_2 [°]	1.2667×10^1	4.4823×10^{-1}	1.1131×10^1	1.4010×10^1
$1/\rho$ [mm]	6.82479×10^{-3}	2.5595×10^{-4}	7.65895×10^{-3}	5.92428×10^{-3}

Table 4.18: The best compromise solution found by finding maximum value of MC_{pk} of three springback parameters β_1 , β_2 , $1/\rho$

C_{pk} values	$C_{pk}^{\beta_1} = 3.62217; C_{pk}^{\beta_2} = 3.27706; C_{pk}^{\rho} = 24051$			
IT values	$IT = 9$			
Solution ID	1736			
Parameters	Mean	Stdev	Min	Max
F_{BHF} [N]	2.7150×10^4	6.6530×10^2	2.5079×10^4	2.9270×10^4
R_d [mm]	2.4013	1.6686×10^{-2}	2.3491	2.4542
R_e [MPa]	5.4999×10^2	1.6703×10^1	4.8229×10^2	6.0456×10^2
R_m [MPa]	8.4001×10^2	20	7.7752×10^2	9.1239×10^2
R_p [mm]	9.95	1.6709×10^{-2}	9.8870	1.0003×10^1
μ	0.1	3.3052×10^{-3}	8.8856×10^{-2}	1.1199×10^{-1}
t [mm]	1.5	1.6682×10^{-2}	1.4476	1.5518
β_1 [°]	-6.1158×10^{-1}	3.5784×10^{-1}	-1.8810	4.7824×10^{-1}
β_2 [°]	9.0027×10^{-2}	4.4857×10^{-1}	-1.5982	1.6313
$1/\rho$ [mm]	4.5243×10^{-3}	6.2305×10^{-5}	4.7692×10^{-3}	4.2682×10^{-3}

$$MC_{pm} = \left(\prod_{i=1}^m C_{pm}^i \right)^{(1/m)} \quad (4.43)$$

In the case of three springback parameters of β_1 , β_2 , and $1/\rho$, the best solution is the one that is a maximum value of the following expression:

$$MC_{pm} = (C_{pm}^{\beta_1} \times C_{pm}^{\beta_2} \times C_{pm}^{1/\rho})^{(1/3)} \quad (4.44)$$

Where, the C_{pm}^i for three output variables β_1 , β_2 , $1/\rho$ is represented by the following expressions:

- $C_{pm}^{\beta_1}$ is defined as follows:

$$C_{pm}^{\beta_1} = \frac{IT}{6\sqrt{\delta_{\beta_1}^2 + \sigma_{\beta_1}^2}} \quad (4.45)$$

- $C_{pm}^{\beta_2}$ is defined as follows:

$$C_{pm}^{\beta_2} = \frac{IT}{6\sqrt{\delta_{\beta_2}^2 + \sigma_{\beta_2}^2}} \quad (4.46)$$

- $C_{pm}^{1/\rho}$ is defined as follows:

$$C_{pm}^{1/\rho} = \frac{IT}{6\sqrt{\delta_{1/\rho}^2 + \sigma_{1/\rho}^2}} \quad (4.47)$$

Similarly, the best alternative is the one that the value of MC_{pm} is maximum. As mentioned above, with any different values of IT , the best solutions found by the C_{pm} is identical.

- With $IT = 3.8$, the best alternative is obtained as shown in Table 4.19. This design configuration satisfies the process yield requirement of 99.99% and the required tolerance interval of 3.8.

4.2.5 Synthesis of results

The best solutions based on the capability indices which have been obtained from the MORDO of U_T hole displacement and three springback parameters of β_1 , β_2 , $1/\rho$ are synthesized in Table 4.20. It is found that the optimal design configuration which is indicated by using the C_{pk} index is dependent upon the IT values. While the optimal design configuration is identical despite different values of IT when using the C_{pm} index.

For springback parameters of β_1 , β_2 , $1/\rho$, the optimal design configuration obtained by C_{pm} meet the IT value smaller than the one attained by C_{pk} . The difference of predicted results of β_1 , β_2 , $1/\rho$ is very small when comparing between the design solutions attained based on C_{pk} and C_{pm} . Whereas, for U_T hole displacement the IT value got from C_{pm} is bigger than the one from C_{pk} . The predicted results of U_T based on these indices are the same.

Table 4.19: The best compromise solution found by finding maximum value of MC_{pm} of three springback parameters $\beta_1, \beta_2, 1/\rho$

Criteria	C_{pm}			
Interval of tolerance	$IT = 3.8$			
Solution ID	1271			
Parameters	Mean	Stdev	Min	Max
F_{BHF} [N]	2.6728×10^4	6.6530×10^2	2.4656×10^4	2.8848×10^4
R_d [mm]	2.4055	1.6686×10^{-2}	2.3532	2.4583
R_e [MPa]	5.4999×10^2	1.6703×10^1	4.8229×10^2	6.0456×10^2
R_m [MPa]	8.4001×10^2	20	7.7752×10^2	9.1239×10^2
R_p [mm]	9.6323	1.6709×10^{-2}	9.5694	9.6853
μ	0.1	3.3052×10^{-3}	8.8856×10^{-2}	1.1199×10^{-1}
t [mm]	1.5	1.6682×10^{-2}	1.4476	1.5518
β_1 [°]	2.0182×10^{-2}	3.9007×10^{-1}	-1.4289	1.2220
β_2 [°]	1.0770×10^{-1}	4.5186×10^{-1}	-1.5421	1.6678
$1/\rho$ [mm]	4.2183×10^{-3}	8.5893×10^{-5}	4.5659×10^{-3}	4.0159×10^{-3}

Table 4.20: Synthesis of the best solutions based on the capability indices

Parameters	IT	C_{pk}	C_{pm}	Solution ID
β_1	9 [°]	3.6222	N/A	1736 (Table 4.18)
β_2	9 [°]	3.2771		
$1/\rho$	9 [mm]	24051		
U_T	11 [mm]	1.335		
β_1	3.8 [°]	N/A	1.6215	1271 (Table 4.19)
β_2	3.8 [°]		1.3634	
$1/\rho$	3.8 [mm]		150.107	
U_T	12 [mm]		1.346	

4.3 Summary of the chapter

The main objective of this chapter is to treat Robust Design Optimization applied for sheet metal forming process design and to propose capability indices-based Pareto multiple objective criteria decision making applied for Robust Design. A couple of major points is summarized as follows:

- The approaches in Robust Design and Reliability-based Design have been reviewed and compared between them. The issues in conventional design optimization and optimization under uncertainty have been also addressed. It has been found that conventional design optimization may not always satisfy the desired targets due to the significant uncertainty that exist in material properties, blank thickness and friction condition. While optimization under uncertainty takes the uncertainties into account as soon as in the design process. In addition, optimization algorithms have been reviewed and investigation shows that the NSGA-II algorithm is the best effective in this case study.
- A multi-objective optimization under uncertainty strategy applied for sheet metal forming process has been introduced. A Pareto multiple objective criteria decision making based on capability indices applied for robust design has been proposed. It has been found that a best solution obtained from Pareto optimal solutions by using the C_{pk} index depends on the tolerance interval (IT). With different values of IT , the best solution is different. Whereas the value of IT does not influence on determining the best alternative by using the C_{pm} index. The best solution found by these indices is identical with any various values of IT . However, in order to verify the capability of obtained optimal design configurations based on C_{pk} and C_{pm} , these design solutions have been determinated to ensure the process yield of 99.99% corresponding to the process fallout of 63 PPM. This proposed approach has been successfully applied to the optimization problems in 2-D and 6-D criteria space.

Conclusions and perspectives

5.1 Conclusions

The two objectives of robust design are to make the mean value close to the target value and to minimize the variability that results from uncertainty represented by noise factors. This thesis has proposed a robust optimization strategy to take aleatory uncertainties in noise factors into account as well as to optimize process design in presence of the uncertainties. In the context of concurrent engineering and FEM numerical simulation, this strategy has been elaborated for responding the challenge in the design process: "How to design for producing robust products?". It is dedicated to sheet metal forming process design. Several key conclusions are drawn from this research including:

- In terms of modeling and FEM simulation, the accuracy of FEM numerical models depends on the accuracy of models used to describe the reality (constitutive equations of material, boundary conditions...) and the accuracy of numerical solution methods (discretization, mass scaling, meshing, contact types...). In addition, it is also up to process parameters (blank holder force, friction condition, workpiece, tooling geometry, drawing velocity...). Investigation of FEM numerical models in this study has been shown that there is a sensitivity threshold at which responses of these FEM numerical models are insensitive to very small variations of input parameters of the process. As a consequence, small variations around nominal values of the input parameters are not correctly propagated by FEM numerical models. In order to be able to build computer experiments based FEM numerical simulation and propagate consistently the uncertainties, we have proposed an FDM-based approach to detect minimum sensitivity threshold of FEM numerical simulation to very small variations of input parameters of the process. This method has been successfully applied for a benchmark problem of Numisheet 2011 of sheet metal draw bending process. Hence, it is necessary to figure out the sensitivity thresholds before executing Design of Experiments.
- Uncertainty is inevitable in any manufacturing process. Therefore, managing the uncertainties in the early product life cycle, particularly as soon as the early design stage is vital. Through uncertainty analysis in sheet metal bending, it has been found that conventional design methods may not always satisfy the desired targets due to the aleatory uncertainties that exist in material properties, sheet thickness, and process parameters. Investigation of these

aleatory uncertainties has shown that they influence significantly on variation of the product performance. In particular, blank thickness and material properties (UTS and YS) are parameters having the greatest influence on the shape variation due to springback.

- Through uncertainty analysis of design configurations obtained by conventional optimization (also known as deterministic design optimization), it is found that there is the deviation in the mean value and the standard deviation in responses of U-shaped sheet metal bending due to the significant aleatory uncertainties in the uncontrollable parameters as shown in Table 4.6. In order to tackle this problem, a robust design optimization strategy applied for sheet metal forming process design has been proposed. This strategy has been successfully applied to the benchmark problem of U-shaped sheet metal bending process.
- A multi-objective optimization under uncertainty strategy applied for sheet metal forming process has been introduced. A Pareto multiple objective criteria decision making based on capability indices applied for robust design has been proposed. It has been found that a best solution obtained from Pareto optimal solutions by using the C_{pk} index depends on the tolerance interval (IT). With different values of IT , the best solution is different. Whereas the value of IT does not influence on determining the best alternative by using the C_{pm} index. The best solution found by this index is identical with any various values of IT . However, in order to verify the capability of obtained optimal design configurations based on C_{pk} and C_{pm} , these design solutions have been determined to ensure the process yield of 99.99% corresponding to the process fallout of 63 PPM. This proposed approach has been successfully applied to the optimization problems in 2-D and 6-D criteria space.

5.2 Perspectives

Several points for future research are recommended on the basis of the knowledge gained and the problems encountered during the study of this thesis:

- For FEM numerical simulation of sheet metal forming processes, an appropriate constitutive model which properly describes the behaviour of material is crucial. One of the significant effects on the quality of the springback prediction is constitutive model of the material. In particular, modeling of the Bauschinger effect and cyclic hardening characteristics of materials is vital. As a point for future research, advanced constitutive models should be adopted in the springback prediction such as the Geng-Wagoner hardening law [65] and the Yoshida-Uemori hardening law [241] which have been proven to describe the springback behavior best. Furthermore, there is still the discrepancy between results obtained from physical process and numerical simulation. This difference results from model assumptions, discretization of the model, contact

types, meshing, mass scaling, etc. Improvement of the numerical methods and the problem modeling is recommended for future research.

- Regarding sensitivity threshold analysis of FEM numerical simulation, this threshold can be improved when the accuracy of numerical model is enhanced. Investigation of sensitivity threshold with finer meshing and lower punch velocity is recommended in perspective. Moreover, the proposed approach for detecting the sensitivity threshold should be tested with different FEM-based software as a point for future work.
- Since metamodels play a very important role in robust design optimization strategy, enhancing the accuracy of metamodeling methods is recommended as a point in future work. Presently, the accuracy of metamodel depends on the choice of which metamodeling method is the best fit of input data.
- In terms of modeling the variations of input parameters, in this thesis there has been seven input parameters under consideration. Adding more the parameters under study is proposed for future research. Especially, consideration of the scatter in anisotropic properties of material is a suggestion. On the other hand, uncertainties in the input parameters in this thesis are taken into account due to part-to-part, coil-to-coil, batch-to-batch, within batch, lab-to-lab variations. It is recommended to investigate uncertainties of the input parameters resulting from within part variations. For example, thickness within part varies differently due to imprecision of rolling process. Likewise, the scatter of process parameters such as holder force, friction between surfaces should be investigated in perspective.
- Concerning geometric tolerance, form tolerances analysis based on modal basis to represent form variations of formed part is suggested for future research.
- Since the optimization strategy is carried out by using numerical models and approximations of the real process, the errors always exist. Validation of obtained optimal design configurations is highly recommended to test in the physical process.

Part II

Summary in French

Résumé

L'objectif ultime de ce travail de thèse est d'évaluer la possibilité de valider et d'optimiser un processus de fabrication en utilisant la simulation numérique en tenant compte des incertitudes irréductibles sur le procédé, les matériaux et la géométrie du produit fabriqué. La prise en compte des incertitudes nécessite de quantifier les effets des variations des paramètres du modèle sur les sorties de celui-ci, en propageant ces variations via la simulation numérique pour évaluer leurs effets sur les sorties. Dans ce travail nous avons proposé une procédure pour déterminer le seuil de sensibilité du modèle numérique afin de construire des plans d'expériences numériques cohérents avec ce seuil. Nous avons également montré que, compte tenu des incertitudes sur les matériaux et la géométrie du produit, il est possible d'optimiser certains paramètres du procédé pour contrôler les effets des incertitudes sur les variations dimensionnelles et morphologiques du produit. Pour cela, nous avons proposé une procédure d'optimisation basée sur un algorithme NSGA-II et une méta-modélisation du procédé. L'application à l'emboutissage d'une tôle en U, retour élastique inclus, montre qu'il s'agit d'un problème de conception robuste pour lequel nous obtenons l'ensemble des compromis entre l'écart à la moyenne et l'écart type d'une fonction "performance" du procédé correctement choisie. Finalement l'analyse de ces résultats nous permet de quantifier le lien entre la notion de robustesse d'une solution optimisée du procédé et les critères de mesure de la qualité du produit.

Mot-clés: incertitude, tôle, travail de la, commande robuste, simulation par ordinateur, décision multicritère

Introduction

Contexte et motivation

Dans un contexte où il est nécessaire de répondre aux défis industriels dans des délais plus courts, et à moindre coût pour une meilleure satisfaction du client, l'ingénierie simultanée s'est imposée comme une solution. L'ingénierie simultanée consiste à réaliser le plus simultanément possible les différentes tâches du processus de développement de produit, plutôt que successivement [201]. Le recouvrement partiel voire total de certaines tâches permet alors de diminuer le temps de développement et d'améliorer la qualité du produit. Une mise en œuvre efficace de l'ingénierie simultanée nécessite des modes d'organisations et des outils informatiques spécifiques [201].

L'emboutissage de tôle est un processus de production qui est très utilisé dans la production de masse, en particulier pour fabriquer des composantes de "caisse en blanc" dans l'industrie automobile comme le montre la Figure 5.1. Plus précisément,

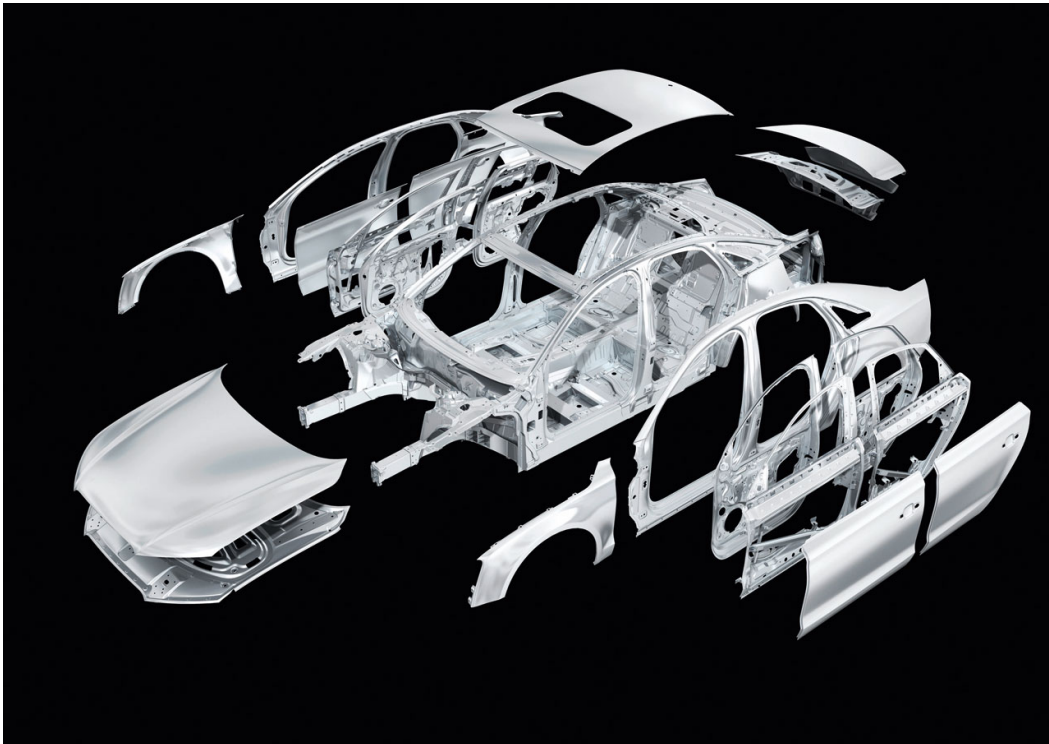


Figure 5.1: Des composantes de "caisse en blanc" d'une voiture.

il y a environ 100 à 150 panneaux métalliques emboutis sur les véhicules (camions légers, automobiles, fourgonnettes, ...) produits aujourd'hui [126]. En raison de

la concurrence de plus en plus sévère, la réduction des coûts et l'amélioration de la productivité sont des exigences que les constructeurs automobiles se doivent de satisfaire. Cependant, la conception d'un processus d'emboutissage est très coûteuse et prend du temps en raison des procédures d'essais et d'erreurs. En effet, une usine automobile doit produire environ 40-50 panneaux différents pour un modèle de voiture ce qui représentent 150-200 matrices d'emboutissage [86]. Par conséquent, il est nécessaire de réduire le temps de conception du processus d'emboutissage et d'éliminer les essais physiques coûteux qui augmentent celui de la fabrication. Les logiciels de simulation par éléments finis accompagnés par les logiciels de CAO pour la définition des modèles géométriques sont des outils aujourd'hui largement utilisés dans la définition des processus d'emboutissage. Un concepteur peut utiliser la simulation d'emboutissage pour évaluer la possibilité de fabrication d'une pièce emboutie sans les frais de fabrication d'un outil physique. Néanmoins, il existe encore, évidemment, une différence entre les résultats de la simulation numérique et ceux de l'expérience physique. Différence encore aujourd'hui inévitable à cause des approximations dans les modèles numériques, ou des variations inattendues des variables d'entrée [88].

D'autre part, malgré les apports de la simulation numérique, les fabricants sont encore confrontés à des défauts comme des amincissements trop importants, des rides et des déchirures sur les pièces embouties. Lorsque ces défauts rédhibitoires sont éliminés, la conception d'un processus d'emboutissage doit encore garantir que les pièces produites satisfassent tout au long de la production les exigences du cahier des charges, malgré les variations (incertitudes) des paramètres d'entrée du processus.

Les variations des propriétés des matériaux, de l'épaisseur du flan, des conditions de lubrification, les dimensions de l'outillage (dus à l'usure) et des paramètres de procédé peuvent être les causes des variations de la performance des pièces produites. Ces variations peuvent avoir des conséquences dans le processus d'assemblage qui suit les opérations d'emboutissage. Cela peut déboucher sur des problèmes de non-qualité. Les sources des variations inhérentes aux flans peuvent venir de la variation de pièce-à-pièce, de lot-à-lot, mais également à l'intérieur du lot au cours du processus de production [126]. Ainsi, en tenant compte de l'incertitude et des variabilités inhérentes et irréductibles, l'optimisation du processus sont les questions essentielles et doivent être résolues pour obtenir une conception de processus robuste du processus d'emboutissage de tôle.

Dans le contexte de l'ingénierie simultanée et de la conception robuste, cette thèse est motivée par une demande pour développer une méthodologie et un concept dans lequel les activités d'ingénierie dans le processus de développement des produits et la production sont intégrées et réalisées simultanément, plus particulièrement la recherche d'une conception de processus robuste le plus insensible possible aux variations inévitables. Cet enjeux de recherche est l'un des problèmes qui est posé par groupe de recherche français nommé "concevoir pour produire robuste" à l'AFM (Association Française de Mécanique) comme suit:

"Comment maîtriser les incertitudes, au plus tôt dans le cycle de vie du produit, en particulier au niveau de la production?"

Problématiques et Objectifs de la thèse

Positionnement de la thèse

Afin de préciser le contexte de ces travaux de thèse, le cycle de vie du produit est utilisé comme référentiel. Alting postule que le cycle de vie d'un produit passe par six phases, comprenant [6]:

- L'analyse du besoin
- Conception/Développement
- Production
- Distribution
- Usage
- Elimination / recyclage

Ces phases du cycle de vie d'un produit sont illustrées dans la figure 5.2. Le cadre de ce travail de recherche par rapport à cette représentation du cycle de vie d'un produit concerne les phases de la conception du produit/développement et de la production de produits.

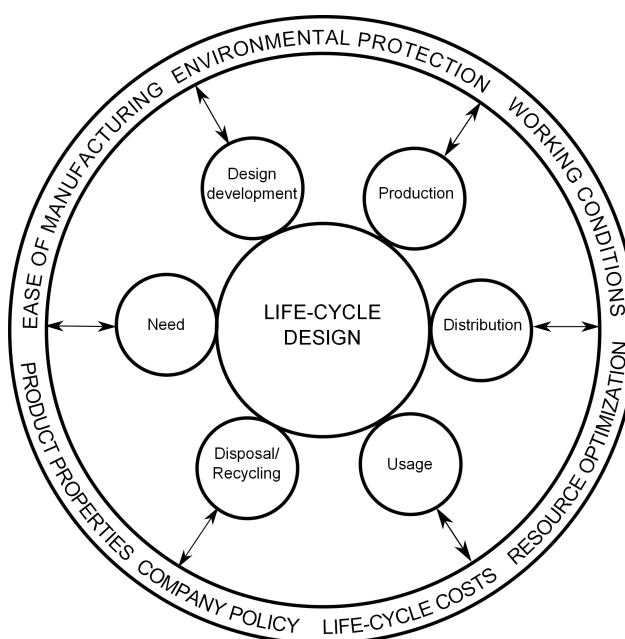


Figure 5.2: Le cycle de vie d'un produit [6]

En particulier, cette thèse a la partie "detailed design" du processus de conception représenté sur la figure 5.3. Plus précisément, ce travail de thèse concerne la conception robuste pour un procédé de formage de tôle métallique.

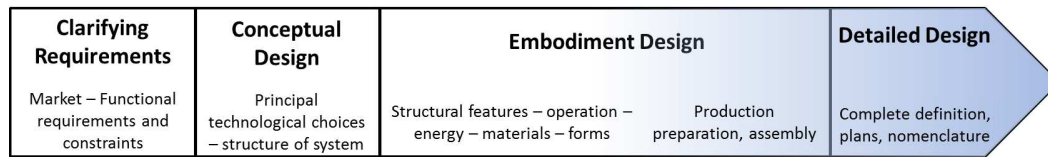


Figure 5.3: Le processus de conception [162],[188], [55].

Problématiques

Les progrès réalisés sur les outils de simulation numérique permettent d'augmenter le niveau de prédictivité et de précision. Cependant la qualité des résultats de ces outils reste dépendante de nombreux facteurs, dont : les caractéristiques fonctionnelles de ces logiciels, les facteurs numériques, les paramètres du procédé, le matériau et la pièce brute comme indiqué sur la figure 5.4 [204]. En outre, les

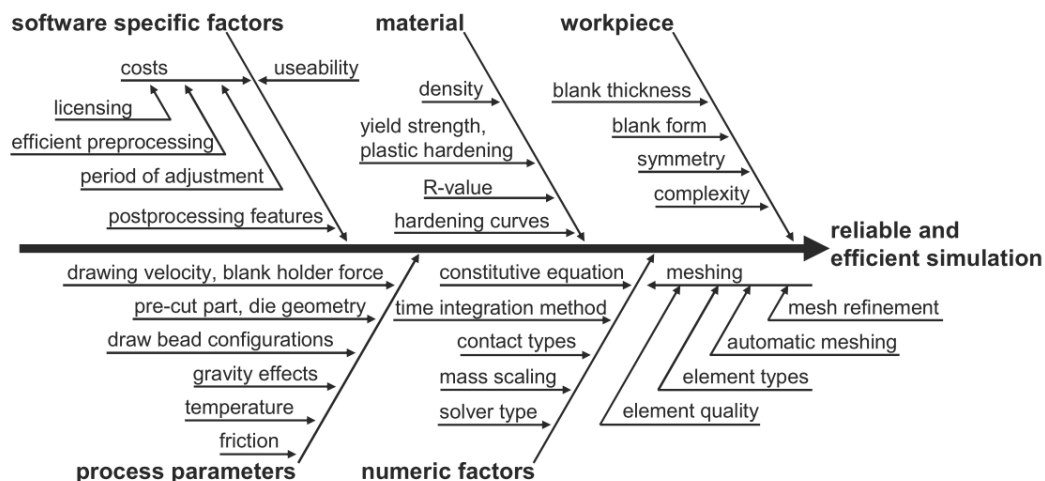


Figure 5.4: Diagramme d'Ishikawa pour simuler le procédé d'emboutissage [204]

modèles numériques basés sur méthode des éléments finis (MEF) ont un comportement déterministe dans la mesure où si l'on relance le code avec les mêmes données d'entrée on obtient des observations identiques. C'est cette absence d'erreur aléatoire qui différencie des expériences numériques des expériences physiques [183]. Les incertitudes sont inévitables dans un processus de fabrication, à toutes les étapes du développement de produit, et pendant tout le cycle de vie du produit. Les incertitudes peuvent conduire à des variations dans les performances des sorties. Les incertitudes proviennent de diverses sources telles que l'imprécision de fabrication, les variations dans les propriétés des matériaux, les variations de dimensions géométriques de la pièce, et les variations de paramètres du procédé. Les sources d'incertitude dans un procédé de formage de tôle de métal sont synthétisées dans la figure 5.5 [154]. Les sources de ces variations inhérentes proviennent de la variation pièce-à-pièce, de lot-à-lot, et l'intérieur du lot au cours du processus de produc-

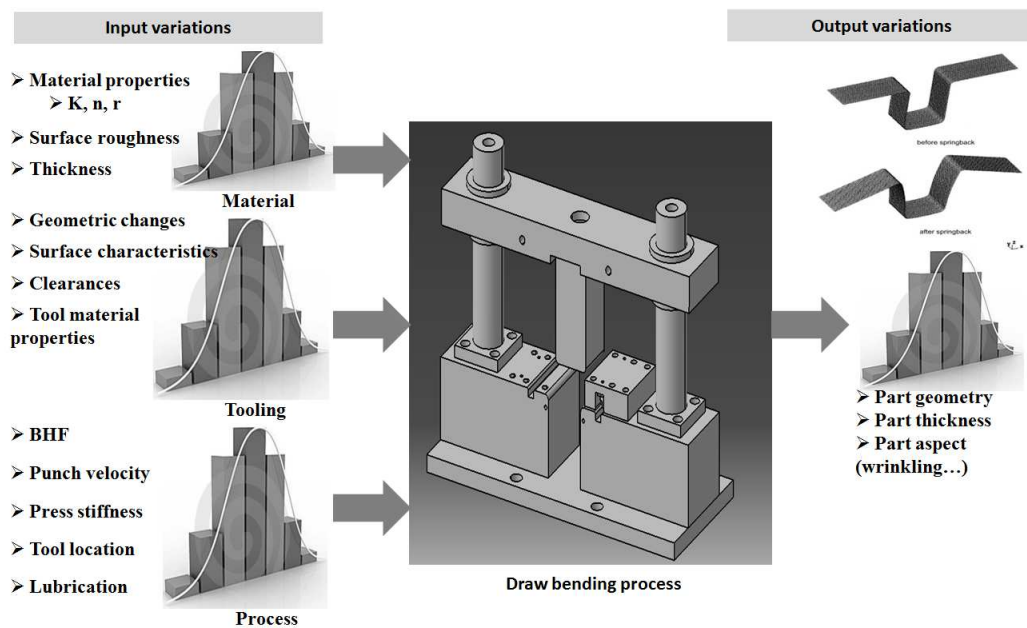


Figure 5.5: Sources d'incertitude dans un procédé de formage de tôle en acier [154].

tion [126]. En particulier, la variabilité des propriétés des matériaux est différente de bobine-à-bobine, de laboratoire-à-laboratoire et d'essai-à-essai. Karthik indique que la dispersion de laboratoire-à-laboratoire est approximativement égale à la dispersion d'essai-à-essai dans un laboratoire. Par contre les variations de bobine-à-bobine présentent généralement plus de dispersions d'essai-à-essai, en particulier dans le sens transversal [98]. Par conséquent, cela conduit à amplifier les variations de performances de la pièce. Afin d'améliorer la qualité, la quantification des incertitudes dans le processus de conception est nécessaire. Des expériences d'ordinateur basées sur des simulations numériques MEF sont l'approche la plus commune pour étudier les problèmes de quantification de l'incertitude [183]. Toutefois, ces expériences informatiques considèrent les outils numériques de type MEF comme une boîte noire, et il est très difficile de modifier ces outils pour améliorer leur précision. En outre, puisque le logiciel numérique type MEF a une précision finie (en raison des erreurs introduites par les méthodes de résolution numériques utilisées comme les erreurs de discrétisation, les erreurs d'approximation, les problèmes de convergence, les erreurs de modélisation, etc), il est nécessaire d'étudier son seuil de sensibilité pour des intervalles de variation des paramètres d'entrée.

Dans la phase de conception détaillée, afin d'assurer le comportement attendus et de satisfaire les exigences fonctionnelles d'une pièce malgré les incertitudes, des tolérances sont affectées à chaque fonction de la pièce. Par conséquent, la définition des tolérances est un élément clé dans l'industrie pour améliorer la qualité des produits et maîtriser les coûts de fabrication. Étant donné que la variation de la performance induite par les incertitudes des entrées de la tôle est assez grande en raison du retour élastique, l'analyse de la tolérance géométrique de la pièce en tôle

est un problème à prendre en considération.

Afin de résoudre ce problème, une méthode de conception robuste, proposée par Taguchi, (aussi connu comme méthode Taguchi) [208], [211] à été développée. Néanmoins, la méthode Taguchi présente plusieurs inconvénients. Puisque Taguchi génère des plans expérimentaux basés sur des tableaux orthogonaux, les conceptions optimales ne peuvent être obtenues que sur ces points d'échantillonnage, tandis que les points intermédiaires ne sont pas évalués. Un autre inconvénient de la méthode Taguchi est l'impossibilité de prendre en compte les effets d'interaction entre les variables de conception [221]. En plus des inconvénients de la méthode Taguchi, la variance de la réponse est provoquée uniquement par les incertitudes des facteurs de bruit. Par conséquent, il est essentiel de construire une stratégie d'optimisation multi-objectif basée sur l'optimisation de la conception robuste (RDO) pour réduire les écarts de performance soumis à des incertitudes dans les deux variables de conception et des facteurs de bruit.

Pour le problème d'optimisation multi-objectif, le front Pareto optimal (POF) représente la solution optimale dans l'espace objectif. Un concepteur sélectionne la solution finale parmi l'ensemble de Pareto sur la base d'exigences supplémentaires, qui peuvent être subjective.

Objectifs de la thèse

L'objectif général de cette thèse est de répondre aux questions:

"Comment maîtriser des incertitudes, au plus tôt dans le cycle de vie du produit, en particulier au niveau de la production?" pour un procédé de formage de tôles à l'aide de simulations numériques basées sur la MEF.

Cet objectif se décline dans cette thèse comme suit:

- Qualifier le niveau de prédictibilité de la simulation numérique MEF du procédé.
- Quantifier les effets des incertitudes sur le procédé de production via la simulation numérique.
- Analyser les incertitudes qui influent sur les tolérances géométriques de la pièce emboutie.
- Optimiser le procédé en présence d'incertitude pour obtenir une pièce emboutie respectant les tolérances spécifiées et cela n'est pas possible remettre en cause de la solution de conception du produit (changement de tolérance, de matériaux, de forme, etc).
- Identifier les meilleures configurations de conception optimale basées sur les indices de capacité.

Méthodes numériques et qualification du modèle EF

Seuil de sensibilité de simulation numérique par méthode EF

Comme présenté dans la Section II, la propagation des incertitudes nécessitent de nombreuses simulations. Pour des très petites variations des paramètres, des techniques de réduction de modèles spécifiques seront développées pour limiter les temps de calculs. Cependant, la simulation numérique MEF est elle-même à précision finie en raison d’erreurs introduites par les méthodes de résolution numérique utilisées (résolution de maillage, contact / frottement, erreur de discrétisation, erreur d’approximation, les problèmes de convergence, etc).

Sensibilité dans l’analyse par éléments finis: montrant seuil de sensibilité

La notion de seuil de sensibilité dans ce travail de recherche vient de l’observation des réponses des simulations MEF, pour lesquelles on observe des résultats incohérents. Le seuil de sensibilité est défini comme un seuil à partir duquel la réponse d’un modèle numérique EF est chaotique à pour de très petite variation d’un paramètre d’entrée.

Illustration sur une poutre en flexion

Dans le cas élémentaire d’un modèle EF en éléments poutre, on peut observer sur la figure 5.6, que une longueur du côté variant autour de sa valeur nominale de -5% à $+5\%$, la réponse calculée par la formule analytique (5.1) et celle de l’analyse numérique EF en 1D sont coïncidentes. Les réponses sont lisses et nettes. La formule analytique de la déflexion de la poutre:

$$\Delta = \frac{12FL^3}{3Ea^4} \quad (5.1)$$

Cependant, lors d’un zoom dans la zone locale de $\pm 0,02\%$ autour de la valeur nominale de $10[mm]$, les réponses calculées par l’analyse numérique EF en 1D avec différentes tailles d’éléments, on observe des sauts correspondants aux valeurs de longueur de côté de $10 \pm 0,01\%$. Tandis que la formule analytique de la flèche donne une réponse lisse et régulière. Ce même problème est également observé lorsque la taille de l’élément diminue. Cela montre bien la limite introduite par la précision finie de la simulation numérique EF.

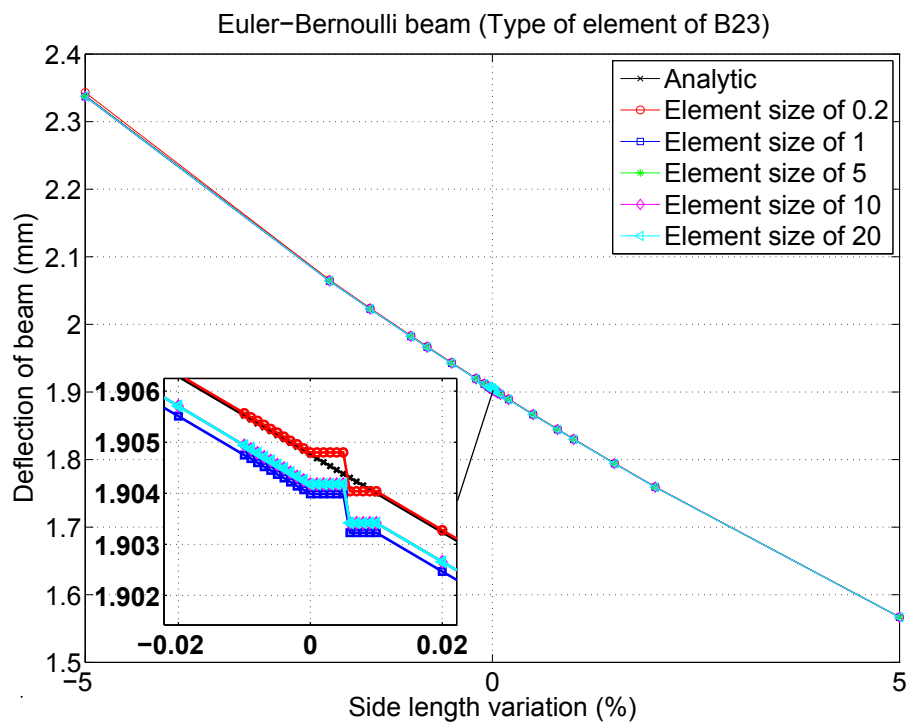


Figure 5.6: Comparaison de flèche calculée analytiquement (5.1) et l'analyse numérique EF en 1D avec différentes tailles d'élément.

Seuil de sensibilité dans la simulation numérique EF de procédé de pliage

Considérons les réponses de retour élastique β_1 , β_2 et ρ par rapport à la variation d'épaisseur de $\pm 5\%$ à $\pm 0,01\%$ autour de la valeur nominale de 1,1 [mm] à 1,6 [mm] comme présenté sur les figures 5.7, 5.8, 5.9.

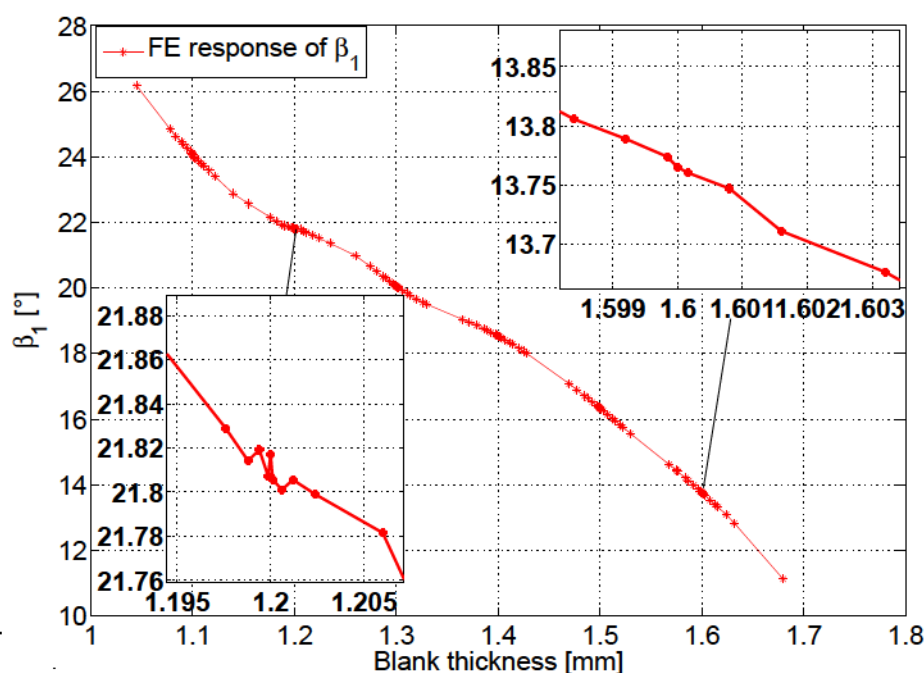


Figure 5.7: évolution d'épaisseur de la tôle par rapport à l'angle β_1 .

On peut voir que les réponses du retour élastique sont régulières et montrent une tendance claire dans la plage globale de variation de 1,1 [mm] 1,6 [mm]. Les réponses de β_1 et β_2 diminuent progressivement avec l'augmentation de l'épaisseur. Alors que la réponse de ρ augmente lorsque l'épaisseur augmente. Néanmoins, on observe des bruits sur les réponses de retour élastique dans une petite plage de variation autour des valeurs nominales d'épaisseur du flan de 1,2 [mm] et 1,6 [mm]. En faisant varier l'épaisseur autour des valeurs nominales (1,2 [mm] et 1,6[mm]) dans un intervalle de $\pm 5\%$ à $\pm 0,01\%$ on observe clairement du bruit sur les réponses du retour élastique. Plus les pas de variations sont petits, donc proches de la valeur nominale et plus l'amplitude du bruit est importante. Par conséquent, cela rend le résultat incohérent et la simulation ne traduit pas correctement les petites variations de l'épaisseur. Un phénomène similaire est également observé sur les réponses du retour élastique par rapport à d'autres valeurs nominales.

A partir de ces résultats, il est intéressant de noter ici qu'il existe bien un seuil de sensibilité en dessous duquel les variations autour d'une valeur nominale ne sont pas correctement propagées par le modèle numérique.

Donc une méthode qui permette d'établir le pas de variation minimal acceptable

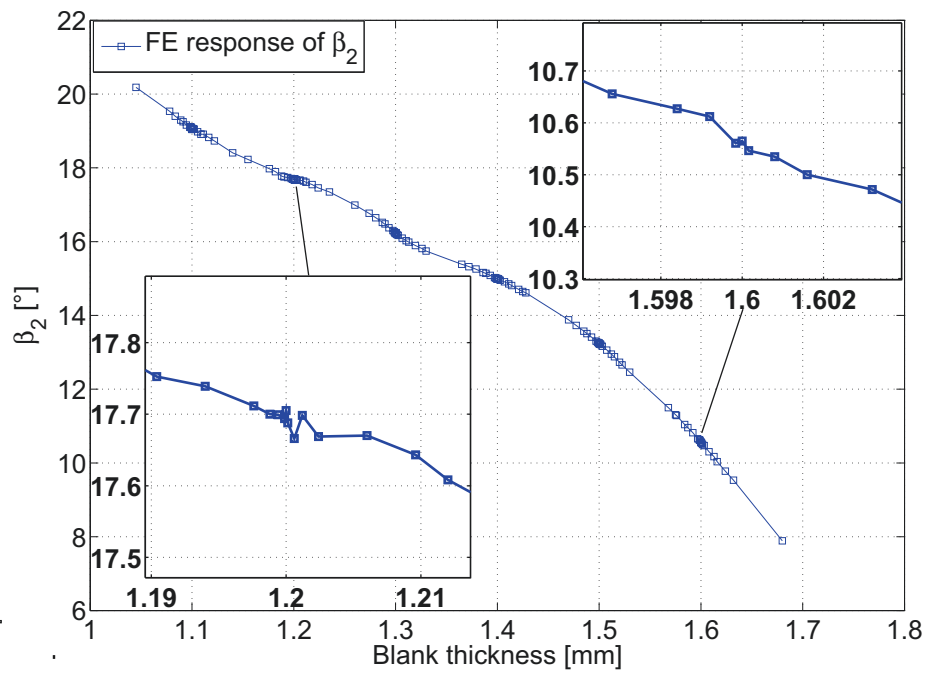


Figure 5.8: évolution d'épaisseur de la tôle par rapport à l'angle β_2 .

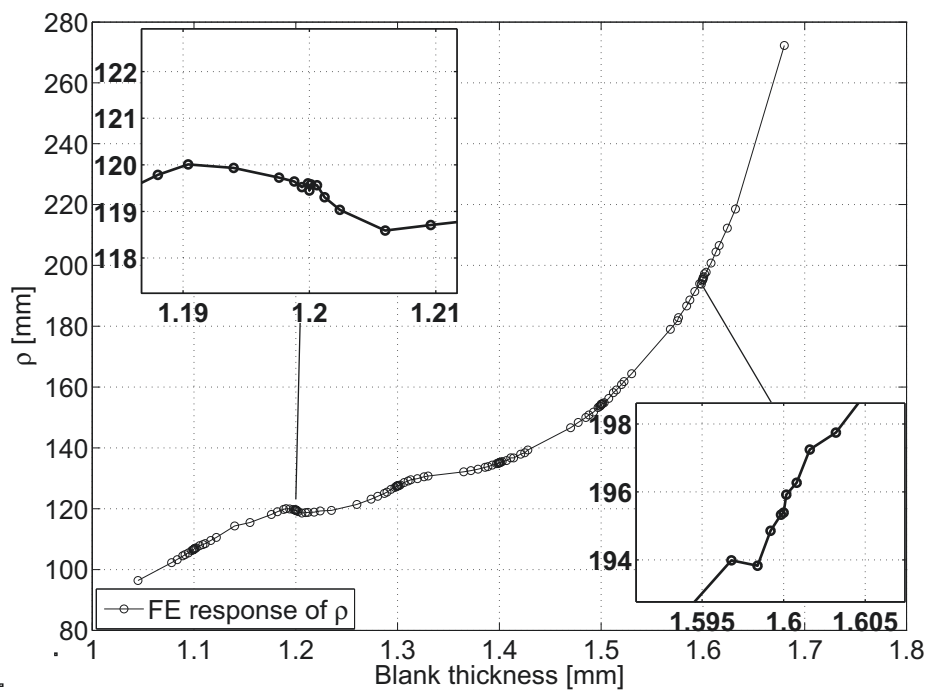


Figure 5.9: évolution d'épaisseur de la tôle par rapport à le rayon ρ .

sur les paramètres d'entrée utilisés dans le plan d'expériences (DOE) est nécessaire afin d'obtenir des réponses fiables par la simulation numérique par MEF. Par conséquent, le pas de variation associé aux incertitudes des paramètres d'entrée doit être bien supérieur au seuil de sensibilité minimal déterminé pour le modèle numérique MEF et le paramètre en question.

Méthodologie proposée pour identifier le seuil de sensibilité de la simulation numérique EF

Pour déterminer le seuil minimum de sensibilité d'un modèle numérique non linéaire EF par rapport aux variations d'un paramètre d'entrée, une approche basée sur l'analyse de la sensibilité de la méthode des différences finies (FDM) est proposée. La procédure proposée se déroule suivant les étapes représentées sur la figure 5.10. Tout d'abord un problème est défini en identifiant les variations des paramètres d'entrée. Les plans d'expériences (DOE) sont utilisés pour échantillonner les valeurs des variables d'entrée qui sont ensuite utilisées dans la simulation numérique EF. Les réponses en sortie sont déterminées et utilisées dans l'identification de seuil de sensibilité en utilisant la méthode des différences finies. Par conséquent, les résultats de seuil de sensibilité sont considérés comme une donnée lors de la saisie de l'intervalle de paramètres d'entrée de la variation de la DOE des expériences numériques.

Afin de réaliser des expériences numériques facilement et afin d'identifier le seuil de sensibilité automatiquement, la simulation du processus de pliage et le retour élastique seront réalisés avec le logiciel Abaqus et les paramètres du retour élastique sont calculés avec Matlab, l'ensemble étant intégré dans le flux de travail de modeFRONTIER.

Pour réduire le temps d'analyse, le calcul est parallélisé sur plusieurs ordinateurs via une procédure spécifique dans modeFRONTIER. Les fichiers d'entrée Abaqus dans lequel les valeurs de variables ont été mises à jour par le DOE sont envoyées au serveur de calcul pour exécuter chaque expérience numérique. Par la suite, les fichiers de résultats sont recopiés sur un ordinateur local afin de déterminer les mesures de retour élastique et calculer la sensibilité.

En théorie, pour une fonction analytique l'approximation de la dérivée par la technique des différences avant, centrale et arrière divergent pour un pas h grand et convergent vers la même limite lorsque le pas h tend asymptotiquement vers zéro. Cependant, ce n'est plus vrai pour une fonction de réponse numérique EF en raison de la précision limitée de modèles numériques.

La technique de détection d'un seuil minimal de sensibilité est la suivante:

Le seuil minimal de sensibilité du modèle numérique EF est identifié pour une valeur du pas de variation pour laquelle l'approximation des différences finies avant, centrale et arrière convergent.

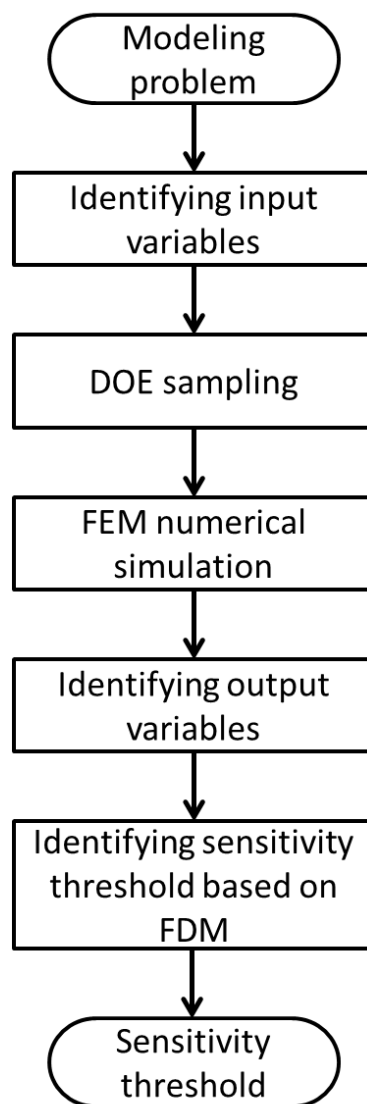


Figure 5.10: Méthodologie proposée pour identifier seuil de sensibilité de la simulation numérique EF.

Exemple d'application

Pour valider la méthode proposée pour l'identification du seuil minimal de sensibilité, un cas plus complexe de simulation numérique processus de pliage de tôle est considéré dans cette partie.

Identification du seuil de sensibilité minimale

Afin de déterminer le seuil minimal de la sensibilité de simulation numérique d'un processus de pliage, le pas de variation h de variables d'entrée comprenant l'épaisseur de la tôle, les propriétés des matériaux, le coefficient de frottement, la force de serre-flan et de la géométrie de l'outillage est réduit progressivement à partir de 20% jusqu'à 0,01% de leurs valeurs nominales.

Les réponses du retour élastique dont β_1 , β_2 et ρ sont considérées comme les fonctions de réponse. Les sensibilités sur ces réponses sont calculées selon la méthode des différences finies.

Les résultats des seuils minimums de sensibilité du processus de pliage de la tôle pour des pas de variation de l'épaisseur de tôle de 20% à 0,01% sont calculés en parallèle avec 25 processeurs sont présentés sur les figures 5.11, 5.12, 5.13.

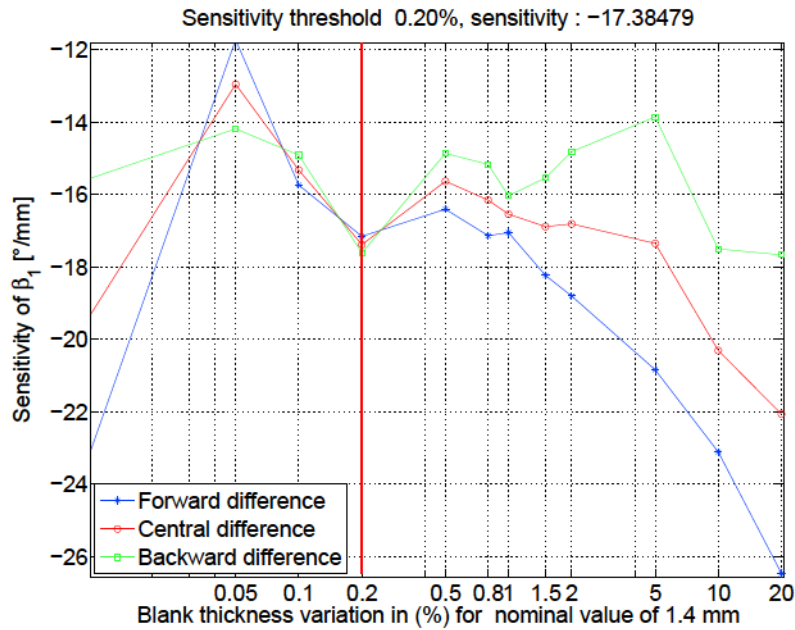


Figure 5.11: Le seuil de sensibilité minimale de la simulation numérique EF du processus de pliage de la tôle par rapport à β_1 pour des variations d'épaisseur de 20% à 0,01%.

On peut observer sur la figure 5.11 que les trois approximations des différences finies avant, arrière et centrale concernant l'angle de retour élastique de β_1 sont divergentes pour des pas supérieur à 20%. Elles se rapprochent ensuite jusqu'au pas

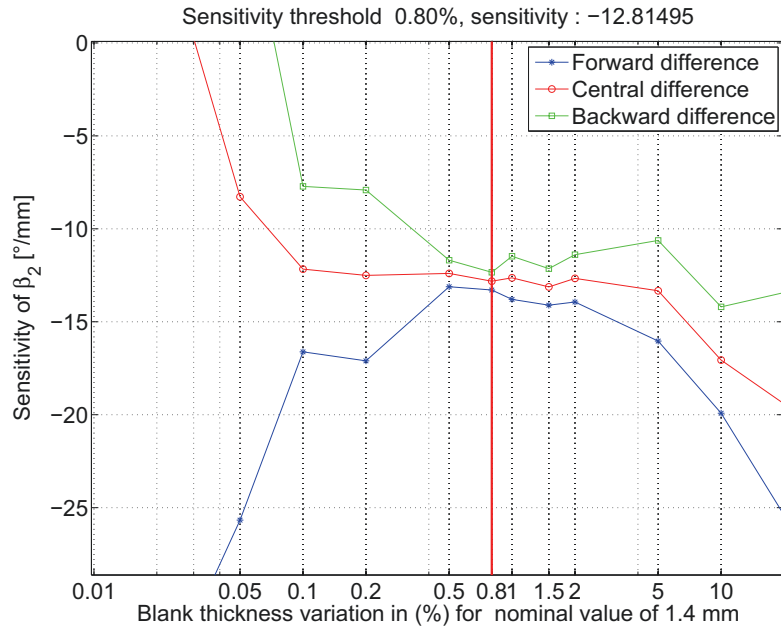


Figure 5.12: Le seuil de sensibilité minimale de la simulation numérique EF du processus de pliage de la tôle par rapport à β_1 pour des variations d'épaisseur de 20% à 0,01%.

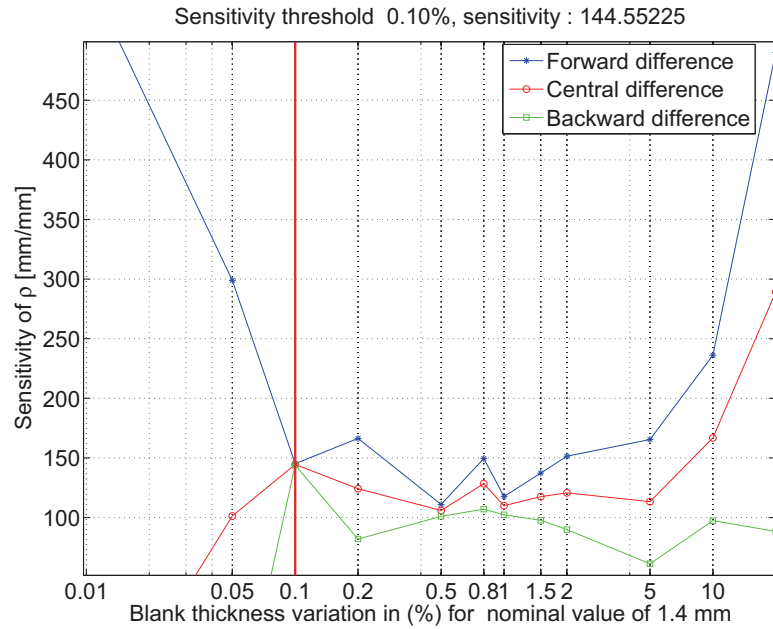


Figure 5.13: Le seuil de sensibilité minimale de la simulation numérique EF du processus de pliage de la tôle par rapport à ρ pour des variations d'épaisseur de 20% à 0,01%.

de 1% puis convergent au pas de 0,2%. Après cela, elles divergent pour des valeurs de pas supérieure à 0,1%. Il est clair que le seuil minimal de sensibilité du modèle numérique EF concernant β_1 par rapport à l'épaisseur du flan peut être fixé à 0,2%. Le même raisonnement, pour l'angle β_2 de la figure 5.12 donne un seuil de 0,8%, et de 0,1% pour le paramètre ρ (cf figure 5.13).

On voit que la simulation numérique MEF propage mal les petites variations d'épaisseur correspond à des pas de variation d'épaisseur du flan plus petits que 0,2%, 0,8% et 0,1% des valeurs nominales, pour les sorties correspondantes respectivement aux angles β_1 , β_2 et ρ le rayon de courbure de la paroi latérale. En conséquence, les réponses numériques de ce modèle MEF ne sont pas fiables lorsque l'intervalle de variation d'épaisseur est plus petit que 0,8% autour de sa valeur nominale. Ce qui signifie que la simulation numérique MEF n'obtient pas de réponses fiables avec un épaisseur du flan de $1,4 \pm 0.0112$ [mm] pour cette étude de cas. De plus, la sensibilité locale des réponses du retour élastique par rapport aux variations d'épaisseur est également déduite de ces résultats. Comme on peut le voir sur les figures 5.11, 5.12, 5.13 la sensibilité locale de β_1 , β_2 , et ρ est $17,38479$ [$^\circ \text{mm}^{-1}$], $12,81495$ [$^\circ \text{mm}^{-1}$] et $144,55225$ [mm mm^{-1}] lorsque l'épaisseur est de 1,4 [mm]. Ces résultats montrent que l'épaisseur influence significativement les réponses du retour élastique. Avec la même méthodologie, le seuil minimal de sensibilité des sept paramètres incluant épaisseur du flan, la limite d'élasticité (YS), la résistance à la traction (UTS), la force de serre-flan (BHF), le coefficient de frottement, le rayon de matrice et le rayon du poinçon sont synthétisés dans le tableau 5.1. Les résultats

Table 5.1: Synthèse du seuil de sensibilité minimale des sept paramètres d'entrée

Paramètre	Seuil de sensibilité concernant β_1 [%]	Seuil de sensibilité concernant β_2 [%]	Seuil de sensibilité concernant ρ [%]	Seuil de sensibilité général de sensibilité [%]	Plage de variation correspondante
t	0.2	0.8	0.1	0.8	1.4 ± 0.0112 [mm]
R_e	1	5	5	5	550 ± 27.5 [MPa]
F_{BHF}	1.5	5	1.5	5	2940 ± 147 [N]
μ	1.5	5	5	5	0.1 ± 0.005
R_d	0.2	5	1	5	7 ± 0.35 [mm]
R_p	1	5	10	10	5 ± 0.5 [mm]
R_m	2	5	2	5	840 ± 42 [MPa]

de la sensibilité sont listés dans le tableau 5.2.

L'analyse des sensibilités du processus de pliage de la tôle

Afin de déterminer l'influence d'un paramètre d'entrée particulier sur le retour élastique, l'analyse des sensibilités peut être réalisée à partir des résultats de la méthode

Table 5.2: La sensibilité de réponse du retour élastique par rapport aux paramètres d'entrée

Paramètre	Sensibilité de β_1	Sensibilité de β_2	Sensibilité de ρ
t	17.3848 [° mm ⁻¹]	12.815 [° mm ⁻¹]	144.5523 [mm mm ⁻¹]
R_e	0.0072 [° MPa ⁻¹]	0.00027 [° MPa ⁻¹]	0.0285 [mm MPa ⁻¹]
F_{BHF}	0.00044 [° N ⁻¹]	0.00056 [° N ⁻¹]	0.00534 [mm N ⁻¹]
μ	26.4348	5.3282	145.9892
R_d	0.0639 [° mm ⁻¹]	0.2547 [° mm ⁻¹]	6.0719 [mm mm ⁻¹]
R_p	0.7132 [° mm ⁻¹]	0.1225 [° mm ⁻¹]	1.1378 [mm mm ⁻¹]
R_m	0.0188 [° MPa ⁻¹]	0.0139 [° MPa ⁻¹]	0.1622 [mm MPa ⁻¹]

proposée pour prédire l'influence du paramètre d'entrée sur les réponses individuelles du retour élastique comme suit:

- Pour l'angle d'ouverture de la paroi β_1 :

$$S_i = \frac{d\beta_1}{dx_i} \xi x_i^{nom} \quad (5.2)$$

- Pour l'angle de la bride β_2 :

$$S_i = \frac{d\beta_2}{dx_i} \xi x_i^{nom} \quad (5.3)$$

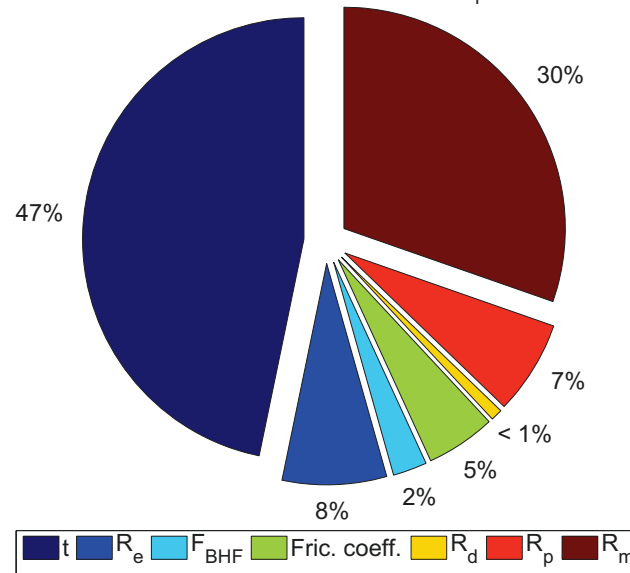
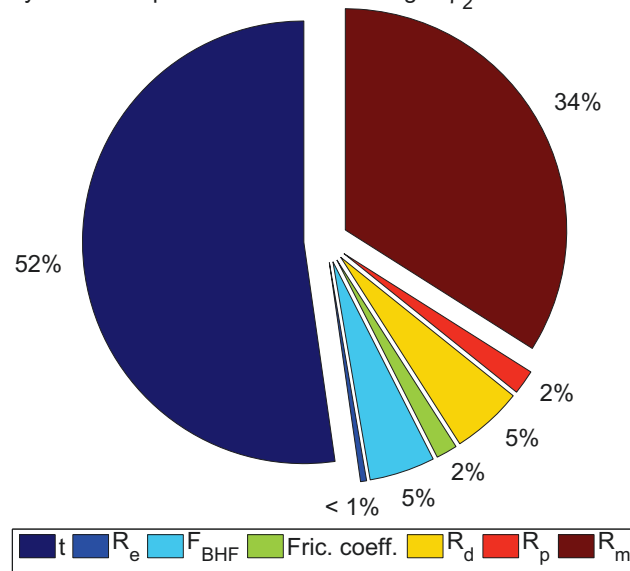
- Pour le rayon de courbure de la paroi latérale ρ :

$$S_i = \frac{d\rho}{dx_i} \xi x_i^{nom} \quad (5.4)$$

où x_i est le $i^{\text{ème}}$ paramètre d'entrée; ξ est le pourcentage de variation et x_i^{nom} est le $i^{\text{ème}}$ paramètre d'entrée à leur valeur nominale.

Les résultats de l'analyse de sensibilité des variables d'entrée contribuant aux réponses du retour élastique de β_1 , β_2 , et ρ sont présentés dans la figure (5.14, 5.15, 5.16).

On peut observer sur la figure 5.14 que l'épaisseur du flan et la résistance à la traction sont les deux paramètres ayant la plus grande influence sur l'angle d'ouverture de la paroi β_1 , suivie par la limite d'élasticité, le rayon du poinçon, le coefficient de frottement, la force de serre-flan et le rayon de matrice. On notera que pour le rayon de matrice, l'influence est quasi-nulle. On peut tirer les mêmes conclusions à propos des deux paramètres les plus influents pour β_2 et ρ . La prise en compte de l'incertitude sur l'épaisseur du flan et des propriétés du matériau dans le processus de conception de procédé, pour maîtriser leurs influences sur les performances de la pièce emboutie, devrait contribuer à la réduction des taux de rejet. Afin de réduire les effets de la variabilité d'épaisseur de la tôle et des propriétés

Sensitivity result of input variables contributing to β_1 at their nominal valueFigure 5.14: L'analyse de sensibilité des variables d'entrée contribuant à la réponse du retour élastique de β_1 à leur valeur nominaleSensitivity result of input variables contributing to β_2 at their nominal valueFigure 5.15: L'analyse de sensibilité des variables d'entrée contribuant à la réponse du retour élastique de β_2 à leur valeur nominale

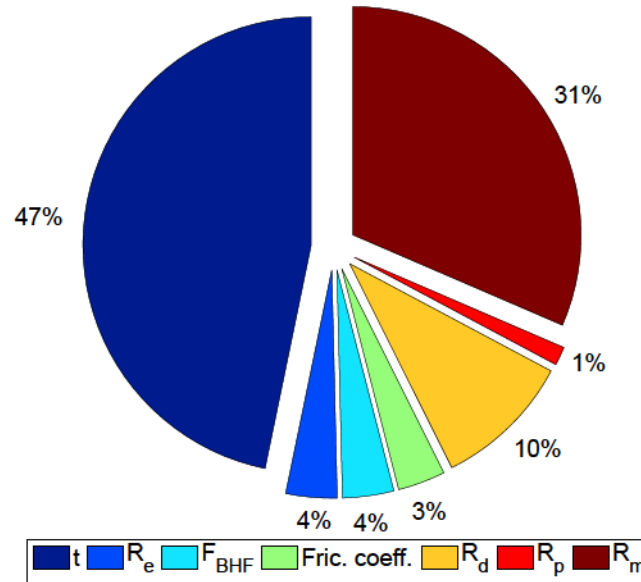
Sensitivity result of input variables contributing to ρ at their nominal value

Figure 5.16: L'analyse de sensibilité des variables d'entrée contribuant à la réponse du retour élastique de ρ à leur valeur nominale

des matériaux et de la géométrie de l'outillage, nous allons rechercher les configurations optimales des paramètres contrôlables du procédé constitués de BHF et des conditions de frottement.

Stratégie pour construire des méta-modèles

Les méta-modèles sont construits selon les 5 premières étapes de la démarche illustrée à la figure 5.17. Les objectifs de l'utilisation des méta-modèles dans cette thèse sont la compréhension et la prédiction des variations dans processus de formage de la tôle. Ensuite, l'exécution des algorithmes d'optimisation sur les méta-modèles pour rechercher des conceptions optimales pour le processus. Les variables d'entrée et de sortie ont été précisées dans la modélisation du processus de formage de tôle. La plage de précision des méta-modèles dépend des objectifs du méta-modèle. Un méta-modèle utilisé pour la prédiction doit être très précis, tandis que pour un méta-modèle utilisé pour la compréhension, il suffit qu'il puisse reproduire une tendance. Les gammes de précisions peuvent être spécifiées par les mesures de validité tels que l'erreur quadratique moyenne (RMSE), l'erreur absolue maximale (MAE). Avant d'échantillonner des variables d'entrée pour construire un DOE, il est nécessaire d'identifier le seuil minimum de sensibilité du modèle EF pour obtenir des résultats de simulation MEF fiables. Le procédé pour identifier ce seuil minimum de sensibilité du modèle EF a été proposé dans la section précédente. L'étape suivante consiste à exécuter les simulations MEF pour l'ensemble des variables d'entrée

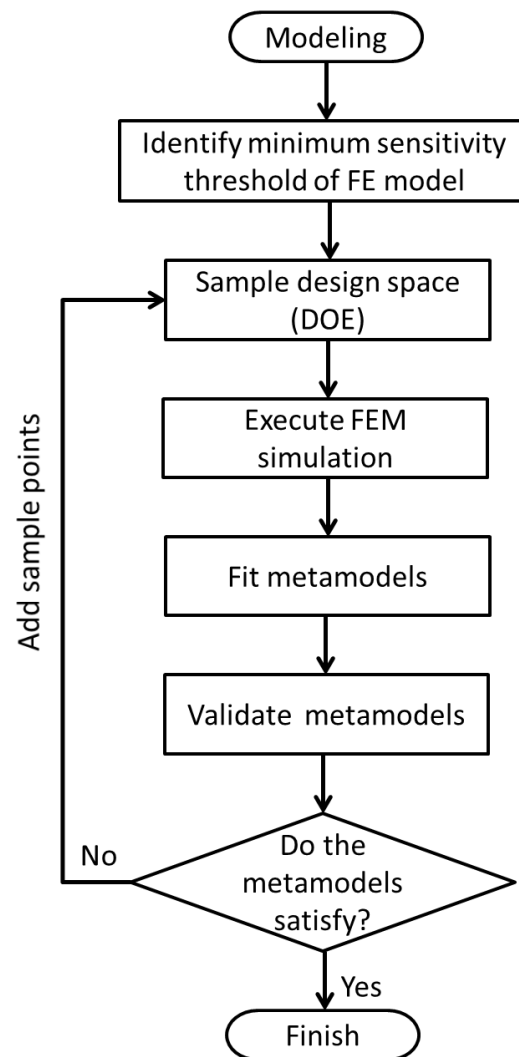


Figure 5.17: Organigramme du processus de métamodélisation

échantillonnées dans DOE. Ensuite, les méta-modèles sont construits avec les valeurs des réponses. Les mesures de validité sont calculées pour comparer la précision du méta-modèle avec la précision requise. Si le méta-modèle ne satisfait pas aux exigences de précision, on peut revenir à l'étape du choix d'un DOE pour ajouter des points expérimentaux (donc d'autres simulations) et par la suite adapter le méta-modèle avec cette information supplémentaire. Ce processus est répété jusqu'à ce que les exigences de précision requises soient satisfaites.

Méta-modèle pour le procédé de formage de tôle

Une simulation MEF du procédé de formage de tôle peut nécessiter généralement plusieurs heures de calculs. Afin d'avoir une évaluation probabiliste (c-à-d: moyenne la variance des sorties) des paramètres des sortie du procédé de formage de tôle, plusieurs milliers d'évaluations sont nécessaires. De plus, pour obtenir la convergence de l'optimisation, plusieurs milliers de points d'échantillonnage sont exigés. Donc, il est impossible d'exécuter une simulation MEF pour chaque évaluation. Alors, il est nécessaire d'utiliser un modèle de substitution pour ce but.

Les variables d'entrée comprennent les tôles d'épaisseur t , la force de serre-flan F_{BHF} , le coefficient de frottement μ , la limite d'élasticité R_e , résistance à la traction R_m , le rayon du poinçon R_p , et celui de la matrice R_d . Les données d'entrée pour la stratégie DOE sont données dans le tableau 5.3, dans lequel les propriétés des matériaux sont tirées de données Arcelormittal [7].

Table 5.3: Les données d'entrée pour la stratégie DOE

Facteurs	Niveaux		
t [mm]	1	1.5	2
F_{BHF} [kN]	2.94	26.47	50
μ	0.04	0.1	0.16
R_e [MPa] [7]	500	550	600
R_m [MPa] [7]	780	840	900
R_p [mm]	2	6	10
R_d [mm]	2	6	10

Le plan d'expériences utilisé pour échantillonner, est un plan factoriel complet à plusieurs niveaux. Cette méthode fonctionne mieux avec moins de huit variables et moins de quatre niveaux. Dans ce cas, nous avons 7 facteurs à 3 niveaux, soit $3^7 = 2187$ points d'échantillonnage initiaux.

Les variables de sortie sont des paramètres retour élastique β_1 , β_2 , ρ . Nous avons besoin de construire un méta-modèle pour chaque variable de sortie:

$$\beta_1 = f_1(t, F_{BHF}, \mu, R_e, R_m, R_p, R_d) \quad (5.5)$$

$$\beta_2 = f_2(t, F_{BHF}, \mu, R_e, R_m, R_p, R_d) \quad (5.6)$$

$$\rho = f_3(t, F_{BHF}, \mu, R_e, R_m, R_p, R_d) \quad (5.7)$$

En comparant entre la précision de plusieurs méta-modèles, il est constaté que la précision de la méthode de RBF est la meilleure comme l'indique le tableau 5.4.

Table 5.4: Comparaison de la précision de métamodèles

RSM	Réponses	MAE	R-carré
Kriging	β_1	7.4591×10^{-5}	0.9999
	β_2	5.6535×10^{-3}	0.9999
	ρ	4.2752×10^{-6}	1
SVD2	β_1	12.0715	0.8727
	β_2	30.8179	0.8829
	ρ	96665.8	0.0768
SVD3	β_1	9.9122	0.9724
	β_2	29.4869	0.9651
	ρ	92667.0694	0.1431
RBF	β_1	9.0596×10^{-11}	1
	β_2	3.2892×10^{-10}	1
	ρ	6.0101×10^{-7}	1
NN	β_1	0.8783	0.9999
	β_2	12.1686	0.9982
	ρ	21912.8576	0.9154

Incertitudes et dispersions géométriques

Catégorisation des incertitudes

Une classification classique des incertitudes est de les séparer en deux types: incertitudes aléatoires et incertitudes épistémiques. Les incertitudes aléatoires sont intrinsèquement de nature stochastique irréductible. Les incertitudes aléatoires pour une tôle emboutie comprennent les variabilités stochastiques dans les propriétés des matériaux, l'épaisseur de la tôle et les caractéristiques de frottement de la surface. Ces incertitudes aléatoires sont considérées comme des variabilités paramétriques. D'autre part, l'incertitude épistémique est due au manque de connaissances ou au caractère incomplet de l'information et elle est subjective et réductible. Les incertitudes épistémiques comprennent des incertitudes sur le modèle utilisé pour décrire la réalité, ses limites et les conditions d'exploitation, également appelées erreurs de forme de modèle [125]. On peut aussi y inclure les erreurs introduites par les méthodes de résolution numérique utilisées (par exemple, les erreurs de discrétisation, les erreurs d'approximation, les problèmes de convergence, ..) [14].

Dans la conception d'un procédé d'emboutissage de tôle basée sur la simulation numérique MEF, les deux types d'incertitudes sont présents. La classification des incertitudes est représenté dans la figure 5.18. D'autre part, sur la base de l'idée

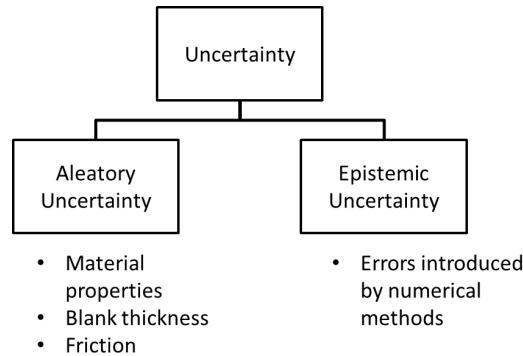


Figure 5.18: Taxonomie des incertitudes dans la conception d'un procédé d'emboutissage de tôle basée sur la simulation numérique MEF.

originale proposée par Taguchi, les paramètres de tous les problèmes de conception peuvent être classés en deux groupes [30]: (1) les facteurs de contrôle composés des entrées que le concepteur est libre de manipuler et (2) des facteurs de bruit, qui sont des entrées qui sont difficiles ou coûteuses à contrôler. La figure 5.19 représente un P-diagramme d'un modèle numérique utilisé pour décrire le produit ou le processus

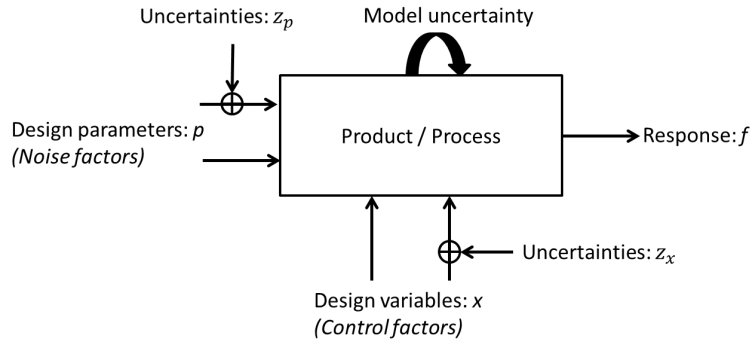


Figure 5.19: P-diagramme

physique réel. Elle représente schématiquement la relation entre l'entrée du modèle et la sortie ou réponse.

Stratégie pour la propagation de l'incertitude

Comme indiqué au chapitre précédent, avant de procéder à la propagation des incertitudes, il est indispensable de construire des méta-modèles qui seront ensuite utilisés pour estimer les moments probabilistes des réponses. En effet plusieurs milliers, voire des millions d'évaluations sont nécessaires pour une évaluation probabiliste, le modèle EF du procédé de formage de tôle ne peut pas être utilisée directement. Par conséquent, une approche pour la propagation de l'incertitude sur la base de méta-modèle est proposée comme indiqué dans figure 5.20.

Après les variables d'entrée aient été identifiées, l'incertitude des paramètres d'entrée est modélisée et représentée par des distributions Gaussienne comme présenté dans le tableau 5.5. L'échantillonnage de Latin Hypercube est ensuite utilisé pour

Table 5.5: Modélisation probabiliste : représentation des incertitudes dans les paramètres d'entrée

Paramètres	Distribution	Bornes d'intervalle	Moyenne	écarte-type
F_{BHF} [kN]	Normal	[2.94,50]	26.47	0.6667
R_d [mm]	Normal	[2,10]	6	0.0167
R_p [mm]	Normal	[2,10]	6	0.0167
R_e [MPa]	Normal	[500,600]	550	16.667
R_m [MPa]	Normal	[780,900]	840	20
μ	Normal	[0.04, 0.16]	0.1	0.0033
t [mm]	Normal	[1,2]	1.5	0.0167

les valeurs des paramètres incertains. Ces points d'échantillonnage sont propagées à travers les méta-modèles pour atteindre moments statistiques des réponses.

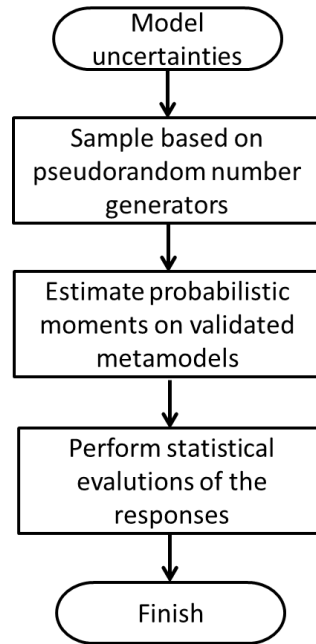


Figure 5.20: Démarche proposée pour la propagation de l'incertitude.

Propagation de distribution

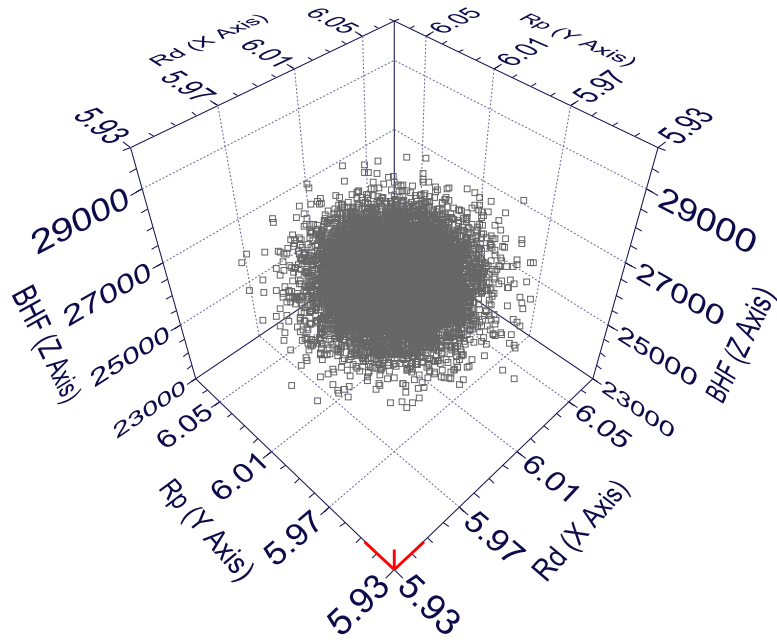
Les paramètres d'entrée sont échantillonnés par LHS comme représentés graphiquement dans la Figure 5.21. Les paramètres d'entrée sont supposés comme des variables aléatoires continues. Cela représente incertitudes aléatoires dans les paramètres d'entrée de pliage de la tôle. L'un des objectifs de propagation de l'incertitude est d'évaluer les moments statistiques des sorties. Figure 5.22 et Table 5.6 montrent la densité de probabilité ainsi que la moyenne et l'écart type β_1 , β_2 et ρ .

Table 5.6: Les deux premiers moments statistiques de β_1 , β_2 and ρ

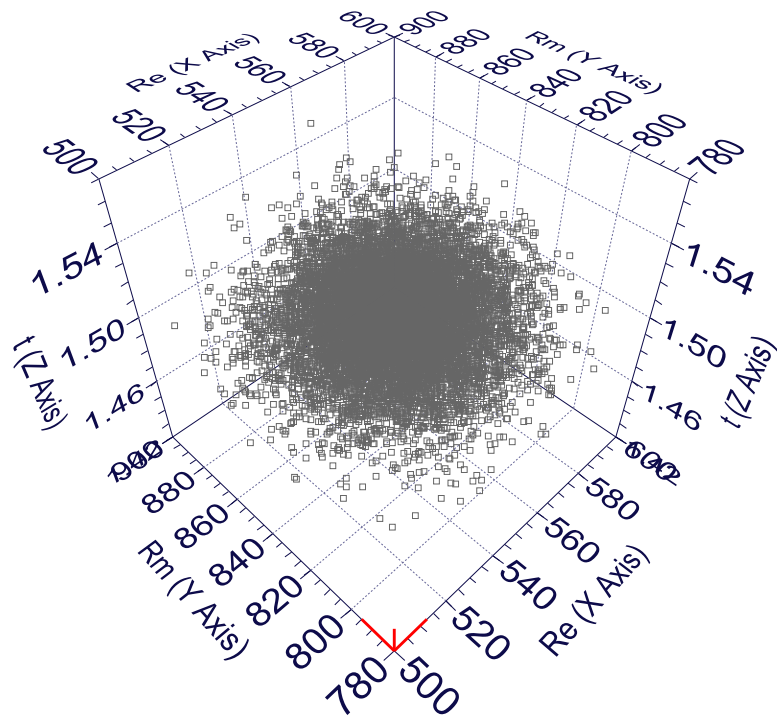
Paramètres	β_1 [°]	β_2 [°]	ρ [mm]
Moyenne	17.823	12.7535	150.854
écarte-type	0.9693	0.745	66.7696

Détermination des variations de performance basé sur l'exigence fonctionnelle

On suppose que les composants sont assemblés entre eux par des rivets. Pour s'assurer qu'il n'y ait pas de problème dans le processus d'assemblage, les composants doivent respecter les spécifications fonctionnelles sur la position des perçages des rivets. Par conséquent, la variation de position d'un trou en raison du retour

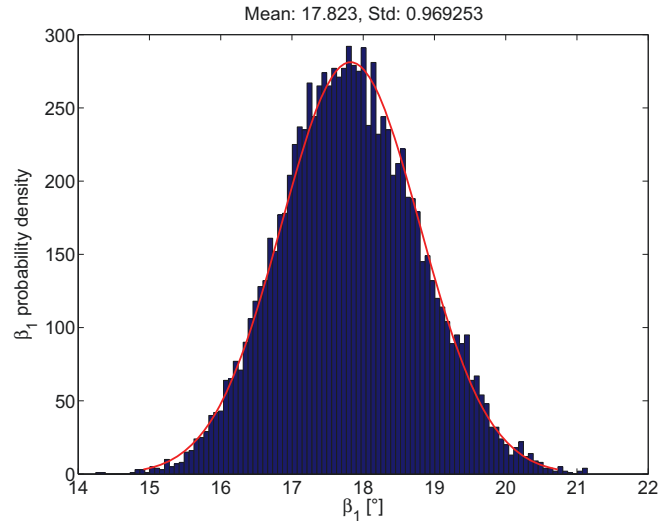
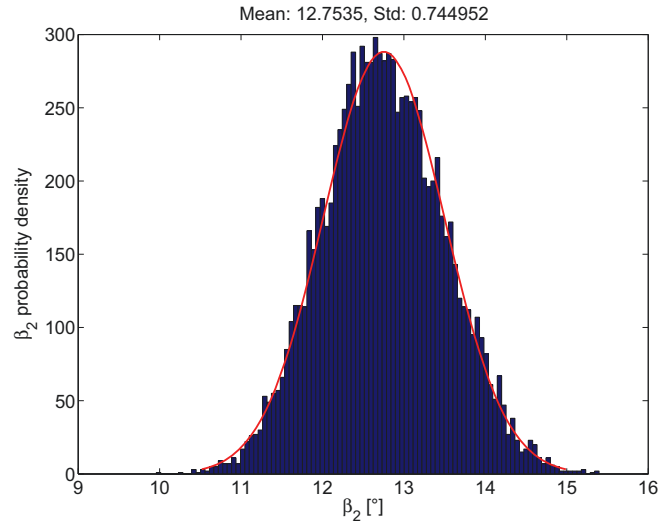
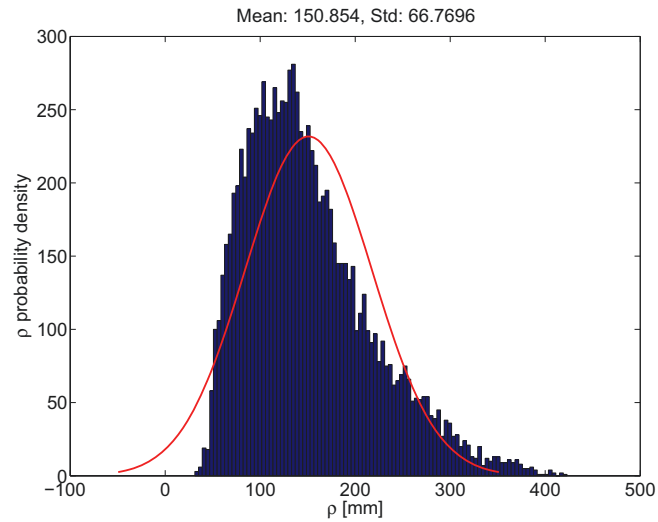


(a) 10000 points d'échantillonnage générés par LHS pour R_d , R_p et F_{BHF}



(b) 10000 points d'échantillonnage générés par LHS pour R_e , R_m et t

Figure 5.21: Les points d'échantillonnage générés par LHS pour les paramètres d'entrée

(a) β_1 probability density(b) β_2 probability density(c) ρ probability densityFigure 5.22: La densité de probabilité de β_1 , β_2 and ρ

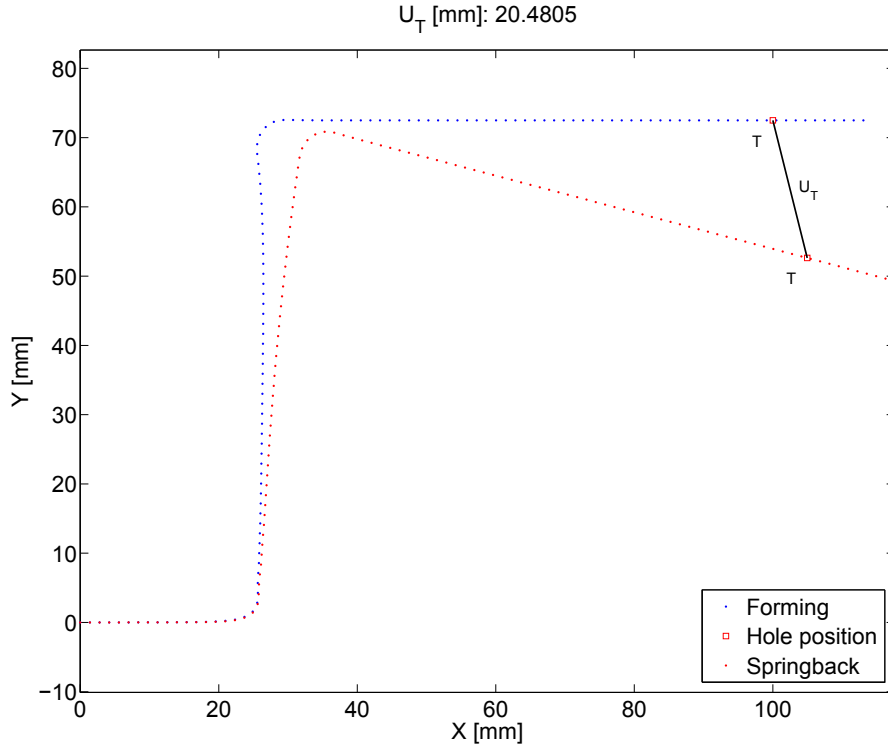


Figure 5.23: La variabilité de la position du trou avant et après le retour élastique.

élastique doit être prise en compte.

La position du trou, marquée par le point T , avant et après le retour élastique avec une moitié de la pièce est présentée dans la Figure 5.23. L'exigence fonctionnelle du trou sur la pièce se traduit par:

- La position du trou à partir du point de référence dans l'axe horizontal est de 100 [mm].
- L'amplitude du déplacement du trou doit être dans l'intervalle de tolérance admissible.

L'amplitude du déplacement de trou est définie par:

$$U_T = \sqrt{(x_T - x_T^0)^2 + (y_T - y_T^0)^2} \quad (5.8)$$

où (x_T^0, y_T^0) est la coordonnée du point T avant retour élastique et (x_T, y_T) est la coordonnée du point T après retour élastique.

Métamodèle et analyse d'incertitude pour U_T

On trouve que le méta-modèle de type RBF présente la meilleure précision pour représenter le U_T comme indiqué dans le tableau 5.7. La Figure 5.24 montre le

Table 5.7: Comparaison de la précision des méta-modèles pour U_T

RSM	Réponses	MAE	R-carré
Krigeage	U_T	1.0258×10^{-4}	0.9999
SVD2	U_T	36.6112	0.8268
SVD3	U_T	38.6366	0.9370
RBF	U_T	5.7494×10^{-10}	1
NN	U_T	16.9244	0.9988

méta-modèles de U_T par rapport à F_{BHF} et R_d . La Figure 5.25 montre la densité

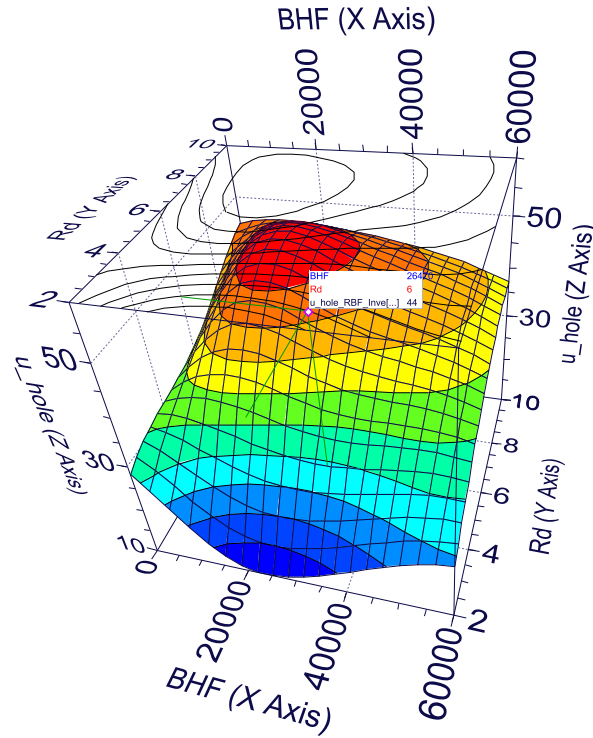


Figure 5.24: Méta-modél de U_T par rapport à F_{BHF} et R_d .

de probabilité ainsi que la moyenne et l'écart-type de déplacement de trou U_T . On peut voir que la variation de la position du trou est importante en raison des incertitudes aléatoires sur les entrées. Le déplacement du trou est assez important, minimiser ce déplacement et sa variation est nécessaire. Une optimisation de type MORDO sera présentée dans le prochain chapitre pour assurer cette minimisation.

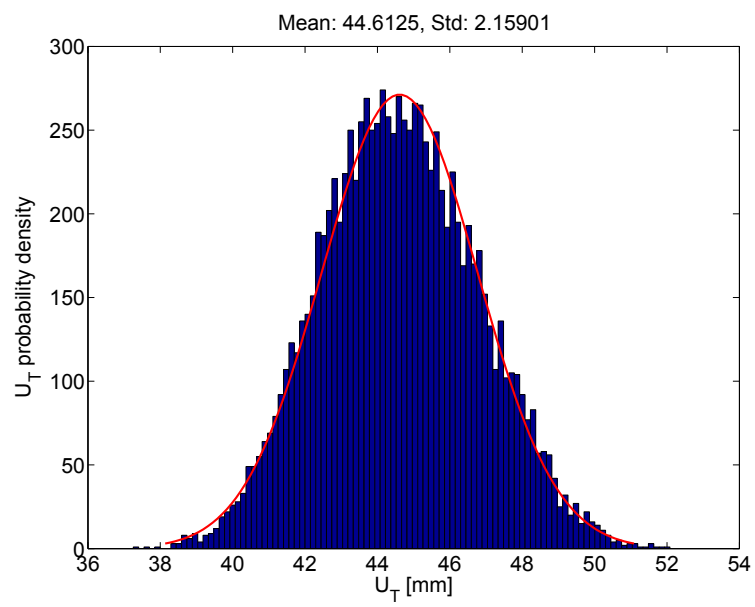


Figure 5.25: La densité de probabilité du déplacement de trou U_T .

Optimisation multi-objectif en présence d'incertitudes

Stratégie d'optimisation multi-objectif sous incertitude pour procédé de formage de tôle

L'objectif de cette thèse est de proposer une stratégie pour l'optimisation multi-objectif de la conception robuste du procédé d'emboutissage de la tôle.

Comme indiqué, les variables d'entrée du processus se classe en deux catégories: les variables de conception (facteurs de contrôle) et les paramètres de conception (facteurs de bruit). En particulier, les variables de conception comprennent trois paramètres:

- Force serrage F_{BHF}
- Rayon de matrice R_d
- Rayon de poinçon R_p

Facteurs de bruit comprennent 4 paramètres:

- épaisseur de la tôle t
- Limite d'élasticité R_e
- Résistance à la traction R_m
- Coefficient de frottement μ

Supposons que les valeurs cibles des paramètres de retour élastique β_1 , β_2 , ρ et trou déplacement U_T sont respectivement 0 [°], 0 [°], $+\infty$ et 0 [mm].

Optimisation multi-objectif et conception robuste

Selon Choi et al. [33] et Allen et al. [4], il existe quatre types de conception robuste.

- Le type I consiste à représenter les incertitudes par des paramètres séparés des variables de conception. Il s'agit alors d'optimiser les variables de conception de façon à ce que les spécifications fonctionnelles soient satisfaites quelques soit les incertitudes sur les facteurs de bruits.
- Le type II consiste à considérer que les incertitudes sont incluses dans les variables de conception.
- Le type III consiste à considérer que les incertitudes sont incluses dans les fonctions du système.

- Le type IV consiste à considérer que les incertitudes sont présentes dans le processus d'analyse du système.

L'approche de conception robuste proposée dans cette thèse relève à la fois du type I et du type II. Dans le type I, la variance de la réponse est provoquée par les variations des facteurs de bruit. Bien que la conception robuste de type II soit différente du type I, la variation de la performance est due à uniquement des variations des facteurs ou des variables de contrôle de conception [30]. L'approche proposée pour le MORDO prend en compte les incertitudes dans les facteurs de contrôle et des incertitudes dans les facteurs de bruit.

L'objectif de l'optimisation robuste est de minimiser à la fois l'écart de la valeur moyenne $\delta = |\mu_f - T|$, et la variance σ_f^2 , de la fonction de la performance, sous les contraintes. La stratégie de conception multi-objectif utilisant l'optimisation de conception robuste est présentée dans la Figure 5.26. Supposons que x est le vecteur des facteurs de contrôle de F_{BHF}, R_d, R_p et z est le vecteur des facteurs de bruit de t, R_e, R_m, μ . La modélisation des incertitudes sur l'épaisseur, les propriétés des matériaux, le coefficient de frottement est représentée par la distribution gaussienne pour des raisons de commodité mathématique car un modèle gaussien peut être spécifié uniquement par ses deux premiers moments.

Table 5.8: Modélisation probabiliste et la représentation des incertitudes dans les paramètres pour le cas de déplacement de trou U_T

Paramètres	Distribution	Moyenne	écarte-type	Bornes d'intervalle
F_{BHF} [kN]	Normal	26.470	0.6667	[4.940, 48]
R_d [mm]	Normal	6	0.0167	[2.05, 9.95]
R_p [mm]	Normal	6	0.0167	[2.05, 9.95]
R_e [MPa]	Normal	550	16.6667	[500, 600]
R_m [MPa]	Normal	840	20	[780, 900]
μ	Normal	0.1	0.0033	[0.04, 0.16]
t [mm]	Normal	2	0.0167	[1, 2]

MORDO de déplacement de trou de U_T

La modélisation probabiliste et la représentation des incertitudes dans les facteurs sont présentées dans le tableau 5.9. Dans le cas où la fonction de performance est le déplacement de trou U_T , la formulation MORDO est représentée comme suit:

$$\text{Find } x \quad (5.9a)$$

$$\text{to minimize} \quad (5.9b)$$

$$F_{obj1}(x) = E[U_T(x, z)] - U_T^{Target} \quad (5.9c)$$

$$F_{obj2}(x) = \sigma(U_T(x, z)) \quad (5.9d)$$

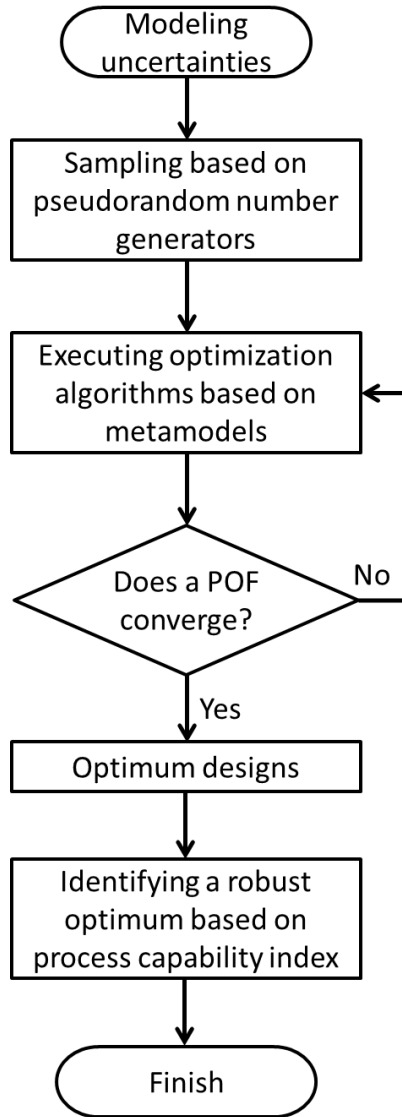
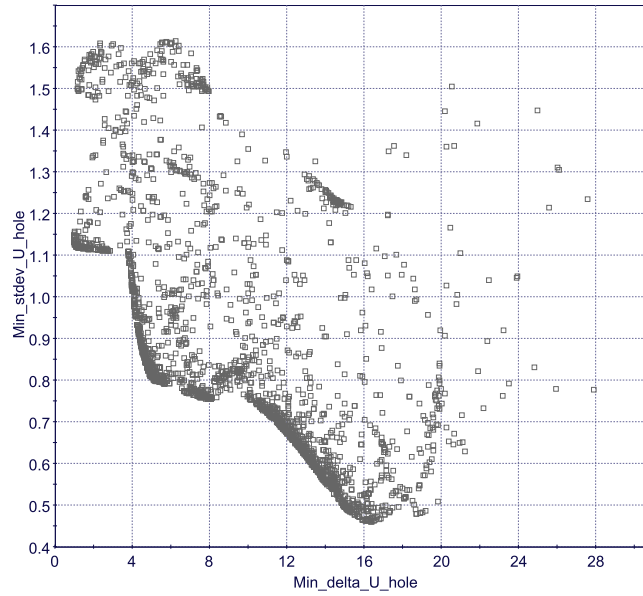


Figure 5.26: A multi-objective design strategy using robust design optimization

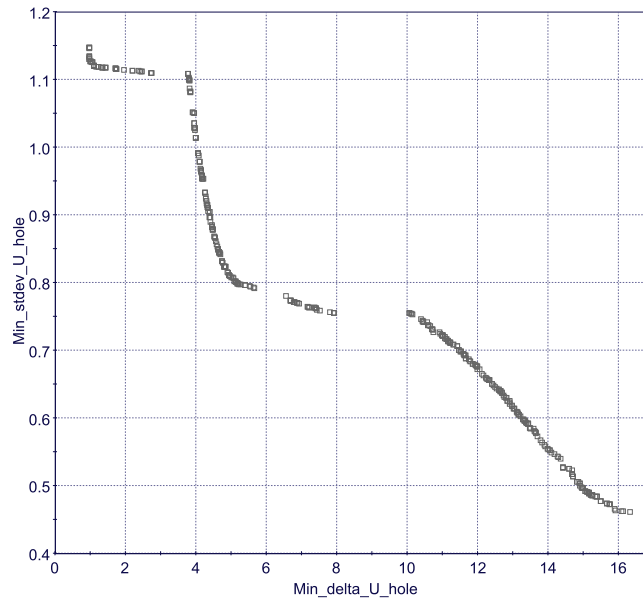
Table 5.9: Modélisation probabiliste et la représentation des incertitudes dans les paramètres pour le cas de déplacement de trou U_T

Paramètres	Distribution	Moyenne	écarte-type	Bornes d'intervalle
F_{BHF} [kN]	Normal	26.470	0.6667	[4.940,48]
R_d [mm]	Normal	6	0.0167	[2.05,9.95]
R_p [mm]	Normal	6	0.0167	[2.05,9.95]
R_e [MPa]	Normal	550	16.6667	[500,600]
R_m [MPa]	Normal	840	20	[780,900]
μ	Normal	0.1	0.0033	[0.04, 0.16]
t [mm]	Normal	2	0.0167	[1,2]

L'algorithme NSGA-II est utilisé dans cette optimisation de MORDO. Cet algorithme a trouvé 425 solutions de conception optimaux graphiquement représentés par le front de Pareto avant (POF) représenté sur la figure 5.27.



(a) Nombre total de conceptions (2500 points)



(b) 425 conceptions optimales sur POF

Figure 5.27: Front optimal de Pareto obtenu de MORDO de déplacement de trou de U_T

MORDO des paramètres de β_1 , β_2 , ρ

Le formulation du problème d'optimisation multi-objectifs de conception robuste avec les trois variables de sortie est la suivante :

$$\text{Find } x \quad (5.10a)$$

$$\text{to minimize} \quad (5.10b)$$

$$F_{obj1}(x) = E[\beta_1(x, z)] - \beta_1^{Target} \quad (5.10c)$$

$$F_{obj2}(x) = E[\beta_2(x, z)] - \beta_2^{Target} \quad (5.10d)$$

$$F_{obj3}(x) = E\left[\frac{1}{\rho(x, z)}\right] - \frac{1}{\rho^{Target}} \quad (5.10e)$$

$$F_{obj4}(x) = \sigma(\beta_1(x, z)) \quad (5.10f)$$

$$F_{obj5}(x) = \sigma(\beta_2(x, z)) \quad (5.10g)$$

$$F_{obj6}(x) = \sigma\left(\frac{1}{\rho(x, z)}\right) \quad (5.10h)$$

De même, les incertitudes dans les paramètres contrôlables et non contrôlables sont modélisés par la distribution gaussienne, comme indiqué dans le Tableau 5.10. Puisqu'il y a six fonctions objectifs, les solutions optimales de Pareto sont représen-

Table 5.10: Modélisation probabiliste et représentation des incertitudes sur les paramètres dans le cas des 3 sorties β_1 , β_2 et ρ

Paramètres	Distribution	Moyenne	écarte-type	Bornes d'intervalle
F_{BHF} [kN]	Normal	26.470	0.6667	[4.940, 48]
R_d [mm]	Normal	6	0.0167	[2.05, 9.95]
R_p [mm]	Normal	6	0.0167	[2.05, 9.95]
R_e [MPa]	Normal	550	16.6667	[500, 600]
R_m [MPa]	Normal	840	20	[780, 900]
μ	Normal	0.1	0.0033	[0.04, 0.16]
t [mm]	Normal	1.5	0.0167	[1, 2]

tées par une hypersurface de dimension six. Cependant, cette hypersurface ne peut pas être représentée graphiquement dans ce cas.

La prise de décision de multi-critère basée sur les indices de capacité

Les résultats de l'optimisation multi-critère de la conception robuste sont des solutions optimales de Pareto. Un des problèmes dans MORDO est de déterminer une conception de compromis qui est gouvernée par plusieurs critères antagonistes. Pour résoudre ce problème, une prise de décision basée sur des indices de capacité de C_{pk} , C_{pm} et I est proposée. Tout d'abord, cette approche est introduite pour le cas de

la conception gouvernée par des deux objectifs avec l'optimisation du déplacement du trou U_T . Ensuite, elle est généralisée à la conception gouvernée par plus de deux objectifs et en particulier appliquée dans le cas de 6 objectifs du MORDO des paramètres de retour élastique de β_1 , β_2 et $1/\rho$.

Prise de décision dans l'espace de critères 2-D

La représentation graphique des indices de capacité de C_{pk} , C_{pm} et I dans lequel l'index C_{pk} est représenté par une forme linéaire, alors que les indices C_{pm} et I sont représentés par la forme quadratique de la figure 5.28. Selon l'indice de capacité

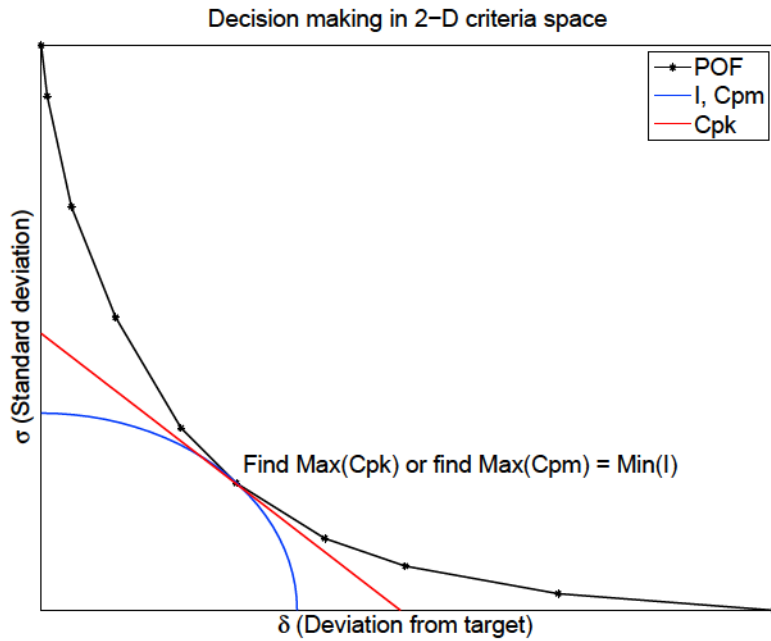


Figure 5.28: La prise de décision dans l'espace des critères 2-D basée sur des indices de capacité

utilisé par un concepteur, une solution de compromis est déterminée.

Comme la valeur cible de U_T est supposée être 0 [mm], la spécification de U_T est représenté par $U_T = 0 \pm IT/2$ [mm].

L'indice de C_{pk}

La meilleure solution est celle qui donne la valeur de C_{pk}^i maximale:

$$C_{pk}^i = \frac{\frac{IT}{2} - |\delta_{U_T}^i|}{3\sigma_{U_T}^i} \quad (5.11)$$

L'indice de C_{pm}

De même, la meilleure solution est celle qui donne la valeur de C_{pk}^i maximale:

$$C_{pm}^i = \frac{IT}{6\sqrt{(\delta_{U_T}^i)^2 + (\sigma_{U_T}^i)^2}} \quad (5.12)$$

L'indice de I

La meilleure solution est celle qui donne la valeur de C_{pk}^i minimale:

$$I^i = \sqrt{(\sigma_{U_T}^i)^2 + (\delta_{U_T}^i)^2} \quad (5.13)$$

La prise de décision dans l'espace de critères 6-D

Puisqu'il y a 6 fonctions objectif donnés, des solutions Pareto optimales sont représentées par une hypersurface de dimensions 6 de $\sigma_{\beta_1}, \sigma_{\beta_2}, \sigma_{1/\rho}, \delta_{\beta_1}, \delta_{\beta_2}, \delta_{1/\rho}$. Ainsi, la recherche d'une meilleure solution de compromis de solutions Pareto optimales en 6-D sera réalisée en combinant les indices de capabilité utilisés à partir de dimensions supérieures à des dimensions inférieures.

Comme mentionné ci-dessus, les valeurs cibles de β_1, β_2 et $1/\rho$ sont supposées être 0 [°] et 0 [mm] respectivement, les spécifications de ces trois variables sont représentées comme $\beta_1 = 0 \pm IT/2$ [°], $\beta_2 = 0 \pm IT/2$ [°] et $1/\rho = 0 \pm IT/2$ [mm].

L'indice de C_{pk}

La meilleure solution est celle qui donne la valeur de MC_{pk} maximale:

$$MC_{pk} = \left(\prod_{i=1}^m C_{pk}^i \right)^{(1/m)} \quad (5.14)$$

Où i est le nombre de variables de sortie.

L'indice de C_{pm}

La meilleure solution est celle qui donne la valeur de MC_{pm} maximale:

$$MC_{pm} = \left(\prod_{i=1}^m C_{pm}^i \right)^{(1/m)} \quad (5.15)$$

L'indice de I

La meilleure solution est celle qui donne la valeur de MI minimale:

$$MI = \left(\prod_{i=1}^m I_i \right)^{(1/m)} \quad (5.16)$$

Synthèse des résultats

Les meilleures solutions en fonction des indices de capacité qui ont été obtenues à partir de la MORDO de déplacement de trou de U_T et trois paramètres de retour élastique de β_1 , β_2 , $1/\rho$ sont synthétisées dans le tableau 5.11. On trouve que la configuration de la conception optimale qui est indiquée en utilisant le C_{pk} indice dépend de la valeurs IT . Bien que la configuration de conception optimale soit identique malgré les différentes valeurs de IT lors de l'utilisation de l'indice de C_{pm} .

Pour les paramètres de retour élastique de β_1 , β_2 , $1/\rho$, la configuration de conception optimale obtenue par C_{pm} satisfait la valeur de IT plus petit que celui atteint par C_{pk} . La différence de résultats prévus de β_1 , β_2 , $1/\rho$ est très petite lorsque l'on compare entre les solutions de conception basées sur C_{pk} et C_{pm} . Alors que pour déplacement de trou de U_T la valeur de IT à partir de C_{pm} est plus grand que celui de C_{pk} . Les résultats prévus de U_T basés sur ces indices sont les mêmes.

Table 5.11: Synthèse des meilleures solutions sur la base des indices de capabilité

Paramètres	IT	C_{pk}	C_{pm}	Solution ID
β_1	9 [°]	3.6222	N/A	1736 (Table 5.12)
β_2	9 [°]	3.2771		
$1/\rho$	9 [mm]	24051		
U_T	11 [mm]	1.335		1112 (Table 5.13)
β_1	3.8 [°]	N/A	1.6215	1271 (Table 5.14)
β_2	3.8 [°]		1.3634	
$1/\rho$	3.8 [mm]		150.107	
U_T	12 [mm]		1.346	1112 (Table 5.15)

Table 5.12: La meilleure solution de compromis trouvé en trouvant valeur maximale de MC_{pk} de trois paramètres retour élastique β_1 , β_2 , $1/\rho$

Valeurs de C_{pk}		$C_{pk}^{\beta_1} = 3.62217$; $C_{pk}^{\beta_2} = 3.27706$; $C_{pk}^{\rho} = 24051$		
Valeurs d'IT		$IT = 9$		
Solution ID		1736		
Paramètres	Mean	Stdev	Min	Max
F_{BHF} [N]	2.7150×10^4	6.6530×10^2	2.5079×10^4	2.9270×10^4
R_d [mm]	2.4013	1.6686×10^{-2}	2.3491	2.4542
R_e [MPa]	5.4999×10^2	1.6703×10^1	4.8229×10^2	6.0456×10^2
R_m [MPa]	8.4001×10^2	20	7.7752×10^2	9.1239×10^2
R_p [mm]	9.95	1.6709×10^{-2}	9.8870	1.0003×10^1
μ	0.1	3.3052×10^{-3}	8.8856×10^{-2}	1.1199×10^{-1}
t [mm]	1.5	1.6682×10^{-2}	1.4476	1.5518
β_1 [°]	-6.1158×10^{-1}	3.5784×10^{-1}	-1.8810	4.7824×10^{-1}
β_2 [°]	9.0027×10^{-2}	4.4857×10^{-1}	-1.5982	1.6313
$1/\rho$ [mm]	4.5243×10^{-3}	6.2305×10^{-5}	4.7692×10^{-3}	4.2682×10^{-3}

Table 5.13: La meilleure solution lors de $C_{pk} = 0.67$, $C_{pk} = 1.00$ and $C_{pk} = 1.33$

Valeurs de C_{pk}		$C_{pk} = 0.67$; $C_{pk} = 1.00$; $C_{pk} = 1.33$		
Valeurs d'IT [mm]		$IT = 6.48$; $IT = 8.72$; $IT = 11$		
Solution ID		1112		
Paramètres	Mean	Stdev	Min	Max
F_{BHF} [N]	4.7778×10^4	6.6530×10^2	4.5707×10^4	4.9898×10^4
R_d [mm]	9.95	1.6686×10^{-2}	9.8977	1.0003×10^1
R_e [MPa]	5.4999×10^2	1.6703×10^1	4.8229×10^2	6.0456×10^2
R_m [MPa]	8.4001×10^2	20	7.7752×10^2	9.1239×10^2
R_p [mm]	2.5346	1.6709×10^{-2}	2.4716	2.5875
μ	0.1	3.3052×10^{-3}	8.8856×10^{-2}	1.1199×10^{-1}
t [mm]	2	1.6682×10^{-2}	1.9476	2.0518
U_T [mm]	9.5960×10^{-1}	1.1340	-2.2829	4.6259

Table 5.14: La meilleure solution de compromis trouvé en trouvant valeur maximale de MC_{pm} de trois paramètres retour élastique β_1 , β_2 , $1/\rho$

Critère	C_{pm}			
Interval de tolérance	$IT = 3.8$			
Solution ID	1271			
Paramètres	Mean	Stdev	Min	Max
F_{BHF} [N]	2.6728×10^4	6.6530×10^2	2.4656×10^4	2.8848×10^4
R_d [mm]	2.4055	1.6686×10^{-2}	2.3532	2.4583
R_e [MPa]	5.4999×10^2	1.6703×10^1	4.8229×10^2	6.0456×10^2
R_m [MPa]	8.4001×10^2	20	7.7752×10^2	9.1239×10^2
R_p [mm]	9.6323	1.6709×10^{-2}	9.5694	9.6853
μ	0.1	3.3052×10^{-3}	8.8856×10^{-2}	1.1199×10^{-1}
t [mm]	1.5	1.6682×10^{-2}	1.4476	1.5518
β_1 [°]	2.0182×10^{-2}	3.9007×10^{-1}	-1.4289	1.2220
β_2 [°]	1.0770×10^{-1}	4.5186×10^{-1}	-1.5421	1.6678
$1/\rho$ [mm]	4.2183×10^{-3}	8.5893×10^{-5}	4.5659×10^{-3}	4.0159×10^{-3}

Table 5.15: La meilleure solution trouvée par l'aide de l'indice de C_{pm}

Critère	C_{pm}			
Solution ID	1112			
Paramètres	Mean	Stdev	Min	Max
F_{BHF} [N]	4.7778×10^4	6.6530×10^2	4.5707×10^4	4.9898×10^4
R_d [mm]	9.95	1.6686×10^{-2}	9.8977	1.0003×10^1
R_e [MPa]	5.4999×10^2	1.6703×10^1	4.8229×10^2	6.0456×10^2
R_m [MPa]	8.4001×10^2	20	7.7752×10^2	9.1239×10^2
R_p [mm]	2.5346	1.6709×10^{-2}	2.4716	2.5875
μ	0.1	3.3052×10^{-3}	8.8856×10^{-2}	1.1199×10^{-1}
t [mm]	2	1.6682×10^{-2}	1.9476	2.0518
U_T [mm]	9.5960×10^{-1}	1.1340	-2.2829	4.6259

Conclusions et perspectives

Conclusions

Les deux objectifs de conception robuste sont de rendre la valeur moyenne proche de la valeur cible et de minimiser la variabilité qui résulte de l'incertitude représentée par des facteurs de bruit. Cette thèse a proposé une stratégie d'optimisation robuste pour prendre en compte les incertitudes aléatoires dans les facteurs de bruit pour optimiser la conception des processus de fabrication en présence des incertitudes. Dans le contexte de l'ingénierie simultanée et la simulation numérique MEF, cette stratégie a été élaborée pour répondre au défi dans le processus de conception: "Comment concevoir pour produire des produits robustes". Il est dédié à la conception de procédé d'emboutissage.

Plusieurs conclusions clés sont tirées de cette recherche :

- En termes de modélisation et de simulation MEF, la précision des modèles numériques MEF dépend de la précision des modèles utilisés pour décrire la réalité (des équations du comportement du matériau, des conditions aux limites ...) et de la précision des méthodes de résolution numériques (discrétisation, facteur de mise à l'échelle de la masse, maillage, types de contact ...). En outre, elle dépend aussi de paramètres du processus (l'effort du serre-flan, des conditions de frottement, de la pièce, de la géométrie de l'outillage, de la vitesse ...). L'étude des modèles numériques MEF a démontré qu'il existe un seuil de sensibilité auquel les réponses de ces des modèles numériques MEF sont insensibles à de très faibles variations des paramètres d'entrée du modèle. En conséquence, des variations inférieures à ce seuil autour de valeurs nominales des paramètres d'entrée ne sont pas correctement propagées par le modèle numériques MEF. Afin d'être capable de construire des expériences numériques basées sur simulation MEF et de propager de manière cohérente ces incertitudes, nous avons proposé une approche basée sur une méthode de différence finie (FDM) pour détecter seuil minimum de sensibilité d'un modèle EF. Cette méthode a été appliquée avec succès pour le problème de référence de pliage de tôle Numisheet2011.
- L'incertitude est inévitable dans un processus de fabrication. Par conséquent, la gestion des incertitudes dans le cycle de vie du produit au début, en particulier dès les phases de conception préliminaire est essentielle. À travers l'analyse des incertitudes du pliage de tôle, nous avons montré que les méthodes de conception classiques ne peuvent pas toujours satisfaire les objectifs souhaités en raison des incertitudes aléatoires qui existent dans les propriétés du matériau, l'épaisseur de la tôle et les paramètres du processus. L'étude de ces incertitudes aléatoires a permis de constater qu'elles influencent de manière significative la variation des performances du produit. En particulier,

l'épaisseur et les propriétés des matériaux vierges sont des paramètres ayant la plus grande influence sur la variation de forme due au retour élastique.

- À travers l'analyse des incertitudes de configurations de conception obtenues par optimisation classique (également connue sous le nom d'optimisation de la conception déterministe), nous avons constaté qu'il existe un écart entre la valeur moyenne et l'écart-type dans les réponses des paramètres de forme du pliage d'une tôle en forme de U en raison des incertitudes aléatoires importantes dans les paramètres incontrôlables. Afin de résoudre ce problème, une stratégie d'optimisation de conception robuste appliquée à la conception d'un processus de pliage de la tôle a été proposée. Cette stratégie a été appliquée avec succès au problème de référence du processus de pliage d'une tôle en U.
- Une stratégie d'optimisation multi-objectif en contexte incertain pour les processus de pliage de tôle a été introduite. Un critère de prise de décision fondé sur les indices de capacité appliqués à la conception robuste a été proposé. Nous avons établi que la meilleure solution, obtenue à partir des solutions optimales de Pareto en utilisant l'indice C_{pk} dépend de l'intervalle de tolérance (IT). Avec différentes valeurs de IT , la meilleure solution est différente. Alors que la valeur de IT n'a pas d'influence sur la détermination de la meilleure alternative en utilisant l'indice C_{pm} . La meilleure solution trouvée par cet indice est identique pour toutes les différentes valeurs de IT . Toutefois, afin de vérifier la capacité de configuration de conceptions optimales obtenues sur la base des indices C_{pk} et C_{pm} , ces solutions de conception ont été déterminées pour assurer un taux de fiabilité du procédé de 99,99 % correspondant à un taux de rebut de 63 PPM. Cette approche a été appliquée avec succès aux problèmes d'optimisation avec les critères s'exprimant dans des espaces en 2 et 6 dimensions.

Perspectives

Plusieurs points pour une recherche future sont proposés sur la base des connaissances acquises et les problèmes rencontrés lors de l'étude de cette thèse:

- Pour la simulation numérique MEF des procédés de formage de la tôle, un modèle de comportement approprié qui décrit correctement le comportement du matériau est crucial. Un des effets significatifs sur la qualité de la prédiction du retour élastique est le modèle de comportement du matériau. En particulier, la modélisation de l'effet Bauschinger et des caractéristiques de durcissement cycliques des matériaux est essentielle. Pour la recherche future, il serait judicieux d'essayer des modèles de comportement avancés pour la prédiction du retour élastique comme la loi d'écrouissage de Geng-Wagoner [65] et la loi d'écrouissage de Yoshida-Uemori[241] qui ont montré que pour décrire le retour élastique elles produisaient un meilleur comportement. En outre, il y a encore l'écart entre les résultats obtenus par un procédé physique

et la simulation numérique. Cette différence résulte des hypothèses du modèle, discrétisation du modèle, les types de contact, du maillage, du facteur de mise à l'échelle de la masse, etc... L'amélioration continue des méthodes numériques et de la modélisation de problèmes reste indispensable pour la recherche future.

- En ce qui concerne l'analyse de sensibilité de seuil de la simulation numérique MEF, ce seuil peut être amélioré lorsque la précision du modèle numérique est améliorée. L'étude du seuil de sensibilité avec un maillage plus fin et une vitesse de poinçon inférieure est recommandée. En outre, l'approche proposée pour détecter le seuil de sensibilité doit être testée avec un différent logiciel basé sur MEF comme un point de départ pour des travaux futurs.
- Puisque les méta modèles jouent un rôle très important dans la stratégie d'optimisation en conception robuste, l'amélioration de la précision des méthodes de méta-modélisation est recommandée comme un point dans les travaux futurs. Actuellement, la précision du méta modèle dépend du choix de la méthode de méta-modélisation la mieux adaptée aux données d'entrée.
- Dans ce travail de thèse nous nous sommes limités à l'usage de sept paramètres d'entrée pour le modèle numérique. L'ajout de plus de paramètres dans l'étude est proposé comme recherche future. En particulier, l'étude de la dispersion des propriétés d'anisotropies du matériau est une suggestion. D'autre part, les incertitudes dans les paramètres d'entrée sont pris en compte en raison des variations de pièce-à-pièce, à l'intérieur du lot, de bobine-à-bobine, de lot-à-lot et de laboratoire-à-laboratoire. Il est recommandé d'étudier les incertitudes des paramètres d'entrée résultant de variations à l'intérieur de pièce. Par exemple, la variation de l'épaisseur dans la pièce en raison de l'imprécision du processus de laminage. De même, la dispersion des paramètres de processus tels que la force serrage, la friction entre les surfaces devrait être approfondie.
- En ce qui concerne la tolérancement géométrique, nous suggérons d'utiliser une analyse des tolérances basée sur une base modale pour représenter les variations de forme des pièces embouties.
- La stratégie d'optimisation est effectuée en utilisant des modèles et des approximations numériques du processus réel, des erreurs existent toujours. Nous recommandons fortement de valider les configurations de conception optimale obtenues en les testant sur un procédé réel.

Appendix

A.1 Equations for calculating the springback paramters

$$\theta_1^0 = \arccos \left(\frac{\vec{ox} \times A\vec{oBo}}{|\vec{ox}| \times |A\vec{oBo}|} \right) \quad (\text{A.1})$$

$$\theta_2^0 = \arccos \left(\frac{\vec{ox} \times A\vec{oBo}}{|\vec{ox}| \times |A\vec{oBo}|} \right) \quad (\text{A.2})$$

$$\theta_1 = \arccos \left(\frac{\vec{ox} \times \vec{AB}}{|\vec{ox}| \times |\vec{AB}|} \right) \quad (\text{A.3})$$

$$\theta_2 = \arccos \left(\frac{\vec{AB} \times \vec{DE}}{|\vec{DE}| \times |\vec{AB}|} \right) \quad (\text{A.4})$$

$$\beta_1 = \theta_1 - \theta_1^0 \quad (\text{A.5})$$

$$\beta_2 = \theta_2^0 - \theta_2 \quad (\text{A.6})$$

$$\rho = \sqrt{(x_A - x_I)^2 + (y_A - y_I)^2} \quad (\text{A.7})$$

Where,

$$x_I = \frac{(b_2 - b_1)}{\left(\frac{1}{a_2} - \frac{1}{a_1}\right)} \quad (\text{A.8})$$

$$y_I = b_1 - \left(\frac{x_I}{a_1}\right) \quad (\text{A.9})$$

$$a_1 = \frac{y_B - y_A}{x_B - x_A} \quad (\text{A.10})$$

$$b_1 = \frac{y_B + y_A}{2} + \frac{x_B + x_A}{2a_1} \quad (\text{A.11})$$

$$a_2 = \frac{y_C - y_A}{x_C - x_A} \quad (\text{A.12})$$

$$b_2 = \frac{y_C + y_A}{2} + \frac{x_C + x_A}{2a_2} \quad (\text{A.13})$$

A.2 Numerical analysis procedures

A.2.1 Dynamic explicit procedure

Starting from the virtual work equation:

$$\int_V T_{ij} \delta u_{i,j} dV = \int_S t_i \delta u_i dS - \int_V \rho \ddot{u}_i \delta u_i dV \quad (\text{A.14})$$

where T_{ij} is the Cauchy stress tensor, $u_{i,j}$ the gradient of the displacements, t_i the traction vector, ρ the density, \ddot{u}_i the acceleration of material particles and δ the variational operator. After being discretized from the principle of virtual work, the equation (A.14) has the form:

$$[M] \ddot{u}^t = F_{ext}^t - F_{int}^t \quad (\text{A.15})$$

where $[M]$ is the mass matrix, F_{ext}^t the external force and F_{int}^t the internal force vector at a time t . An explicit central-difference time integration rule is used in the explicit dynamics procedure to perform a large number of small time increments efficiently. The explicit central-difference operator satisfies the dynamic equilibrium equations at the beginning of the increment, t ; the accelerations calculated at time t are used to advance the velocity solution to time $t + \Delta t/2$ and the displacement solution to time $t + \Delta t$. The equations of motion for the body are integrated using the explicit central-difference integration rule:

$$\dot{u}_{(i+\frac{1}{2})}^N = \dot{u}_{(i-\frac{1}{2})}^N + \frac{\Delta t_{i+1} + \Delta t_{(i)}}{2} \ddot{u}_{(i)}^N \quad (\text{A.16})$$

$$u_{(i+1)}^N = u_{(i)}^N + \Delta t_{(i+t)} \dot{u}_{(i+\frac{1}{2})}^N \quad (\text{A.17})$$

where u^N is a degree of freedom and the subscript i refers to the increment number in an explicit dynamics step. The central-difference integration operator is explicit in the sense that the kinematic state is advanced using known values of $\dot{u}_{(i-\frac{1}{2})}^N$ and $\ddot{u}_{(i)}^N$ from the previous increment. In order to compensate for possible density manipulations, the equation (A.15) must be introduced by an artificial damping term:

$$[M] \ddot{u}^t + [C] \dot{u}^t = F_{ext}^t - F_{int}^t \quad (\text{A.18})$$

where $[C]$ is the damping matrix and \dot{u} the velocity. Since the central-difference operator is conditionally stable, the stable time increment is given by:

$$\Delta t_{stable} \leq \frac{2}{\omega_{max}} \approx \frac{L^e}{C_d} \approx \frac{L^e}{\sqrt{\frac{E}{\rho}}} \quad (\text{A.19})$$

where ω_{max} is the highest frequency of the system; L^e is the element length in the mesh; C_d is the wave speed of the material; E is the Young's modulus of the material; ρ is the mass density.

Most sheet metal forming analyses require too much computer time to be run in their physical time scale because the actual time period of forming events is large by explicit dynamics. Thus, it is critical to reduce the time of the analysis. There are two methods for speeding up the analysis:

- Artificially increase the punch velocity so that the same forming process occurs in a shorter step time. This method is called load rate scaling.
- Artificially increase the mass density of the elements so that the stability limit increases, allowing the analysis to take fewer increments. This method is called mass scaling.

In order to ensure that dynamic effects are insignificant on the output results, the kinetic-to-internal energy ratio is required less than about 5%.

A.2.2 Static implicit procedure

The virtual work equation which body forces are not considered has the form:

$$\int_V T_{ij} \delta u_{i,j} dV = \int_S t_i \delta u_i dS \quad (\text{A.20})$$

After being transformed into a known configuration in time yielding, the equation (A.20) is defined as follows:

$$\int_V [dT_{ij} - T_{kj} du_{i,k} + T_{ij} du_{k,k}] \delta u_{i,j} dV = \int_S t_i \delta u_i dS \quad (\text{A.21})$$

A stiffness equation obtain after discretizing from the principle of virtual work:

$$[K(u)]u = F \quad (\text{A.22})$$

The static implicit procedure is executed according to an incremental step-by-step solution in which it is assumed that the static equilibrium configuration of a body is defined at the increment t . The configuration at the time $t + \Delta t$ attains by means of an iterative procedure, based on each iteration on the solution of the following finite element governing equations [3]:

$$([K_L]_t^t + [K_{NL}]_t^t) \Delta U^{(i)} = R^{t+\Delta t} - F_{t+\Delta t}^{t+\Delta t, (i-1)} \quad (\text{A.23})$$

$$U^{t+\Delta t, (i)} = U^{t+\Delta t, (i-1)} + \Delta U^{(i)} \quad (\text{A.24})$$

where $[K_L]_t^t$ is the linear strain incremental stiffness mastrix at the time t measured with respect to the configuration at the same time t ; $[K_{NL}]_t^t$ the non-linear strain incremental stiffness matrix at the time t , which contains the term due to the non-linear relationship between strains and displacements; $\Delta U^{(i)}$ the vector of the increments of the nodal point displacements calculated in the iteration i ; $R^{t+\Delta t}$ the vector of the externally applied nodal point loads at the time $t + \Delta t$ which include the ones deriving from the thermal stresses; $F_{t+\Delta t}^{t+\Delta t, (i-1)}$ the vector of the nodal point forces equivalent to the element stresses at the time $t + \Delta t$ and measured with respect to the configurations at the same time $t + \Delta t$, calculated by means of the solution of

the previous iteration; and $U^{t+\Delta t,(i)}$ and $U^{t+\Delta t,(i-1)}$ the nodal displacement vectors at the time $t + \Delta t$, calculated at the i and the $(i-1)$ iterations respectively.

The results of sheet metal forming analysis are represented by the incremental displacement field and by the stresses and strain incremental fields.

A.3 Input data for sensitivity threshold identification

h variation step (%)	Blank thickness (mm)	Yield strength (MPa)	UTS (MPa)	Blank holder force (N)	Friction coefficient	Die radius (mm)	Punch radius (mm)
-20	1.12	440	672	2352	0.08	5.6	4
-10	1.26	495	756	2646	0.09	6.3	4.5
-5	1.33	522.5	798	2793	0.095	6.65	4.75
-2	1.372	539	823.2	2881.2	0.098	6.86	4.9
-1.5	1.379	541.75	827.4	2895.9	0.0985	6.895	4.925
-1	1.386	544.5	831.6	2910.6	0.099	6.93	4.95
-0.8	1.3888	545.6	833.28	2916.48	0.0992	6.944	4.96
-0.5	1.393	547.25	835.8	2925.3	0.0995	6.965	4.975
-0.2	1.3972	548.9	838.32	2934.12	0.0998	6.986	4.99
-0.1	1.3986	549.45	839.16	2937.06	0.0999	6.993	4.995
-0.05	1.3993	549.725	839.58	2938.53	0.09995	6.9965	4.9975
-0.01	1.39986	549.945	839.916	2939.706	0.09999	6.9993	4.9995
0	1.4	550	840	2940	0.1	7	5
+0.01	1.40014	550.055	840.084	2940.294	0.10001	7.0007	5.0005
+0.05	1.4007	550.275	840.42	2941.47	0.10005	7.0035	5.0025
+0.1	1.4014	550.55	840.84	2942.94	0.1001	7.007	5.005
+0.2	1.4028	551.1	841.68	2945.88	0.1002	7.014	5.01
+0.5	1.407	552.75	844.2	2954.7	0.1005	7.035	5.025
+0.8	1.4112	554.4	846.72	2963.52	0.1008	7.056	5.04
+1	1.414	555.5	848.4	2969.4	0.101	7.07	5.05
+1.5	1.421	558.25	852.6	2984.1	0.1015	7.105	5.075
+2	1.428	561	856.8	2998.8	0.102	7.14	5.1
+5	1.47	577.5	882	3087	0.105	7.35	5.25
+10	1.54	605	924	3234	0.11	7.7	5.5
+20	1.68	660	1008	3528	0.12	8.4	6

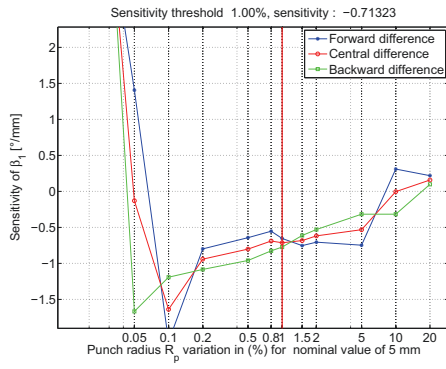
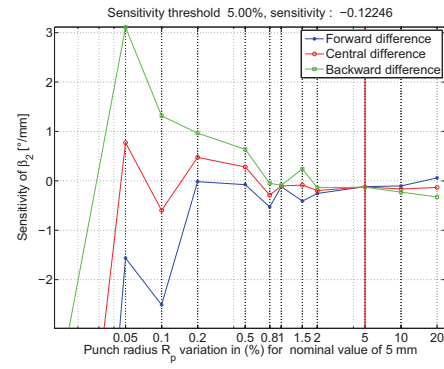
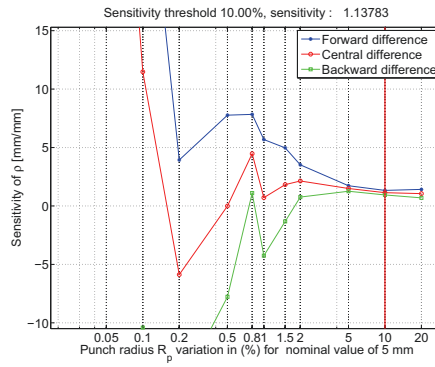
Table A.1: The input parameters for indentifying sensitivity threshold

A.4 Results of sensitivity threshold identification

A.4.1 Punch radius

Parameter	Sensitivity threshold of β_1 (%)	Sensitivity threshold of β_2 (%)	Sensitivity threshold of ρ (%)	General sensitivity threshold of R_p (%)	Corresponding variation range of R_p
R_p	1	5	10	10	$5 \pm 0.5\text{mm}$

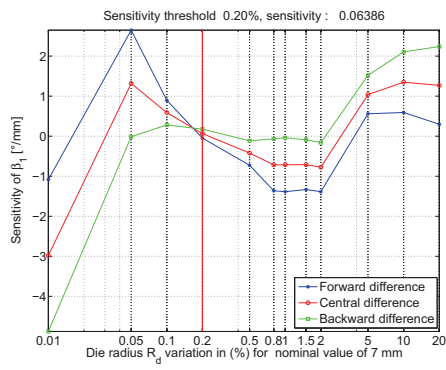
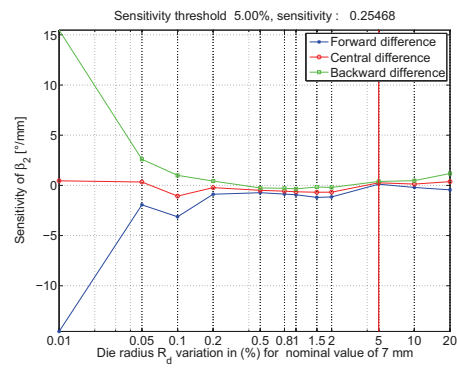
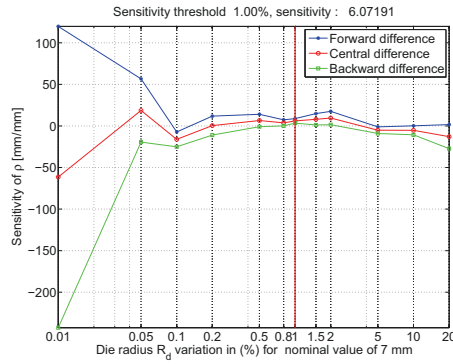
Table A.2: Synthesis of punch radius sensitivity threshold

(a) β_1 (b) β_2 (c) ρ

A.4.2 Die radius

Parameter	Sensitivity threshold of β_1 (%)	Sensitivity threshold of β_2 (%)	Sensitivity threshold of ρ (%)	General sensitivity threshold of R_d (%)	Corresponding variation range of R_d
R_d	0.2	5	1	5	$7 \pm 0.35\text{mm}$

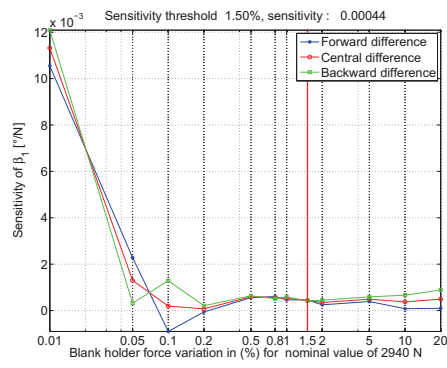
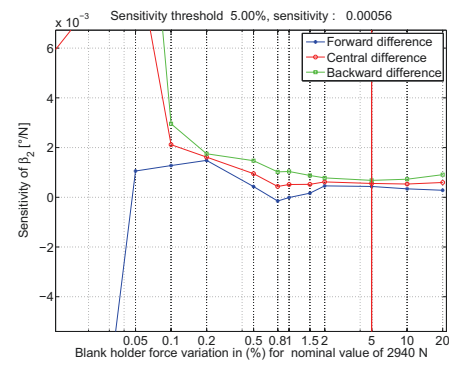
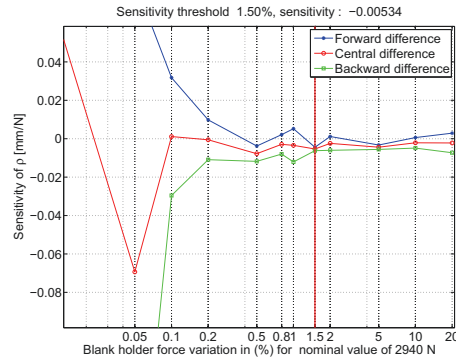
Table A.3: Synthesis of die radius sensitivity threshold

(a) β_1 (b) β_2 (c) ρ

A.4.3 Blank holder force

Parameter	Sensitivity threshold of β_1 (%)	Sensitivity threshold of β_2 (%)	Sensitivity threshold of ρ (%)	General sensitivity threshold of BHF (%)	Corresponding variation range of BHF
F_{BHF}	1.5	5	1.5	5	$2940 \pm 147\text{N}$

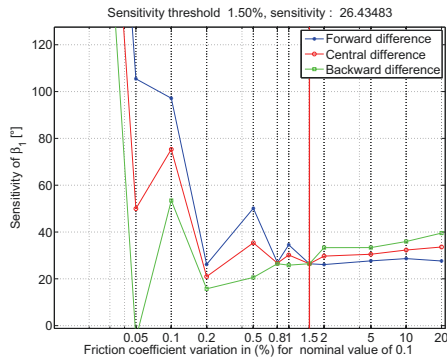
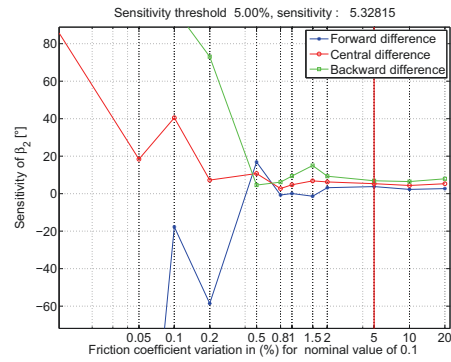
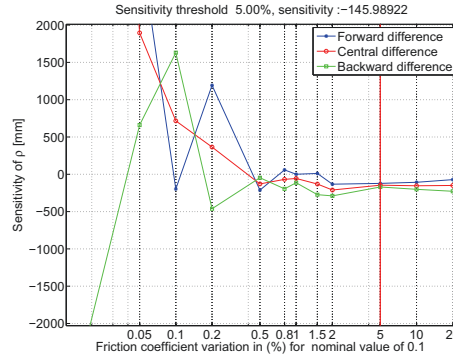
Table A.4: Synthesis of blank holder force sensitivity threshold

(a) β_1 (b) β_2 (c) ρ

A.4.4 Friction coefficient

Parameter	Sensitivity threshold of β_1 (%)	Sensitivity threshold of β_2 (%)	Sensitivity threshold of ρ (%)	General sensitivity threshold of fric. coeff.(%)	Corresponding variation range of fric. coeff.
μ	1.5	5	5	5	0.1 ± 0.005

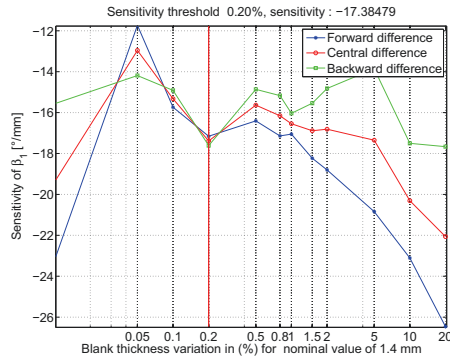
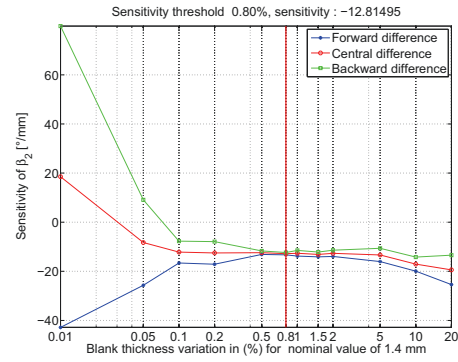
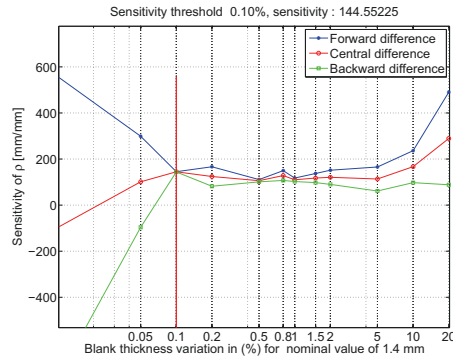
Table A.5: Synthesis of friction coefficient sensitivity threshold

(a) β_1 (b) β_2 (c) ρ

A.4.5 Blank thickness

Parameter	Sensitivity threshold of β_1 (%)	Sensitivity threshold of β_2 (%)	Sensitivity threshold of ρ (%)	General sensitivity threshold of blank thickness (%)	Corresponding variation range of blank thickness
t	0.2	0.8	0.1	0.8	1.4 \pm 0.0112mm

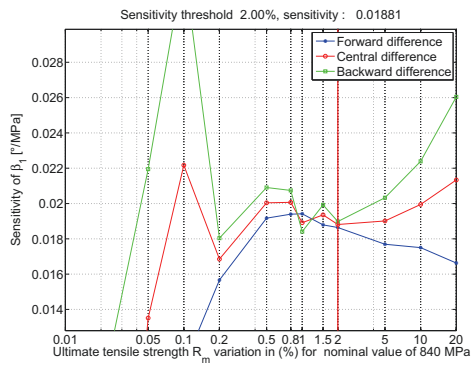
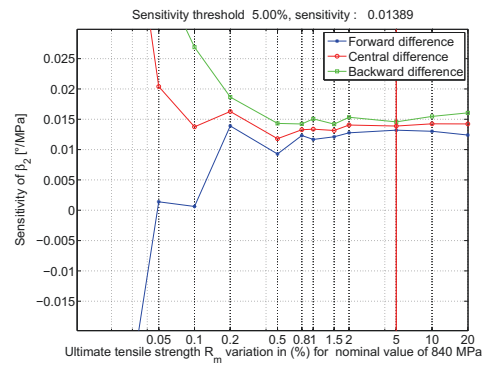
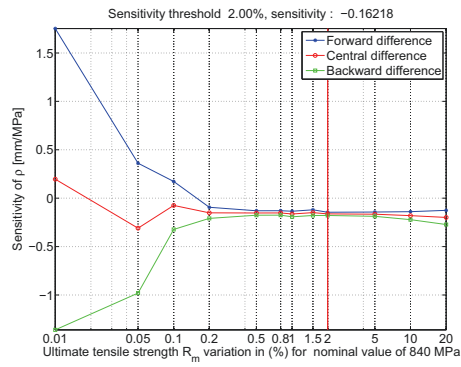
Table A.6: Synthesis of blank thickness sensitivity threshold

(a) β_1 (b) β_2 (c) ρ

A.4.6 Ultimate tensile strength

Parameter	Sensitivity threshold of β_1 (%)	Sensitivity threshold of β_2 (%)	Sensitivity threshold of ρ (%)	General sensitivity threshold of UTS(%)	Corresponding variation range of UTS
R_m	2	5	2	5	840 \pm 42MPa

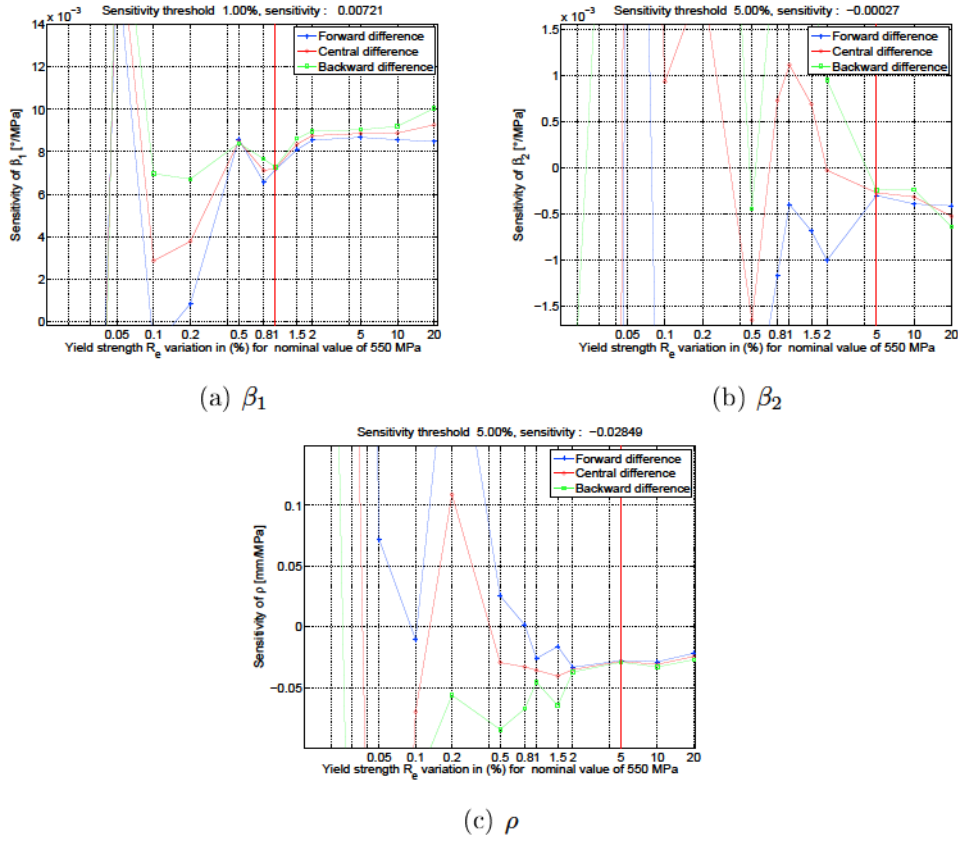
Table A.7: Synthesis of UTS sensitivity threshold

(a) β_1 (b) β_2 (c) ρ

A.4.7 Yield strength

Parameter	Sensitivity threshold of β_1 (%)	Sensitivity threshold of β_2 (%)	Sensitivity threshold of ρ (%)	General sensitivity threshold of YS(%)	Corresponding variation range of YS
R_e	1	5	5	5	550 \pm 27.5MPa

Table A.8: Synthesis of yield strength sensitivity threshold



A.5 Metamodeling techniques

A.5.1 Response Surface Methodology

Polynomial functions with an increasing complexity are fitted through the observations y or the response parameters. Equation 2.47 may be written in matrix notation as [142]:

$$y = X\beta + \varepsilon \quad (\text{A.25})$$

where X is a matrix containing the levels of independent variables, β is a vector of regression coefficients, and ε is a vector of random error terms. Note that the design matrix X can incorporate non-linear terms with respect to the variables. The order of these terms is referred to as the order of the polynomial model. The metamodel is given by:

$$\hat{y} = X\beta \quad (\text{A.26})$$

where the unknown regression coefficients β are determined by minimizing the sum of the squares of the errors ε_i at the training points. The least squares function is:

$$L = \sum_{i=1}^n \varepsilon_i^2 = \varepsilon^T \varepsilon = (y - X\beta)^T (y - X\beta) \quad (\text{A.27})$$

The least squares estimators must satisfy $\frac{\partial L}{\partial \beta}|_{\hat{\beta}} = 0$. After simplifying, the least squares estimator of β is:

$$\hat{\beta} = (X^T X)^{-1} X^T y \quad (\text{A.28})$$

The response prediction \hat{y}_0 at untried point x_0 is given by the explicit function:

$$\hat{y}_0 = x_0^T \hat{\beta} \quad (\text{A.29})$$

The variance at this location is given by [142]:

$$\text{Var}(\hat{y}_0) = \sigma^2 x_0^T (X^T X)^{-1} x_0 \quad (\text{A.30})$$

The prediction uncertainty of the metamodel is given by the square root of the variance of Equation A.30 as $\sqrt{\text{Var}(\hat{y}_0)}$.

The difference between the observation y_i and the fitted value \hat{y}_i is a residual denoted by:

$$e = y_i - \hat{y}_i \quad (\text{A.31})$$

A.5.2 Kriging

Since computer simulations are deterministic in nature, the same input parameters will yield exactly the same result, they are not subject to measurement error. Hence, the remaining error ε in Equation 2.47 should formally be zero [185]. Consequently, Sacks et al. [183] proposed an approach of Design and Analysis of Computer Experiments (DACE) in which Kriging is used as an interpolation technique. The metamodel can interpolate exactly through the response values at the training points.

The Equation 2.47 can be written by using Kriging as follows:

$$y = X\beta + Z(x) \quad (\text{A.32})$$

where the random error term ε in Equation 2.47 is replaced by a stochastic part $Z(x)$ to compute the exact predictions at the available training points. $Z(x)$ is

assumed to be a Gaussian stochastic process with zero mean, process variance σ_Z^2 , and spatial covariance function given by:

$$\text{cov}(Z(x_i), Z(x_j)) = \sigma_Z^2 R(x_i, x_j) \quad (\text{A.33})$$

where $R(x_i, x_j)$ describes the correlation between the known measurement points x_i and x_j . The correlation function R determines the shape of the metamodel between measurement points. This correlation function is specified by the user. The case of a Gaussian exponential correlation function is given by:

$$R(\theta, x_i, x_j) = \exp^{-\theta(x_i - x_j)^2} \quad (\text{A.34})$$

In the case of m design variables are present, the correlation function depends on the m one-dimensional correlation functions as follows:

$$R(\theta, x_i, x_j) = \prod_{l=1}^m \exp^{-\theta_l(x_{il} - x_{jl})^2} \quad (\text{A.35})$$

The entries of the vectors $\theta = \{\theta_1, \theta_2, \dots, \theta_m\}^T$ and the distance between the known measurement points x_i and x_j determine the structure of $R(\theta, x_i, x_j)$.

Similar to RSM, a Kriging metamodel is fitted in order to minimize the mean square error between the Kriging metamodel $\hat{y}(x)$ and the true model but unknown response function $y(x)$ [183]:

$$\min \quad E(\hat{y}(x) - y(x))^2 \quad (\text{A.36a})$$

$$\text{s.t.} \quad E(\hat{y}(x) - y(x)) = 0 \quad (\text{A.36b})$$

In other words, the mean square error is minimized subject to the unbiasedness constraint that ensures there is no systematic error between the metamodel and the true function. The Best Linear Unbiased Predictor (BLUP) \hat{y}_0 at an untried point x_0 is now given by [185]:

$$\hat{y}_0 = x_0^T \beta + r_0^T R^{-1}(y - X\beta) \quad (\text{A.37})$$

where X is the design matrix containing the training points. The vector r_0 contains the correlation between the point (x_0, y_0) and the known measurement (x_i, y_i) . R is a matrix containing the correlation between the training points given by Equation A.34.

A.5.3 Radial Basis Functions

Radial Basis Functions (RBF) are powerful tool for multivariate scattered data interpolation [52]. Since RBF are interpolant response surfaces they pass exactly through training points. The method uses linear combinations of a radially symmetric function based on Euclidean distance to approximate response functions.

Given a training set of n points sampled from a function $f(x): \mathbb{R}^d \rightarrow \mathbb{R}$,

$$f(x_i) = f_i, i = 1, \dots, n, \quad (\text{A.38})$$

a RBF interpolant has the form

$$s(x) = \sum_{j=1}^n c_j \phi(\|x - x_j\|/\delta), \quad (\text{A.39})$$

where $\|\cdot\|$ is the Euclidean norm in the d -dimensional space, and δ a fixed *scaling parameter*. The *radial function* $\phi(r): [0, +\infty) \rightarrow \mathbb{R}$ is suitable fixed function. So the RBF interpolant s is simply a linear combination of identical spherical symmetric functions, centered at the n different training points sites.

The coefficient c_j represents the free parameters of the RBF model. Their values are obtained by imposing the interpolation equations:

$$s(x_i) = f(x_i) = f_i, \forall i = 1, \dots, n. \quad (\text{A.40})$$

By defining the symmetrical matrix A (termed the collocation matrix of the RBF) as

$$A_{ij} = \phi(\|x_i - x_j\|/\delta), i, j = 1, \dots, n, \quad (\text{A.41})$$

the interpolation equations can be expressed as

$$s(x_i) = \sum_{j=1}^n A_{ij} c_j = f_i, \forall i = 1, \dots, n. \quad (\text{A.42})$$

or in matrix form as

$$A.c = f \quad (\text{A.43})$$

If the matrix A is nonsingular, the unknown coefficients vector is obtained by inverting the linear system of equations:

$$c = A^{-1}.f \quad (\text{A.44})$$

A key point for obtaining a unique solution is the nonsingularity of the matrix A : this depends only on the choice of the radial function ϕ .

For so-called *positive definite* (PD) radial functions, the matrix A is positive definite for every choice of training points, and the linear system Equation A.43 has a unique solution.

In case of so-called *conditionally positive definite* (CPD) radial functions, the RBF interpolant form has to be changed. In order to guarantee a unique solution, an additional polynomial term has to be introduced in Equation A.39:

$$s(x) = \sum_{j=1}^n c_j \phi(\|x - x_j\|/\delta) + p_m(x) \quad (\text{A.45})$$

Here m represents the degree of the polynomial, and it depends only on the choice of ϕ . The polynomial term has the form

$$p_m(x) = \sum_{j=1}^q b_j \pi_j(x) \in \mathbb{P}_m^d, \quad (\text{A.46})$$

where $\{\pi_j(x)\}$ is a basis of the linear space \mathbb{P}_m^d containing all real-valued polynomials in d variables of degree m . The q is the dimension of the polynomial space \mathbb{P}_m^d , and it is equal to $q = \binom{m+d}{d}$

There exist many different kinds of radial basis function. In ModeFRONTIER, five different radial functions are available: Gaussians (G), Duchon's Polynomial Spline (PS), Hardy's MultiQuadrics (MQ), Inverse MultiQuadrics (IMQ), and Wendland's Compactly Supported C^2 (W2) as presented in Table A.9.

Table A.9: Available radial functions

Radial functions	Form	Type
G	$\phi(r) = \exp(-r^2)$	PD
PS	$\phi(r) = \begin{cases} r^3 & \text{dodd} \\ r^2 \log(r) & \text{deven} \end{cases}$	$m = (d+1)/2$ $m = d/2$
MQ	$\phi(r) = (1 + r^2)^{(1/2)}$	m=0
IMQ	$\phi(r) = (1 + r^2)^{(-1/2)}$	PD
W2	$\phi(r) = \begin{cases} (1-r)^3 + (3r+1) & d=1 \\ (1-r)^4 + (4r+1) & d=2,3 \\ (1-r)^5 + (5r+1) & d=4,5 \end{cases}$	PD

A.5.4 Neural Networks

A neural network is composed of neurons (single unit perceptrons) which are multiple linear regression models with a nonlinear transformation on y . If the inputs to each neuron are denoted $\{x_1, x_2, \dots, x_n\}$, and the regression coefficients are denoted by the weights w_i , then the output y might be given by

$$y = \frac{1}{1 + e^{-\eta/T}} \quad (\text{A.47})$$

where $\eta = \sum w_i x_i + \beta$ (where β is the 'bias value' of a neuron) and T is the slope parameter of the sigmoid defined by the user. A *neural network* is then created by assembling the neurons into an architecture; the most common of which is the multi-layer feedforward architecture as shown in Figure A.8. There are two main issues in building a neural network: (1) specifying the architecture and (2) training the neural network to perform well with reference to a training set. This is equivalent to (i) specifying a regression model, and (ii) estimating the parameters of the model given a set of data [32].

Training a neural network is the determination of the proper values for all weights w_i , in the architecture and is usually done by back-propagation [181]; this requires a set of n training data points $\{(x_1, y_1), (x_2, y_2), \dots, (x_p, y_p)\}$. For a network with output y , the performance is

$$E = \sum_p (y_p - \hat{y}_p)^2 \quad (\text{A.48})$$

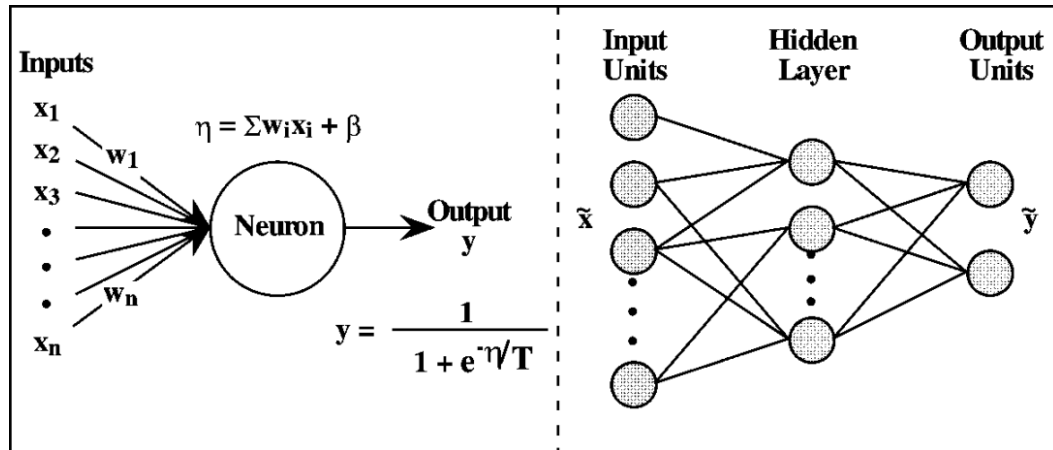


Figure A.8: Typical neuron and architecture. (a) Single unit per caption; (b) feed-forward two-layer architecture [200].

where \hat{y}_p is the output that results from the network given input x_p , and E is the total error of the system. The weights are then adjusted in the proportion to

$$\frac{\partial E}{\partial y} \frac{\partial y}{\partial w_{ij}} \quad (\text{A.49})$$

Nomenclature

β_1	The wall opening angle
β_2	The flange angle
μ	Friction coefficient
ρ	The side wall curl radius
F_{BHF}	Blank holder force
R_d	Die radius
R_e	Yield strength
R_m	Ultimate tensile strength
R_p	Punch radius
t	Blank thickness
U_T	Hole displacement
AFM	Association Française de Mécanique
ARMOGA	Adaptive Range Multi-Objective Genetic Algorithms
BHF	Blank Holder Force
BIW	Body-In-White
CAD	Computer Aided Design
CCD	Central Composite Design
CDF	Cumulative Distribution Function
CE	Concurrent Engineering
DO	Deterministic Optimization
DOE	Design of Experiments
DOF	Degrees of Freedom
DP	Dual Phase
DPMO	Defects Per Million Opportunities
EF	Élément Finis

FDM	Finite Difference Method
FEM	Finite Element Method
FFD	Full Factorial Design
I/O	Input/Output
IT	Interval of Tolerance
LCS	Latin Hypercube Sampling
MCS	Monte Carlo Sampling
MEF	Méthode des Éléments Finis
MOGA-II	Improved Multi-objective Genetic Algorithm
MOPSO	Multi-objective Particle Swarm Optimization
MORDO	Multi-objective Robust Design Optimization
MOSA	Multi-objective Optimization Simulated Annealing
NCR	Non-conformity Rate
NSGA-II	Elitist Non-dominated Sorting Genetic Algorithm
PDF	Probability Density Function
POF	Pareto optimal front
PPM	Parts Per Million
R & D	Research & Development
RBDO	Reliability Based Design Optimization
RDO	Robust Design Optimization
RS	Random Sampling
RSM	Response Surface Methodology
SNR	Signal-to-Noise Ratio
UTS	Ultimate Tensile Strength
WSM	Weighted Sum Method
YS	Yield Strength

Bibliography

- [1] Abdullah, A., Sapuan, S., Samad, Z., and Aziz, N. (2012). A comprehensive review of experimental approaches used in the measurement of springback. *Advances in Natural & Applied Sciences*, 6(2). (Cited on pages 9 and 13.)
- [2] Adragna, P.-A. (2007). *Tolérancement des Systèmes Assemblés, une approche par le Tolérancement Inertiel et Modal*. PhD thesis, Université de Savoie. (Cited on pages 91, 92 and 93.)
- [3] Alberti, N. and Fratini, L. (2004). Innovative sheet metal forming processes: numerical simulations and experimental tests. *Journal of materials processing technology*, 150(1):2–9. (Cited on page 221.)
- [4] Allen, J. K., Seepersad, C., Choi, H., and Mistree, F. (2006). Robust design for multiscale and multidisciplinary applications. *Journal of Mechanical Design*, 128(4):832–843. (Cited on pages 11, 113, 114, 115, 116, 117, 120, 122, 149 and 205.)
- [5] Allen, M. and Maute, K. (2004). Reliability-based design optimization of aeroelastic structures. *Structural and Multidisciplinary Optimization*, 27(4):228–242. (Cited on page 134.)
- [6] Alting, L. (1993). Life-cycle design of products: a new opportunity for manufacturing enterprises. *Concurrent Engineering: Automation, Tools and Techniques*, A. Kusiak (ed.), Wiley Inc, New York. (Cited on pages 9, 12, 5, 6 and 177.)
- [7] Arcelormittal (2014). Dual phase steels. (Cited on pages 63, 64 and 194.)
- [8] Arora, J. S. Introduction to optimum design, 1989. *McGraw-Mill Book Company*. (Cited on page 127.)
- [9] Askey, R. and Wilson, J. A. (1985). *Some basic hypergeometric orthogonal polynomials that generalize Jacobi polynomials*, volume 319. American Mathematical Soc. (Cited on page 82.)
- [10] Aspenberg, D. (2011). Robust optimisation of structures: Evaluation and incorporation of variations in simulation based design. (Cited on pages 34 and 132.)
- [11] Atzema, E., Abspoel, M., Kömmelt, P., and Lambriks, M. (2009). Towards robust simulations in sheet metal forming. *International Journal of Material Forming*, 2(1):351–354. (Cited on page 134.)
- [12] Atzema, E. H. and Kömmelt, P. (2007). Modelling parameter interdependence in stochastic simulations of stamping: Yield locus. In *IDDRG Congress*, pages 195–204. (Cited on page 134.)

-
- [13] Ben-Haim, Y. and Elishakoff, I. (1990). *Convex models of uncertainty in applied mechanics*, volume 112. Elsevier Amsterdam. (Cited on page 78.)
- [14] Beyer, H.-G. and Sendhoff, B. (2007). Robust optimization—a comprehensive survey. *Computer methods in applied mechanics and engineering*, 196(33):3190–3218. (Cited on pages 93 and 197.)
- [15] Bonte, M. H. A. (2007). *Optimisation strategies for metal forming processes*. University of Twente. (Cited on pages 12, 128, 129, 130, 131 and 132.)
- [16] Booker, A., Conn, A., Dennis, J., Frank, P., Serafini, D., Torczon, V., and Trosset, M. (1996). Multi-level design optimization: a boeing/ibm/rice collaborative project. *1996 Final Report, ISSTECH-96*, 31. (Cited on page 30.)
- [17] Booker, A. J. (1998). Design and analysis of computer experiments. *AIAA paper*, pages 98–4757. (Cited on pages 9 and 30.)
- [18] Box, G. (1988). Signal-to-noise ratios, performance criteria, and transformations. *Technometrics*, 30(1):1–17. (Cited on page 120.)
- [19] Box, G. E. and Behnken, D. W. (1960). Some new three level designs for the study of quantitative variables. *Technometrics*, 2(4):455–475. (Cited on page 29.)
- [20] Box, G. E. and Wilson, K. (1951). On the experimental attainment of optimum conditions. *Journal of the Royal Statistical Society. Series B (Methodological)*, 13(1):1–45. (Cited on page 32.)
- [21] Boyles, R. A. (1991). The taguchi capability index. *Journal of Quality Technology*, 23:17–26. (Cited on pages 92 and 93.)
- [22] Breitzkopf, P., Naceur, H., Rassineux, A., and Villon, P. (2005). Moving least squares response surface approximation: formulation and metal forming applications. *Computers & Structures*, 83(17):1411–1428. (Cited on page 129.)
- [23] Breitung, K. (1984). Asymptotic approximations for multinormal integrals. *Journal of Engineering Mechanics*, 110(3):357–366. (Cited on page 126.)
- [24] Bucher, C. G. (1988). Adaptive sampling—an iterative fast monte carlo procedure. *Structural Safety*, 5(2):119–126. (Cited on page 78.)
- [25] Chaloner, K., Verdinelli, I., et al. (1995). Bayesian experimental design: A review. *Statistical Science*, 10(3):273–304. (Cited on page 30.)
- [26] Chan, L. K., Cheng, S. W., and Spiring, F. A. (1988). A new measure of process capability: Cpm. *Journal of Quality Technology*, 20(3):162–175. (Cited on page 92.)
- [27] Chen, P. and Koç, M. (2007). Simulation of springback variation in forming of advanced high strength steels. *Journal of materials processing technology*, 190(1):189–198. (Cited on page 33.)

- [28] Chen, V. C., Tsui, K.-L., Barton, R. R., and Meckesheimer, M. (2006). A review on design, modeling and applications of computer experiments. *IIE transactions*, 38(4):273–291. (Cited on page 31.)
- [29] Chen, W., Allen, J. K., Mavris, D. N., and Mistree, F. (1996a). A concept exploration method for determining robust top-level specifications. *Engineering Optimization + A35*, 26(2):137–158. (Cited on page 122.)
- [30] Chen, W., Allen, J. K., Tsui, K.-L., and Mistree, F. (1996b). A procedure for robust design: minimizing variations caused by noise factors and control factors. *Journal of Mechanical Design*, 118(4):478–485. (Cited on pages 11, 94, 120, 121, 149, 197 and 206.)
- [31] Chen, W., Tsui, K.-L., Allen, J. K., and Mistree, F. (1995). Integration of the response surface methodology with the compromise decision support problem in developing a general robust design procedure. In *Proceedings of the 1995 ASME Design Engineering Technical Conference, September*, pages 17–20. (Cited on page 122.)
- [32] Cheng, B. and Titterton, D. M. (1994). Neural networks: A review from a statistical perspective. *Statistical science*, pages 2–30. (Cited on page 233.)
- [33] Choi, H.-J. (2005). *A robust design method for model and propagated uncertainty*. PhD Thesis, Georgia Institute of Technology, Atlanta. (Cited on pages 11, 79, 80, 116, 117, 122, 123, 149 and 205.)
- [34] Chongthairungruang, B., Uthaisangsuk, V., Suranuntchai, S., and Jiratheeranant, S. (2013). Springback prediction in sheet metal forming of high strength steels. *Materials & Design*, 50:253–266. (Cited on page 14.)
- [35] Chung, W., Cho, J., and Belytschko, T. (1998). On the dynamic effects of explicit fem in sheet metal forming analysis. *Engineering Computations*, 15(6):750–776. (Cited on page 23.)
- [36] Clarke, S. M., Griebisch, J. H., and Simpson, T. W. (2005). Analysis of support vector regression for approximation of complex engineering analyses. *Journal of mechanical design*, 127(6):1077–1087. (Cited on page 33.)
- [37] Couto, P. R. G., Damasceno, J. C., and de Oliveira, S. P. (2013). Monte carlo simulations applied to uncertainty in measurement. (Cited on pages 10 and 76.)
- [38] Cressie, N. (1988). Spatial prediction and ordinary kriging. *Mathematical Geology*, 20(4):405–421. (Cited on page 32.)
- [39] Currin, C., Mitchell, T., Morris, M., and Ylvisaker, D. (1991). Bayesian prediction of deterministic functions, with applications to the design and analysis of computer experiments. *Journal of the American Statistical Association*, 86(416):953–963. (Cited on page 30.)

- [40] Dantan, J., Gayton, N., Qureshi, A., Lemaire, M., and Etienne, A. (2013). Tolerance analysis approach based on the classification of uncertainty (aleatory/epistemic). In *The Twelfth CIRP Conference on Computer Aided Tolerancing*, volume 128, pages 287 – 293. Elsevier. (Cited on page 75.)
- [41] De Boor, C. and Ron, A. (1990). On multivariate polynomial interpolation. *Constructive Approximation*, 6(3):287–302. (Cited on pages 32 and 33.)
- [42] De Souza, T. and Rolfe, B. (2008). Multivariate modelling of variability in sheet metal forming. *Journal of materials processing technology*, 203(1):1–12. (Cited on page 34.)
- [43] Deb, K. (2001). *Multi-objective optimization using evolutionary algorithms*, volume 16. John Wiley & Sons. (Cited on pages 135 and 138.)
- [44] Deb, K., Agrawal, S., Pratap, A., and Meyarivan, T. (2000). A fast elitist non-dominated sorting genetic algorithm for multi-objective optimization: Nsga-ii. *Lecture notes in computer science*, 1917:849–858. (Cited on pages 137 and 138.)
- [45] Deb, K. and Goel, T. (2001). Controlled elitist non-dominated sorting genetic algorithms for better convergence. In *Evolutionary Multi-Criterion Optimization*, pages 67–81. Springer. (Cited on page 137.)
- [46] Deb, K., Pratap, A., Agarwal, S., and Meyarivan, T. (2002). A fast and elitist multiobjective genetic algorithm: Nsga-ii. *Evolutionary Computation, IEEE Transactions on*, 6(2):182–197. (Cited on page 135.)
- [47] Del Prete, A., Primo, T., and Strano, M. (2010). The use of fea packages in the simulation of a drawing operation with springback, in the presence of random uncertainty. *Finite Elements in Analysis and Design*, 46(7):527–534. (Cited on page 134.)
- [48] Ditlevsen, O., Olesen, R., and Mohr, G. (1986). Solution of a class of load combination problems by directional simulation. *Structural Safety*, 4(2):95–109. (Cited on page 31.)
- [49] Diwekar, U. M. (2003). A novel sampling approach to combinatorial optimization under uncertainty. *Computational Optimization and Applications*, 24(2-3):335–371. (Cited on page 86.)
- [50] Doltsinis, I. and Kang, Z. (2004). Robust design of structures using optimization methods. *Computer Methods in Applied Mechanics and Engineering*, 193(23):2221–2237. (Cited on pages 131 and 132.)
- [51] Du, X. and Chen, W. (2000). Methodology for managing the effect of uncertainty in simulation-based design. *AIAA journal*, 38(8):1471–1478. (Cited on page 74.)

- [52] Dyn, N., Levin, D., and Rippa, S. (1986). Numerical procedures for surface fitting of scattered data by radial functions. *SIAM Journal on Scientific and Statistical Computing*, 7(2):639–659. (Cited on pages 32 and 231.)
- [53] Eldred, M. S., Giunta, A. A., Wojtkiewicz, S., and Trucano, T. G. (2002). Formulations for surrogate-based optimization under uncertainty. In *9th AIAA/ISSMO Symposium on Multidisciplinary Analysis and Optimization, Atlanta, GA*. (Cited on page 134.)
- [54] Englund, S. and Rackwitz, R. (1993). A benchmark study on importance sampling techniques in structural reliability. *Structural Safety*, 12(4):255–276. (Cited on page 78.)
- [55] Etienne, A. (2007). *Intégration Produit/Process par les concepts d’activités et de caractéristiques clés-Application à l’optimisation de l’allocation des tolérances géométriques*. PhD thesis, Université de Metz. (Cited on pages 9, 12, 6 and 178.)
- [56] Evans, D. H. (1972). An application of numerical integration techniques to statistical tolerancing, iii - general distributions. *Technometrics*, 14(1):23–35. (Cited on page 78.)
- [57] Fang, H. and Horstemeyer, M. F. (2006). Global response approximation with radial basis functions. *Engineering Optimization*, 38(04):407–424. (Cited on page 32.)
- [58] Fiessler, B., Rackwitz, R., and Neumann, H.-J. (1979). Quadratic limit states in structural reliability. *Journal of the Engineering Mechanics Division*, 105(4):661–676. (Cited on page 78.)
- [59] Fishburn, P. C. (1967). Letter to the editor-additive utilities with incomplete product sets: Application to priorities and assignments. *Operations Research*, 15(3):537–542. (Cited on page 143.)
- [60] Forcellese, A., Fratini, L., Gabrielli, F., and Micari, F. (1998). The evaluation of springback in 3d stamping and coining processes. *Journal of Materials Processing Technology*, 80:108–112. (Cited on page 23.)
- [61] Friedman, J. H. (1991). Multivariate adaptive regression splines. *The annals of statistics*, pages 1–67. (Cited on page 32.)
- [62] Fu, J. C. and Wang, L. (2002). A random-discretization based monte carlo sampling method and its applications. *Methodology and Computing in Applied Probability*, 4(1):5–25. (Cited on page 31.)
- [63] Fung, G. E. and Box, C. A. (1986). Studies in quality improvement: Minimizing transmitted variation by parameter design. (Cited on page 120.)

- [64] Geng, L. and Wagoner, R. (2002). Role of plastic anisotropy and its evolution on springback. *International Journal of Mechanical Sciences*, 44(1):123–148. (Cited on page 24.)
- [65] Geng, L. and Wagoner, R. H. (2000). Springback analysis with a modified hardening model. *SAE Transactions: Journal of Materials & Manufacturing*, 109:365–375. (Cited on pages 168 and 216.)
- [66] Giraud-Moreau, L. and Lafon, P. (2002). A comparison of evolutionary algorithms for mechanical design components. *Engineering Optimization*, 34(3):307–322. (Cited on page 137.)
- [67] Giunta, A. A., Balabanov, V., Haim, D., Grossman, B., Mason, W. H., Watson, L. T., and Haftka, R. T. (1997). Multidisciplinary optimization of a supersonic transport using design of experiments theory and response surface modeling. (Cited on page 29.)
- [68] Giunta, A. A., Wojtkiewicz, S. F., Eldred, M. S., et al. (2003). Overview of modern design of experiments methods for computational simulations. In *Proceedings of the 41st AIAA Aerospace Sciences Meeting and Exhibit, AIAA-2003-0649*. (Cited on page 86.)
- [69] Goel, T., Vaidyanathan, R., Haftka, R. T., Shyy, W., Queipo, N. V., and Tucker, K. (2007). Response surface approximation of pareto optimal front in multi-objective optimization. *Computer Methods in Applied Mechanics and Engineering*, 196(4):879–893. (Cited on page 135.)
- [70] Goldberg, D. E. (1989). *Genetic Algorithms in Search, Optimization and Machine Learning*. Addison-Wesley Longman Publishing Co., Inc., Boston, MA, USA, 1st edition. (Cited on page 135.)
- [71] Gomes, C., Onipede, O., and Lovell, M. (2005). Investigation of springback in high strength anisotropic steels. *Journal of Materials Processing Technology*, 159(1):91–98. (Cited on page 24.)
- [72] Govik, A., Nilsson, L., and Moshfegh, R. (2012). Finite element simulation of the manufacturing process chain of a sheet metal assembly. *Journal of Materials Processing Technology*, 212(7):1453–1462. (Cited on pages 11 and 106.)
- [73] Grierson, D. E. (2008). Pareto multi-criteria decision making. *Advanced Engineering Informatics*, 22(3):371–384. (Cited on page 145.)
- [74] Guo, J. and Du, X. (2007). Sensitivity analysis with mixture of epistemic and aleatory uncertainties. *AIAA journal*, 45(9):2337–2349. (Cited on pages 10 and 74.)
- [75] H. Huh, K. Chung, S. H. W. C. (2011). Benchmark study of the 8th international conference and workshop on numerical simulation of 3d sheet metal forming

- processes. *Proceedings of Numisheet 2011*. (Cited on pages 5, 9, 15, 16, 36, 38, 39, 42, 43 and 86.)
- [76] He, N. and Wagoner, R. (1996). Springback simulation in sheet metal forming. Master's thesis, Ohio State University. (Cited on page 23.)
- [77] Helton, J. C. and Davis, F. J. (2003). Latin hypercube sampling and the propagation of uncertainty in analyses of complex systems. *Reliability Engineering & System Safety*, 81(1):23–69. (Cited on page 86.)
- [78] Hill, R. (2002). A theory of the yielding and plastic flow of anisotropic metals. *Proceedings of the Royal Society of London. Series A. Mathematical and Physical Sciences*, 193:281–297. (Cited on page 40.)
- [79] Hoffman, F. O. and Hammonds, J. S. (1994). Propagation of uncertainty in risk assessments: the need to distinguish between uncertainty due to lack of knowledge and uncertainty due to variability. *Risk Analysis*, 14(5):707–712. (Cited on pages 74 and 75.)
- [80] Hohenbichler, M. and Rackwitz, R. (1983). First-order concepts in system reliability. *Structural safety*, 1(3):177–188. (Cited on page 125.)
- [81] Hou, B., Wang, W., Li, S., Lin, Z., and Xia, Z. C. (2010). Stochastic analysis and robust optimization for a deck lid inner panel stamping. *Materials & Design*, 31(3):1191–1199. (Cited on page 134.)
- [82] Hsiang, T. (1985). A tutorial on quality control and assurance—the taguchi methods. In *ASA Annual Meeting*. Las Vegas Nevada, USA. (Cited on page 92.)
- [83] Hu, J., Marciniak, Z., and Duncan, J. (2002). *Mechanics of sheet metal forming*. Butterworth-Heinemann. (Cited on pages 9, 12, 13 and 18.)
- [84] Huang, B. and Du, X. (2007). Analytical robustness assessment for robust design. *Structural and Multidisciplinary Optimization*, 34(2):123–137. (Cited on page 85.)
- [85] Huang, H.-Z. (1995). Reliability analysis method in the presence of fuzziness attached to operating time. *Microelectronics Reliability*, 35(12):1483–1487. (Cited on page 74.)
- [86] I.Drishtikona (2009). Sheet metal stamping in automotive industry. (Cited on pages 3 and 176.)
- [87] Jansson, T., Andersson, A., and Nilsson, L. (2005). Optimization of draw-in for an automotive sheet metal part: an evaluation using surrogate models and response surfaces. *Journal of Materials Processing Technology*, 159(3):426–434. (Cited on page 129.)

- [88] Jansson, T., Nilsson, L., and Moshfegh, R. (2008). Reliability analysis of a sheet metal forming process using monte carlo analysis and metamodels. *Journal of materials processing technology*, 202(1):255–268. (Cited on pages 4, 34, 131 and 176.)
- [89] Jin, R., Chen, W., and Simpson, T. W. (2001). Comparative studies of meta-modelling techniques under multiple modelling criteria. *Structural and Multidisciplinary Optimization*, 23(1):1–13. (Cited on pages 29 and 33.)
- [90] Jin, R., Chen, W., and Sudjianto, A. (2002). On sequential sampling for global metamodeling in engineering design. In *ASME 2002 International Design Engineering Technical Conferences and Computers and Information in Engineering Conference*, pages 539–548. American Society of Mechanical Engineers. (Cited on page 31.)
- [91] Jin, R., Chen, W., and Sudjianto, A. (2005). An efficient algorithm for constructing optimal design of computer experiments. *Journal of Statistical Planning and Inference*, 134(1):268–287. (Cited on page 31.)
- [92] Jin, R., Du, X., and Chen, W. (2003). The use of metamodeling techniques for optimization under uncertainty. *Structural and Multidisciplinary Optimization*, 25(2):99–116. (Cited on page 63.)
- [93] Johnson, M. E., Moore, L. M., and Ylvisaker, D. (1990). Minimax and maximin distance designs. *Journal of statistical planning and inference*, 26(2):131–148. (Cited on page 30.)
- [94] Juran, J. M. (1962). Quality control handbook. In *Quality control handbook*. McGraw-Hill. (Cited on page 90.)
- [95] Kalpakjian, S. and Schmid, S. R. (2010). *Manufacturing processes for engineering materials*. Pearson education. (Cited on pages 9 and 14.)
- [96] Kane, V. E. (1986). Process capability indices. *Journal of Quality Technology*, 18(1):41–52. (Cited on page 90.)
- [97] Kang, Z. (2005). Robust design optimization of structures under uncertainties. (Cited on pages 120 and 134.)
- [98] Karthik, V., Comstock Jr, R., Hershberger, D., and Wagoner, R. (2002). Variability of sheet formability and formability testing. *Journal of materials processing technology*, 121(2):350–362. (Cited on pages 7 and 179.)
- [99] Keane, A. and Nair, P. (2005). *Computational approaches for aerospace design: the pursuit of excellence*. John Wiley & Sons. (Cited on pages 11, 46, 47, 48, 77, 80, 81, 123, 124 and 129.)

- [100] Kennedy, M. C. and O'Hagan, A. (2001). Bayesian calibration of computer models. *Journal of the Royal Statistical Society: Series B (Statistical Methodology)*, 63(3):425–464. (Cited on page 74.)
- [101] Kini, S. D. (2004). *An approach to integrating numerical and response surface models for robust design of production systems*. PhD thesis, The Ohio State University. (Cited on pages 34 and 134.)
- [102] Kleiber, M., Rojek, J., and Stocki, R. (2002). Reliability assessment for sheet metal forming operations. *Computer methods in applied mechanics and engineering*, 191(39):4511–4532. (Cited on page 131.)
- [103] Kleijnen, J. P. and Sargent, R. G. (2000). A methodology for fitting and validating metamodels in simulation. *European Journal of Operational Research*, 120(1):14–29. (Cited on pages 9, 26 and 27.)
- [104] Klir, G. J. (2004). Generalized information theory: aims, results, and open problems. *Reliability Engineering & System Safety*, 85(1):21–38. (Cited on page 77.)
- [105] Klir, G. J. and Wierman, M. J. (1999). *Uncertainty-based information: elements of generalized information theory*, volume 15. Springer. (Cited on page 77.)
- [106] Kloess, A., Mourelatos, Z., and Meernik, P. (2004). Probabilistic analysis of an automotive body-door system. *International journal of vehicle design*, 34(2):101–125. (Cited on page 31.)
- [107] Knowles, J. D. and Corne, D. W. (2000). Approximating the nondominated front using the pareto archived evolution strategy. *Evolutionary computation*, 8(2):149–172. (Cited on page 137.)
- [108] Koch, P. N. (1998). *Hierarchical modeling and robust synthesis for the preliminary design of large scale complex systems*. (Cited on page 30.)
- [109] Koehler, J. and Owen, A. (1996). Computer experiments. *Handbook of statistics*, 13(13):261–308. (Cited on page 30.)
- [110] Kotz, S. and Johnson, N. L. (1993). *Process capability indices*. CRC Press. (Cited on page 91.)
- [111] Langley, P. and Simon, H. A. (1995). Applications of machine learning and rule induction. *Communications of the ACM*, 38(11):54–64. (Cited on page 32.)
- [112] Ledoux, Y., Samper, S., Favreliere, H., Formosa, F., Pairel, E., and Arrieux, R. (2006). Optimisation of a stamping process by a design of experiment linked to a modal analysis of geometric defects. *Archives of civil and mechanical engineering*, 6(1):5–17. (Cited on pages 11 and 87.)

- [113] Ledoux Y., S. P. and S., S. (2010). Optimization method for stamping tools under reliability constraints using genetic algorithms and finite element simulations. *Journal of Materials Processing Technology*, 210:474–486. (Cited on page 34.)
- [114] Lee, K.-H. and Park, G.-J. (2001). Robust optimization considering tolerances of design variables. *Computers & Structures*, 79(1):77–86. (Cited on page 131.)
- [115] Lee, K.-H. and Park, G.-J. (2006). A global robust optimization using kriging based approximation model. *JSME International Journal Series C*, 49(3):779–788. (Cited on pages 113 and 134.)
- [116] Lee, S. and Yang, D. (1998). An assessment of numerical parameters influencing springback in explicit finite element analysis of sheet metal forming process. *Journal of Materials Processing Technology*, 80:60–67. (Cited on page 23.)
- [117] Lee, S. H. and Kwak, B. M. (2006). Response surface augmented moment method for efficient reliability analysis. *Structural safety*, 28(3):261–272. (Cited on page 78.)
- [118] Lemaitre, J. and Chaboche, J.-L. (1990). *Mechanics of solid materials*. Cambridge university press. (Cited on page 24.)
- [119] Levi, F., Gobbi, M., and Mastinu, G. (2005). An application of multi-objective stochastic optimisation to structural design. *Structural and Multidisciplinary Optimization*, 29(4):272–284. (Cited on page 132.)
- [120] Li, K., Carden, W., and Wagoner, R. (2002a). Simulation of springback. *International Journal of Mechanical Sciences*, 44(1):103–122. (Cited on page 23.)
- [121] Li, K., Geng, L., and Wagoner, R. (1999). Simulation of springback with the draw/bend test. In *Intelligent Processing and Manufacturing of Materials, 1999. IPMM'99. Proceedings of the Second International Conference on*, volume 1, pages 91–104. IEEE. (Cited on page 23.)
- [122] Li, X., Yang, Y., Wang, Y., Bao, J., and Li, S. (2002b). Effect of the material-hardening mode on the springback simulation accuracy of v-free bending. *Journal of Materials Processing Technology*, 123(2):209–211. (Cited on page 24.)
- [123] Lin, P. T., Gea, H. C., and Jaluria, Y. (2011). A modified reliability index approach for reliability-based design optimization. *Journal of Mechanical Design*, 133(4):044501. (Cited on page 126.)
- [124] Lin, Y. (2004). An efficient robust concept exploration method and sequential exploratory experimental design. (Cited on page 31.)
- [125] Mahadevan, S. and Rebba, R. (2006). Inclusion of model errors in reliability-based optimization. *Journal of Mechanical Design*, 128(4):936–944. (Cited on pages 93 and 197.)

- [126] Majeske, K. D. and Hammett, P. C. (2003). Identifying sources of variation in sheet metal stamping. *International Journal of Flexible Manufacturing Systems*, 15(1):5–18. (Cited on pages 3, 4, 7, 175, 176 and 179.)
- [127] Makinouchi, A. (1993). Numisheet '93: proceedings of the 2nd international conference numerical simulation of 3-d sheet metal forming processes ; verification of simulation with experiment ; isehara, flee2006, 31. august - 2. september 1993. (Cited on page 86.)
- [128] Makinouchi, A. (1996). Sheet metal forming simulation in industry. *Journal of materials processing technology*, 60(1):19–26. (Cited on pages 9, 22 and 23.)
- [129] Makinouchi, A., Teodosiu, C., and Nakagawa, T. (1998). Advance in fem simulation and its related technologies in sheet metal forming. *CIRP Annals-Manufacturing Technology*, 47(2):641–649. (Cited on page 21.)
- [130] Manteufel, R. D. (2001). Distributed hypercube sampling algorithm. In *Third AIAA non-deterministic approaches forum paper AIAA-2001-1673, 42nd structures, structural dynamics, and materials conference*. (Cited on page 86.)
- [131] Marretta, L. and Di Lorenzo, R. (2010). Influence of material properties variability on springback and thinning in sheet stamping processes: a stochastic analysis. *The International Journal of Advanced Manufacturing Technology*, 51(1-4):117–134. (Cited on page 33.)
- [132] Marretta, L., Ingarao, G., and Di Lorenzo, R. (2010). Design of sheet stamping operations to control springback and thinning: a multi-objective stochastic optimization approach. *International Journal of Mechanical Sciences*, 52(7):914–927. (Cited on pages 11 and 87.)
- [133] Martins, J. R. (2006). Sensitivity analysis workshop, stanford march 2006. (Cited on pages 48 and 49.)
- [134] Mattiasson, K. (1995). *Simulation of springback in sheet metal forming*. (Cited on page 22.)
- [135] McKay, M., Beckman, R., and Conover, W. (2000). A comparison of three methods for selecting values of input variables in the analysis of output from a computer code. *Technometrics*, 42(1):55–61. (Cited on page 80.)
- [136] McKay, M. D., Beckman, R. J., and Conover, W. J. (1979). Comparison of three methods for selecting values of input variables in the analysis of output from a computer code. *Technometrics*, 21(2):239–245. (Cited on page 85.)
- [137] Melchers, R. (1989). Importance sampling in structural systems. *Structural safety*, 6(1):3–10. (Cited on page 78.)
- [138] Messac, A. (1996). Physical programming-effective optimization for computational design. *AIAA journal*, 34(1):149–158. (Cited on page 137.)

- [139] Miettinen, K. (1999). *Nonlinear multiobjective optimization*, volume 12. Springer. (Cited on pages 135 and 137.)
- [140] Mitchell, T. J. (1974). An algorithm for the construction of “d-optimal” experimental designs. *Technometrics*, 16(2):203–210. (Cited on pages 27 and 29.)
- [141] Montgomery, D. C. (2008). *Design and analysis of experiments*. John Wiley & Sons. (Cited on page 120.)
- [142] Montgomery, D. C. and Myers, R. H. (1995). Response surface methodology: process and product optimization using designed experiments. *Raymond H. Myers and Douglas C. Montgomery. A Wiley-Interscience Publications*. (Cited on pages 27, 29, 32, 63, 229 and 230.)
- [143] Moore, R. E. (1966). *Interval analysis*, volume 2. Prentice-Hall Englewood Cliffs. (Cited on pages 77, 78 and 83.)
- [144] Morestin, F. and Boivin, M. (1996). On the necessity of taking into account the variation in the young modulus with plastic strain in elastic-plastic software. *Nuclear Engineering and Design*, 162(1):107–116. (Cited on page 25.)
- [145] Morris, M. D. and Mitchell, T. J. (1995). Exploratory designs for computational experiments. *Journal of statistical planning and inference*, 43(3):381–402. (Cited on page 30.)
- [146] Mullur, A. A. and Messac, A. (2005). Extended radial basis functions: more flexible and effective metamodeling. *AIAA journal*, 43(6):1306–1315. (Cited on page 33.)
- [147] Murata, T. and Ishibuchi, H. (1995). Moga: Multi-objective genetic algorithms. In *Evolutionary Computation, 1995., IEEE International Conference on*, volume 1, page 289. IEEE. (Cited on page 137.)
- [148] Myers, R. H., Montgomery, D. C., and Anderson-Cook, C. M. (2009). *Response surface methodology: process and product optimization using designed experiments*, volume 705. John Wiley & Sons. (Cited on page 135.)
- [149] Naceur, H., Guo, Y., and Ben-Elechi, S. (2006). Response surface methodology for design of sheet forming parameters to control springback effects. *Computers & structures*, 84(26):1651–1663. (Cited on page 129.)
- [150] Narasimhan, N. and Lovell, M. (1999). Predicting springback in sheet metal forming: an explicit to implicit sequential solution procedure. *Finite Elements in Analysis and Design*, 33(1):29–42. (Cited on page 23.)
- [151] Natrella, M. (2010). Nist/sematech e-handbook of statistical methods. (Cited on page 110.)

- [152] Negoita, C., Zadeh, L., and Zimmermann, H. (1978). Fuzzy sets as a basis for a theory of possibility. *Fuzzy sets and systems*, 1:3–28. (Cited on pages 78 and 83.)
- [153] Nguyen, D. and Widrow, B. (1990). Improving the learning speed of 2-layer neural networks by choosing initial values of the adaptive weights. In *Neural Networks, 1990., 1990 IJCNN International Joint Conference on*, pages 21–26. IEEE. (Cited on page 70.)
- [154] Nguyen, V. D., Adragna, P.-A., and Lafon, P. (2013). Assessment of sensitivity of numerical simulation in sheet metal forming process applied for robust design. In *Smart Product Engineering*, pages 493–503. Springer. (Cited on pages 9, 12, 7, 8, 178 and 179.)
- [155] Nie, J. and Ellingwood, B. R. (2005). Finite element-based structural reliability assessment using efficient directional simulation. *Journal of engineering mechanics*, 131(3):259–267. (Cited on page 31.)
- [156] Oberkampf, W. L., DeLand, S. M., Rutherford, B. M., Diegert, K. V., and Alvin, K. F. (2002). Error and uncertainty in modeling and simulation. *Reliability Engineering & System Safety*, 75(3):333–357. (Cited on page 75.)
- [157] Oberkampf, W. L., Diegert, K. V., Alvin, K. F., and Rutherford, B. M. (1998). Variability, uncertainty, and error in computational simulation. *ASME-PUBLICATIONS-HTD*, 357:259–272. (Cited on page 74.)
- [158] Oliveira, M., Alves, J., Chaparro, B., and Menezes, L. (2007). Study on the influence of work-hardening modeling in springback prediction. *International Journal of Plasticity*, 23(3):516–543. (Cited on page 24.)
- [159] Owen, A. (1995). A collection of orthogonal array generators. (Cited on page 30.)
- [160] Owen, A. B. (1992). Orthogonal arrays for computer experiments, integration and visualization. *Statistica Sinica*, 2(2):439–452. (Cited on page 30.)
- [161] Owen, A. B. (1997). Monte carlo variance of scrambled net quadrature. *SIAM Journal on Numerical Analysis*, 34(5):1884–1910. (Cited on page 86.)
- [162] Pahl, G., Beitz, W., Feldhusen, J., and Grote, K.-H. (2007). *Engineering design: a systematic approach*, volume 157. Springer. (Cited on pages 9, 12, 6 and 178.)
- [163] Palmer, K. D. (1998). Data collection plans and meta models for chemical process flowsheet simulators. (Cited on page 30.)
- [164] Papadrakakis, M., Lagaros, N. D., and Tsompanakis, Y. (1998). Structural optimization using evolution strategies and neural networks. *Computer methods in applied mechanics and engineering*, 156(1):309–333. (Cited on page 32.)

- [165] Park, D., Kang, J., Hong, J., and Oh, S. (1999). Springback simulation by combined method of explicit and implicit fem. In *Proceedings of NUMISHEET*, volume 99, pages 35–40. (Cited on page 23.)
- [166] Park, G.-J., Lee, T.-H., Lee, K. H., and Hwang, K.-H. (2006). Robust design: an overview. *AIAA journal*, 44(1):181–191. (Cited on pages 11, 114, 116, 119, 120, 133 and 134.)
- [167] Park, J.-S. (1994). Optimal latin-hypercube designs for computer experiments. *Journal of statistical planning and inference*, 39(1):95–111. (Cited on page 30.)
- [168] Pé, V. M., rez, Renaud, J. E., and Watson, L. T. (2002). Adaptive experimental design for construction of response surface approximations. *AIAA journal*, 40(12):2495–2503. (Cited on page 33.)
- [169] Pearn, W. (1992). Distribution and inferential properties of process capability indices. *Journal of Quality Technology*, 24(2):216–231. (Cited on pages 92 and 93.)
- [170] Pearn, W.-L. and Shu, M.-H. (2004). Measuring manufacturing capability based on lower confidence bounds of c pmk applied to current transmitter process. *The International Journal of Advanced Manufacturing Technology*, 23(1-2):116–125. (Cited on page 93.)
- [171] Phadke, M. S. (1995). *Quality engineering using robust design*. Prentice Hall PTR. (Cited on page 120.)
- [172] Plante, R. D. (2001). Process capability: a criterion for optimizing multiple response product and process design. *IIE Transactions*, 33(6):497–509. (Cited on pages 160 and 162.)
- [173] Poles, S., Rigoni, E., and Robic, T. (2004). Moga-ii performance on noisy optimization problems. In *International Conference on Bioinspired Optimization Methods and their Applications, Ljubljana, Slovenia*. (Cited on page 138.)
- [174] Post, J. (2004). *On the constitutive behaviour of Sandvik Nanoflex: modelling, experiments and multi-stage forming*. University of Twente. (Cited on page 129.)
- [175] Pozo Fernández, C., Guillén Gosálbez, G., Sorribas Tello, A., and Jiménez Esteller, L. (2012). Identifying the preferred subset of enzymatic profiles in nonlinear kinetic metabolic models via multiobjective global optimization and pareto filters. *PLoS ONE*, 2012, vol. 7, núm. 9, e43487. (Cited on pages 12 and 136.)
- [176] Ragai, I., Lazim, D., and Nemes, J. A. (2005). Anisotropy and springback in draw-bending of stainless steel 410: experimental and numerical study. *Journal of Materials Processing Technology*, 166(1):116–127. (Cited on page 25.)
- [177] Rahman, S. and Xu, H. (2004). A univariate dimension-reduction method for multi-dimensional integration in stochastic mechanics. *Probabilistic Engineering Mechanics*, 19(4):393–408. (Cited on page 78.)

- [178] Repalle, J. and Grandhi, R. V. (2005). Design of forging process variables under uncertainties. *Journal of materials engineering and performance*, 14(1):123–131. (Cited on page 131.)
- [179] Rosenblatt, M. (1952). Remarks on a multivariate transformation. *The annals of mathematical statistics*, pages 470–472. (Cited on page 125.)
- [180] Rubinstein, R. Y. and Kroese, D. P. (2011). *Simulation and the Monte Carlo method*, volume 707. John Wiley & Sons. (Cited on page 84.)
- [181] Rumelhart, D. E., Widrow, B., and Lehr, M. A. (1994). The basic ideas in neural networks. *Communications of the ACM*, 37(3):87–92. (Cited on page 233.)
- [182] Sacks, J., Schiller, S. B., and Welch, W. J. (1989a). Designs for computer experiments. *Technometrics*, 31(1):41–47. (Cited on page 32.)
- [183] Sacks, J., Welch, W. J., Mitchell, T. J., Wynn, H. P., et al. (1989b). Design and analysis of computer experiments. *Statistical science*, 4(4):409–423. (Cited on pages 7, 29, 30, 32, 178, 179, 230 and 231.)
- [184] Sahai, A., Schramm, U., Buranathiti, T., Chen, W., Cao, J., and Xia, C. Z. (2004). Sequential optimization and reliability assessment method for metal forming processes. In *AIP CONFERENCE PROCEEDINGS*, volume 712, pages 2009–2013. IOP INSTITUTE OF PHYSICS PUBLISHING LTD. (Cited on page 131.)
- [185] Santner, T. J., Williams, B. J., and Notz, W. (2003). *The design and analysis of computer experiments*. Springer. (Cited on pages 230 and 231.)
- [186] Sasaki, D. and Obayashi, S. (2005). Efficient search for trade-offs by adaptive range multi-objective genetic algorithms. *Journal of Aerospace Computing, Information, and Communication*, 2(1):44–64. (Cited on pages 12, 136 and 137.)
- [187] Sasena, M., Parkinson, M., Goovaerts, P., Papalambros, P., and Reed, M. (2002). Adaptive experimental design applied to ergonomics testing procedure. In *ASME 2002 International Design Engineering Technical Conferences and Computers and Information in Engineering Conference*, pages 529–537. American Society of Mechanical Engineers. (Cited on page 31.)
- [188] Scaravetti, D. (2004). *Formulation préalable d’un problème de conception, pour l’aide à la décision en conception préliminaire*. PhD thesis, Ecole nationale supérieure d’arts et métiers-ENSAM. (Cited on pages 9, 12, 6 and 178.)
- [189] Schuëller, G. I. and Jensen, H. A. (2008). Computational methods in optimization considering uncertainties—an overview. *Computer Methods in Applied Mechanics and Engineering*, 198(1):2–13. (Cited on page 134.)
- [190] Sen, P. and Yang, J.-B. (1998). *Multiple criteria decision support in engineering design*, volume 4. Springer London. (Cited on page 137.)

- [191] Seo, H. S. and Kwak, B. M. (2002). Efficient statistical tolerance analysis for general distributions using three-point information. *International journal of production research*, 40(4):931–944. (Cited on page 78.)
- [192] Shafer, G. (1976). *A mathematical theory of evidence*, volume 1. Princeton university press Princeton. (Cited on pages 77 and 78.)
- [193] Shewry, M. and Wynn, H. (1988). Maximum entropy sampling with application to simulation codes. In *Proceedings of the 12th World Congress on Scientific Computation*, volume 2, pages 517–519. (Cited on page 30.)
- [194] Simpson, J. A., Weiner, E. S., et al. (1989). *The Oxford english dictionary*, volume 2. Clarendon Press Oxford. (Cited on page 73.)
- [195] Simpson, T. W. (1998). *A concept exploration method for product family design*. PhD thesis, Citeseer. (Cited on page 30.)
- [196] Simpson, T. W., Allen, J. K., and Mistree, F. (1998). Spatial correlation metamodels for global approximation in structural design optimization. In *ASME Design Engineering Technical Conferences*. (Cited on page 30.)
- [197] Simpson, T. W., Chen, W., Allen, J. K., and Mistree, F. (1996). Conceptual design of a family of products through the use of the robust concept exploration method. In *Proceedings of the 6th AIAA/NASA/USAF Multidisciplinary Analysis & Optimization Symposium*, pages 1535–1545. (Cited on page 122.)
- [198] Simpson, T. W., Lin, D. K., and Chen, W. (2001a). Sampling strategies for computer experiments: design and analysis. *International Journal of Reliability and Applications*, 2(3):209–240. (Cited on page 31.)
- [199] Simpson, T. W., Maier, J. R., and Mistree, F. (2001b). Product platform design: method and application. *Research in engineering Design*, 13(1):2–22. (Cited on page 122.)
- [200] Simpson, T. W., Poplinski, J., Koch, P. N., and Allen, J. K. (2001c). Metamodels for computer-based engineering design: survey and recommendations. *Engineering with computers*, 17(2):129–150. (Cited on pages 5, 9, 13, 27, 28, 29, 63 and 234.)
- [201] Sohlenius, G. (1992). Concurrent engineering. *Annals of the CIRP*, 41:645–655. (Cited on pages 3 and 175.)
- [202] Steiner, S., Abraham, B., and MacKay, J. (1997). Understanding process capability indices. *Institute for Improvement of Quality and Productivity, Department of Statistics and Actuarial Science, University of Waterloo, Waterloo, Ontario N2L 3G1*. (Cited on page 90.)
- [203] Steuer, R. E. (1989). *Multiple criteria optimization: theory, computation, and application*. Krieger Malabar. (Cited on page 135.)

- [204] Stockinger, A. and Meerkamm, H. (2000). Virtual dimensional product validation by integration of simulations. In *International Conference on Engineering Design, ICED'09, 24-27 august 2009, Stanford University, Stanford, CA, USA.*, pages 181–192. (Cited on pages [9](#), [12](#), [7](#), [34](#) and [178](#).)
- [205] Strano, M. (2006). Optimization under uncertainty of sheet-metal-forming processes by the finite element method. *Proceedings of the Institution of Mechanical Engineers, Part B: Journal of Engineering Manufacture*, 220(8):1305–1315. (Cited on pages [131](#) and [134](#).)
- [206] Sullivan, L. P. (1984). Reducing variability: a new approach to quality. *Quality Progress*, 17(7):15–21. (Cited on page [90](#).)
- [207] Swift, H. (1952). Plastic instability under plane stress. *Journal of the Mechanics and Physics of Solids*, 1(1):1–18. (Cited on page [40](#).)
- [208] Taguchi, G. (1986). *Introduction to quality engineering: designing quality into products and processes*. (Cited on pages [8](#), [113](#), [114](#), [120](#) and [180](#).)
- [209] Taguchi, G. (1987). Systems of experimental design: engineering methods to optimize quality and minimize cost. *Quality Resources, White Plains, New York*. (Cited on page [120](#).)
- [210] Taguchi, G., Chowdhury, S., and Taguchi, S. (2000). *Robust engineering*. McGraw-Hill Professional. (Cited on page [120](#).)
- [211] Taguchi, G. and Clausing, D. (1990). Robust quality. *Harvard Business Review*, 68(1):65–75. (Cited on pages [8](#), [113](#) and [180](#).)
- [212] Taherizadeh, A., Ghaei, A., Green, D. E., and Altenhof, W. J. (2009). Finite element simulation of springback for a channel draw process with drawbead using different hardening models. *International Journal of Mechanical Sciences*, 51(4):314–325. (Cited on page [24](#).)
- [213] Tang, B. (1993). Orthogonal array-based latin hypercubes. *Journal of the American Statistical Association*, 88(424):1392–1397. (Cited on page [30](#).)
- [214] Tang, S. (1987). Analysis of springback in sheet forming operation. *Advanced Technology of Plasticity 1987.*, 1:193–197. (Cited on page [23](#).)
- [215] Tannert, C., Elvers, H.-D., and Jandrig, B. (2007). The ethics of uncertainty. *EMBO reports*, 8(10):892–896. (Cited on page [73](#).)
- [216] Tekkaya, A. and Martins, P. (2009). Accuracy, reliability and validity of finite element analysis in metal forming: a user’s perspective. *Engineering Computations*, 26(8):1026–1055. (Cited on page [95](#).)
- [217] Teodosiu, C. and Hu, Z. (1995). Evolution of the intragranular microstructure at moderate and large strains: modelling and computational significance. In *Proc. Numiform*, volume 95, pages 173–182. (Cited on page [24](#).)

- [218] Thunnissen, D. (2003). Uncertainty classification for the design and development of complex systems. *3rd Annual Predictive Methods Conference, Newport Beach, California, June 2003*. (Cited on page 73.)
- [219] Triantaphyllou, E. (2000). *Multi-criteria decision making methods a comparative study*. Springer. (Cited on page 143.)
- [220] Tsui, K.-L. (1992). An overview of taguchi method and newly developed statistical methods for robust design. *Iie Transactions*, 24(5):44–57. (Cited on page 120.)
- [221] Tsui, K.-L. (1996). A critical look at taguchi’s modelling approach for robust design. *Journal of Applied Statistics*, 23(1):81–96. (Cited on pages 8, 120 and 180.)
- [222] Tvedt, L. (1983). Two second-order approximations to the failure probability. *Section on structural reliability*. (Cited on page 127.)
- [223] Valente, M. and Traversa, D. (1999). Springback calculation of sheet metal parts after trimming and flanging. In *Proceedings of NUMISHEET*, volume 99, pages 59–64. (Cited on page 23.)
- [224] Varadarajan, S., CHEN*, W., and Pelka, C. J. (2000). Robust concept exploration of propulsion systems with enhanced model approximation capabilities. *Engineering Optimization+ A35*, 32(3):309–334. (Cited on page 32.)
- [225] Verma, R. K. and Haldar, A. (2007). Effect of normal anisotropy on springback. *Journal of materials processing technology*, 190(1):300–304. (Cited on page 25.)
- [226] Vira, C. and Haimes, Y. Y. (1983). *Multiobjective decision making: theory and methodology*. Number 8. North-Holland. (Cited on page 137.)
- [227] Voce, E. (1955). A practical strain-hardening function. *Metallurgia*, 51(307):219–226. (Cited on page 24.)
- [228] Wagoner, R., Carden, W., Carden, W., and Matlock, D. (1997). Springback after drawing and bending of metal sheets. In *Proceedings of the IPMM*, pages 1–10. (Cited on page 22.)
- [229] Wagoner, R. H., Lim, H., and Lee, M.-G. (2013). Advanced issues in springback. *International Journal of Plasticity*, 45:3–20. (Cited on page 14.)
- [230] Walker, J. (1986). Practical application of variance reduction techniques in probabilistic assessments. In *the Second International Conference on Radioactive Waste Management*, pages 517–521. (Cited on page 31.)
- [231] Wang, G. G. (2003). Adaptive response surface method using inherited latin hypercube design points. *Journal of Mechanical Design*, 125(2):210–220. (Cited on page 31.)

- [232] Wang, G. G. and Shan, S. (2007). Review of metamodeling techniques in support of engineering design optimization. *Journal of Mechanical Design*, 129(4):370–380. (Cited on pages 9, 25, 26 and 60.)
- [233] Wang, G. G. and Simpson, T. (2004). Fuzzy clustering based hierarchical metamodeling for design space reduction and optimization. *Engineering Optimization*, 36(3):313–335. (Cited on page 31.)
- [234] Wang, G. G., Wang, L., and Shan, S. (2005). Reliability assessment using discriminative sampling and metamodeling. In *2005 SAE World Congress*, pages 11–14. (Cited on page 31.)
- [235] Wang, L., Shan, S., and Wang, G. G. (2004). Mode-pursuing sampling method for global optimization on expensive black-box functions. *Engineering Optimization*, 36(4):419–438. (Cited on page 31.)
- [236] Wiebenga, J. H. (2014). Robust design and optimization of forming processes. (Cited on pages 12, 120, 131, 132 and 134.)
- [237] Wiener, N. (1938). The homogeneous chaos. *American Journal of Mathematics*, pages 897–936. (Cited on page 81.)
- [238] Wu, C.-W., Pearn, W.-L., and Kotz, S. (2009). An overview of theory and practice on process capability indices for quality assurance. *International Journal of Production Economics*, 117(2):338–359. (Cited on pages 91 and 93.)
- [239] Xiu, D. and Karniadakis, G. E. (2002). The wiener-askey polynomial chaos for stochastic differential equations. *SIAM Journal on Scientific Computing*, 24(2):619–644. (Cited on page 82.)
- [240] Xu, W., Ma, C., Li, C., and Feng, W. (2004). Sensitive factors in springback simulation for sheet metal forming. *Journal of Materials Processing Technology*, 151(1):217–222. (Cited on page 23.)
- [241] Yoshida, F. and Uemori, T. (2003). A model of large-strain cyclic plasticity and its application to springback simulation. *International Journal of Mechanical Sciences*, 45(10):1687–1702. (Cited on pages 168 and 216.)
- [242] Youn, B. D., Xi, Z., Wells, L. J., and Wang, P. (2006). Enhanced dimension-reduction (edr) method for sensitivity-free uncertainty quantification. In *Proceedings of 11th AIAA/ISSMO multidisciplinary analysis and optimization conference, Portsmouth, VA, USA*. (Cited on page 78.)
- [243] Yu, H. Y. (2009). Variation of elastic modulus during plastic deformation and its influence on springback. *Materials & Design*, 30(3):846–850. (Cited on page 25.)

- [244] Yuen, W. (1990). Springback in the stretch-bending of sheet metal with non-uniform deformation. *Journal of materials processing technology*, 22(1):1–20. (Cited on page 23.)
- [245] Zadeh, L. A. (1965). Fuzzy sets. *Information and control*, 8(3):338–353. (Cited on pages 77, 78 and 83.)
- [246] Zang, C., Friswell, M., and Mottershead, J. (2005). A review of robust optimal design and its application in dynamics. *Computers & structures*, 83(4):315–326. (Cited on pages 11, 115, 116, 117, 120 and 133.)
- [247] Zang, T. A., Hemsch, M. J., Hilburger, M. W., Kenny, S. P., Luckring, J. M., Maghami, P., Padula, S. L., and Stroud, W. J. (2002). *Needs and opportunities for uncertainty-based multidisciplinary design methods for aerospace vehicles*. National Aeronautics and Space Administration, Langley Research Center. (Cited on page 74.)
- [248] Zhang, W. (2007a). *Design for uncertainties of sheet metal forming process*. PhD thesis, The Ohio State University. (Cited on pages 11, 117 and 132.)
- [249] Zhang, W. (2007b). *Design for uncertainties of sheet metal forming process*. PhD thesis, The Ohio State University. (Cited on pages 12, 34, 124 and 125.)
- [250] Zhang, W. and Shivpuri, R. (2009). Probabilistic design of aluminum sheet drawing for reduced risk of wrinkling and fracture. *Reliability Engineering & System Safety*, 94(2):152–161. (Cited on page 131.)
- [251] Zhang, Y. and Der Kiureghian, A. (1995). Two improved algorithms for reliability analysis. In *Reliability and Optimization of Structural Systems*, pages 297–304. Springer. (Cited on page 126.)
- [252] Zhao, Y.-G. and Ono, T. (1999). New approximations for sorm: Part 1. *Journal of engineering mechanics*, 125(1):79–85. (Cited on page 127.)
- [253] Zitzler, E., Thiele, L., Zitzler, E., Zitzler, E., Thiele, L., and Thiele, L. (1998). *An evolutionary algorithm for multiobjective optimization: The strength pareto approach*, volume 43. Citeseer. (Cited on page 137.)
- [254] Zou, T., Mahadevan, S., Mourelatos, Z., and Meernik, P. (2002). Reliability analysis of automotive body-door subsystem. *Reliability Engineering & System Safety*, 78(3):315–324. (Cited on page 31.)
- [255] Zou, T., Mourelatos, Z. P., Mahadevan, S., and Tu, J. (2003). An indicator response surface-based monte carlo method for efficient component and system reliability analysis. In *ASME 2003 International Design Engineering Technical Conferences and Computers and Information in Engineering Conference*, pages 45–54. American Society of Mechanical Engineers. (Cited on page 31.)

About the author

Von Dim NGUYEN was born on December 7th 1984 in Thai Nguyen, Vietnam. His academic cursus is summarized as follows:

- 1999-2002 High school, Thai Nguyen High school, Thai Nguyen, Vietnam
- 2002-2007 Engineer's degree, in Mechanical Engineering, Thai Nguyen University of Technology (TNUT), Thai Nguyen, Vietnam. Specialisation: Manufacturing Engineering.
- 2010-2011 Master's degree, in Knowledge Integration in Mechanical Production, Arts et Métiers ParisTech, Center of Paris, France. The studies included internships at Laboratory of Design, Manufacturing and Control (LCFC), Arts et Métiers ParisTech, Center of Metz, France. The Master thesis is on Modeling and Simulation of Manufacturing Process.
- 2012-2014 PhD in Mechanical Systems and Materials (SMM), Charles Delaunay Institute (ICD), Laboratory of Mechanical Systems and Concurrent Engineering (LASMIS), University of Technology of Troyes (UTT), Troyes, France. Subject: Validation and robust optimization of deep drawing process by simulation in the presence of uncertainty.

Publications

Journal publications

1. V. D. Nguyen, P.-A. Adragna, and P. Lafon, "Identifying sensitivity threshold in FEM numerical simulation," in *Journal of Finite Elements in Analysis and Design*. Submitted, Elsevier, 2014, pp. .
2. V. D. Nguyen, P. Martin, "Product design-Process selection-Process planning Integration based on Modeling and Simulation," in *The International Journal of Advanced Manufacturing Technology*. Springer. Published online on 11 october 2014.

International conference proceedings

1. V. D. Nguyen, P.-A. Adragna, and P. Lafon, "Assessment of sensitivity of numerical simulation in sheet metal forming process applied for robust design," in *Smart Product Engineering*. Springer, 2013, pp. 493-503.
2. V. D. Nguyen, P.-A. Adragna, and P. Lafon, "Predicting the effects of material and process parameters on springback by FEM numerical simulation in sheet metal forming," 10th International Conference on MOdeling, Optimization and SIMlation - MOSIM14 - November 5-7-2014, Nancy - France, "Toward circular Economy".
3. P.-A. Adragna, S. Ali, A. Durupt, V. D. Nguyen, P. Lafon, "Influence of part geometrical tolerancing in the REFM methodology," *Proceedings of Joint Conference on Mechanical, Design Engineering & Advanced Manufacturing*, Toulouse, 18-20 june 2014.
4. V. D. Nguyen, P.-A. Adragna, and P. Lafon, "Multi-objective optimization under uncertainty and decision-making support for sheet metal forming," 18th International ESAFORM Conference on Material Forming, Graz -Austria, 15 - 17 April 2015.

Von Dim NGUYEN

Doctorat : Systèmes Mécaniques et Matériaux

Année 2015

Validation et optimisation robuste d'un procédé d'emboutissage par simulation en contexte incertain

L'objectif ultime de ce travail de thèse est d'évaluer la possibilité de valider et d'optimiser un processus de fabrication en utilisant la simulation numérique en tenant compte des incertitudes irréductibles sur le procédé, les matériaux et la géométrie du produit fabriqué. La prise en compte des incertitudes nécessite de quantifier les effets des variations des paramètres du modèle sur les sorties de celui-ci, en propageant ces variations via la simulation numérique pour évaluer leurs effets sur les sorties. Dans ce travail nous avons proposé une procédure pour déterminer le seuil de sensibilité du modèle numérique afin de construire des plans d'expériences numériques cohérents avec ce seuil. Nous avons également montré que, compte tenu des incertitudes sur les matériaux et la géométrie du produit, il est possible d'optimiser certains paramètres du procédé pour contrôler les effets des incertitudes sur les variations dimensionnelles et morphologiques du produit. Pour cela, nous avons proposé une procédure d'optimisation basée sur un algorithme NSGA-II et une méta-modélisation du procédé. L'application à l'emboutissage d'une tôle en U, retour élastique inclus, montre qu'il s'agit d'un problème de conception robuste pour lequel nous obtenons l'ensemble des compromis entre l'écart à la moyenne et l'écart type d'une fonction « performance » du procédé correctement choisie. Finalement l'analyse de ces résultats nous permet de quantifier le lien entre la notion de robustesse d'une solution optimisée du procédé et les critères de mesure de la qualité du produit.

Mots clés : incertitude - tôle, travail de la - commande robuste - simulation par ordinateur - décision multicritère.

Validation and Robust Optimization of Deep Drawing Process by Simulation in the Presence of Uncertainty

The ultimate objective of this thesis is to evaluate the possibility to validate and optimize a manufacturing process using numerical simulation and taking into account the irreducible uncertainties in the process, materials and geometry of manufactured product. Taking into account the uncertainties requires quantifying the effects of variations of model parameters on the outputs, by propagating these variations via computer simulation to assess their effects on the outputs. In this work, we have proposed a procedure to determine the sensitivity threshold of the numerical model to build numerical Design of Experiments consistent with this threshold. We have also shown that, given the uncertainties in the materials and the geometry of the product, it is possible to optimize certain process parameters to control the effects of uncertainties on the dimensional and morphological variations of the product. For this, we have proposed an optimization procedure based on NSGA-II algorithm and a meta-modeling of the process. The application for deep drawing of a U-shaped sheet metal part, springback included shows that it is a robust design problem for which we get all the compromise between the deviation from the mean and standard deviation of a "performance" depending on the process correctly chosen. Finally, the analysis of these results allows us to quantify the relationship between the notion of robustness of an optimized solution of the process and criteria for measuring the quality of the product.

Keywords: uncertainty - sheet-metal forming - robust design - numerical simulation - sensitivity threshold - uncertainty propagation - robust design optimization.

Thèse réalisée en partenariat entre :

